UNIVERSITY OF CALIFORNIA
RIVERSIDE

N-Heterocyclic Silyl and Silylene Metal Complexes Within a PSiP Framework: Synthesis, Structure and Reactivity

A Dissertation submitted in partial satisfaction
of the requirements for the degree of

Doctor of Philosophy

In

Chemistry

By

Amy Marie Jehl

June 2019

Dissertation Committee:
Dr. W. Hill Harman, Chairperson
Dr. David Martin
Dr. Vincent Lavallo

The Dissertation of Amy Marie Jehl is approved:

_____

_____

_____

Committee Chairperson

University of California, Riverside

Acknowledgements

Thank you, Dr. Hill Harman, for allowing me the opportunity to work in your laboratory. The almost six years in your lab will be an experience forever remembered and appreciated largely because of your patience, kindness and guidance. I have learned a tremendous amount working in your lab and developed skills I never dreamed to acquire. Your guidance through the program has allowed for my success not only in the laboratory but also in the classroom leading students. Also, I would like to express my thanks to committee members Dr. David Martin and Dr.Vincent Lavallo. Acknowledgement is also given to members of the Harman lab who have all supported my academic endeavors including Marissa Barrientos-Lane, Laura Essex, Jordan Taylor, Colomba Sanchez-Marsetti and Alex McSkimming. Thank you for your friendship and help through the years. I've been fortunate to meet, learn from, and work with each of you. Thanks also to Dr Dan Borchardt (NMR), Dr. Rena Hayashi (Academic Coordinator for Sci. Labs), Dr. Fook Tham and Dr. Charlene Tsay (XRD diffraction experiments) and Prisciliano Saavedra (Chem. Sci. Stockroom), who have been extremely helpful in my time at UCR.

This journey started with Dr. John Haan, an amazing undergraduate research advisor and mentor who allowed me the opportunity to work in his lab at CSUF. You provided me with the confidence to pursue graduate school and it is greatly appreciated.

Much acknowledgment is owed to my family who are incredibly supportive and inspiring. This body of work is dedicated to you. Especially my mother who is fond of saying "Every day is like a coin, be careful how you spend it." This work represents many coins. Thank you for the drive to always learn and persevere. Sincere props to Marie

Anstead, as well, who has always been an inspiration and an incredible sister. Finally, John Jehl, my awesome husband, thank you for your bottomless pit of patience through this journey. I am fortunate to call you my best friend and husband. I could not have done any of this without you, John.

To my Family

ABSTRACT OF THE DISSERTATION

N-Heterocyclic Silyl and Silylene Metal Complexes Within a PSiP Framework: Synthesis, Structure and Reactivity

by

Amy Marie Jehl

Doctor of Philosophy, Graduate Program in Chemistry
University of California, Riverside, June 2019
Dr. W. Hill Harman, Chairperson

N-heterocyclic carbenes (NHC) are strong Lewis bases that have demonstrated broad utility as ligands for transition metal (TM) catalysts. Silicon analogues, N-heterocyclic silylenes (NHSi), are comparatively less well studied. The decreased π–π overlap between the Si 3p orbital and adjacent nitrogen lone pairs creates a more accessible vacant orbital on Si, resulting in increased ambiphilic character. When bound to a transition metal, this empty orbital presents an opportunity to cooperatively bind and activate substrate molecules. To increase the stability of a potential metal–silylene complex we targeted the diphosphine ligand precursor 1,2-bis($R_2PCH_2NCH_2$)C_6H_4 (R = alkyl or aryl), first reported by Yamashita and Nozaki in the construction of a boron-anchored pincer. Reported here are $(P^{Cy})_2Si$ pincer ligands and their TM–silylene complexes for small molecule activation. The bimetallic dinickel disilylene complex, $(P^{Cy})_4Ni_2Si_2$, is reactive with dihydrogen, phenol, thiophenol and diphenyl disulfide, resulting in addition of the E–H or E–E bond (E = H, O, or S) across the Ni_2Si_2 core and the conversion of the silylene ligands to bridging

silyls. We also investigated the reactivity of $(P^{Cy})_4Ni_2Si_2$ with CO_2. Addition of excess CO_2 to $(P^{Cy})_4Ni_2Si_2$ revealed a new product, $(P^{Cy})_4Ni_2(\mu\text{-}CO)Si_2O$, featuring a bridging CO across the two Ni centers and a Si–O–Si linkage. This product corresponds to the direct deoxygenation of CO_2 and the transfer of the oxygen atom to the silylene ligands. CO dissociation is observed under certain conditions to give an oxo-bridged 16 e^- $(P^{Cy})_4Ni_2(Si_2O)$ complex that can also be synthesized via direct O-atom transfer to $(P^{Cy})_4Ni_2Si_2$. A transient side-bound CO_2 intermediate was hypothesized to initially form across one of the two Ni^0–silylene interactions prior to C=O bond cleavage and the formation of $(P^{Cy})_4Ni_2(\mu\text{-}CO)Si_2O$. Trapping experiments with TMSCl support this hypothesis, as an intermediate can be isolated, $(P^{Cy})_4NiClNi(CO)Si_2O$-TMS, featuring a terminal Ni–CO and a trimethylsiloxyl moiety on one of the two Si centers, suggesting the cooperativity of the Ni–Si bond in activating CO_2. This work highlights the promise of using TM–silylene interactions for the cooperative activation of small molecules.

Table of Contents

List of Schemes

List of Figures

List of Tables

CHAPTER 1 Syntheses of PSiP Silane Precursor Ligands for Metal Coordination

1.1 Abstract

We report here the synthesis and characterization of three new silane ligand precursors using an *o*-phenylenediamine-derived diphosphine ligand, 1,2-bis($R_2PCH_2NH)C_6H_4$ (R = cyclohexyl), for the purposes of ligating transition metal centers in a step towards the synthesis of transition metal (TM) silylene complexes. The ligand precursor, 1,2-bis($R_2PCH_2NH)C_6H_4$ (R = alkyl or aryl), was first reported by Yamashita and Nozaki for preparation of boryl-anchored pincer ligands. With the groups of Hill and Whited we have developed Si-based analogues. Three new silane ligand precursors: (1,2-$C_6H_4)(NCH_2P(Cy)_2)_2SiCl_2$, (1,2-$C_6H_4)(NCH_2P(Cy)_2)_2SiClH$, and (1,2-$C_6H_4)(NCH_2P(Cy)_2)_2SiH_2$ are synthesized in good yield and have been characterized by a range of NMR spectroscopies, in addition to mass spectrometry or elemental analysis.

1.2 Introduction

New ligand platforms developed around the concept "frustrated Lewis pairs" FLP, have been an effective way to facilitate small molecule activation.[1] Incorporating main-group atoms as a Lewis acid, such as boron, within aryl boranes have facilitated activation of dihydrogen and carbon dioxide as reported in the work of Wagner.[2,3] Harman and Taylor demonstrated a diborothrene bis(phosphino) ligand capable of activating small molecule substrates including molecular oxygen, ethylene and carbon dioxide.[4] The work detailed here investigates the use of silicon as a main group substitute for boron to facilitate FLP

type chemistry when bound to an electron rich metal center within a bis(phosphino) cheating ligand framework.

In the 1980s silylenes were first reported as non-isolable reaction intermediates.[5] The first report of an isolable N-heterocyclic silylene by Denk and West demonstrated the potential for accessing new ligand frameworks in which a divalent silicon species could be isolated.[6] Since this discovery N-heterocyclic silylenes have been an emergent class of ligands that catalyze a variety of organic transformations when bound to various transition metal fragments.[7] As powerful as they have proved, NHSis have yet to be strong competitors with NHCs in homogeneous catalysis.[8] Despite this, increased reports of various TM–silylene complexes, their activity for both non-catalytic small molecule activation and catalysis of various organic transformations, demonstrates continued active research interest in this relatively new field. This is emphasized in the multiple reviews written on silylenes and transition metal complexes spanning several years.[8–11]

Development of silicon containing precursor ligands is one approach in accessing silylene ligands for transition metal coordination for the potential of small molecule activation. Early reports from Lappert, Gehrhus, West and Denk established protocols in isolating stable silylenes.[12–15] Typically, the 'free' silylene ligand is generated using a reductant (Na, K, KC_8, etc), followed by addition of a transition metal source to generate transition metal silylene complexes or transition metal silyl(silylene) complexes.[14] Utilizing Si–Cl or Si–H bond activation within silane precursor ligands is also an established route to TM-silicon containing complexes as demonstrated in the work of Berry, Whited and Dixon.[16–18] The targeted ligand framework for this work was an *o*-

phenylenediamine-derived bis(phosphine) ligand precursor 1,2-bis($R_2PCH_2NH)C_6H_4$ (R = alkyl or aryl), first reported by Yamashita and Nozaki used in the preparation of boryl-anchored pincer ligand.[19] Lin and Peters later reported the boryl-anchored pincer ligand to bind cobalt and demonstrated its ability for reversible H_2 activation.[20] With respect to installing silicon, it was the groups of Hill and Whited who have developed Si-based analogues, in addition to the work we report here.[17,21]

1.2.1 *N*-Heterocyclic Silylenes

N-heterocyclic silylene ligands have demonstrated ability to facilitate various chemical transformations just as their more well-known congener, N-heterocyclic carbenes (NHC). NHC ligands are strong σ-donating L-type ligands with essentially no π-acceptor character.[2] The isoelectronic congeners of the heavier group 14 elements, e.g. silylenes and germylenes, have gained increased research interest since the first isolable five membered N-heterocyclic silylene was synthesized by Denk in 1994.[6] More recent TM–(NHSi) complexes have demonstrated interesting binding modes with new reports made each year.[5,6,7] These heavy atom NHC analogues possess substantially different properties than their carbene counterparts due in part to the poor overlap between the 2p nitrogen lone pairs and the more diffuse *n*p orbital ($n > 2$) on the group 14 center.[8] (Figure 1.2-1, top diagram)

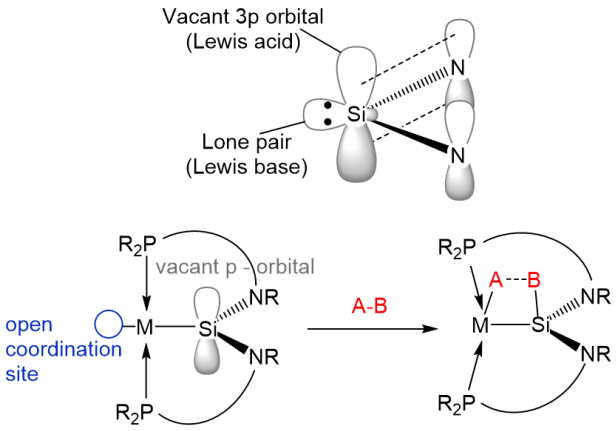

Figure 1.2-1 Electronic configuration of free N-heterocyclic silylene with diffuse 3p orbital demonstrating ambiphilic character (top diagram). NHSi bound to a metal center, followed by subsequent reactivity with a small molecule, AB, across metal–silicon interaction (bottom scheme).

As a result the silicon center is significantly more Lewis acidic than in analogous carbenes, a feature proven in some preliminary studies of TM–silylene reactivity.[6,9] The electrophilicity, as a result of the more diffuse p-orbital at silicon, makes these complexes ideal candidates to target small molecule activation in a pseudo frustrated Lewis pair (FLP)-type chemistry.[1] As with stable carbenes, silylenes are generally found to be in the singlet state with a lone pair of electrons which reside in a forward facing sp^2-orbital in addition to possessing an empty 3p orbital.[8,22] These features contribute to their Lewis acidity and basicity, and this is largely responsible for their reactive nature. Specifically, the empty 3p orbital located on silicon, in addition to strong σ-donating abilities, suggests the possibility of cooperative reactivity with a metal center in activating a small molecule substrate (Figure 1.2-1, bottom diagram).[10,23]

1.2.2 Pincer Ligands [PXP] with Donor Atom X = B, C, P, N, and Si

Phosphines are known to be strong σ-donors and have been implemented into countless transition metal-ligand frameworks. Additionally, they have played a large part in homogenous catalysis as ancillary and chelating ligands.[24] The tunability of both electronic and steric effects at the two donor phosphine arms, in addition to the central donor atom, X, makes tridentate ligand frameworks appealing platforms with many possibilities for improvement and fine tuning for potential TM–complexes. Tridentate ligand frameworks featuring chelating phosphine donors are known to be versatile ligands. Traditionally tridentate pincer type ligands are of the form EXE with X as a central donor atom, usually within some aromatic backbone and E as a two electron Lewis donor.[11]

There are a variety of pincer complexes [PXP] that feature various central donor atoms where X is carbon, nitrogen, boron, phosphorous or silicon that have gone on to bind a metal center. The first reported ligand with carbon as a central atom donor was reported in 1975 with the seminal work of Shaw.[25] The first boron-based pincer ligand was reported in 2007 by Bourissou, Maron and coworkers.[26] This discovery was shortly followed in 2009 by Yamashita, Nozaki and co-workers who reported boron as a central atom within an amido stabilized bis(phosphine) framework.[19] Hill and Peters went on to form a variety of metal complexes based on the Yamashita and Nozaki ligand framework. [20] Nitrogen has also been employed as a donor atom within a pincer framework with the first report in 1971 of a PNP ligand made by Nelson and co-workers.[27] Continued implementation employing nitrogen as a donor within a PNP ligand framework largely continued by Milstein and co-workers.[28,29]

With respect to silicon there have been several groups throughout the years that have incorporated silicon into a pincer ligand framework. Turculet and co-workers in 2007 installed silicon between two *o*-phenylene rings creating several PSiP ligand frameworks with varying substituents on phosphorous and silicon, all of which have been widely used.[30] Additionally, these PSiP ligands have been demonstrated to afford several complexes featuring various transition metals with interesting reactivity.[30–33] Milstein and Iwasawa continued to demonstrate the PSiP ligand framework to be a powerful platform by providing additional variations to the ligand, in addition to installing various transition metals to form novel complexes. [34–36] In 2014 Dixon and Hill, followed by Whited demonstrated the *o*-phenylenediamine derived bis-phosphine ligand as successful in installing silicon.[21,37] The aforementioned representative PXP ligand frameworks with X = C, B, P, N, and Si as central donor atoms is summarized in Figure 1.2-2.

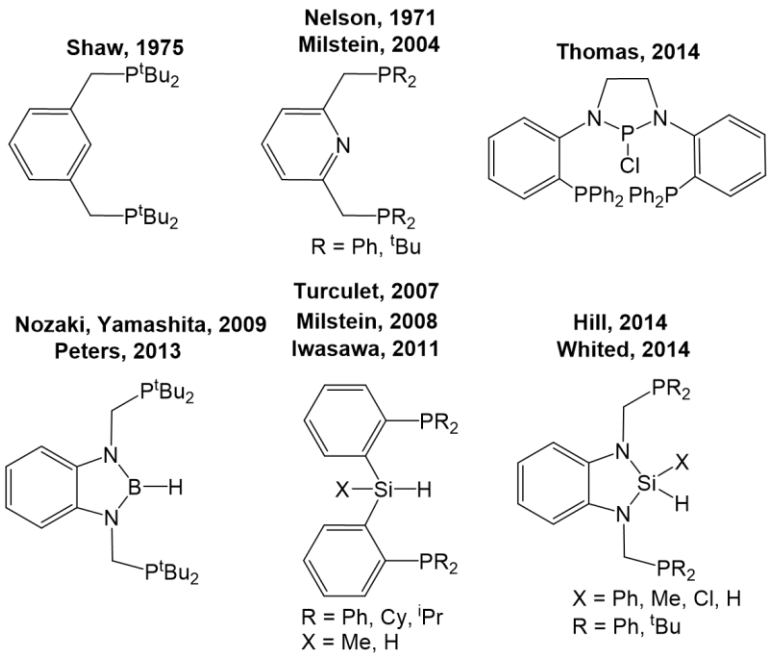

Figure 1.2-2. Representative examples of PXP ligand frameworks where X represents carbon, boron, phosphorous, nitrogen and silicon as a central donor atom for potential metal complexes.

1.3 Results and Discussion

Our goal was to target a potentially chelating bis(phosphine) silane precursor ligand, taking advantage of a pincer ligand framework to increase the stability of a potential metal-silylene complex. The ligand precursor (1,2-C_6H_4)($NHCH_2P(Cy)_2$)$_2$ has been described previously and was an ideal starting point as it has been shown to support various electrophiles to form boryl, phosphoryl and silyl compounds that have gone on to bind transition metals and form complexes within pincer frameworks.[19,21,38,39] Three new forms of the silane precursor ligands: (1,2-C_6H_4)($NCH_2P(Cy)_2$)$_2SiCl_2$, **1**; (1,2-C_6H_4)($NCH_2P(Cy)_2$)$_2$SiClH, **2** and (1,2-C_6H_4)($NCH_2P(Cy)_2$)$_2SiH_2$, **3**, were synthesized. In a similar fashion reported by Dixon and Hill, the newly reported silane precursors, compounds **1** and **2**, are made by treating the previously reported ligand precursor (1,2-C_6H_4)($NHCH_2P(Cy)_2$)$_2$ with the appropriate chlorosilane in the presence of triethylamine (Scheme 1.3-1).[19]

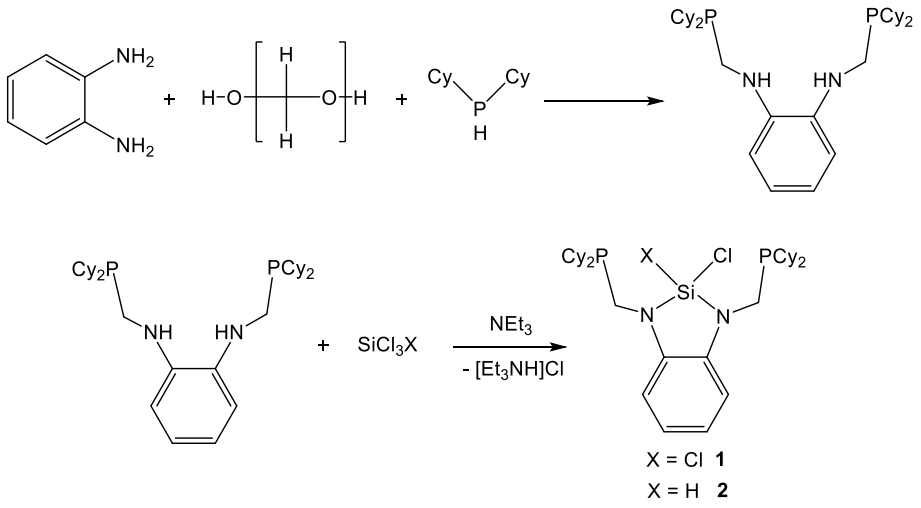

Scheme 1.3-1 Synthesis of silane precursor ligands **1** and **2** from ligand precursor 1,2-bis (dicyclohexylphosphinoamino)benzene.

The ligand precursor, **3**, was made via addition of (teeda)$SiCl_2H_2$ which has been previously reported as a convenient silane source by Whited and Grubbs in making silane precursor ligands of the form PSiP (Scheme 1.3-2).[37,40]

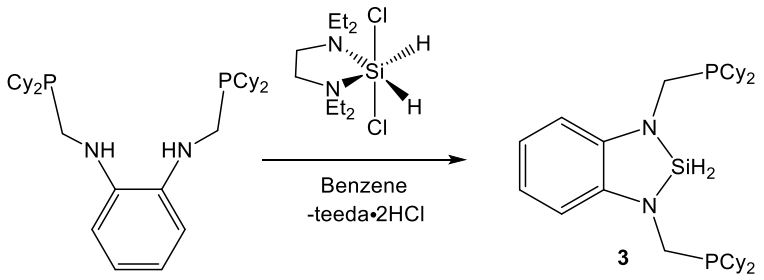

Scheme 1.3-2 Synthesis of silane ligand precursor in which (teeda)$SiCl_2H_2$ affords the silicon dihydrido ligand precursor, **3**, with the loss of teeda receiving two equivalents of HCl.[37]

The air and moisture sensitive silane precursor ligands were characterized by mass spectrometry and a range of NMR spectroscopies. For **1**: $^{31}P\{H\}$: δ –13.59, ^{29}Si: HSQC –29.57, Accurate mass (LIFDIMS): 624.2740; **2**: $^{31}P\{^1H\}$: δ –11.48; ^{29}Si: HSQC –30.26; and for **3**: $^{31}P\{H\}$: δ –5.02, ^{29}Si: HSQC, –39.96, Accurate mass (LIFDIMS); 556.3534.

We pursued the synthesis of the free silylene as a possible direct and general route to metal–silylene complexes of these ligands. However, the free silylene of **1** and **2** proved challenging to isolate by reduction of either **1** and **2** using a number of conditions and reducing agents (Na, K, KC_8, etc.) (Scheme 1.3-3). These reducing conditions resulted in a variety of products and intractable mixtures. Dehydrohalogenation with N-heterocyclic carbene (NHC) was also explored as a complimentary means of generating the free silylene of **2** as it has been demonstrated previously as an alternative means to generate free silylene of certain silane containing precursor ligands.[41] Treatment of **2** with NHC was unsuccessful in generating the free silylene of **2** and instead resulted in complicated

mixtures or no reaction depending on the NHC reagent. The free silylene may be inherently unstable as it lacks the kinetic protection of bulky flanking groups which are typically necessary for the isolation of these compounds.[42]

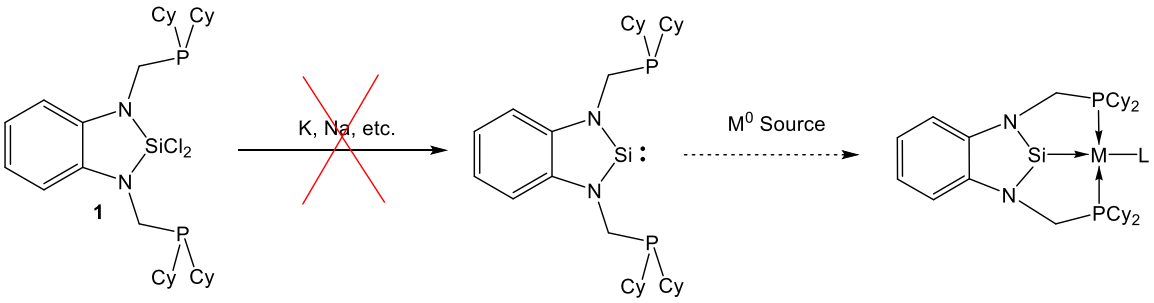

Scheme 1.3-3 Possible synthetic route to access metal–silyl complexes with the $(^{Cy}P)_2Si$ ligand framework. Attempt to access a metal–silylene via this synthetic route with **1** proved difficult and afforded intractable mixtures of products.

We discovered an alternative route to access metal–silyl complexes with the $(^{Cy}P)_2Si$ ligand framework. In spite of failure to initially generate the free silylene, metalation of the silane precursor ligands of **1** and **2** proved successful. This was accomplished via oxidative addition of Si–Cl bond of **1** or base-assisted metalation of **2** as the first step to access various metal–silylene complexes of the group 10 metals, further discussed in Chapter 2 (Scheme 1.3-4). This proved an ideal alternative method to pursue the synthesis of metal–silylene complexes due to the possibility of a two-electron reduction of the metal–silyl to afford potential metal–silylene complexes.

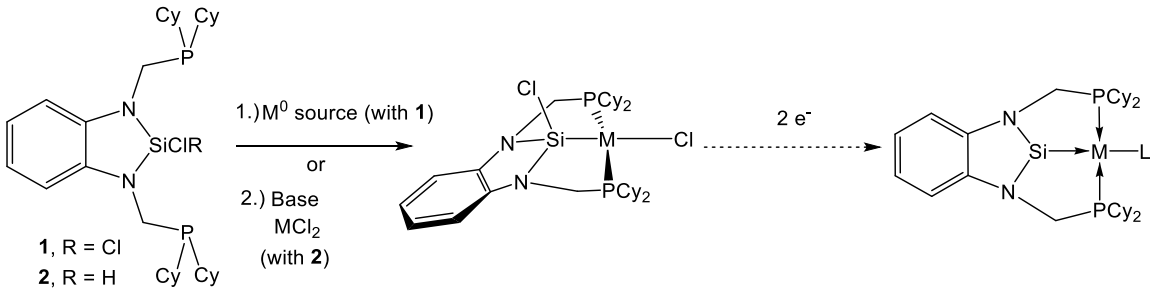

Scheme 1.3-4 Synthetic routes for silane precursor ligands **1** and **2** to form metal–silyl complexes, followed by two electron reduction for the generation of potential metal–silylene complexes.

1.4 Concluding Remarks

The synthesis and characterization of the hydroscopic and air-sensitive silane precursor ligands **1**, **2**, and **3** are reported here with each silane precursor isolated in good yield as a white crystalline solid from concentrated solutions of ether. Given the free silylene complexes of **1**, **2**, and **3** proved difficult to isolate, metalation of the new silane ligand precursors proved successful and is reported in Chapter 2 of this work.

1.5 Ligand Synthesis

1.5.1 Standard Synthetic Methods and Materials

All manipulations were carried out under an atmosphere of N_2 using a GloveBox or standard Schlenk techniques. All dry solvents were passed through a purification solvent system from JC Meyer Solvent Systems followed by storage over 4 Å molecular sieves. Tetrahydrofuran and diethyl ether were dried over sodium metal and benzophenone until ketal test was purple, followed by distillation under an atmosphere of nitrogen and storage over 4 Å molecular sieves. Deuterated solvents were subject to three freeze, pump, thaw cycles for deoxygenation and stored over sieves at least 12 hours prior to use. Dicylcohexylphoshine[43] and (teeda)SiH_2Cl_2[44] were made according to the literature

procedures or at times the dicylcohexylphoshine was purchased from Strem Chemicals Inc. and used without further purification. Tetrachlorosilane and trichlorosilane were purchased and distilled under a nitrogen atmosphere prior to use to ensure HCl was not present. Triethylamine was dried over CaH for twelve hours and distilled under an atmosphere of nitrogen prior to use. Spectroscopic data was collected using a Varian 500, Bruker 400 or 600 MHz instrument. Chemical shifts in ^{1}H NMR are referenced to deuterated solvents. Chemical shifts in ^{31}P NMR are referenced to phosphoric acid and ^{29}Si NMR are referenced to a trimethylvinylsilane standard (TMS). Original ^{29}Si NMR spectra were processed using MestReNova 11.0.4 to eliminate background signal from the borosilicate NMR tube. All spectroscopic data was taken at room temperature unless otherwise noted. X-ray diffraction was performed on a Bruker-AXS diffractometer. Mass spectra were recorded using either an Agilent LCTOF mass spectrometer or a Waters GCT high-resolution mass spectrometer operating in LIFDI mode. Elemental analyses were performed by Midwest Microlab, LLC, Indianapolis, IN.

1.5.2 (1,2-C_6H_4)($NCH_2P(Cy)_2$)$_2SiCl_2$ (**1**)

To a stirred solution of 11.12 g (21.03 mmol) 1-2-bis(phosphinomethylamino)[19] in 60 mL THF, triethylamine, 7.33 mL, (52.57 mmol) was added. To this mixture, 3.00 mL (23.00 mmol) of tetrachlorosilane was added dropwise with stirring. After 12 hours the volatiles were removed in *vacuo*. The resulting residue was dissolved in ether, filtered through Celite and the filtrate pumped down to dryness. Recrystallization from ether gave **1** as a colorless crystalline solid (7.64 g, 58 % yield) after first crop collection. ^{1}H NMR (500 MHz, C_6D_6) δ 7.09 (dd, J = 5.4, 3.6 Hz, 2H, Ar-H), 6.99 (dd, J = 5.7, 3.4 Hz, 2H, Ar-H), 3.52 (s, 4H,

methine C-H), 1.86 (d, *J* = 8.9 Hz, 4H, cyclohexyl C-H), 1.75 (d, *J* = 13.5 Hz, 4H, cyclohexyl C-H), 1.65 (q, *J* = 10.3, 9.1 Hz, 9H, cyclohexyl C-H), 1.59 (m, 4H), 1.21 (m, 18H, cyclohexyl C-H). $^{31}P\{^{1}H\}$ NMR (202 MHz, C_6D_6) δ -13.59. ^{29}Si HSQC (60 MHz, C_6D_6) δ -29.57, ^{1}H NMR (300 MHz, C_6D_6) δ 3.54. ^{13}C NMR (126 MHz, C_6D_6) δ 137.87 (Ar-C), 118.95 (Ar-C), 109.65 (Ar-C), 38.20 (methane-C), 29.40 (cyclohexyl-C), 27.12 (cyclohexyl-C), 26.36 (cyclohexyl-C). Calculated Mass for Compound with Molecular Formula $C_{32}H_{54}N_2SiP_2$: 624.2752. Measured Mass for Compound with Molecular Formula $C_{32}H_{54}N_2SiP_2$: 624.2740. Elemental Analysis Predicted for $C_{32}H_{54}N_2SiP_2$: C, 61.43; H, 8.38; N, 4.48. Elemental Analysis Measured for $C_{32}H_{54}N_2SiP_2$: C, 61.13, 8.29, N, 4.36

1.5.3 (1,2-C_6H_4)($NCH_2P(Cy)_2$)$_2$SiHCl (**2**)

To a stirred solution of 2.077 g (3.93 mmol) of 1,2-bis(phosphinomethylamino)[19] in 60 mL THF, triethylamine, 1.16 mL, (8.25 mmol) was added. To this mixture, 0.44 mL (4.32 mmol) of trichlorosilane was added dropwise with stirring. After 12 hours the volatiles were removed in *vacuo*. The resulting residue was dissolved in ether under inert atmosphere, filtered through Celite and the filtrate pumped down to dryness. Recrystallization from ether at –35 °C overnight gave **2** as a colorless crystalline solid (1.267 g, 55 % yield) after second crop collection. ^{1}H NMR (300 MHz, Benzene-d_6) δ 7.26 (t, *J* = 8.8 Hz, 1H), 7.04 (dd, *J* = 5.7, 3.3 Hz, 2H), 6.91 (dd, *J* = 5.7, 3.4 Hz, 2H), 3.45 (d, *J* = 13.5, 6.6 Hz, 4H), 1.86 (d, *J* = 12.4 Hz, 2H), 1.75 (d, *J* = 11.3 Hz, 2H), 1.70 – 1.48 (m, 20H), 1.39 – 1.16 (m, 10H), 1.16 – 0.98 (m, 10H). $^{31}P\{^{1}H\}$ NMR (121 MHz, C_6D_6) δ -11.48. ^{29}Si HSQC (60 MHz, C_6D_6) δ -30.26.

1.5.4 (1,2-C_6H_4)($NCH_2P(Cy)_2$)$_2SiH_2$ (**3**)

Complex **3** was prepared in an analogous fashion, with a slightly modified procedure, to a previously reported silane precursor ligand.[37] To a stirring solution of 1,2-bis(phosphinomethylamino)[19] in 15 mL benzene, (teeda)SiH_2Cl_2, (0.8544 g, 3.126 mmol) in a slurry of benzene, was slowly added over the course of a few minutes. Yield after recrystallization from ether gave **3** as colorless solid in 80 % yield after first crop collection. ^{1}H NMR (500 MHz, Benzene-d_6) δ 7.04 (dd, J = 5.5, 3.3 Hz, 2H), 6.73 (dd, J = 5.5, 3.3 Hz, 2H), 6.62 (t, J = 6.9 Hz, 2H), 3.28 (s, 4H), 1.77 (d, J = 11.7 Hz, 5H), 1.70 (d, J = 14.5 Hz, 3H), 1.66 – 1.60 (m, 8H), 1.59 – 1.53 (m, 8H), 1.30 – 1.14 (m, 8H), 1.13 – 1.03 (m, 8H). ^{31}P{^{1}H} NMR ^{31}P NMR (202 MHz, C_6D_6) δ -5.02. ^{29}Si HSQC (119 MHz, C_6D_6) δ -36.96 ^{13}C NMR (126 MHz, C_6D_6) δ 142.44, 118.33, 107.77, 38.70, 33.25, 29.97, 28.86, 27.42, 27.33, 26.69. Calculated Mass for compound with molecular formula $C_{32}H_{54}N_2SiP_2$: 556.3526. Measured Mass in LIFDI mode for compound with molecular formula $C_{32}H_{54}N_2SiP_2$ [M^+]: 556.3534.

1.6 References

(1) Stephan, D. W.; Erker, G. *Angewandte Chemie - International Edition* **2010**, *49* (1), 46–76.

(2) Prey, S. E.; Bolte, M.; Lerner, H.-W.; Wagner, M.; von Grotthuss, E. *Angewandte Chemie International Edition* **2018**, *57* (50), 16491–16495.

(3) Bolte, M.; Holthausen, M. C.; Lerner, H.-W.; Diefenbach, M.; von Grotthuss, E.; Wagner, M. *Angewandte Chemie International Edition* **2016**, *55* (45), 14067–14071.

(4) Taylor, J. W.; McSkimming, A.; Guzman, C. F.; Hill Harman, W. *J. Am. Chem. Soc* **2017**, *139*, 52.

(5) Iwamoto, T.; Ishida, S. *Organosilicon Compounds: Theory and Experiment (Synthesis)* **2017**, 361–532.

(6) Denk, M.; Lennon, R.; Hayashi, R.; West, R.; Belyakov, A. V.; Verne, H. P.; Haaland, A.; Wagner, M.; Metzler, N. *Journal of the American Chemical Society* **1994**, *116* (6), 2691–2692.

(7) Fürstner, A.; Krause, H.; Lehmann, C. W. *Chemical Communications* **2001**, *1* (22), 2372–2373.

(8) Asay, M.; Jones, C.; Driess, M. *Chemical Reviews* **2011**, *111* (2), 354–396.

(9) Blom, B.; Gallego, D.; Driess, M. *Inorganic Chemistry Frontiers* **2014**, *1* (2), 134.

(10) Hill, N. J.; West, R. *Journal of Organometallic Chemistry* **2004**, *689* (24 SPEC. ISS.), 4165–4183.

(11) Raoufmoghaddam, S.; Zhou, Y.-P.; Wang, Y.; Driess, M. *Journal of Organometallic Chemistry* **2017**, *829*, 2–10.

(12) West, R.; Denk, M.; Jutzi, P.; Möhrke, A.; Straus, D. A.; Grumbine, S. D.; Tilley, T. D.; Grumbine, S. K.; Arnold, F. P.; Rheingold, A. L. *J. Chem. Soc., Chem. Commun* **1994**, *68* (2), 5599–5601.

(13) Gehrhus, B.; Hitchcock, P. B.; Lappert, M. F.; Maciejewski, H. *Organometallics* **2002**, *17* (26), 5599–5601.

(14) Denk, M.; Hayashi, R. K.; West, R. *J. Chem. Soc., Chem. Commun.* **1994**, 33–34.

(15) Gehrhus, B.; Lappert, M. F.; Heinicke, J.; Boese, R.; Bläser, D.; Denk, M.; Lennon, R.; Hayashi, R.; West, R.; Belyakov, A. V.; et al. *J. Chem. Soc., Chem. Commun.* **1995**, *116* (19), 1931–1932.

(16) Yoo, H.; Carroll, P. J.; Berry, D. H. *Journal of the American Chemical Society* **2006**, *128* (18), 6038–6039.

(17) Whited, M. T.; Deetz, A. M.; Boerma, J. W.; Derosha, D. E.; Janzen, D. E. *Organometallics* **2014**, *33*, 5073.

(18) Dixon, L. S. H.; Hill, A. F.; Sinha, A.; Ward, J. S. *Organometallics* **2014**, *33* (3), 653–658.

(19) Segawa, Y.; Yamashita, M.; Nozaki, K. *Organometallics* **2009**, *28*, 6234–6242.

(20) Lin, T.-P.; Peters, J. C. *Journal of the American Chemical Society* **2013**, *135* (41), 15310–15313.

(21) Dixon, L. S. H.; Hill, A. F.; Sinha, A.; Ward, J. S. *Organometallics* **2014**, *33* (3), 653–658.

(22) Soleilhavoup, M.; Bertrand, G. *Accounts of Chemical Research* **2015**, *48* (2), 256–266.

(23) Boehme, C.; Frenking, G. *Journal of the American Chemical Society* **1996**, *118* (8), 2039–2046.

(24) Vougioukalakis, G. C.; Grubbs, R. H. *Chemical Reviews* **2010**, *110* (3), 1746–1787.

(25) Shaw, B. L.; Uttley, M. F. *JCS Dalton Chem. Comtn.* **1975**, *918* (3), 1890.

(26) Sircoglou, M.; Bontemps, S.; Mercy, M.; Saffon, N.; Takahashi, M.; Bouhadir, G.; Maron, L.; Bourissou, D. *Angewandte Chemie - International Edition* **2007**, *46* (45), 8583–8586.

(27) Dahlhoff, W. V; Nelson, S. M.; Kelly, S. J.; Ford, G. H. *J. Chem. Soc (A)* **1971**, 388.

(28) Zhang, J.; Gandelman, M.; Shimon, L. J. W.; Rozenberg, H.; Milstein, D. *Organometallics* **2004**, *23* (17), 4026–4033.

(29) Fogler, E.; Iron, M. A.; Zhang, J.; Ben-David, Y.; Diskin-Posner, Y.; Leitus, G.; Shimon, L. J. W.; Milstein, D. *Inorganic Chemistry* **2013**, *52* (19), 11469–11479.

(30) MacInnis, M. C.; Maclean, D. F.; Lundgren, R. J.; Mcdonald, R.; Turculet, L. *Organometallics* **2007**, *26* (26), 6522–6525.

(31) MacLean, D. F.; McDonald, R.; Ferguson, M. J.; Caddell, A. J.; Turculet, L. *Chemical Communications* **2008**, No. 41, 5146–5148.

(32) Morgan, E.; MacLean, D. F.; McDonald, R.; Turculet, L. *Journal of the American Chemical Society* **2009**, *131* (40), 14234–14236.

(33) Mitton, S. J.; Mcdonald, R.; Turculet, L. *Organometallics* **2009**, *28*, 5122–5136.

(34) Korshin, E. E.; Leitus, G.; Shimon, L. J. W.; Konstantinovski, L.; Milstein, D. *Inorganic Chemistry* **2008**, *47* (16), 7177–7189.

(35) Takaya, J.; Iwasawa, N. *Organometallics* **2009**, *28* (23), 6636–6638.

(36) Takaya, J.; Iwasawa, N. *Journal of the American Chemical Society* **2008**, *130* (46), 15254–15255.

(37) Whited, M. T.; Deetz, A. M.; Boerma, J. W.; Derosha, D. E.; Janzen, D. E. *Organometallics* **2014**, *33* (19), 5070–5073.

(38) Lin, T. P.; Peters, J. C. *Journal of the American Chemical Society* **2013**, *135* (41), 15310–15313.

(39) Murphy, L. J.; Hollenhorst, H.; McDonald, R.; Ferguson, M.; Lumsden, M. D.; Turculet, L. *Organometallics* **2017**, *36* (19), 3709–3720.

(40) Whited, M. T.; Grubbs, R. H. *Accounts of Chemical Research* **2009**, *42* (10), 1607–1616.

(41) Cui, H.; Shao, Y.; Li, X.; Kong, L.; Cui, C. *Organometallics* **2009**, *28*, 5191.

(42) Hopkinson, M. N.; Richter, C.; Schedler, M.; Glorius, F. *Nature Chemistry* **2014**, *510* (7506), 485–496.

(43) Busacca, C. A.; Lorenz, J. C.; Grinberg, N.; Haddad, N.; Hrapchak, M.; Latli, B.; Lee, H.; Sabila, P.; Saha, A.; Sarvestani, M.; et al. *Organic Letters* **2005**, *7* (19), 4277–4280.

(44) Kloos, S. D.; Boudjouk, P. *Inorganic Syntheses*; Darensbourg, M., Y., E., Eds.; Wiley: New York, **1998**; Vol. 32.

1.7 Spectroscopic Data and Figures

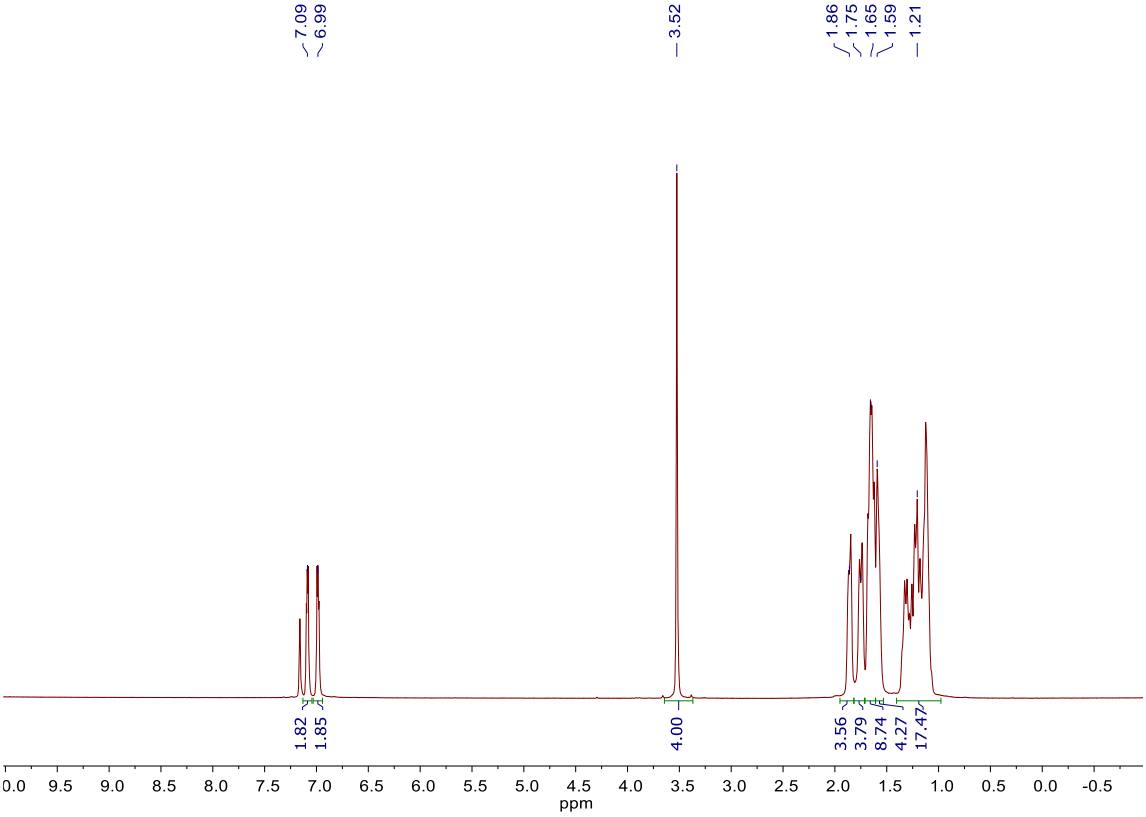

Figure 1.7-1 ^{1}H NMR of **1** in C_6D_6 at 500 MHz.

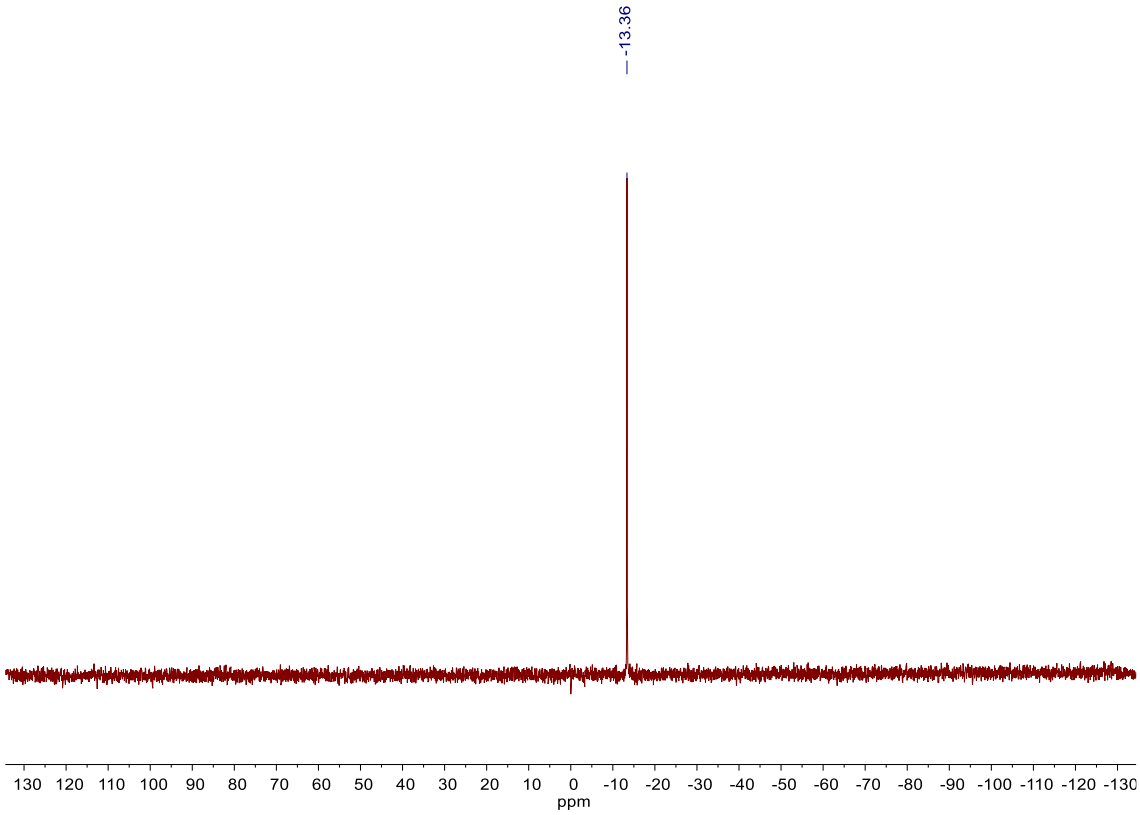

Figure 1.7-2 $^{31}P\{^{1}H\}$ NMR of **1** in C_6D_6 at 202 MHz.

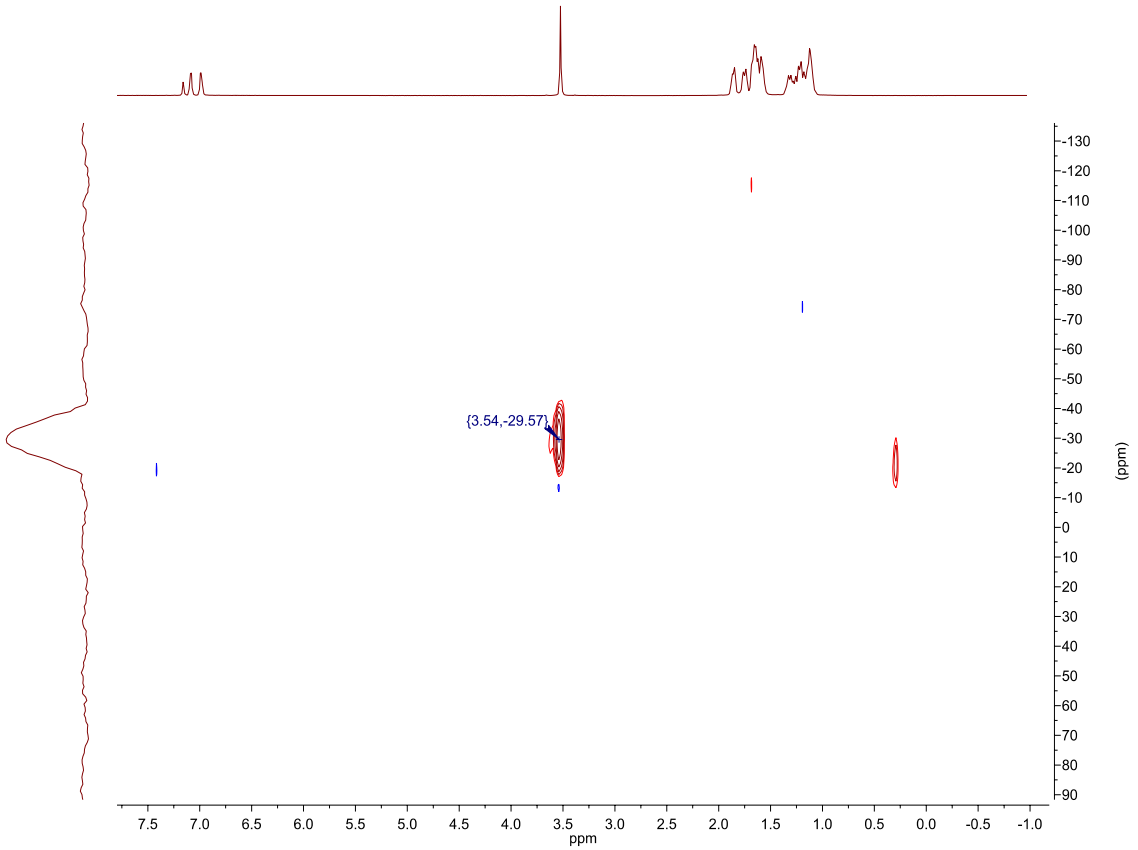

Figure 1.7-3 ^{29}Si HSQC of **1** in C_6D_6 at 60 MHz.

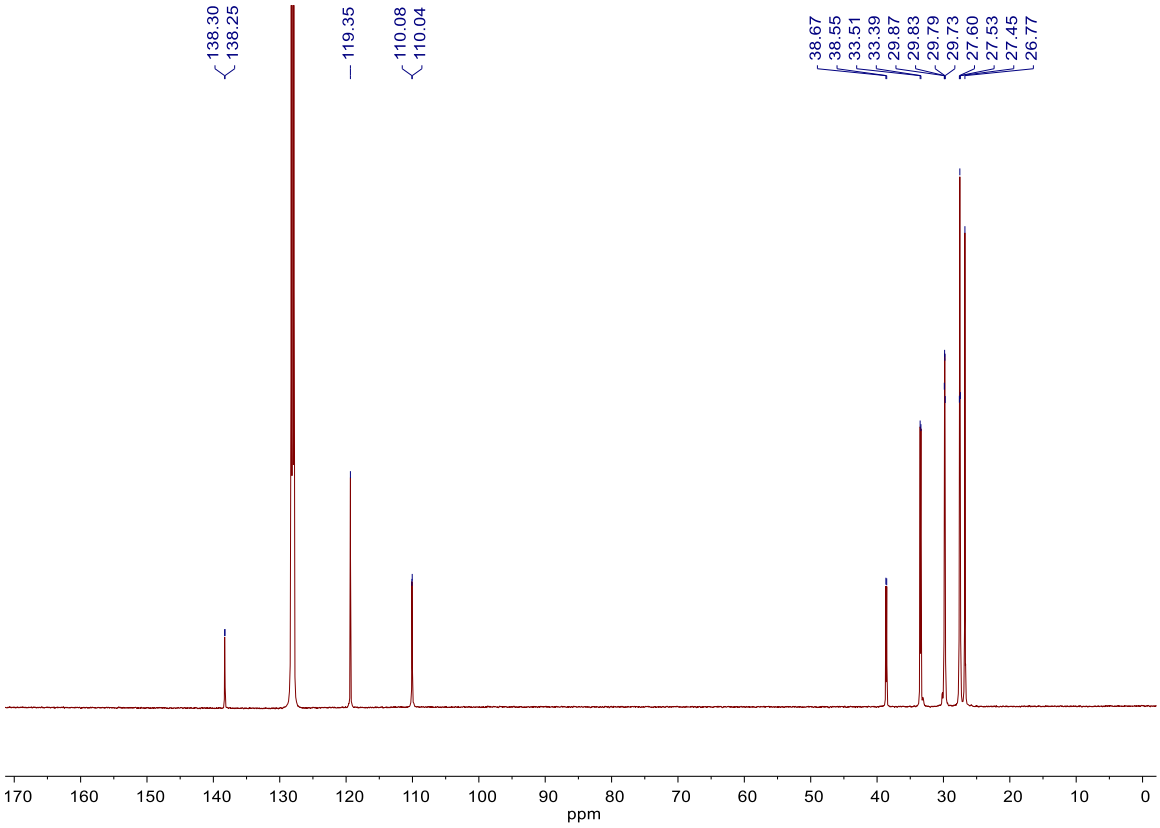

Figure 1.7-4 ^{13}C NMR of **1** in C_6D_6 at 126 MHz.

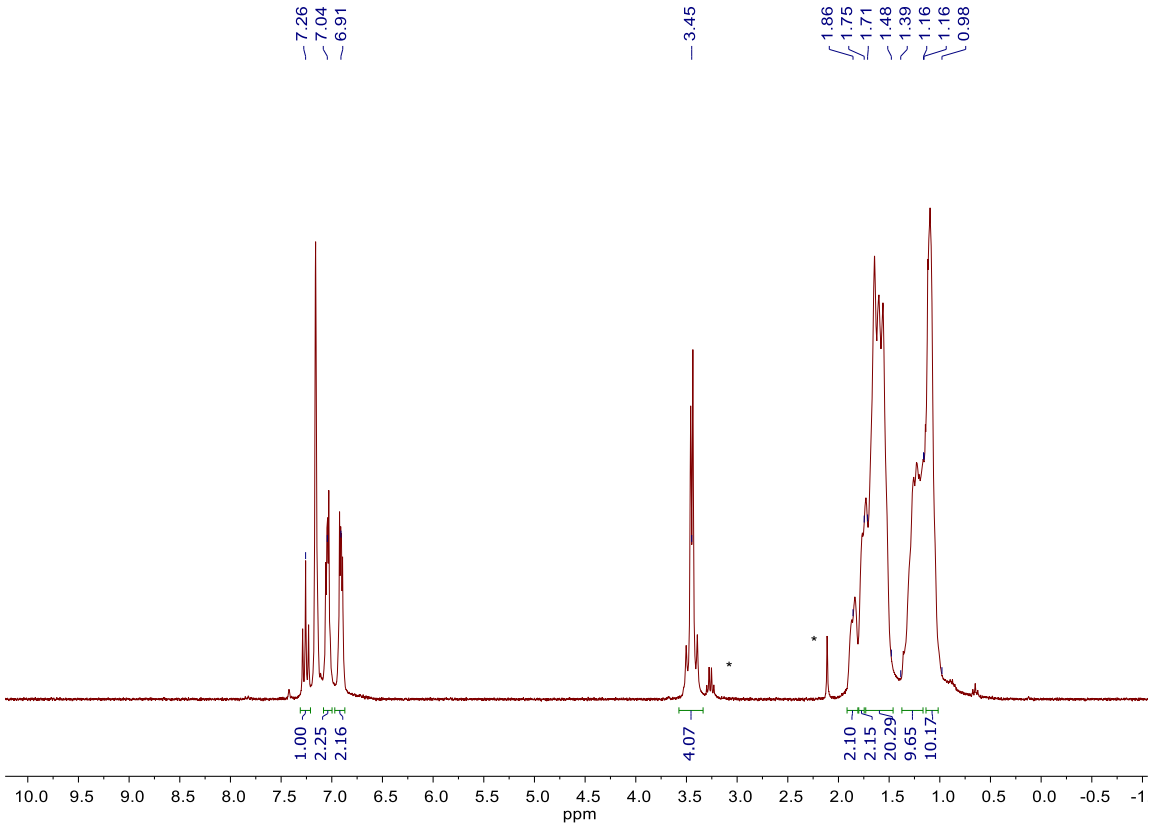

Figure 1.7-5 ^{1}H NMR of **2** in C_6D_6 at 300 MHz.

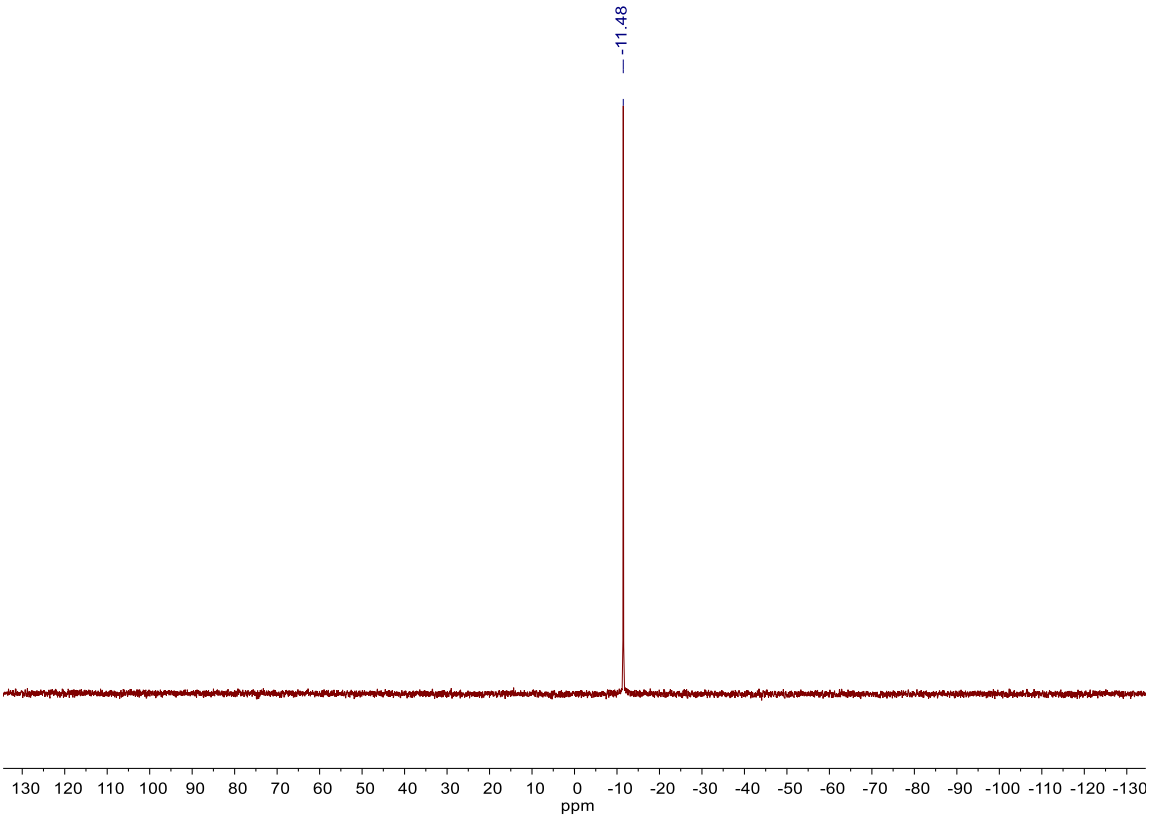

Figure 1.7-6 $^{31}P\{^{1}H\}$ NMR of **2** in C_6D_6 at 121 MHz.

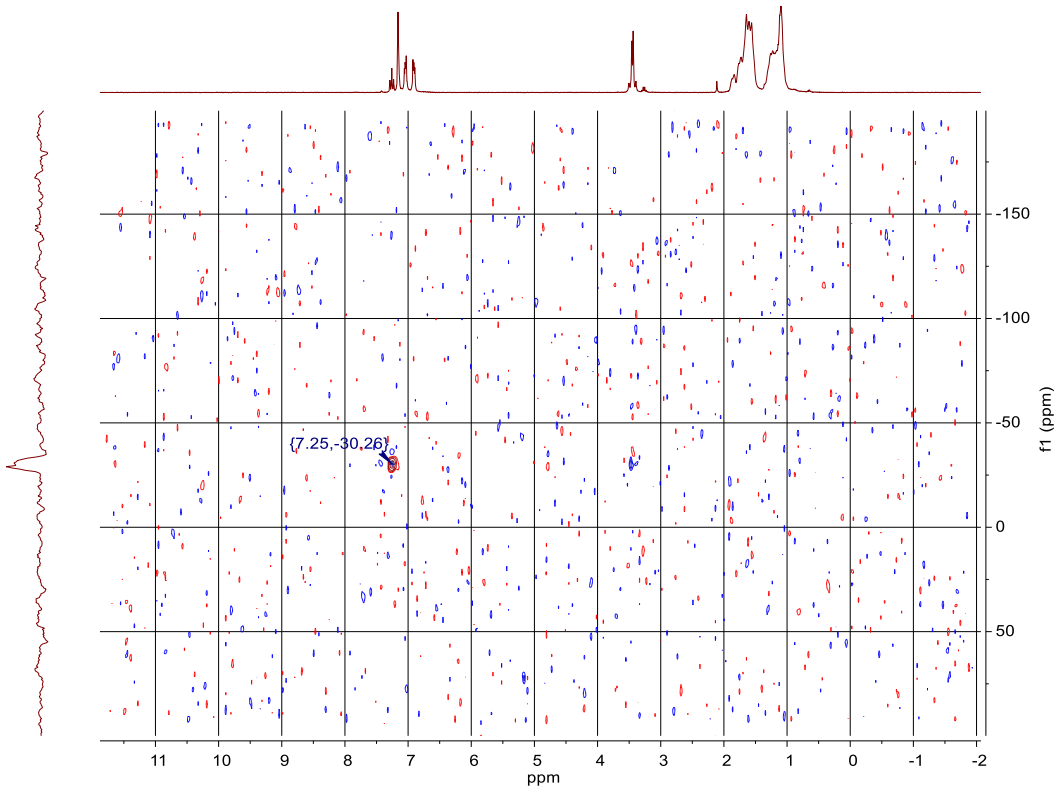

Figure 1.7-7 ^{29}Si HSQC of **2** in C_6D_6 at 60 MHz.

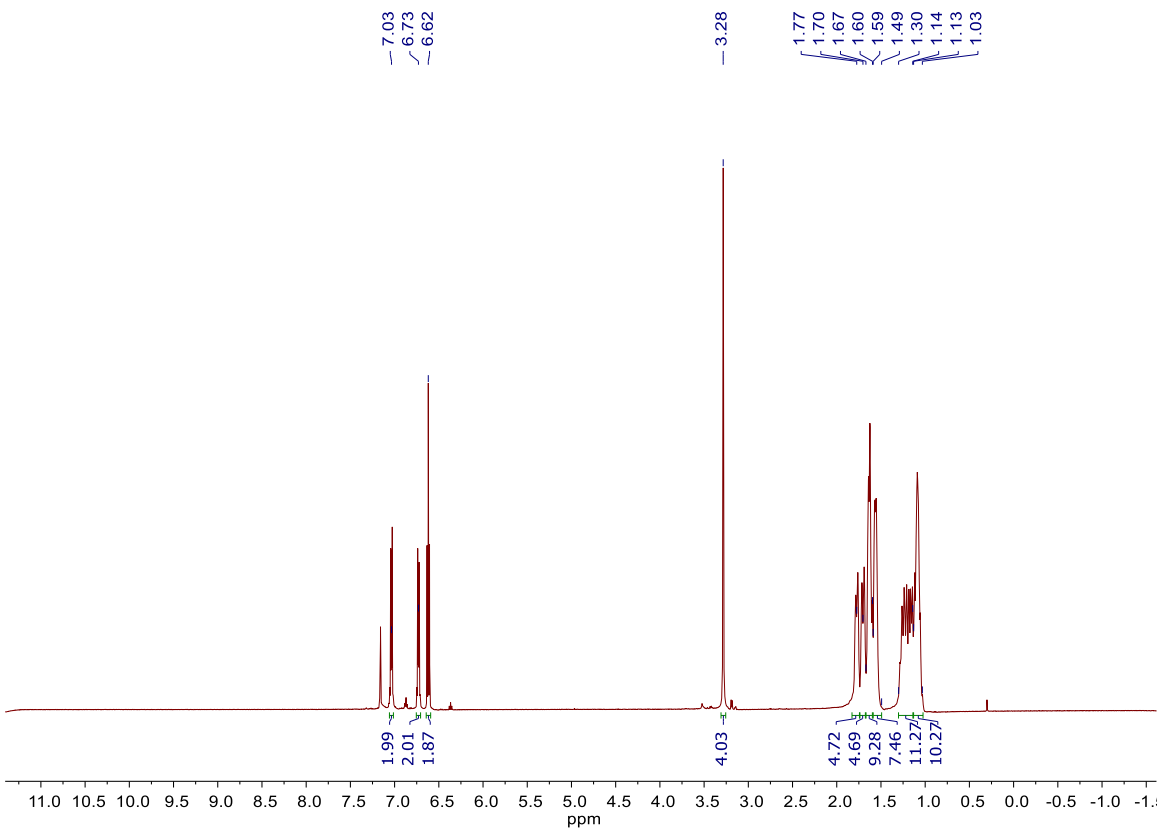

Figure 1.7-8 ^{1}H NMR **3** in C_6D_6 at 500 MHz.

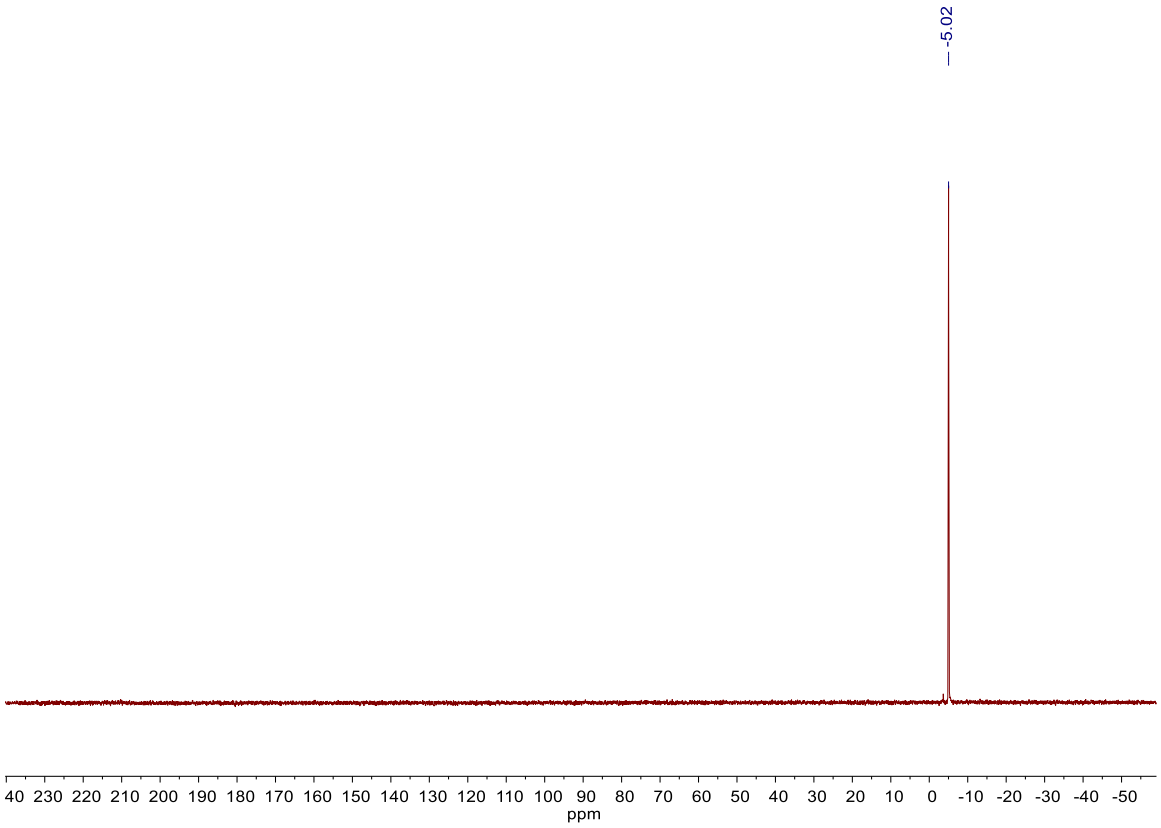

Figure 1.7-9 $^{31}P\{^{1}H\}$ of **3** in C_6D_6 at 202 MHz.

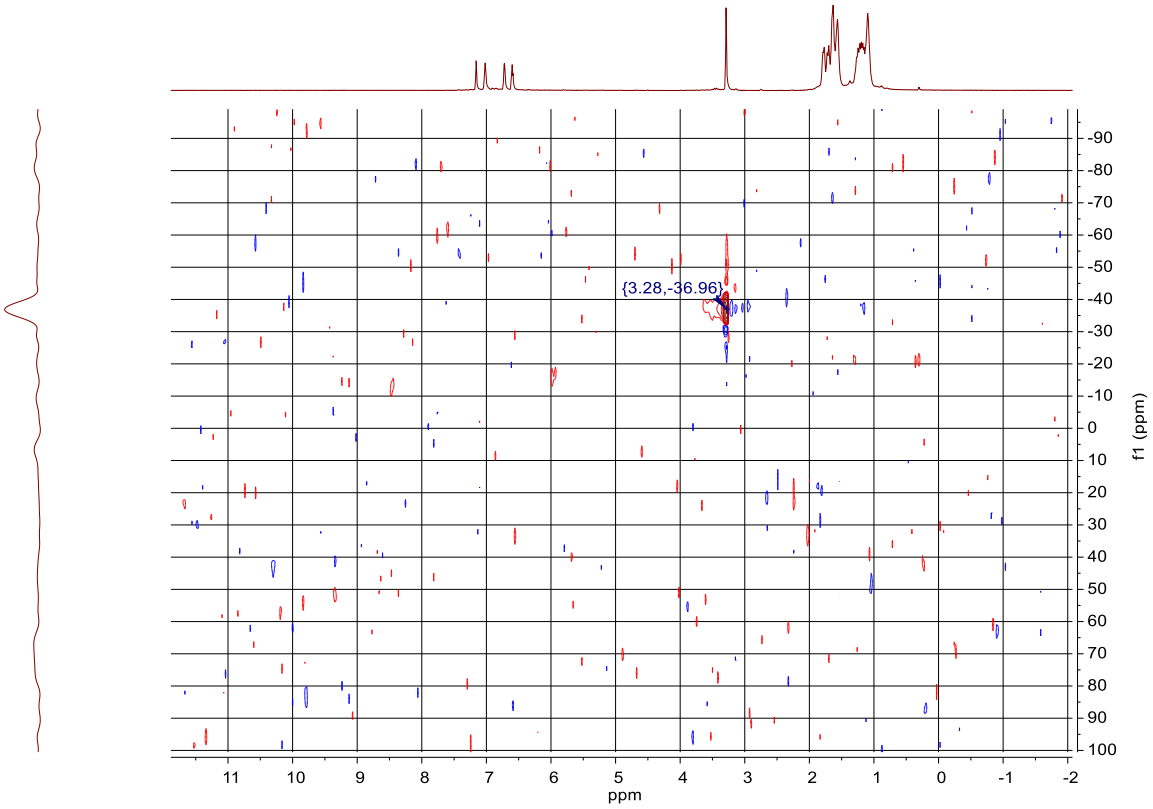

Figure 1.7-10 ^{29}Si HSQC of **3** in C_6D_6 at 119 MHz.

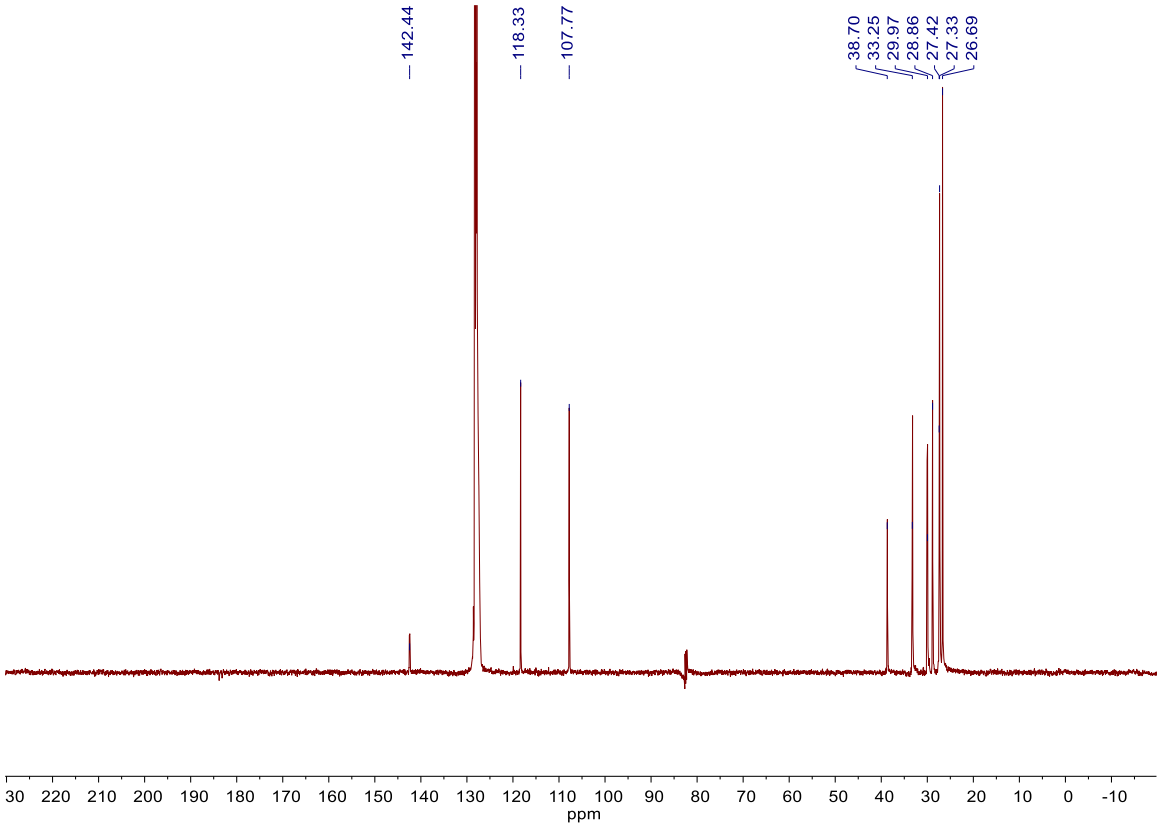

Figure 1.7-11 ^{13}C NMR of **3** in C_6D_6 at 126 MHz.

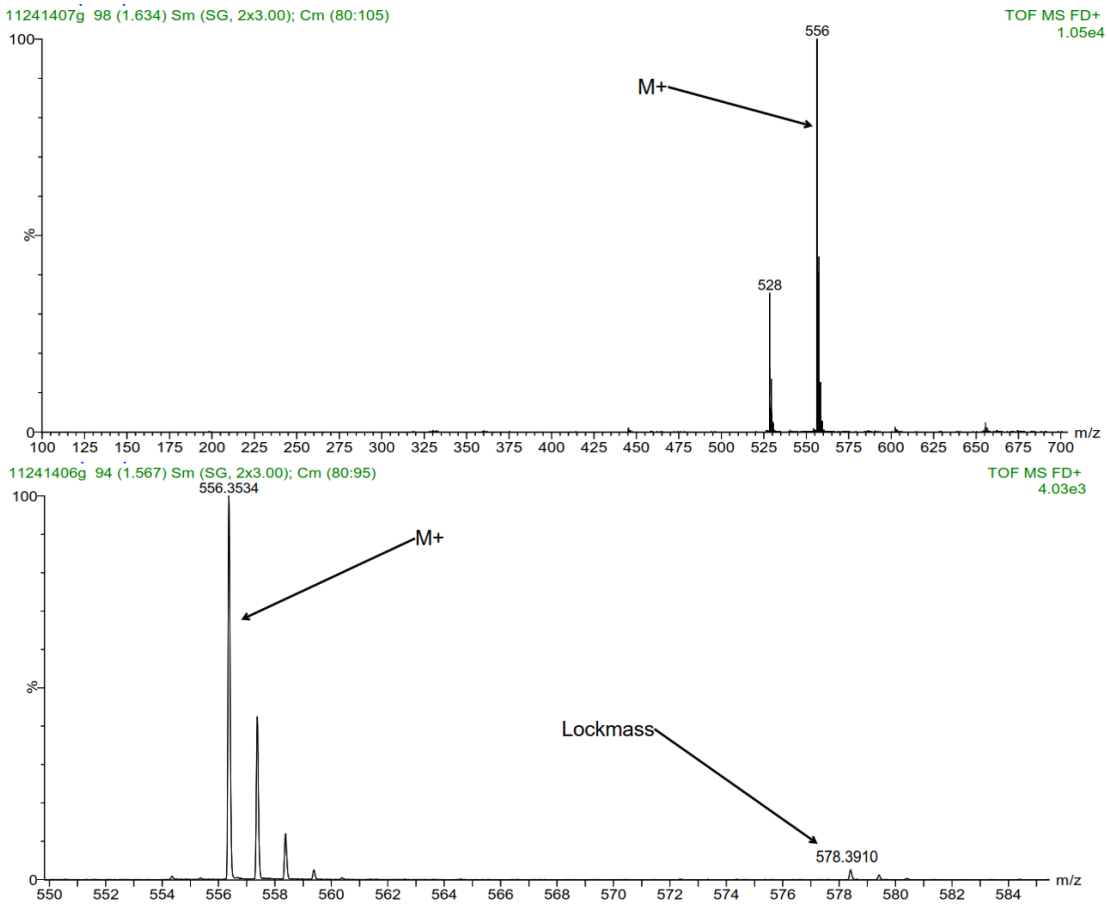

Figure 1.7-12. Mass spectrometry operating in LIFDI mode for **3.**

CHAPTER 2 Metalation of Silane Pincer Precursor Ligands

2.1 Abstract

The synthesis and characterization of three new group 10 TM–silyl complexes featuring $(^{Cy}P)_2Si$ ligand framework; $(1,2\text{-}C_6H_4)(NCH_2P(Cy)_2)_2SiNiCl_2$, $(1,2\text{-}C_6H_4)(NCH_2P(Cy)_2)_2SiPdCl_2$ and $(1,2\text{-}C_6H_4)(NCH_2P(Cy)_2)_2SiPtCl_2$ are reported here with the aim of using these complexes as precursors to gain access to TM–silylene complexes under reducing conditions. The Ni, Pd and Pt–silyl complexes can be accessed one of two ways from silane precursor ligands, **1** and **2** (Chapter 1). Each TM–silyl has been fully characterized spectroscopically and by mass spectrometry. Metalation using cobalt and the silane precursor ligand **1** with $Co_2(CO)_8$ proved successful for the synthesis of a dicobalt(I)carbonyl silylene and is also reported here.

2.2 Introduction

Various PSiP ligand frameworks have been shown to successfully form metal–silyl complexes featuring a wide range of metal centers including nickel, iron and cobalt with work using silicon based analogues attributed to the laboratories of Hill and Whited.[1,2] In addition, many laboratories have established metal centers installed within a PSiP framework using metals from groups 6–10 on the periodic table. Metal-silyl complexes make appealing precursors because of the potential for reductant addition to potentially form silylene metal complexes. The work of Xiong and coworkers have gone on to demonstrate a cobalt PSiP complex to participate in Kumada coupling reactions.[2] Electing to use a PSiP pincer ligand framework Whited and coworkers have demonstrated the

synthesis of a cationic ruthenium (II) silylene.[3] It was the work of Turculet, Iwasawa and Milstein groups who initially explored the chemistry of silicon as a central silyl donor within a PSiP framework.[4–6] In 2014 Ward and Dixon, making use of a PSiP framework, demonstrated the first NHSi installed as the central donor.[7] It is noted that protocols for silyl formation followed by metalation are attributed to the work of Berry, Ward, Dixon and Hill.[7–9]

Recently in 2018 Ozerov and Whited demonstrated the synthesis of a PSiP-cobalt metal-silyl complex which after hydride abstraction from silicon using trityl tetrakis-(pentafluorophenyl)borate ($[Ph_3C][BArF_{20}]$) affords the first reported cationic base free cobalt–silylene.[10] Silylene complexes featuring cobalt are relatively rare and as such are actively pursued for TM-silylene formation given cobalt is an inexpensive non-noble metal. Representative and noteworthy metal-silyl and silylene complexes are depicted in Figure 2.2-1.

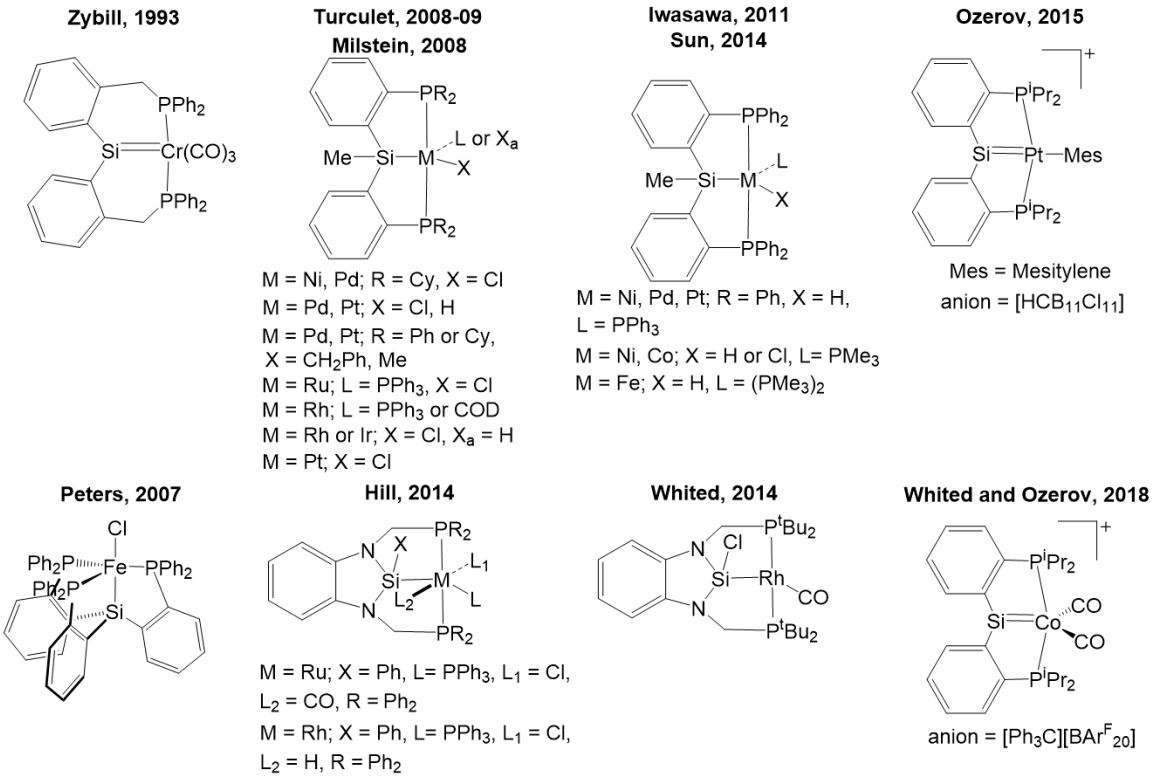

Figure 2.2-1 Representative metal–silyl and silylene complexes within PSiP framework.

Metal–silyl complexes make appealing precursors because one can imagine addition of reductant may afford the targeted metal silylene complexes. The work reported here describes the synthesis of the group 10 Ni, Pd, and Pt metal–silyls within a $(^{cy}P)_2Si$ ligand framework. Additionally, reported in the latter part of this chapter is the synthesis of a bimetallic cobalt (I) carbonyl silylene.

2.3 Results and Discussion

2.3.1 Nickel, $(1,2\text{-}C_6H_4)(NCH_2P(Cy)_2)_2SiNiCl_2$ (**4**)

Treatment of $Ni(COD)_2$ or $Ni(PPh_3)_4$ in THF to a suspension of NN-dichlorosilane ligand precursor **1** results in the oxidative addition of a Si–Cl bond to give $(1,2\text{-}C_6H_4)(NCH_2P(Cy)_2)_2SiNiCl_2$, **4**, as an air sensitive orange precipitate in good yield (73 %)

with an exact mass by LIFDIMS of 682.2089. The nickel (II) silyl, **4**, can alternatively be synthesized from the hydrochlorosilane ligand precursor **2** in a metal-chelated base-assisted route in the presence of excess triethylamine and $NiCl_2$. These routes, including a third, to obtain the diamagnetic Ni–silyl complex **4** are shown in Scheme 2.3-1.

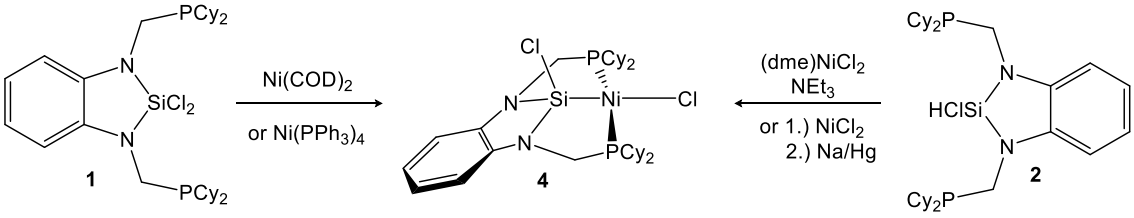

Scheme 2.3-1. Synthesis of Ni(II)–silyl **4** through oxidative addition of Ni(0) source into Si–Cl bond of **1** (from left to right) or metal chelated base assisted metalation with $NiCl_2$ from **2** and/or metal-ligand chelation with **2** using $NiCl_2$ followed by in-situ reduction (from left to right).

The ^{31}P NMR of **4** has a single resonance at room temperature at δ 67.93 ppm that is significantly downfield from the precursor ligands **1** and **2** (δ –13.36 and δ –11.48, respectively), and is consistent with metal binding. The $^{29}Si\{^{1}H\}$ NMR of **4** features a triplet resonance at δ 62.08 ppm with silicon–phosphorous coupling of 53.2 Hz. Variable temperature NMR experiments revealed the bridging methylene protons are diastereotopic at a low temperature of –60 °C, while at room temperature they appear as a resolved single resonance at a δ 3.3 ppm (refer to section 2.7). The molecular structure of **4** was confirmed by single crystal X-ray diffraction. The solid-state structure of **4** features a distorted square planar nickel center bound to a distorted tetrahedral silicon. The solid-state structure of **4** also has a Ni–Si bond length of 2.1468(5) Å. These solid-state features and spectroscopic data are consistent with those previously reported for nickel in PSiP chelating ligand framework to form Ni–silyl complexes.[1,11]

2.3.2 Palladium, (1,2-C_6H_4)($NCH_2P(Cy)_2$)$_2$$SiPdCl_2$ (**5**)

Using the same general synthetic route to synthesize **4**, palladium can also be installed into the silane precursor ligands **1** and **2**. Addition of one equivalent of palladium (0) tetrakistriphenylphosphine to a solution of **1** in THF results in the oxidative addition of the Si–Cl bond to from the Pd(II)silyl, **5**. After stirring for one hour, a single peak is observed in the $^{31}P\{^1H\}$ NMR shifted significantly downfield from the silane precursor ligand **1**. Removal of THF to obtain a concentrated solution, followed by addition of ether, results in the precipitation of **5** as a pale-yellow solid in 60 % yield after collection. Several washings with ether are necessary to remove the four equivalents of free triphenylphosphine generated in the reaction. Further recrystallization from DCM/ether slow diffusion can also be done to obtain spectroscopically pure **5** in 40% yield. An alternative route to obtain **5** includes addition of $PdCl_2$ to silane precursor **2** in THF via metal chelation in the presence of triethylamine. These synthetic routes to access **5** from **1** and **2** are outlined in Scheme 2.3-2.

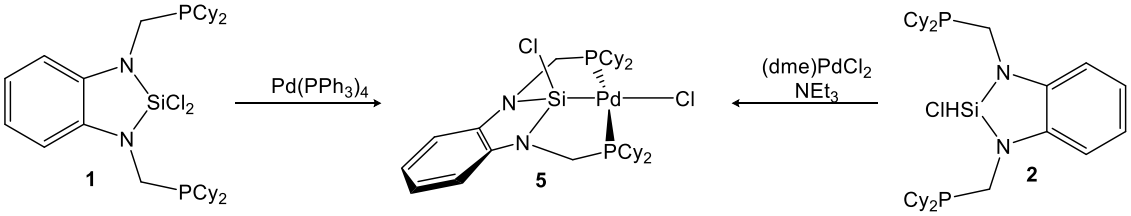

Scheme 2.3-2. Synthetic routes to access Pd(II)–silyl, **5**, via oxidative addition of Pd(0) into Si–Cl bond of **1** (left to right) or a base-assisted metal chelation route from **2** using $PdCl_2$ (right to left).

Inspection of the ^1H NMR of both **4** and **5** reveals an interesting difference in the methylene proton splitting patterns for each complex. In the ^1H NMR for the Pd–silyl complex, **5**, the

methylene protons appear as doublet of triplets coupling pattern at room temperature. This is in contrast to the methylene protons of **4** which appear as a broad singlet in the ^{1}H NMR at the same temperature. This may be a result of the PMP angles, potentially increasing the up-down orientation of the individual protons within the methylene groups to reveal more pronounced coupling as the PMP angle increases down the Group 10 triad. For example, examination of the solid-state structure of **4** reveals a PMP bond angle of 152.41(2) versus that of **5** which is 154.60(2). This observation has been noted in a previously reported study of Group 10 metal complexes within a SCS ligand framework by Gebbink and van Koten.[12]

The ^{31}P{^{1}H} NMR of **5** displays a single resonance at δ 74.30 ppm. Additionally, the ^{29}Si{^{1}H} NMR displays a single resonance at a shift of δ 63.73 ppm with no evident phosphorous–silicon coupling as seen in the ^{29}Si{^{1}H} NMR for **4**, which exhibits a triplet. The molecular structure of **5** was confirmed by single crystal X-ray diffraction, a crystal of which was grown by my lab co-worker Marissa Barrientos, and is displayed in thermal ellipsoid representation at 50% probability in section 2.7 of this work. The solid-state structure of **5** features a distorted square planar palladium center bound to a distorted tetrahedral silicon similar to the geometry coordination revealed in the solid-state structure of **4**. The Si–Pd bond distance of **5** featured within the XRD is 2.2236(5) Å which is similar in distance but slightly longer than that of **4** (Si–Ni, 2.1468(5) Å).

2.3.3 Platinum, (1,2-C_6H_4)($NCH_2P(Cy)_2$)$_2$$SiPtCl_2$ (**6**)

As with the nickel and palladium analogues in the group 10 metal-silyl series, the platinum-silyl can be synthesized using similar synthetic routes. When one equivalent of

ethylenebis(triphenylphosphine)platinum(0) is added to **1** in a solution of minimum THF, **6** is formed as the result of Pt(0) oxidative addition into the Si–Cl bond of the precursor ligand **1**. Alternatively, **6** can be accessed using $PtCl_2$ in a metal-chelated base-assisted route from silane ligand precursor **2** (Scheme 2.3-3).

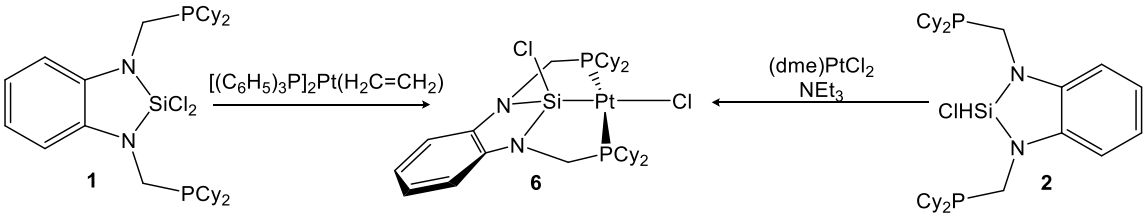

Scheme 2.3-3. Synthetic routes to access **6** via oxidative additive of Pt(0) into Si–Cl bond of **1** (from left to right) and base assisted metal-chelation from **2** in the presence of triethylamine (right to left).

As mentioned previously in discussion of the **4** and **5**, is the differences in the ^{1}H NMR with descension of the Group 10 metal-silyl complexes. A comparison of the ^{1}H NMR of complexes **4**, **5** and **6** can be seen in Section 2.7. Noteworthy are the splitting patterns of the methylene protons within each ^{1}H NMR of the group 10 metal-silyl complexes which may be attributed to the increasing PMP bond angles revealed in the solid-state structures down the group 10 triad.

2.3.4 Cobalt, $SiCo_2P_2(CO)_5$ (**7**)

The attempt to make the low valent monometallic Co–CO complex resulted instead in the novel bimetallic Co(I)Silylene, **7**. (Scheme 2.3-4). The bimetallic cobalt(I) silylene can be synthesized upon treatment of 1.1 equivalents of dicobalt octacarbonyl to dichlorosilane ligand precursor **1** in a solution of THF at which time an immediate color change to deep crimson red is observed. Heating at +60 °C for 24 hours results in a color change from deep

red to an emerald green solution, after which time the ^{31}P NMR indicates the reaction is complete. Removal of THF, extraction with hexane followed by filtration through a pad of Celite, and subsequent concentration of hexane yields **7** in 70 % yield as a fine yellow powder.

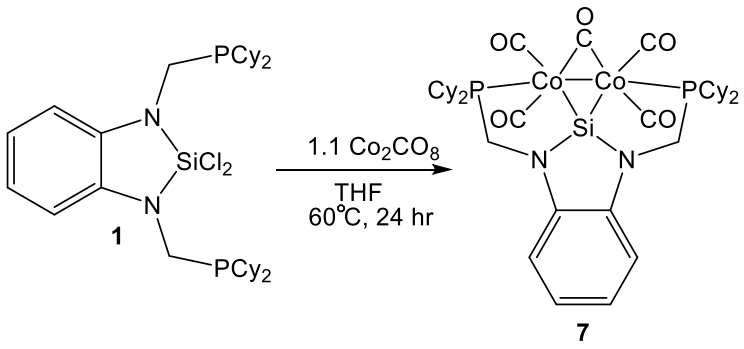

Scheme 2.3-4 Synthesis of **7** upon addition of $Co_2(CO)_8$ to **1**.

The solid-state structure of **7** features a Co–Co bond with a distance of 2.613 Å (cf. Co_2CO_8, $d_{Co–Co}$= 2.700 Å)[13] which is consistent with the distance for a Co–Co bond as indicted by a Cambridge Structure Database (CSD) search. The average cobalt metal bond length according to CSD is 2.539 Å. The solid-state structure indicates the presence of one silylene ligand bridging the two cobalt centers. In 1993 the Nicholson laboratory demonstrated the preparation and structure of silicon–cobalt carbonyl clusters.[14] These silicon–cobalt clusters offer an interesting comparison to **7** as some feature a singly bridging silicon across two cobalt centers. However, in contrast to previously reported silicon-cobalt clusters **7** features a single N-heterocyclic silylene ligand, which a literature search indicates as relatively rare.

Complex **7** features a broad resonance at room temperature in the ^{31}P NMR at δ 93 ppm. Additionally, at room temperature the four methylene protons feature broad resonances in the ^{1}H NMR (See section 2.7). The asymmetry observed in the solid-state structure is consistent with variable temperature ^{1}H NMR experiments. At low temperature the splitting of the two groups of methylene protons are resolved in the ^{1}H NMR of **7** at –40 °C in d^{8}-toluene as each have different chemical environments. The protons in one set of methylene groups displays as a pseudo triplet split by its neighboring proton in addition to the neighboring phosphorous atom. The other set of methylene protons display a splitting pattern in the ^{1}H NMR as a doublet of doublets, likely due to the up down orientation of the protons, which split each other and are further split through two bond coupling with the nearby phosphorous atom. As asymmetry is observed given the inequivalence of the methylene protons in the ^{1}H NMR, it is also revealed in the ^{13}C NMR (See Section 2.7) for complex **7** for the three groups of carbonyl ligands in addition to the methylene carbon atoms. The two carbon atoms for the methylene protons each give rise to a resonance at a of δ 38.14 ppm and 36.68 ppm in the ^{13}C NMR at a temperature of –40 °C, with each peak displaying a different splitting pattern based on its orientation with respect to the neighboring phosphorus atoms. Additional information obtained from the ^{13}C NMR of **7** at a temperature of –40 °C indicates a resonance for the one bridging carbonyl ligand across the two cobalt centers at a shift of 247.57 ppm. Two resonances for the terminal carbonyl ligands is also evident at δ 210.30 ppm and 204.96 ppm, the latter being consistent with previously reported cobalt carbonyl compounds containing terminal CO-ligands.[15] It should be noted that at room temperature each carbonyl resonance was not observed as a

sharp peak but instead as a broad signal around 240 ppm. This is likely due to the rapid interconversion of the CO ligands in solution at room temperature due to the benzylidene ring interconversion above and below the plane of the silicon center. Fortunately, the resonance for the three distinct carbonyl ligands can be resolved at low temperature (See Section 2.7). Comparable spectroscopic features have been reported with similar PSiP ligand framework in the lab of Sun and coworkers.[2,16] In 2008 the lab of Gebbink and van Koten carried out similar variable temperature studies on group 10 metals within a SCS ligand framework containing methylene linkers bound to the sulfur donor atoms.[12]

2.4 Concluding Remarks

The successful synthesis of the air sensitive group 10 metal-silyl complexes of nickel, palladium and platinum was accomplished, all in good yield. With these metal-silyl complexes access to metal-silylene complexes are demonstrated and discussed in Chapter 3 of this work. Additionally, it was shown that cobalt can successfully be installed in the $(^{Cy}P)_2Si$ ligand framework using dicobalt(0)octacarbonyl. The Co(I)Silylene features a Co–Co bond and could be useful for catalyzing reactions that require a strong metal-metal interaction, as the rigidity causes the metals to be locked in place.

Recently in 2018, Whited and Oservov have demonstrated access to a base free cobalt-silylene within a PSiP ligand framework.[10] Reported here is the synthesis and characterization of a bimetallic silylene. A literature search reveals bimetallic cobalt-silane complexes are relatively rare. Additionally, no such reports of N-heterocyclic silylene bimetallic cobalt complexes were found to be reported during the preparation of this document. Cobalt-silylene complexes may prove useful for small molecule reactivity such

as C–H bond activation in addition to hydroformulation reactions and these studies with that of **7** warrant further investigation.[17] The latter types of reactivity are important characteristics for any potential catalyst used for alternative energy sources.[18]

2.5 Syntheses of Group 10 Metal–Silyl Complexes and Cobalt (I) Silylene

2.5.1 Standard Synthetic Methods and Materials

Standard synthetic methods and materials are the same as reported in Chapter 1.

2.5.2 Nickel, (1,2-C_6H_4)($NCH_2P(Cy)_2$)$_2SiNiCl_2$ (**4**)

To a stirred solution of N,N-dichlorosilane, **1**, (2.28 g, 3.64mmol) in THF (20 mL), $Ni(COD)_2$ (1.00 g, 3.64 mmol) in THF (20 mL) was added. After two hours of stirring at room temperature, a bright orange precipitate formed and was collected. Recrystallization using DCM/ether resulted in 1.83 g (73 % yield) of orange crystalline solid after first crop collection. Crystals suitable for XRD analysis were grown from THF/ether at room temperature. ^{1}H NMR (400 MHz, C_6D_6) δ 6.97 (dd, *J* = 5.6, 3.3 Hz, 2H), 6.75 (dd, *J* = 5.6, 3.3 Hz, 2H), 3.24 (s, 4H), 2.32 (ddd, *J* = 12.3, 9.3, 2.8 Hz, 2H), 2.16 (d, *J* = 12.9 Hz, 2H), 2.04 (d, *J* = 13.3 Hz, 4H), 1.95 (dt, *J* = 11.6, 3.7 Hz, 2H), 1.79 – 1.61 (m, 7H), 1.48 (dt, *J* = 22.1, 12.5 Hz, 12H), 1.33 (qd, *J* = 12.5, 2.8 Hz, 2H), 1.20 – 1.03 (m, 8H), 1.03 – 0.89 (m, 2H). ^{31}P{^{1}H} NMR (162 MHz, C_6D_6) δ 67.93. ^{29}Si{^{1}H} NMR (119 MHz, C_6D_6) δ 62.08 (t, $J_{Si\text{-}P}$= 53.2 Hz). ^{13}C NMR (126 MHz, C_6D_6) δ 142.95, 119.69, 111.12, 42.73, 42.63, 42.54, 35.80, 35.74, 35.68, 35.39, 35.32, 35.25, 30.37, 29.01, 28.93, 27.86, 27.34, 27.29, 27.24, 27.18, 27.14, 27.02, 26.98, 26.94, 26.85, 26.79, 26.74, 26.28, 26.02. LIFDIMS Exact Mass calculated for $C_{32}H_{52}Cl_2N_2NiP_2Si$: 682.2106. LIFDIMS Exact Mass measured for $C_{32}H_{52}Cl_2N_2NiP_2Si$: 682.2089.

2.5.3 Palladium, (1,2-C_6H_4)($NCH_2P(Cy)_2$)$_2$$SiPdCl_2$ (**5**)

To a stirred solution of N,N-dichlorosilane, **1**, (1.00 g, 1.59 mmol) in minimum THF, $Pd(PPh_3)_4$ (1.83 g, 1.59 mmol) dissolved in THF was added. After two hours of stirring at room temperature, a pale-yellow precipitate formed and was collected. Recrystallization using THF/Ether mixture resulted in 0.850 g (73 % yield) of yellow crystalline solid after first crop collection. Crystals suitable for XRD analysis were grown from concentrated benzene at room temperature. ^{1}H NMR (400 MHz, C_6D_6) δ 6.96 (dd, *J* = 5.6, 3.3 Hz, 2H), 6.74 (dd, *J* = 5.6, 3.4 Hz, 2H), 3.24 (qt, *J* = 13.4, 3.4 Hz, 4H), 2.55 (t, *J* = 11.3 Hz, 2H), 2.10 (d, *J* = 10.1 Hz, 2H), 2.01 – 1.80 (m, 8H), 1.77 – 1.61 (m, 6H), 1.45 (d, *J* = 10.9 Hz, 10H), 1.23 (q, *J* = 11.3, 10.5 Hz, 4H), 1.02 (qt, *J* = 21.0, 9.6 Hz, 13H). ^{31}P{^{1}H} NMR (162 MHz, C_6D_6) δ 74.30. ^{29}Si{^{1}H} NMR (119 MHz, C_6D_6) δ 63.73. ^{13}C NMR (151 MHz, C_6D_6) δ 142.09, 119.75, 111.00, 41.77, 41.71, 41.64, 34.85, 34.78, 34.72, 30.26, 28.72, 28.59, 27.45, 27.00, 26.96, 26.92, 26.87, 26.83, 26.79, 26.75, 26.70, 26.65, 26.60, 26.19, 25.76. LIFDIMS Exact Mass calculated for $C_{32}H_{52}Cl_2N_2PdP_2Si$: 730.1787 LIFDIMS Exact Mass measured for $C_{32}H_{52}Cl_2N_2PdP_2Si$, [$M^+$]: 732.1801

2.5.4 Platinum, (1,2-C_6H_4)($NCH_2P(Cy)_2$)$_2$$SiPtCl_2$ (**6**)

To a stirred solution of N,N-dichlorosilane, **1**, (0.013 g, 0.020 mmol) in minimum THF, ethylenebis(triphenylphosphine)platinum(0) (0.015 g, 0.020 mmol) dissolved in minimum THF, was slowly added. After two hours of stirring at room temperature, a pale-yellow precipitate formed and was collected. Recrystallization using DCM/Ether mixture resulted in 0.012 g (75 % yield) of yellow crystalline solid after first crop collection. Crystals suitable for XRD analysis were grown from concentrated DCM/ether layering at –35 ºC.

^{1}H NMR (400 MHz, C_6D_6) δ 6.95 (dd, *J* = 5.6, 3.3 Hz, 2H), 6.76 (dd, *J* = 5.6, 3.4 Hz, 2H), 3.44 (dt, *J* = 13.8, 4.3 Hz, 2H), 3.18 (dt, *J* = 13.7, 3.0 Hz, 2H), 2.80 – 2.66 (m, 2H), 2.16 (d, *J* = 11.0 Hz, 2H), 2.05 (dd, *J* = 11.2, 6.5 Hz, 4H), 1.90 (dt, *J* = 6.9, 3.4 Hz, 4H), 1.82 – 1.70 (m, 4H), 1.63 (d, *J* = 12.5 Hz, 3H), 1.52 – 1.38 (m, 13H), 1.22 – 0.89 (m, 16H). ^{31}P{^{1}H} NMR (162 MHz, C_6D_6) δ 72.30 ($J_{P\text{-}Pt}$ = 2976.0 Hz). ^{29}Si NMR (119 MHz, C_6D_6) δ 56.83 (t, $J_{Si\text{-}Pt}$ = 11.0 Hz, $J_{Si\text{-}Pt}$ = 1663.2). ^{13}C NMR (151 MHz, C_6D_6) δ 143.10, 119.92, 112.05, 44.24, 44.15, 44.07, 35.73, 35.65, 35.57, 33.37, 33.29, 33.21, 30.28, 28.10, 27.22, 26.88, 26.85, 26.79, 26.68, 26.64, 26.59, 26.53, 26.49, 26.22, 25.70. LIFDIMS Exact Mass calculated for $C_{32}H_{52}Cl_2N_2PdP_2Si$: 819.2400, LIFDIMS Exact Mass measured for $C_{32}H_{52}Cl_2N_2PdP_2Si$, [$M^+$]: 820.2437

2.5.5 Cobalt, $SiCo_2P_2(CO)_5$ (**7**)

To a stirred solution of NN-dichlorosilane, **1**, 0.050 g (0.080 mmol) in THF 1.1 equivalents of $Co_2(Co)_8$ (0.030 g) was added. An immediate color change from colorless to deep crimson red was observed. Heating overnight at +60 °C in a Strauss flask resulted in another color change from red to green. ^{31}P NMR was checked after 12 hours of heating and revealed a single new broad resonance. All solvent was removed and the green glaze extracted with 3x2 mL portions of hexane, followed by filtration through a pad of Celite. Concentration of hexane extracts afforded 0.040 g of **7** as a yellow powder in 60 % yield. ^{1}H NMR (500 MHz, Toluene-d_8, - 60 °C) δ 7.96 (dd, *J* = 5.6, 3.2 Hz, 2H), 7.61 (dd, *J* = 5.6, 3.4 Hz, 2H), 4.24 (t, *J* = 11.3 Hz, 2H), 3.99 (dd, *J* = 12.7, 4.8 Hz, 2H), 3.07 – 3.01 (m, 3H), 2.94 – 2.80 (m, 7H), 2.64 (d, *J* = 10.7 Hz, 6H), 2.52 (t, *J* = 15.3 Hz, 4H), 2.40 (d, *J* = 6.6 Hz, 2H), 2.36 – 2.29 (m, 4H), 2.21 (t, *J* = 6.7 Hz, 0H), 2.16 (d, *J* = 12.2 Hz, 1H), 2.08

(d, J = 10.8 Hz, 2H), 2.06 – 1.93 (m, 2H), 1.92 – 1.85 (m, 2H), 1.80 (q, J = 12.3, 11.3 Hz, 2H). $^{31}P\{^{1}H\}$ NMR (202 MHz, Toluene-d_8, 20 °C) δ 93.62. ^{13}C NMR (126 MHz, Toluene-d_8, - 60 °C) δ 247.57, 210.30, 204.96, 139.88 (d, J = 9.4 Hz), 119.10, 109.27, 38.33 (d, J = 26.7 Hz), 36.87 (dd, J = 31.3, 17.7 Hz), 28.79, 28.41, 27.85, 27.34 (t, J = 9.4 Hz), 26.27 (t, J = 12.5 Hz), 26.00. ^{29}Si NMR (119 MHz, Toluene-d_8) δ 160.04 (t, J = 19.3 Hz). LIFDIMS Accurate Mass calculated for $C_{37}H_{52}Co_2N_2O_5P_2Si$: 829.1779, LIFDIMS Accurate Mass measured for $C_{37}H_{52}Co_2N_2O_5P_2Si$: 812.1769.

2.6 References

(1) Iluc, V. M.; Hillhouse, G. L. *Tetrahedron* **2006**, *62* (32), 7577–7582.

(2) Xiong, Z.; Li, X.; Zhang, S.; Shi, Y.; Sun, H. *Organometallics* **2016**, *35* (3), 357–363.

(3) Whited, M. T.; Zhang, J.; Ma, S.; Nguyen, B. D.; Janzen, D. E. *Dalton Transactions* **2017**, *46* (43), 14757–14761.

(4) Korshin, E. E.; Leitus, G.; Shimon, L. J. W.; Konstantinovski, L.; Milstein, D. *Inorganic Chemistry* **2008**, *47* (16), 7177–7189.

(5) Takaya, J.; Iwasawa, N. *Journal of the American Chemical Society* **2008**, *130* (46), 15254–15255.

(6) Mitton, S. J.; Mcdonald, R.; Turculet, L. *Organometallics* **2009**, *28*, 5122–5136.

(7) Dixon, L. S. H.; Hill, A. F.; Sinha, A.; Ward, J. S. *Organometallics* **2014**, *33* (3), 653–658.

(8) Whited, M. T.; Deetz, A. M.; Boerma, J. W.; Derosha, D. E.; Janzen, D. E. *Organometallics* **2014**, *33* (19), 5070–5073.

(9) Yoo, H.; Carroll, P. J.; Berry, D. H. *Journal of the American Chemical Society* **2006**, *128* (18), 6038–6039.

(10) Zhang, J.; Foley, B. J.; Bhuvanesh, N.; Zhou, J.; Janzen, D. E.; Whited, M. T.; Ozerov, O. V. *Organometallics* **2018**, *37* (21), 3956–3962.

(11) Smith, E. E.; Du, G.; Fanwick, P. E.; Abu-Omar, M. M. *Organometallics* **2010**, *29* (23), 6527–6533.

(12) Kruithof, C. A.; Dijkstra, H. P.; Lutz, M.; Spek, A. L.; Gebbink, R. J. M. K.; Van Koten, G. *Organometallics* **2008**, *27* (19), 4928–4937.

(13) Garcia, T. Y.; Fettinger, J. C.; Olmstead, M. M.; Balch, A. L. *Chem. Commun* **2009**, 7143–7145.

(14) Tiel, M. Van; Mackay, K. M.; Nicholson, B. K. *Joumal of Organometallic Chemistry* **1993**, *462*, 79–87.

(15) Bungu, P. N.; Otto, S. *Journal of the Chemical Society. Dalton Transactions* **2007**, No. 27, 2876–2884.

(16) Wu, S.; Li, X.; Xiong, Z.; Xu, W.; Lu, Y.; Sun, H. *Organometallics* **2013**, *32*, 23.

(17) Ghosh, C. K.; G Graham, W. A. *J. Am. Chem. Soc.* **1987**, *109* (2), 4727–4728.

(18) Benson, E. E.; Kubiak, C. P.; Sathrum, A. J.; Smieja, J. M. *Chemical Society reviews* **2009**, *38* (1), 89–99.

2.7 Spectroscopic Data, Figures and Tables

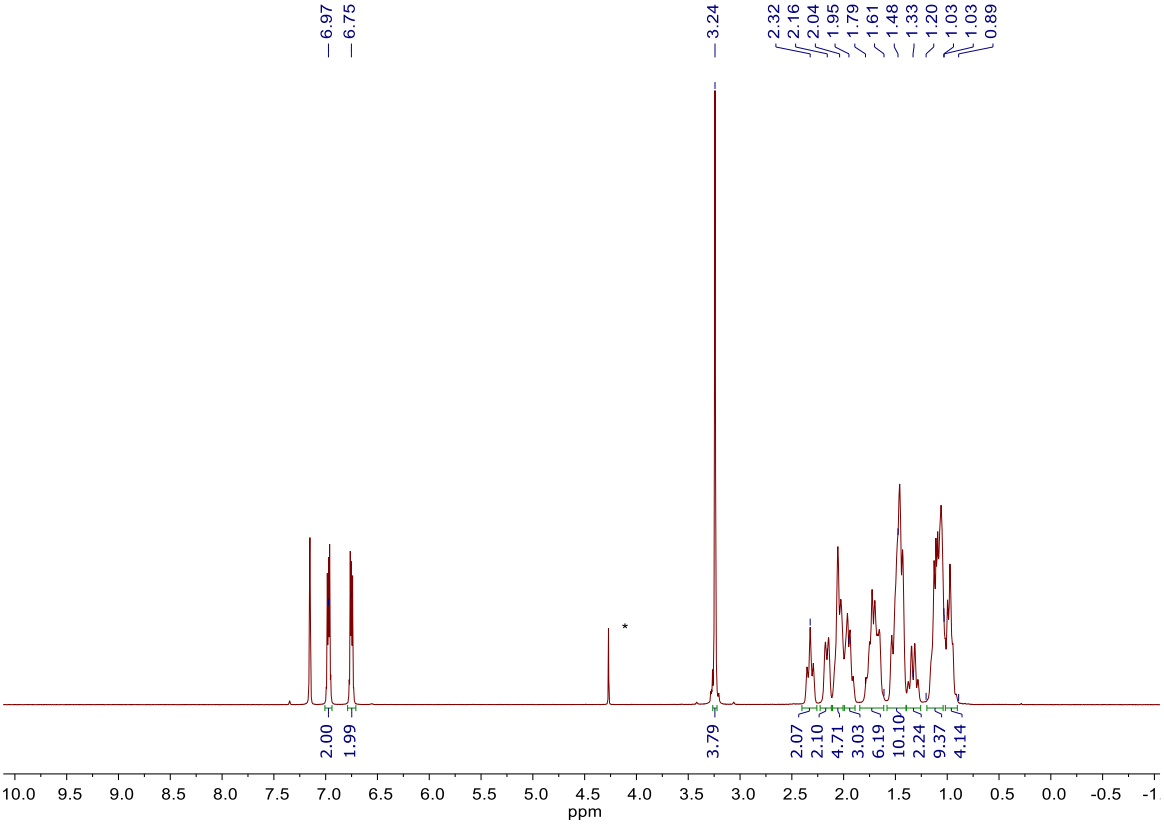

Figure 2.7-1 ^{1}H NMR of (1,2-C_6H_4)($NCH_2P(Cy)_2$)$_2$$SiNiCl_2$, **4**, on a 400 MHz instrument in C_6D_6. *denotes DCM.

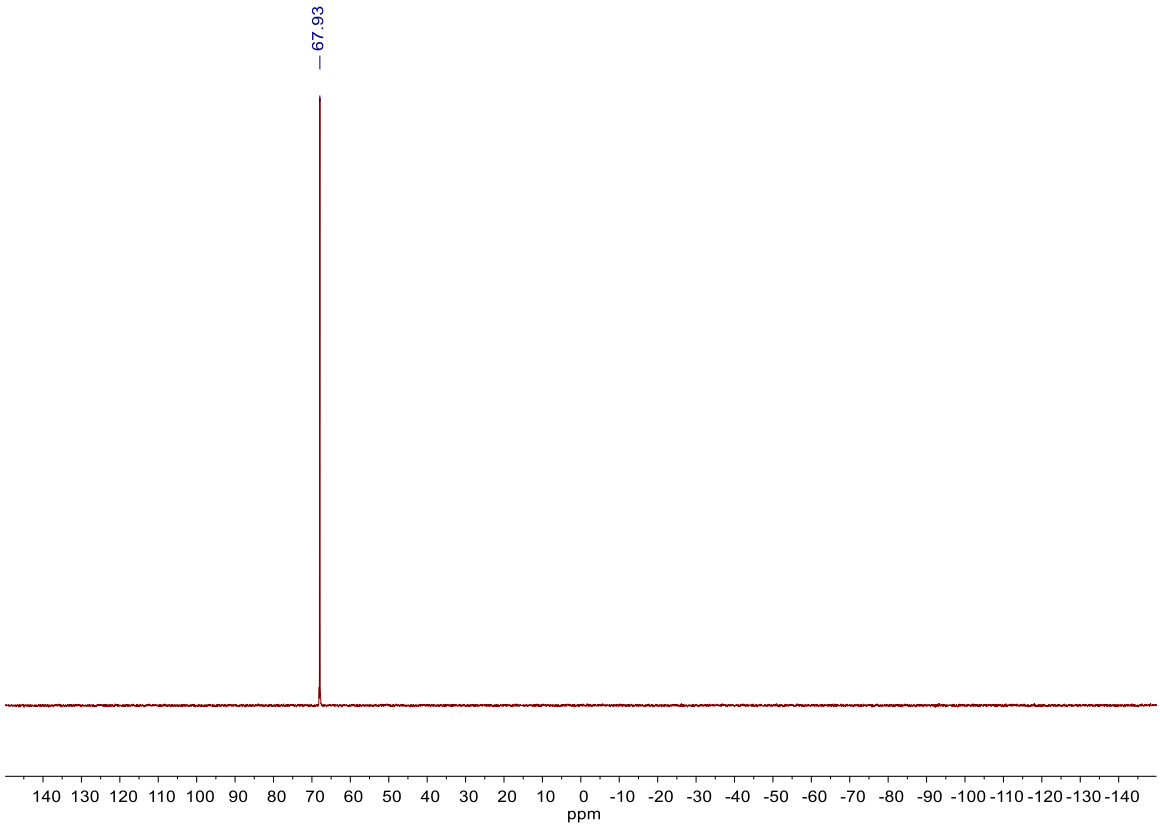

Figure 2.7-2 $^{31}P\{^{1}H\}$ NMR of (1,2-C_6H_4)($NCH_2P(Cy)_2$)$_2SiNiCl_2$, **4**, at 162 MHz in C_6D_6.

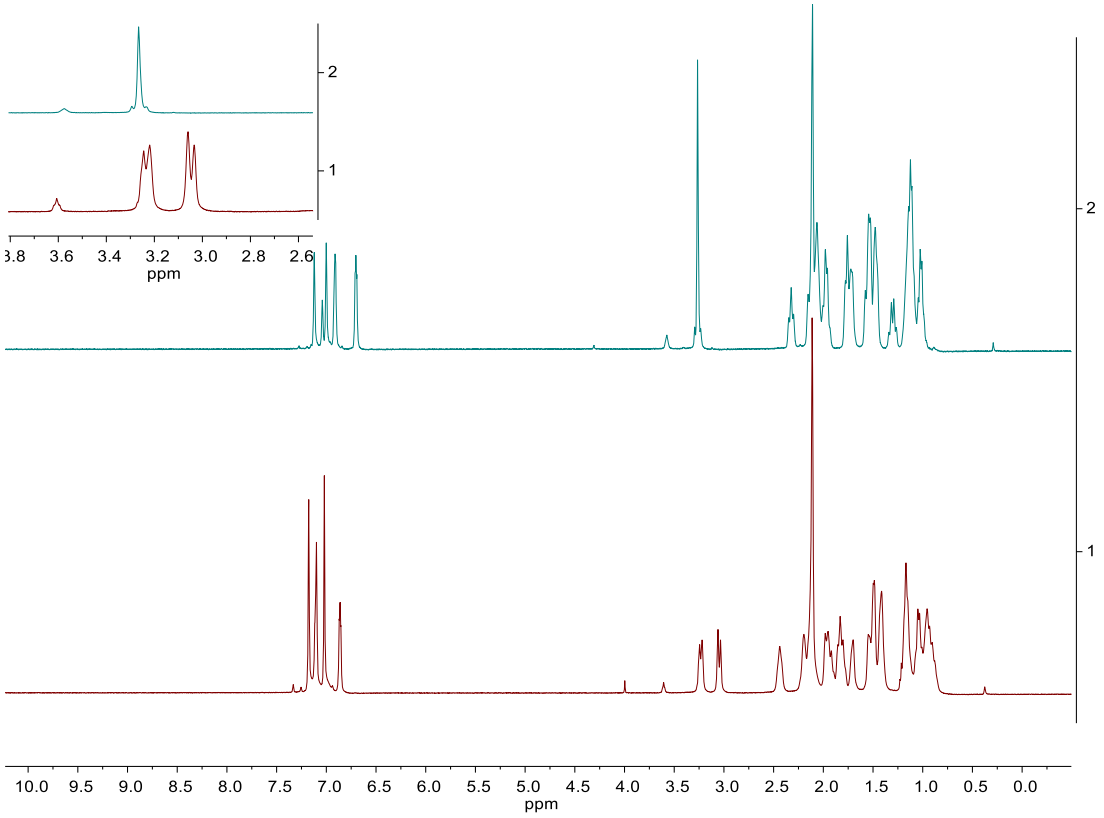

Figure 2.7-3 Variable temperature ^{1}H NMR of $(1,2\text{-}C_6H_4)(NCH_2P(Cy)_2)_2SiNiCl_2$, **4**, at +20° C (top spectrum) and –60° C (bottom spectrum) in d_8-toluene at 500 MHz. Top left magnified inset demonstrates the bridging methylene protons coalesce as a broad singlet at +20° C (top left inset, spectrum 2) while at low temperature the methylene protons resolve to reveal a doublet of doublet splitting pattern at a temperature of –60° C(top left inset, spectrum 1).

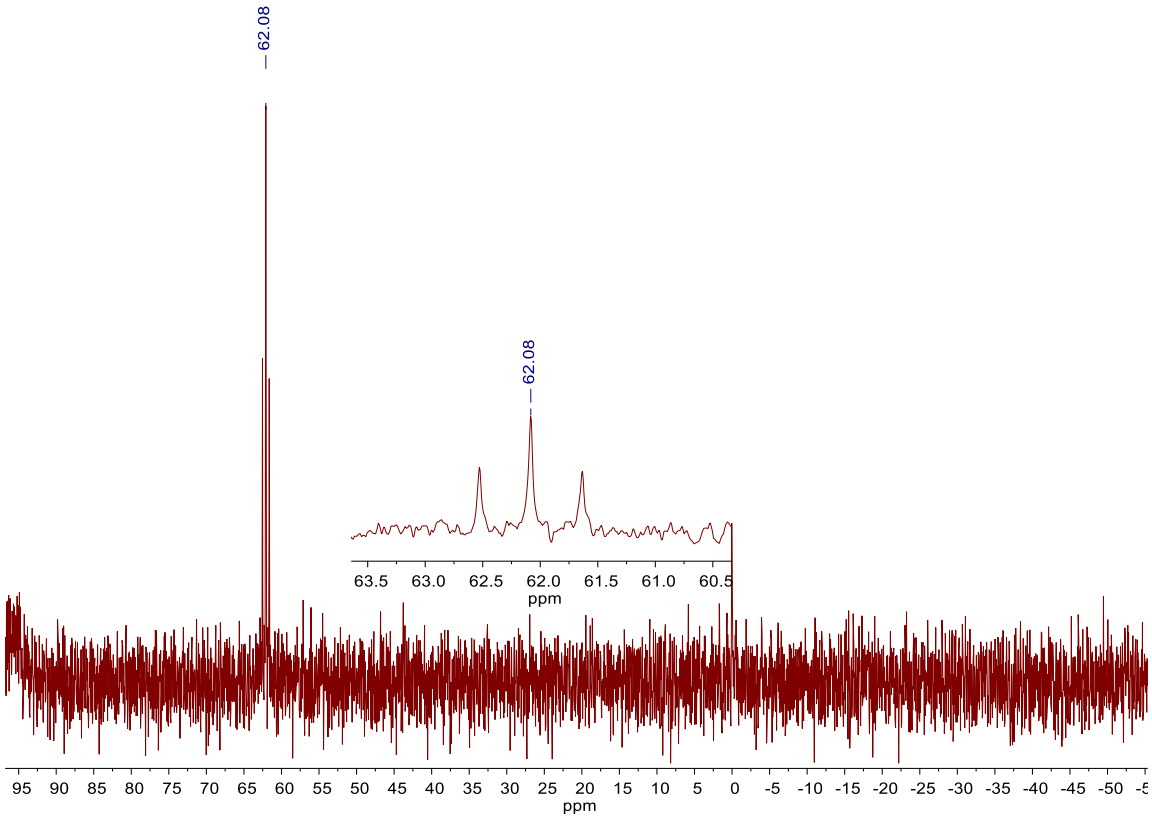

Figure 2.7-4 $^{29}Si\{^{1}H\}$ NMR of $(1,2\text{-}C_6H_4)(NCH_2P(Cy)_2)_2SiNiCl_2$, **4**, at 119 MHz in C_6D_6.

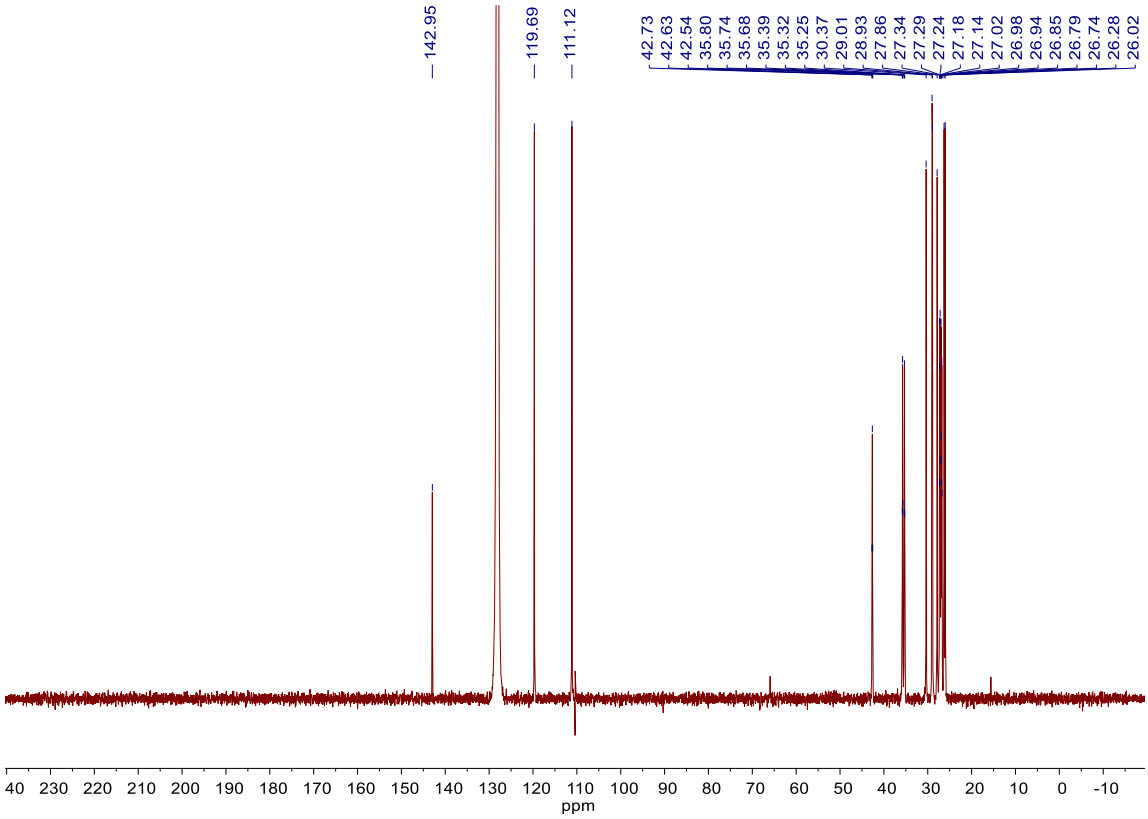

Figure 2.7-5. ^{13}C NMR of $(1,2\text{-}C_6H_4)(NCH_2P(Cy)_2)_2SiNiCl_2$, **4**, at 126 MHz instrument in C_6D_6.

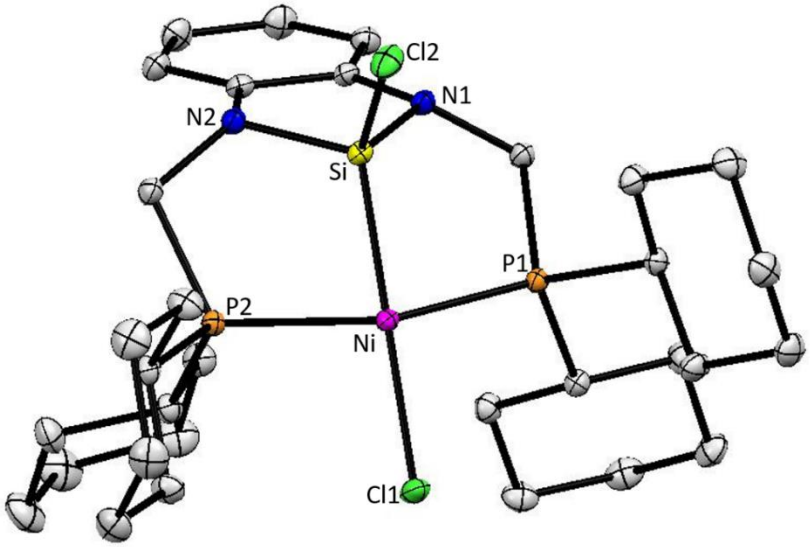

Figure 2.7-6. Thermal ellipsoid plot at 50% probability of $(1,2\text{-}C_6H_4)(NCH_2P(Cy)_2)_2SiNiCl_2$, **4**, Magenta, yellow, blue, orange, green and gray ellipsoids represent nickel, silicon, nitrogen, phosphorus, chlorine and carbon atoms, respectively. Hydrogen atoms are omitted for clarity.

Table 2.7-1 Crystallographic data for $(1,2\text{-}C_6H_4)(NCH_2P(Cy)_2)_2SiNiCl_2$, **4**.

Identification code	hh61AB6_0m-I2a	
Empirical formula	$C_{32}H_{52}Cl_2N_2NiP_2Si$	
Formula weight	684.39	
Temperature	100(2) K	
Wavelength	0.71073 Å	
Crystal system	Monoclinic	
Space group	I 2/a	
Unit cell dimensions	a = 19.4944(7) Å	α = 90°.
	b = 13.8942(5) Å	β = 98.1386(5)°.
	c = 25.1424(13) Å	γ = 90°.
Volume	6741.5(5) Å^3	
Z	8	
Density (calculated)	1.349 mg/m^3	
Absorption coefficient	0.889 mm^{-1}	
F(000)	2912	
Crystal size	0.565 x 0.399 x 0.296 mm^3	
θ range for data collection	1.679 to 30.508°.	
Index ranges	$-27 \le h \le 27$, $-19 \le k \le 19$, $-35 \le l \le 35$	
Reflections collected	97155	
Independent reflections	10287 [R_{int} = 0.0242]	
Completeness to θ = 25.242°	100.00%	
Absorption correction	Semi-empirical from equivalents	
Refinement method	Full-matrix least-squares on F^2	
Data / restraints / parameters	10287 / 0 / 361	
Goodness-of-fit on F^2	1.049	
Final R indices [$I > 2\sigma_1$]	R_1= 0.0208, wR_2 = 0.0546	
R indices (all data)	R_1= 0.0235, wR_2 = 0.0563	
Largest diff. peak and hole	0.470 and -0.221 e/Å^3	

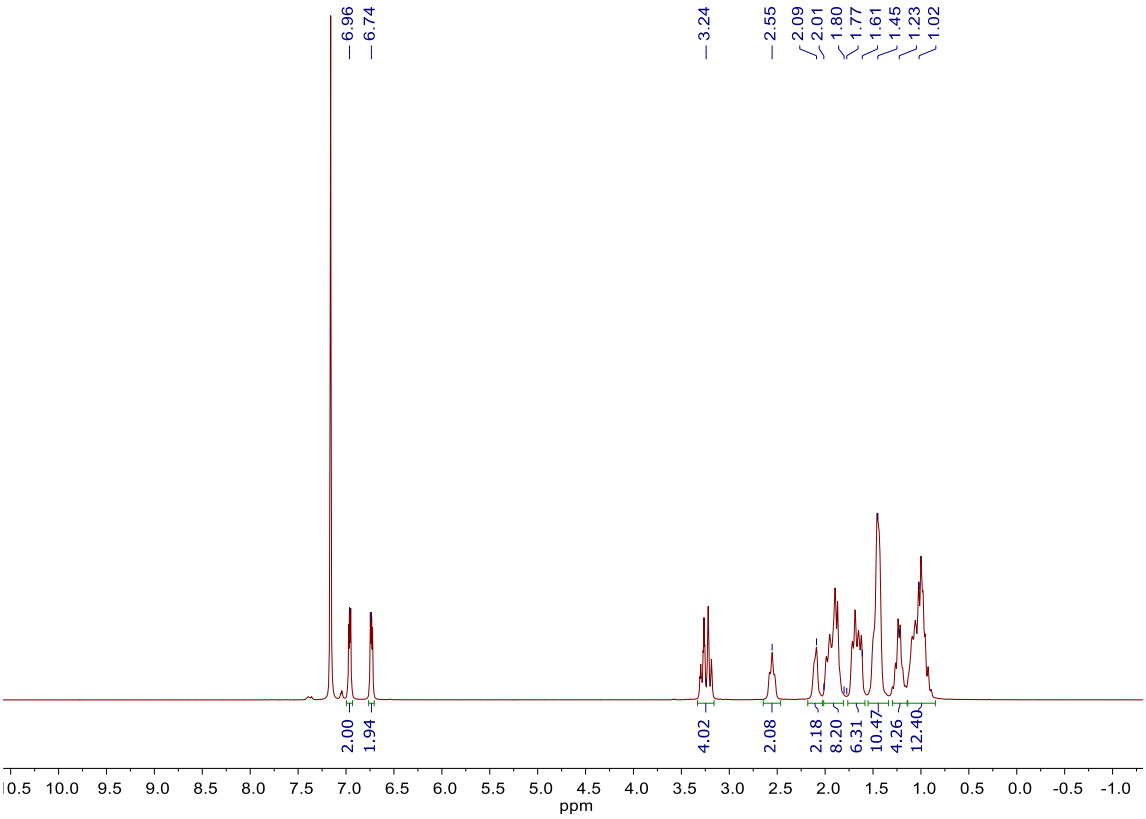

Figure 2.7-7. ^{1}H NMR of $(1,2\text{-}C_6H_4)(NCH_2P(Cy)_2)_2SiPdCl_2$, **5**, at 400 MHz in C_6D_6.

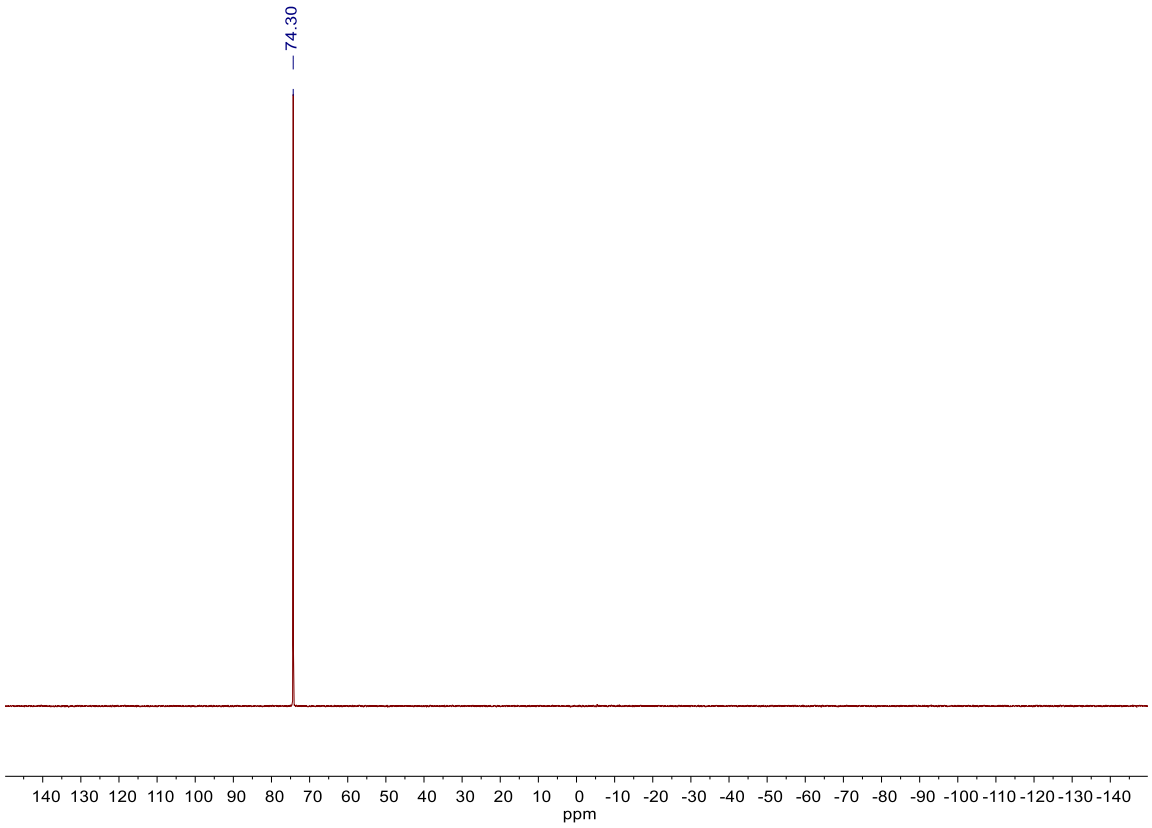

Figure 2.7-8 $^{31}P\{^{1}H\}$ NMR of (1,2-C_6H_4)($NCH_2P(Cy)_2$)$_2$$SiPdCl_2$, **5**, at 162 MHz in C_6D_6.

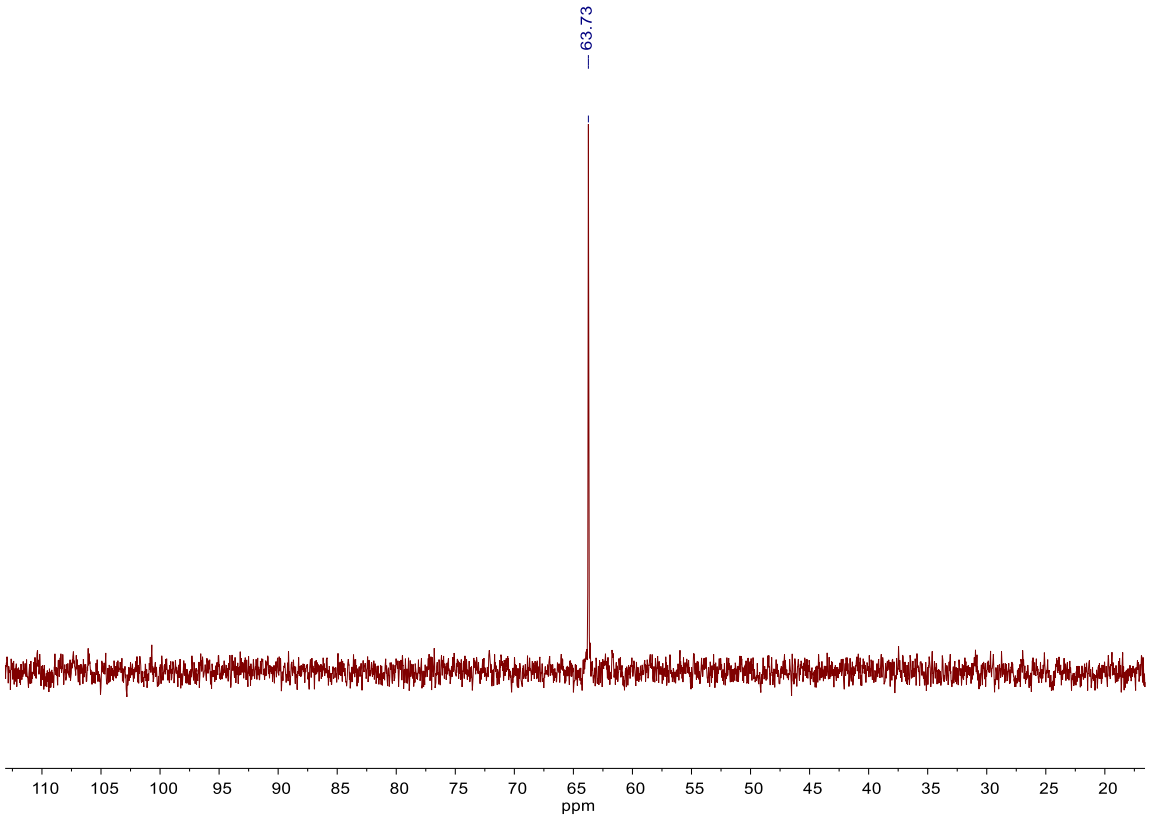

Figure 2.7-9 $^{29}Si\{^{1}H\}$ NMR of $(1,2\text{-}C_6H_4)(NCH_2P(Cy)_2)_2SiPdCl_2$, **5**, at 119 MHz in C_6D_6.

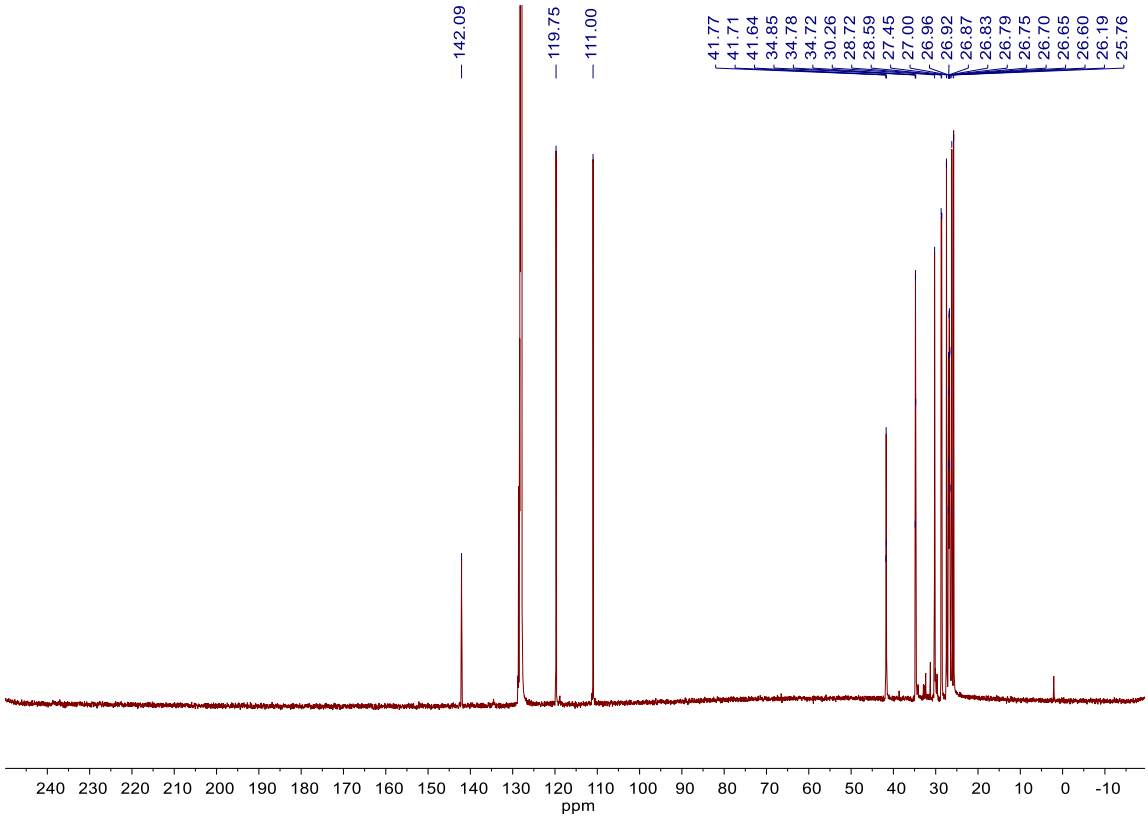

Figure 2.7-10 ^{13}C NMR of $(1,2\text{-}C_6H_4)(NCH_2P(Cy)_2)_2SiPdCl_2$, **5**, at 151 MHz in C_6D_6**.**

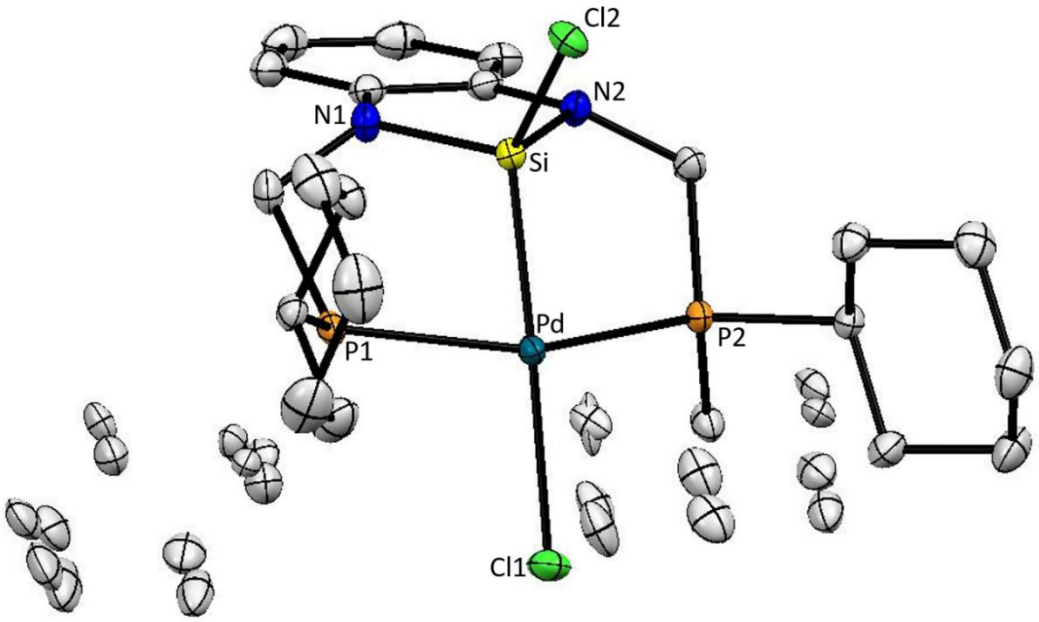

Figure 2.7-11 Thermal ellipsoid plot at 50% probability of (1,2-C_6H_4)($NCH_2P(Cy)_2$)$_2$$SiPdCl_2$, **5**. Dark green, yellow, blue, orange, green and gray ellipsoids represent palladium, silicon, nitrogen, phosphorus, chlorine and carbon respectively. Hydrogen atoms and solvent molecules are omitted for clarity. There was one disordered molecule of (1,2-C_6H_4)($NCH_2P(Cy)_2$)$_2$$SiPdCl_2$ and half a disordered molecule of benzene present in the asymmetric unit of the unit cell. Two of the four cyclohexyl-groups were modeled with disorder (cyclohexyl-disordered site occupancy ratios were 51%/49% and 53%/47%). The disordered benzene was located at the inversion center (benzene disordered site occupancy ratio was 32%/18%).

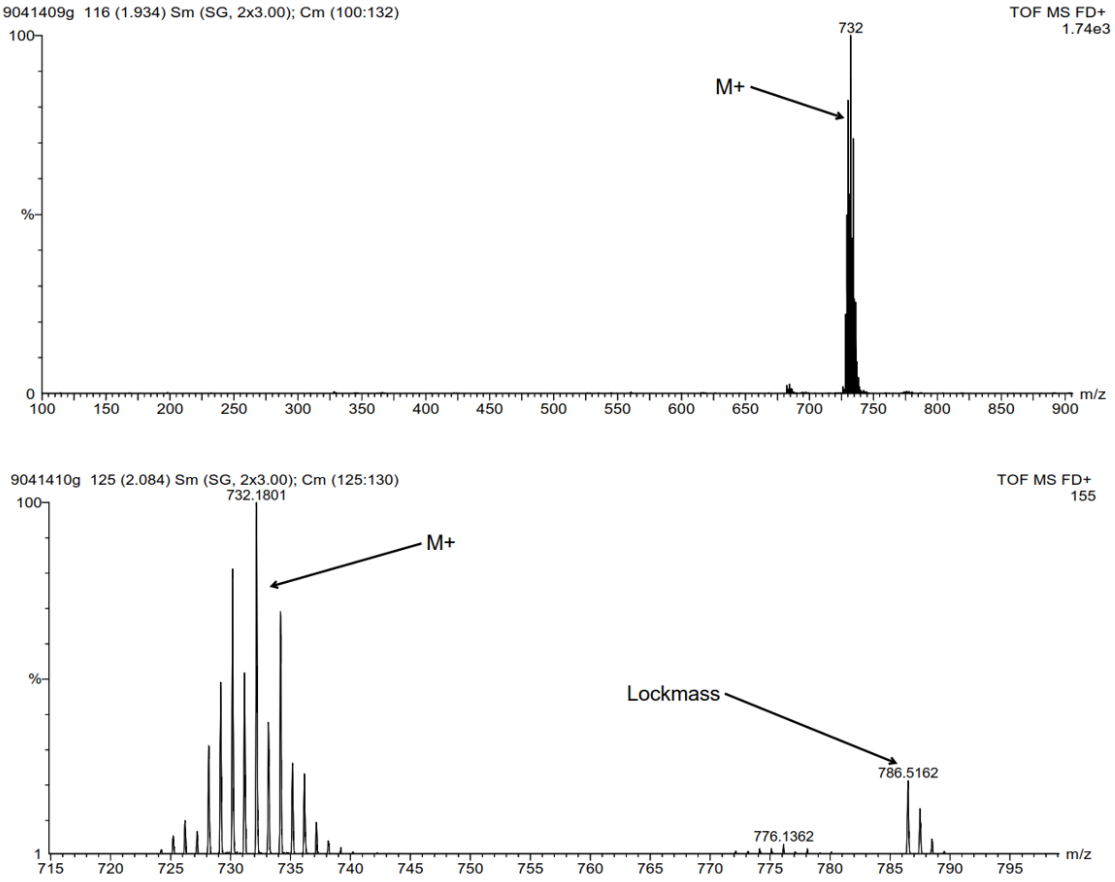

Figure 2.7-12 Mass spectrometry operating in LIFDI mode for (1,2-C_6H_4)($NCH_2P(Cy)_2$)$_2SiPdCl_2$, **5**.

Table 2.7-2 Crystallographic data for $(1,2\text{-}C_6H_4)(NCH_2P(Cy)_2)_2SiPdCl_2$, **5**.

Identification code	hh279MB15_0m	
Empirical formula	$C_{35}H_{55}Cl_2N_2P_2PdSi$	
Formula weight	771.14	
Temperature	100(2) K	
Wavelength	0.71073 Å	
Crystal system	Monoclinic	
Space group	P 21/n	
Unit cell dimensions	a = 11.2329(8) Å	α = 90°.
	b = 24.6246(18) Å	β = 112.7621(11)°.
	c = 14.4180(11) Å	γ = 90°.
Volume	3677.5(5) $Å^3$	
Z	4	
Density (calculated)	1.393 Mg/m^3	
Absorption coefficient	0.796 mm^{-1}	
F(000)	1612	
Crystal size	0.272 x 0.253 x 0.132 mm^3	
Theta range for data collection	1.654 to 30.508°.	
Index ranges	$-16 \le h \le 16$, $-35 \le k \le 35$, $-20 \le l \le 20$	
Reflections collected	87873	
Independent reflections	11235 [R_{int} = 0.0440]	
Completeness to θ = 25.242°	100.00%	
Absorption correction	Semi-empirical from equivalents	
Refinement method	Full-matrix least-squares on F^2	
Data / restraints / parameters	11235 / 584 / 548	
Goodness-of-fit on F^2	1.032	
Final R indices [$I > 2\sigma_1$]	R_1 = 0.0266, wR_2 = 0.0593	
R indices (all data)	R_1 = 0.0340, wR_2 = 0.0629	
Largest diff. peak and hole	1.041 and -0.518 e/$Å^{-3}$	

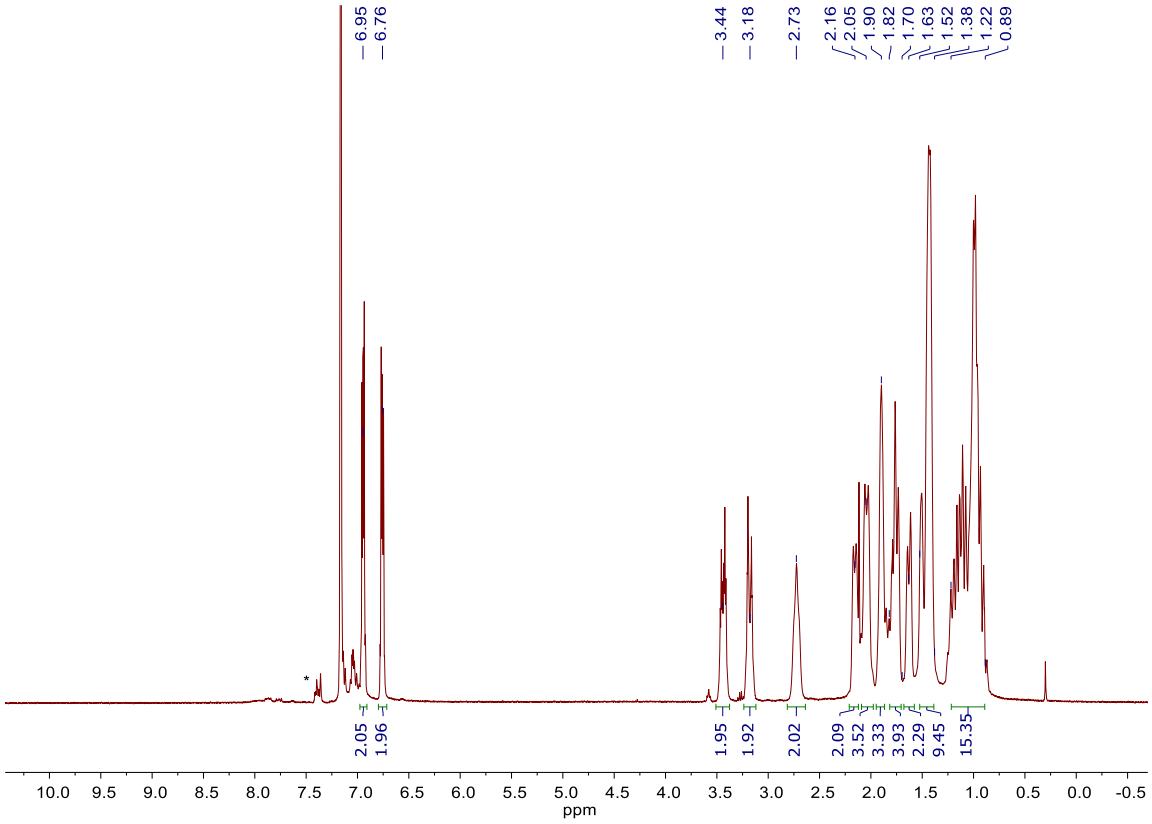

Figure 2.7-13 ^{1}H NMR of (1,2-C_6H_4)($NCH_2P(Cy)_2$)$_2$$SiPtCl_2$, **6**, at 400 MHz in C_6D_6.

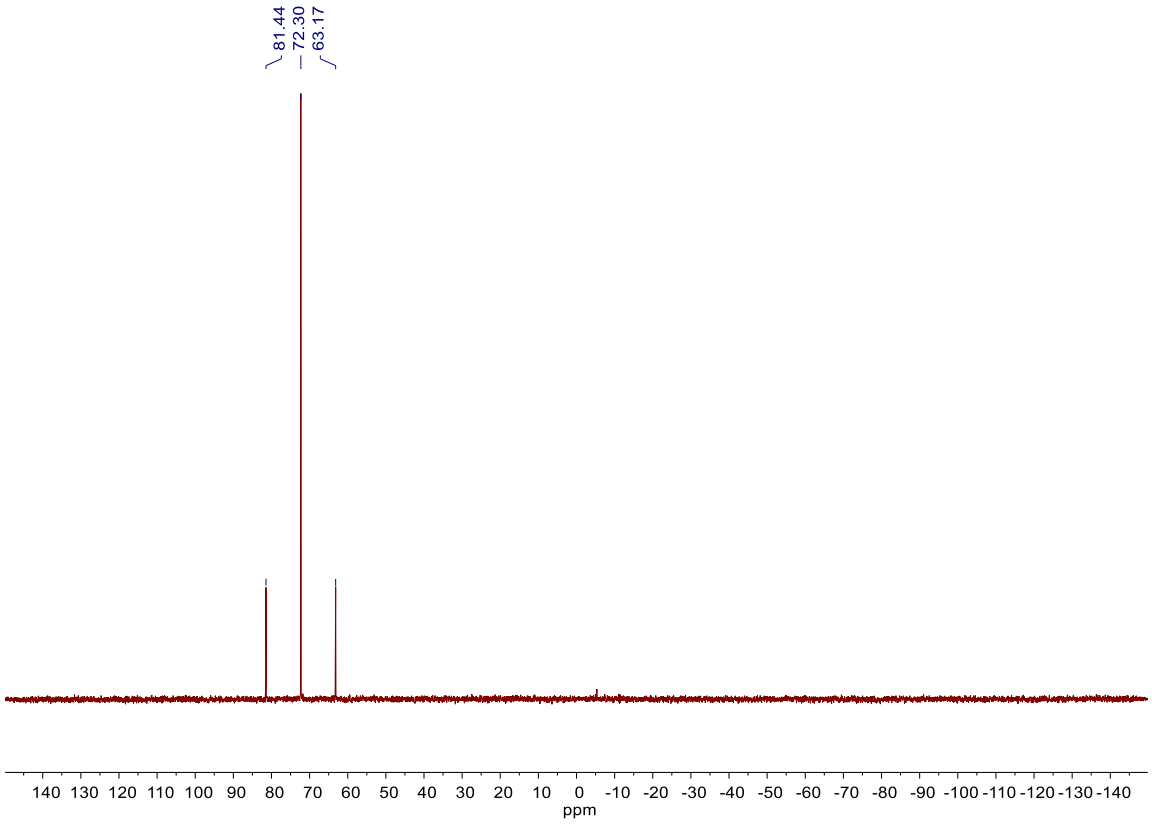

Figure 2.7-14 $^{31}P\{^{1}H\}$ NMR of (1,2-C_6H_4)($NCH_2P(Cy)_2$)$_2$$SiPtCl_2$, **6**, at 162 MHz in C_6D_6 featuring P–Pt (J = 2976.0 Hz) coupling.

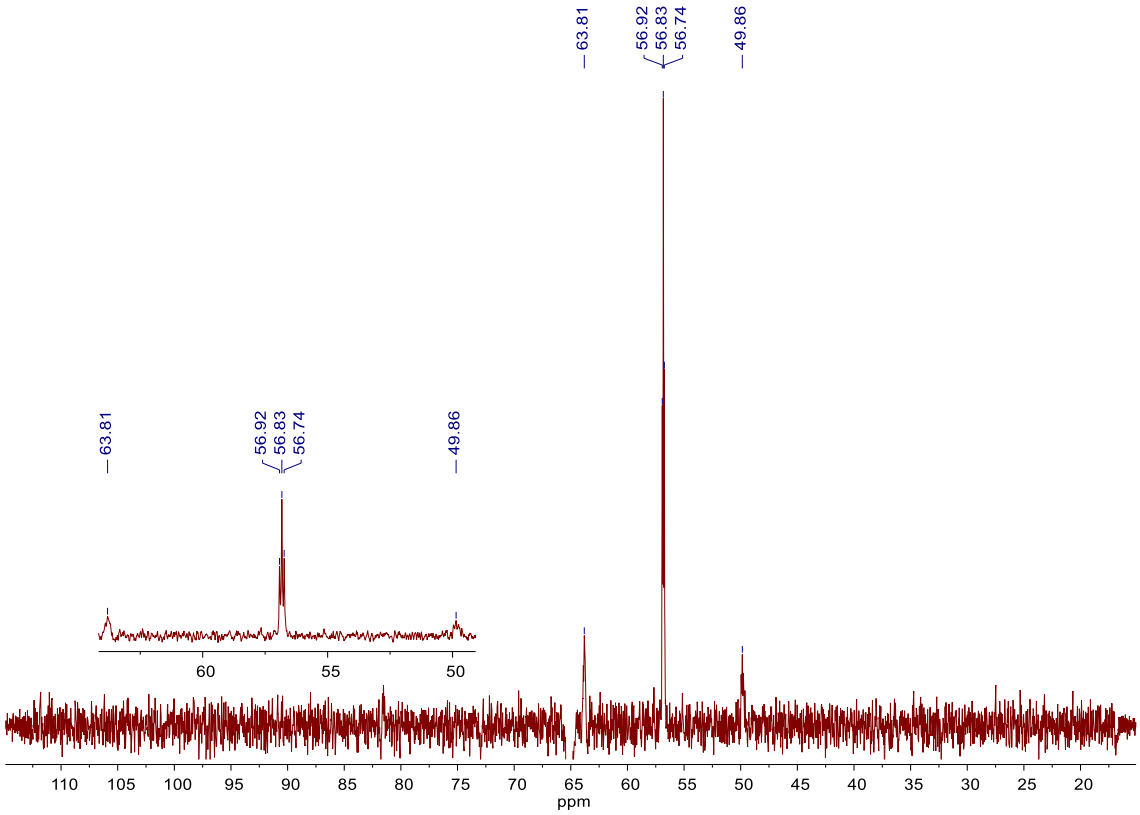

Figure 2.7-15 $^{29}Si\{^{1}H\}$ NMR of $(1,2\text{-}C_6H_4)(NCH_2P(Cy)_2)_2SiPtCl_2$, **6**, at 162 MHz in C_6D_6 featuring Si–P (J = 11.0 Hz) and Si-Pt (J = 1663.2 Hz) coupling.

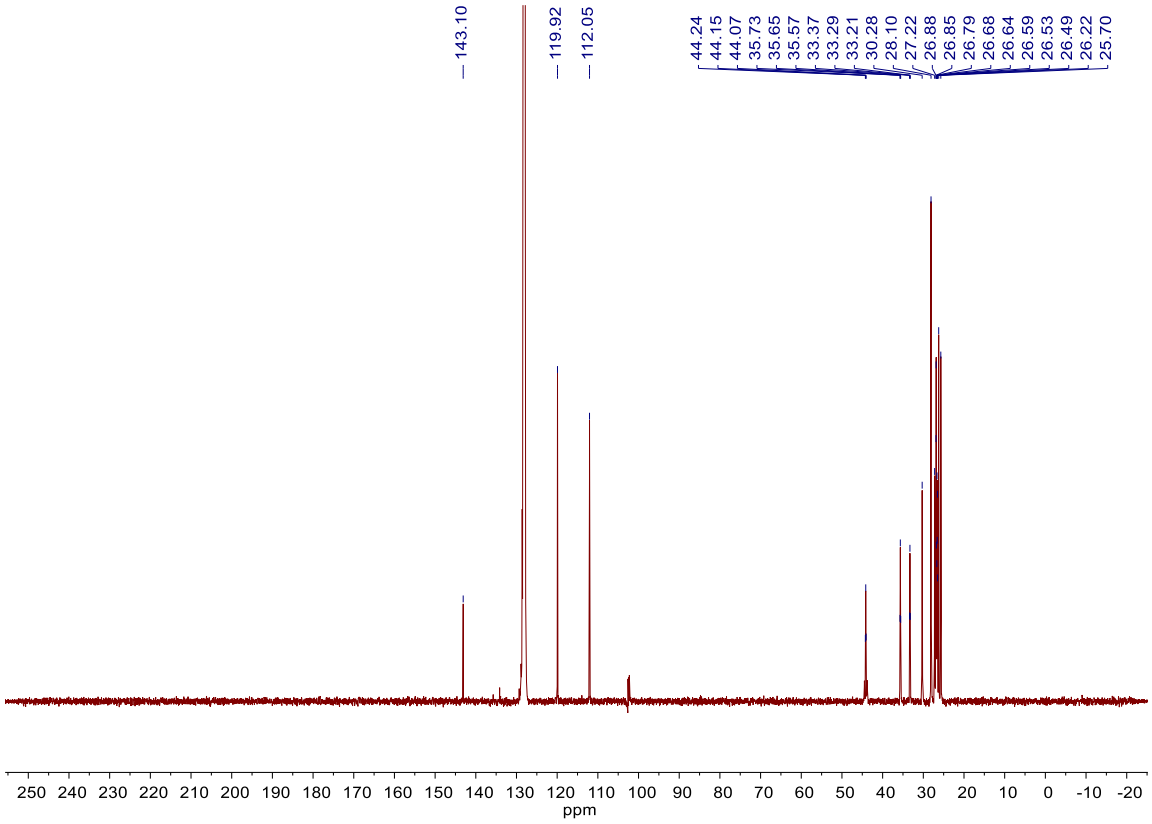

Figure 2.7-16 ^{13}C NMR of $(1,2\text{-}C_6H_4)(NCH_2P(Cy)_2)_2SiPtCl_2$, **6**, at 151 MHz in C_6D_6.

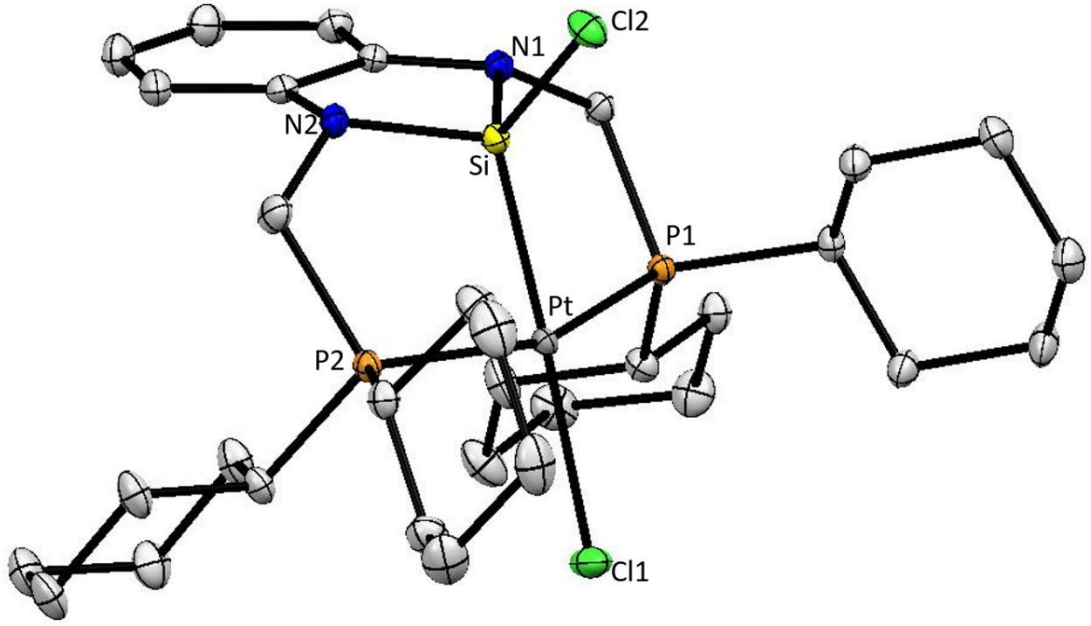

Figure 2.7-17 Thermal ellipsoid plot at 50% probability of (1,2-C_6H_4)($NCH_2P(Cy)_2$)$_2$$SiPtCl_2$, **6**. Dark gray, yellow, blue, orange, green and light gray ellipsoids represent platinum, silicon, nitrogen, phosphorus, chloride and carbon, respectively. Hydrogen atoms and solvent molecules have been omitted for clarity. Compound **6** crystallizes in the monoclinic centrosymmetric space group P21/c with one molecule of **6** and one molecule of diethyl ether per asymmetric unit.

Table 2.7-3 Crystallographic data for $(1,2\text{-}C_6H_4)(NCH_2P(Cy)_2)_2SiPtCl_2$, **6**.

Identification code	hh293ab	
Empirical formula	$C_{36}H_{62}Cl_2N_2OP_2PtSi$	
Formula weight	894.89	
Temperature	100(2) K	
Wavelength	0.71073 Å	
Crystal system	Monoclinic	
Space group	$P2_1/c$	
Unit cell dimensions	a = 14.2103(5) Å	α = 90°.
	b = 12.3672(4) Å	β = 99.1736(14)°.
	c = 22.5412(8) Å	γ = 90°.
Volume	3910.8(2) $Å^3$	
Z	4	
Density (calculated)	1.520 Mg/m^3	
Absorption coefficient	3.867 mm^{-1}	
F(000)	1824	
Crystal color	colourless	
Crystal size	0.277 x 0.257 x 0.222 mm^3	
Theta range for data collection	1.830 to 30.996°	
Index ranges	$-20 \le h \le 20$, $-17 \le k \le 17$, $-32 \le l \le 32$	
Reflections collected	82624	
Independent reflections	12477 [R_{int} = 0.0343]	
Completeness to θ = 25.242°	100.00%	
Absorption correction	Semi-empirical from equivalents	
Refinement method	Full-matrix least-squares on F^2	
Data / restraints / parameters	12477 / 0 / 408	
Goodness-of-fit on F^2	1.052	
Final R indices [$I > 2\sigma_1$ = 11389 data]	R_1 = 0.0191, wR_2 = 0.0411	
R indices (all data)	R_1 = 0.0232, wR_2 = 0.0424	
Largest diff. peak and hole	1.759 and -0.805 e/$Å^{-3}$	

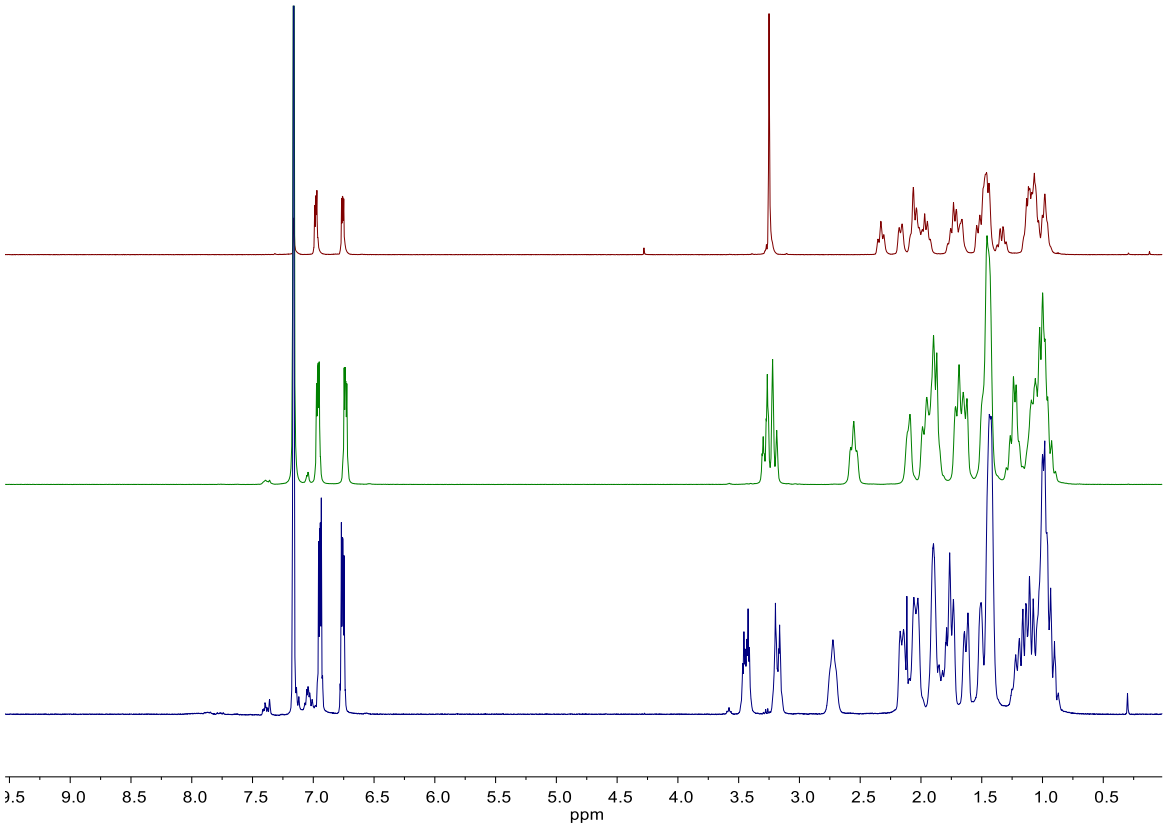

Figure 2.7-18 Stacked ^{1}H NMR in C_6D_6 at 500 MHz at room temperature of **4**, **5**, and **6** for comparative purposes. Note the methylene proton splitting patterns in the alkyl region as the metal–silyl complexes descend down the group 10 triad. Top red spectrum, **4**; middle green spectrum, **5**; bottom purple spectrum, **6**.

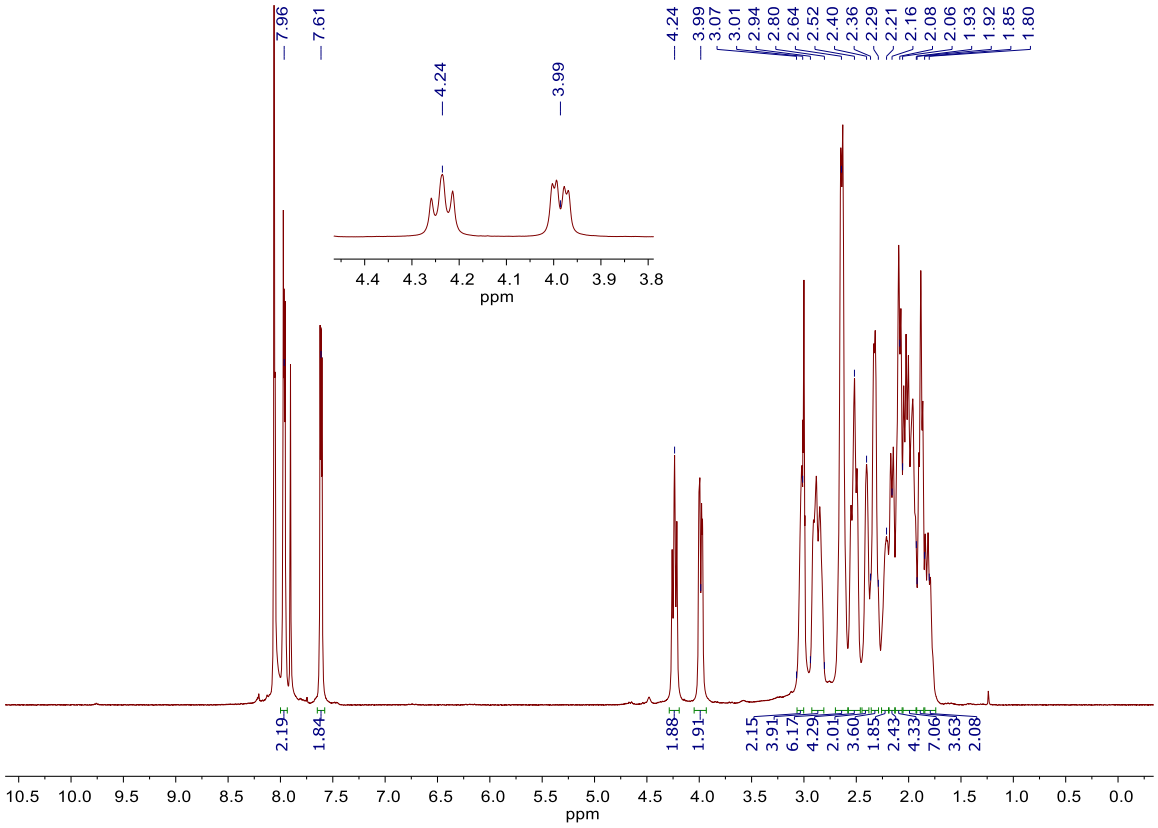

Figure 2.7-19 ^{1}H NMR at –60 °C of $SiCo_2P_2(CO)_5$, **7**, in d_8-toluene at 500 MHz.

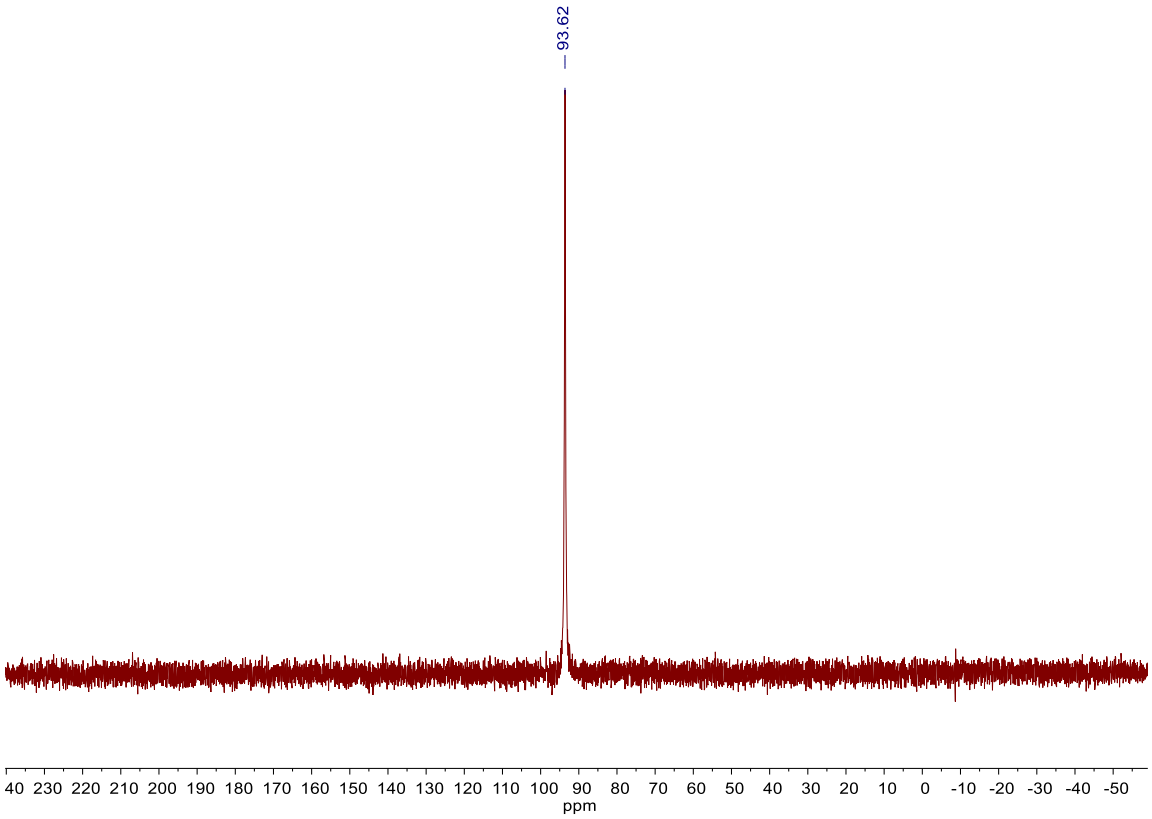

Figure 2.7-20 $^{31}P\{^{1}H\}$ NMR of $SiCo_2P_2(CO)_5$, **7**, in d_8-toluene at +20 °C at 202 MHz.

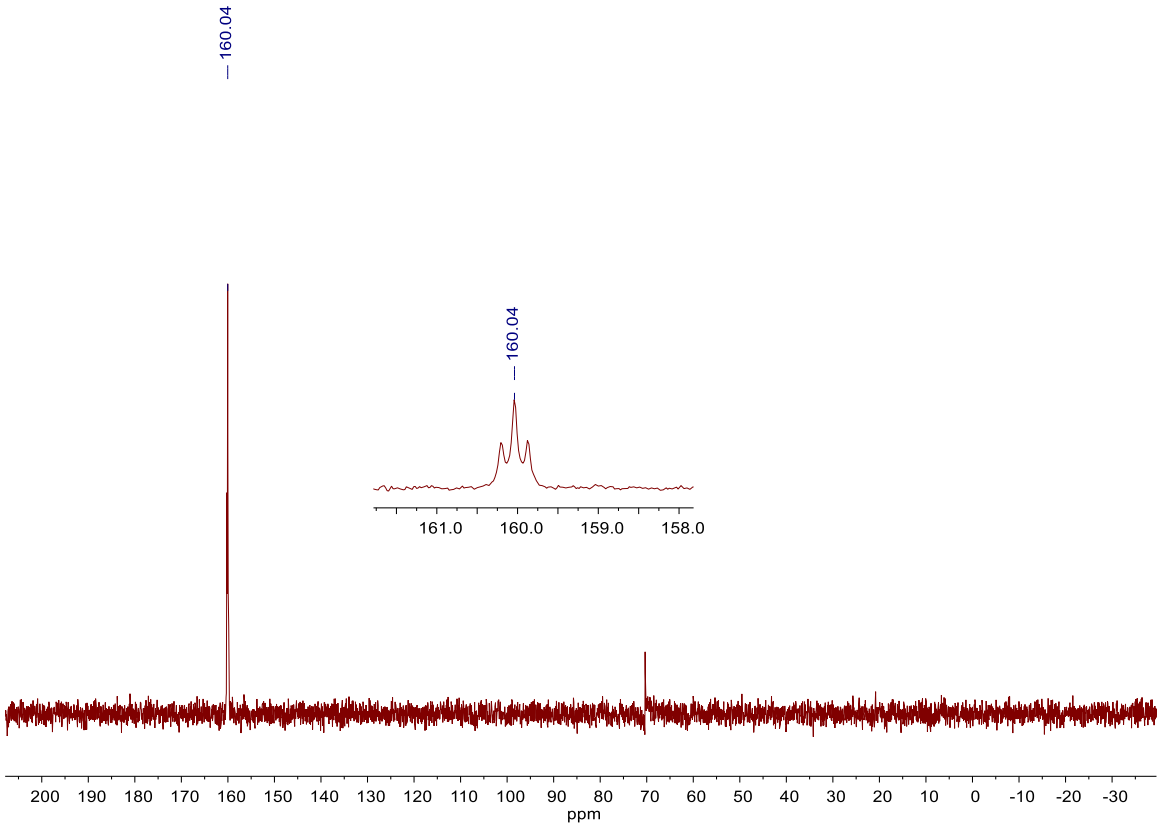

Figure 2.7-21 $^{29}Si\{^{1}H\}$ NMR of $SiCo_2P_2(CO)_5$, **7**, in d_8-toluene at +20 °C at 119 MHz. Note artifact at +70 ppm at spectrum centered frequency.

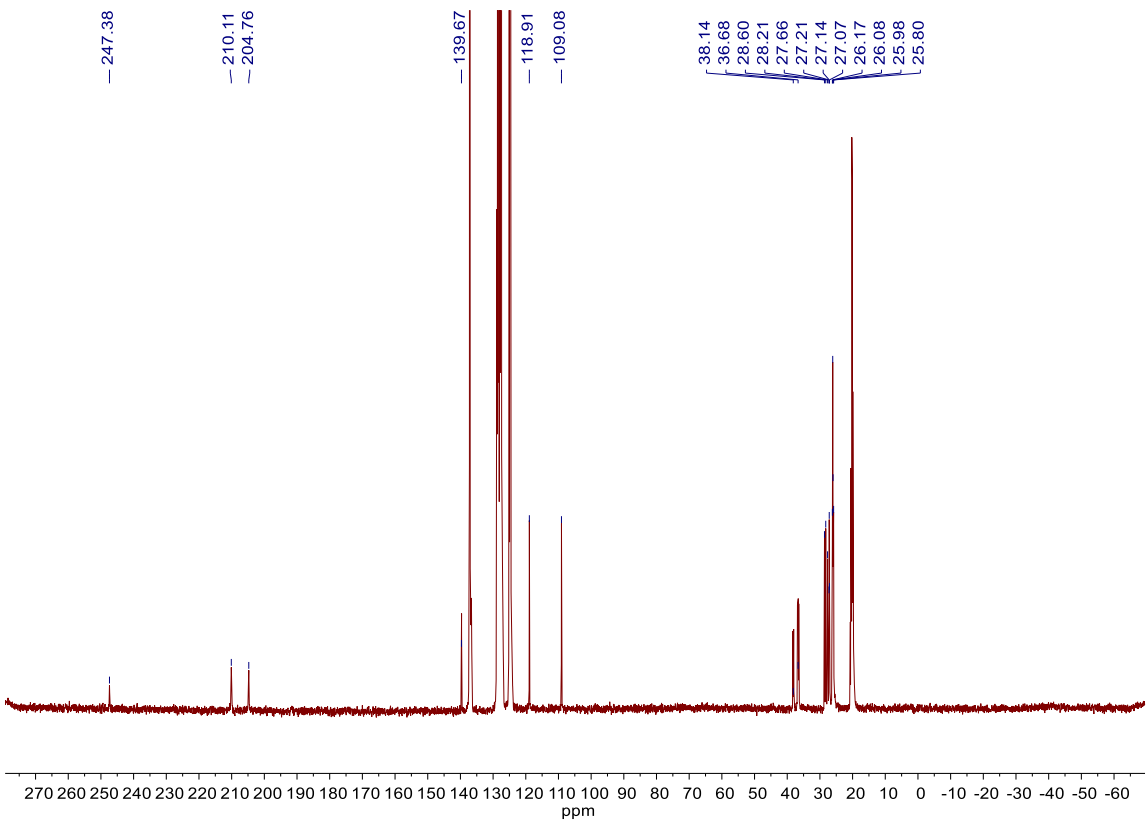

Figure 2.7-22 ^{13}C NMR at –40 °C of $SiCo_2P_2(CO)_5$, **7**, in d_8-toluene at 126 MHz.

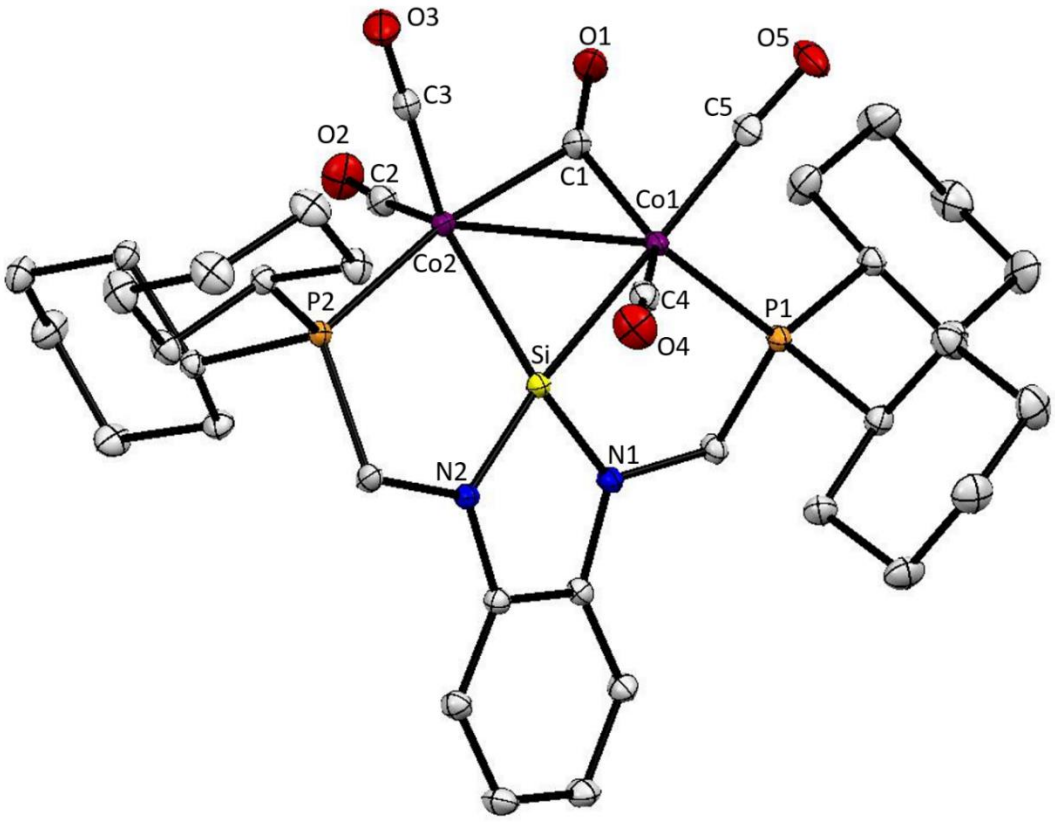

Figure 2.7-23 Thermal ellipsoid plot at 50% probability of $SiCo_2P_2(CO)_5$, **7**. Purple, yellow, blue, orange, red and light gray ellipsoids represent cobalt, silicon, nitrogen, phosphorus, oxygen and carbon, respectively. Hydrogen atoms and solvent molecules have been omitted for clarity.

Table 2.7-4 Crystallographic data for $SiCo_2P_2(CO)_5$, **7**.

Identification code	hh17AB3_0m	
Empirical formula	$C_{37}H_{52}Co_2N_2O_5P_2Si$	
Formula weight	812.69	
Temperature	100(2) K	
Wavelength	0.71073 Å	
Crystal system	Monoclinic	
Space group	P 21/n	
Unit cell dimensions	a = 14.8322(4) Å	α = 90°.
	b = 16.6724(5) Å	β = 98.858(1)°.
	c = 15.5676(5) Å	γ = 90°.
Volume	3803.8(2) $Å^3$	
Z	4	
Density (calculated)	1.419 mg/m^3	
Absorption coefficient	1.032 mm^{-1}	
F(000)	1704	
Crystal size	0.483 x 0.339 x 0.219 mm^3	
θ range for data collection	1.765 to 30.506°.	
Index ranges	$-21 \le h \le 21$, $-23 \le k \le 23$, $-22 \le l \le 22$	
Reflections collected	109814	
Independent reflections	11608 [R_{int} = 0.0308]	
Completeness to θ = 25.242°	99.90%	
Absorption correction	Semi-empirical from equivalents	
Refinement method	Full-matrix least-squares on F^2	
Data / restraints / parameters	11608 / 0 / 442	
Goodness-of-fit on F^2	1.056	
Final R indices [$I > 2\sigma_1$]	R_1 = 0.0232, w R_2 = 0.0588	
R indices (all data)	R_1 = 0.0282, w R_2 = 0.0615	
Largest diff. peak and hole	0.495 and -0.207 e/$Å^{-3}$	

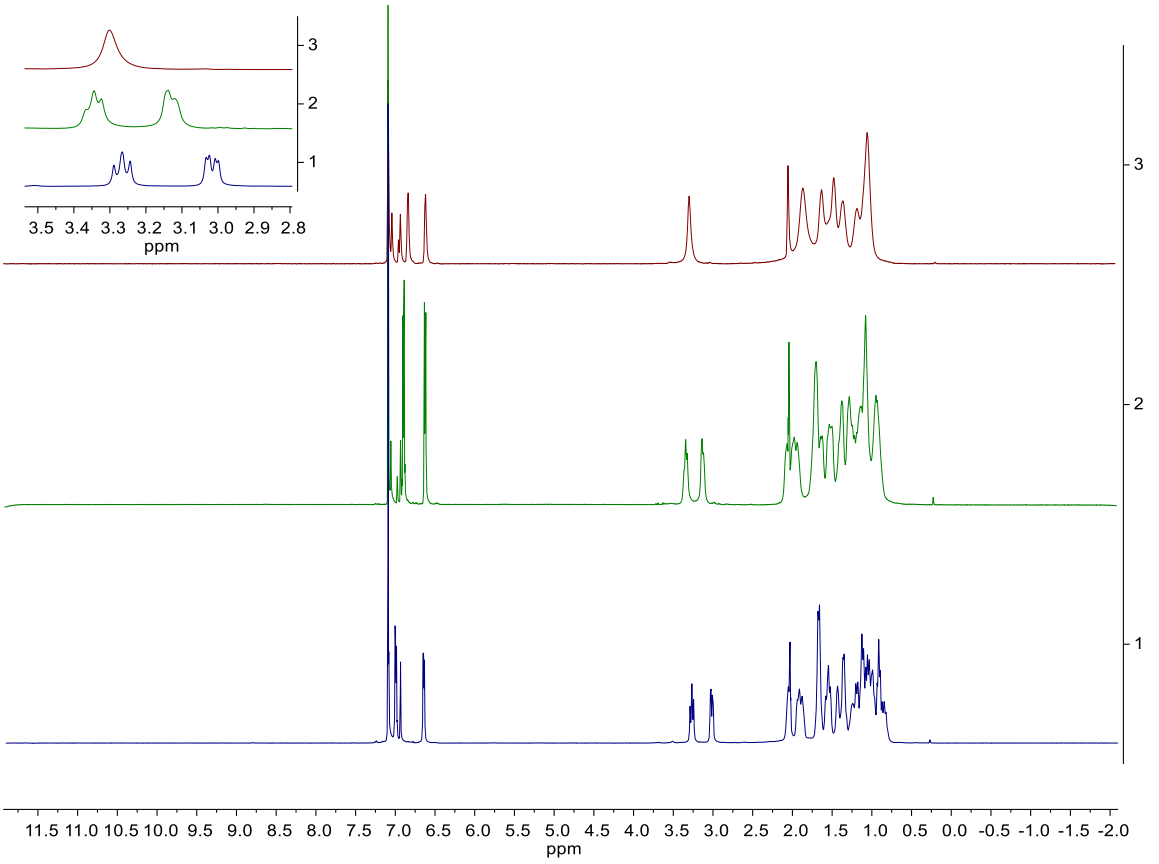

Figure 2.7-24 Variable temperature ^{1}H NMR of $SiCo_2P_2(CO)_5$, **7**, at selected temperatures in d_8-toluene at 500 MHz. Spectrum 1, 2 and 3 at –40 °C, +20 °C and +60 °C, respectively. Left top inset shows the methylene protons resolve at – 40 °C (bottom purple spectrum 1) and coalesce at +60 °C (top red spectrum 3).

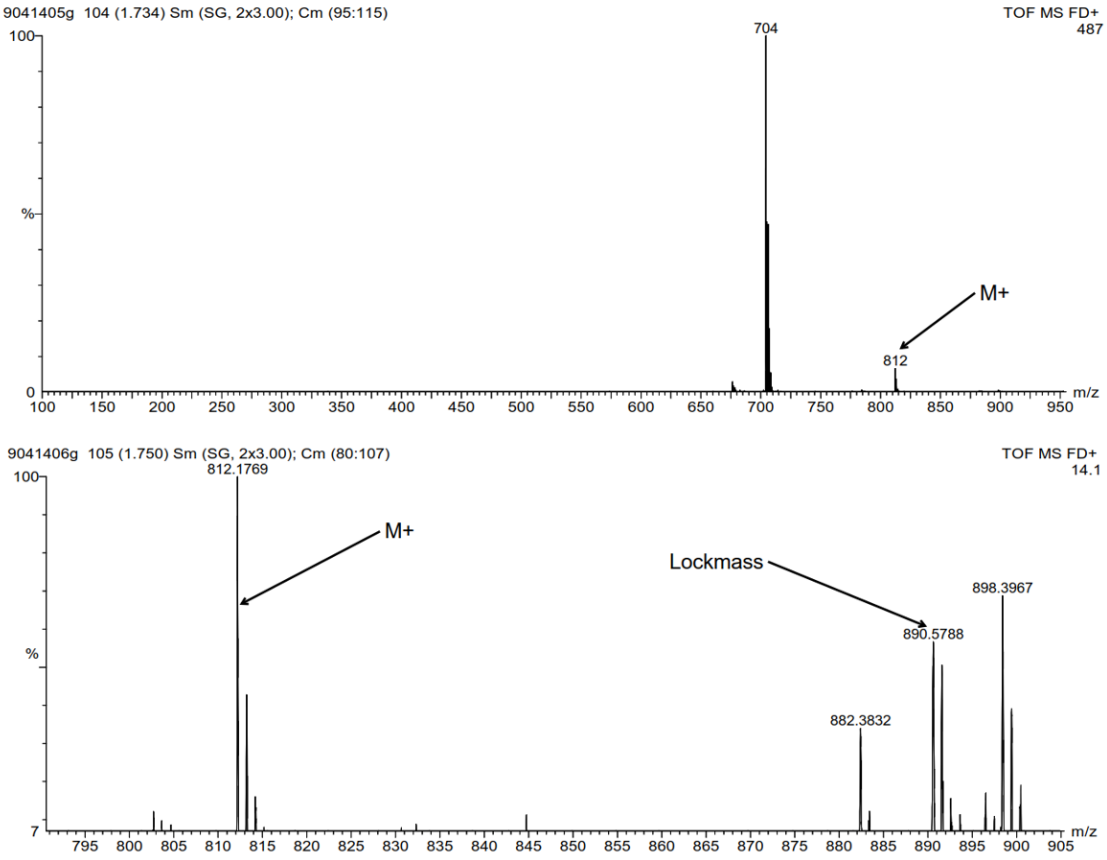

Figure 2.7-25 Mass Spectrometry for **7** operating in LIFDI mode.

CHAPTER 3 Reduction of Metal (II) Silyl Complexes

3.1 Abstract

The synthesis and isolation of monometallic M(II)–silyl complexes of Ni, Pd and Pt have been accessed by Si–Cl or Si–H bond activation and are discussed in Chapter 2 of this work. Reported here is the two-electron reduction of the Ni(II) and Pd(II)–silyl, **5** and **6**, respectively, which result in dimerization products to give dinickel and dipalladium disilylene complexes. The dinickel disilylene complex, $(P^{Cy})_4Ni_2Si_2$, features an asymmetric Ni_2Si_2 core with two phosphine donor atoms ligated to each nickel center and one bridging silylene ligated to each of the two Ni sites. In the presence of triphenylphosphine and reductant the monometallic Ni(0)–silylene can be accessed to give $(P^{Cy})_2SiNi(PPh_3)_2$ in good yield. The monometallic Ni(0)–silylene features a distorted tetrahedral Ni atom ligated to three phosphorous donor atoms and one silylene ligand that is distorted trigonal planar in geometry. The dipalladium disilylene complex $(P^{Cy})_4Pd_2Si_2$ is also introduced and its water addition product is reported.

3.2 Introduction

Isolable silylene ligands for the synthesis of TM-silylene complexes are largely attributed to the work of West, Denk, Driess, Roesky, Lappert and Tilley [1–9] Prior to many of these reports, it was the work of Zybill and coworkers in 1987 that demonstrated the potential of an isolable Fe–Silylene with stabilization provided by sterically bulky heteroatoms.[10]

Over the years a number of significant contributions have been made to further the TM–silylene field of study with classifications assigned in one of four ways as depicted in Figure 3.2-1.[7]

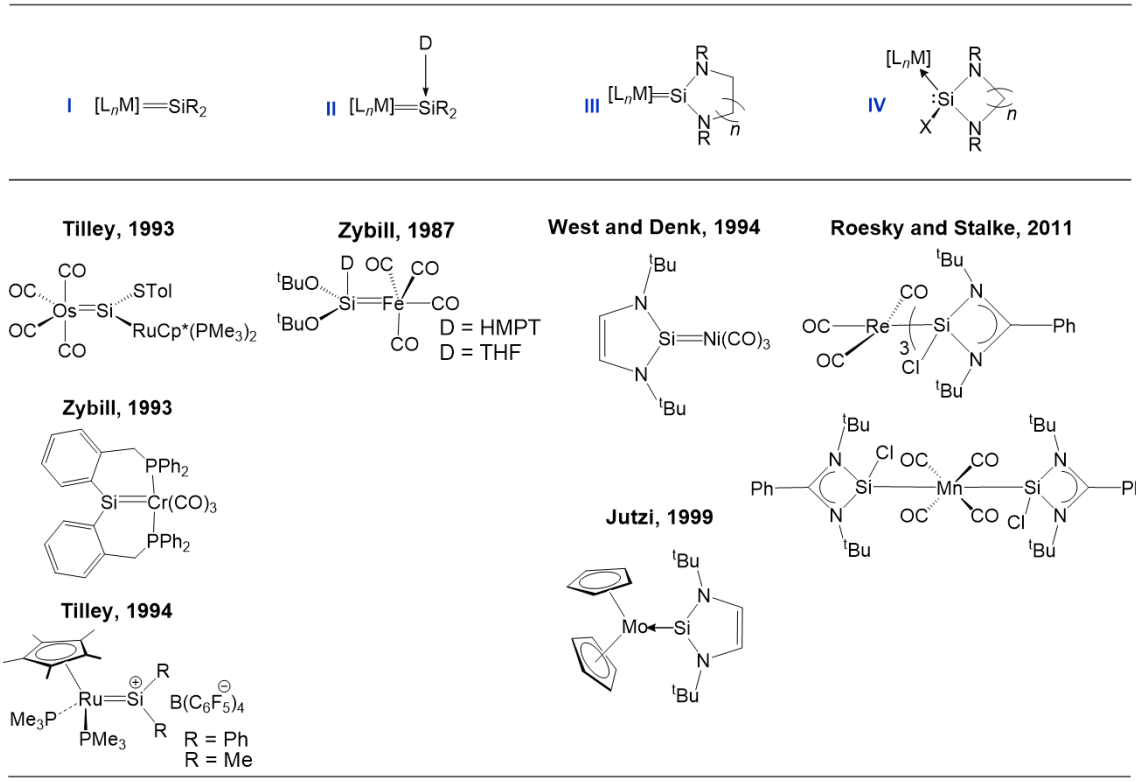

Figure 3.2-1. Transition metal–silylene classes featuring notable examples for each classification.

Type I represents the silicon analogue to Fisher (singlet carbene, with σ donation and π accepting abilities when bound to a metal), or Schrock (triplet carbene, σ and π donating abilities when bound to a metal) type carbene complexes. Type II represents a class of TM-silylene complexes which contain base-stabilized silylene ligands. TM–NHSi complexes are represented as Type III and IV. Type III includes those complexes with *n* representing some unsaturated backbone and Type IV featuring a halide or hydride stabilized silicon site with *n* representing a bulky aromatic or aliphatic group. With the work of Tilley and

co-workers in 1993 and 1994 the isolation of the first 'base-free' Osmium and Ruthenium silylene complexes were reported which can be classified as Type I.[1,11–13] Early work of Zybill and coworkers demonstrated the isolation of a Chromium–Silylene complex which was synthesized via photochemical 1,2-shift of the phospane ligands.[14] Additionally, in 1997 Tilley and coworkers demonstrated the cycloaddition of isocyanates with Rhodium–silylene complexes.[6] Denk, Hayashi and West reported in 1994 the structure and synthesis of donor free bis(silylene) complex, $[Ni\{(^{tBu}N–CH=CH–N^{tBu})Si\}_2\}(CO)_2]$, categorized as Type II and depicted in Figure 3.2-1. The latter capable of being isolated upon addition of a metal (0) source to free NHSi ligand.[2] In more recent years generation of the free silylene has been used by several investigators including the work of Aldridge who has developed novel silylenes and stannylenes capable of activating small molecules.[15,16] Bergman and Tilley have reported the synthesis and isolation of base free reactive silylene complexes of the form $[Cp^*(PMe_3)Ir(SiR_2)(H)][X]$, (X = OTf, R = Mes,; X = $B(C_6F_5)_4$, R = Ph), as reaction intermediates, the result of Si–H activation and silicon redistribution reactions in migration mechanisms from silicon to the metal center.[17] Transition metal N-heterocyclic silylenes which are base stabilized represents a fourth classification of TM-Silylene. Roesky and coworkers in 2006 reported the syntheses of Group 7 stable and isolable monomeric chlorosilylene complexes (Figure 3.2-1).[3,18]

Several synthetic routes to silylene complexes are possible some of which include; anionic substituent abstraction from a TM-silyl, coordination of free silylene to a M^0 source, and alpha hydrogen migration.[7,19,20] Additionally, in recent years NHCs have been used in the synthesis of novel TM–silylene complexes, most notably in the work of Inoue.[21]

Additionally, highlighted in the work of Baceiredo, Kato and Rodriguez is the report of a phosphine stabilized silylene hydrido complex, which are relatively rare.[22]

The first base free nickel (0) complex featuring two N-heterocyclic silylene ligands was reported by Denk, Hayashi and West in 1994.[2] Gehrhus and Lappert in 1997 followed this with the second base free Ni(0) complex featuring multiple silylene ligands. This involved the coordination of the free silylene, $Si[(NCH_2Bu^t)_2C_6H_4\text{-}1,2]$, to nickel and platinum with the use of $NiCl_2(PPh_3)_2$ and $PtCl_2(PPh_3)_2$. Fürstner and coworkers demonstrated a NHSi-Pd^0 complex featuring two silylene capable of Suzuki reactions in 2001.[23] With Inoue and coworkers came the first report of a novel bis(NHSi) ligand and went on to demonstrate its use as a precatalyst when coordinated to nickel for the formation of C–C bonds.[4,24] Recently in 2017 Driess reported a bis(NHSi) $Ni_2Si_2H_2$ complex for the hydrogenation of olefins.[25]

We report here the syntheses of base free nickel and palladium silylene complexes. Notably, the dinickel disilylene, $(P^{Cy})_4Ni_2Si_2$, features two bridging N-heterocyclic silylene ligands, one to each nickel site, with each nickel center additionally ligated to two phosphine donor atoms.

3.3 Results and Discussion

3.3.1 $(P^{Cy})_4Ni_2Si_2$ (**8**)

With the aim of synthesizing a TM–silylene complex, reduction of **4** was attempted. When an orange solution of **4** in benzene is treated with two equivalents of potassium naphthalenide an immediate color change to deep red is observed and within two hours a new broad resonance appears downfield from **4** (δ 67 ppm) at δ 84.73 ppm as a single

product. We were surprised to discover not a monometallic nickel-silylene as predicted, but rather the dimeric dinickel disilylene, $(P^{Cy})_4Ni_2Si_2$, **8**, as depicted in Figure 3.3-1.

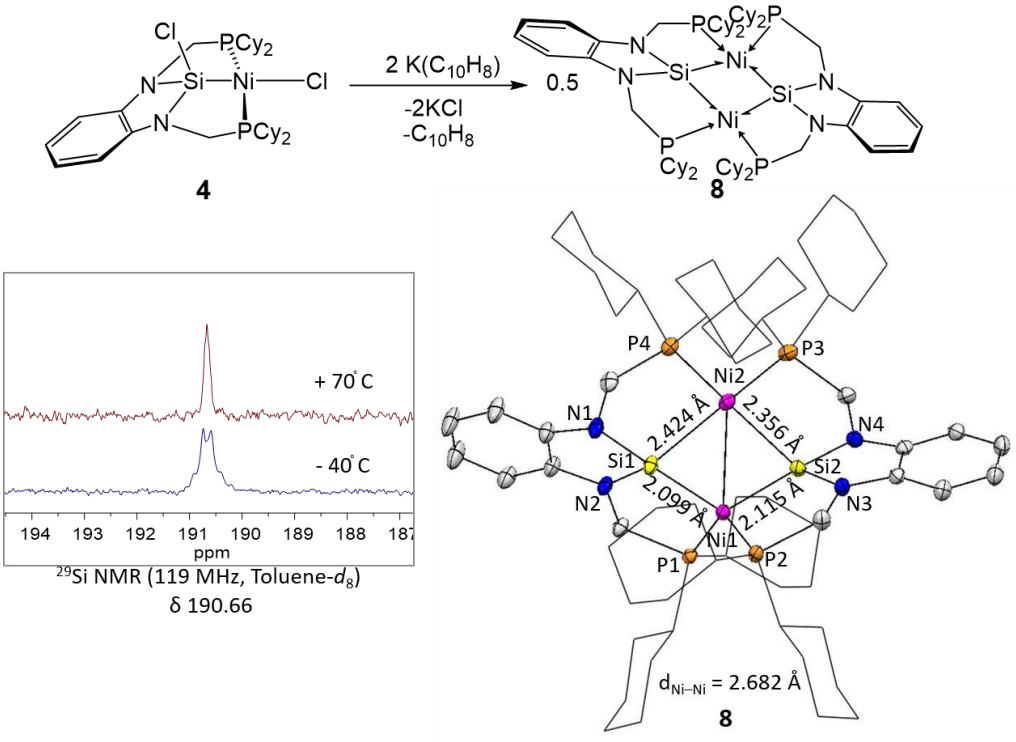

Figure 3.3-1. Synthesis of **8** via reaction of two equivalents of potassium naphthalenide to **4** (top). Magnified silicon resonance from direct $^{29}Si\{^1H\}$ NMR spectrum for **8** at selected temperatures (bottom left). XRD in ellipsoid representation of **8** at 50% probability featuring asymmetric core (bottom right). Notable bond lengths (Å): Ni(1)–Si(1) = 2.0989(6), Ni(1)–Si(2) = 2.1149(7), Ni(2)–Si(1) = 2.4245(7), Ni(2)–Si(2) = 2.3564(6), Ni(1)---Ni(2) = 2.6823(6), Ni(1)–P(1) = 2.1673(9), Ni(1)–P(2) = 2.1590(7), Ni(2)–P(3) = 2.2144(6) and Ni(2)–P(4) = 2.2011(6).

Potassium naphthalenide was the reductant of choice as repeated attempts with the reduction of **4** in the presence of excess potassium metal in benzene or sodium amalgam in THF resulted in mixtures of products, including the formation of a bridging $P_4Ni_2Si_2(\mu\text{-H})_2$ silyl dimer (discussed in Chapter 4). The solid-state structure revealed twined molecules, both featuring asymmetry in the two molecules of **8**, with similar bond distances. The asymmetry of **4** is revealed on the entire compound with two bridging

silylene ligands bonded to each nickel center with two phosphorus donors ligated to each of the nickel atoms. This asymmetry is highlighted in the bond lengths between the Ni and Si atoms within the core of the complex; Si(1) and Si(2) have short bond lengths to Ni(1) of 2.0989(6) and 2.1149(7) Å, respectively. In contrast longer bond lengths are revealed for Si(1) and Si(2) to Ni(2) as 2.4245(7) and 2.3564(6) Å, respectively. This shorter bond length is presumably attributed to the stronger π-donation from silicon to nickel as a dative interaction, while the longer bond lengths represent sigma character between nickel into the P_z orbital of silicon. Additionally, revealed in the solid-state structure of **8** is the varied coordination geometry about each nickel center. The calculated geometry index[26,27] for Ni(2) (τ_4 = 0.67 and τ_4' = 0.35) is suggestive of a geometry coordination consistent with a seesaw geometry, between square planar and tetrahedral. This is in contrast to Ni(1) which has a coordination geometry consistent with tetrahedral, (τ_4 = 0.85 and τ_4' = 0.83). The Ni–Si distances are consistent with previously reported Ni–silylene complexes but slightly shorter than the monometallic donor stabilized Si(II)X[$Ni(CO)_3$] (X = H and Cl) complexes reported by Driess which features Ni–Si distances ranging from 2.236(1) – 2.275(1) Å. These lengths are also similar to distances observed with the Ni–silylene complexes reported by Roesky.[28,29] Asymmetry is also revealed in the P–Ni distances suggesting stronger back donation within the shorter P–Ni bonds which have distances for P(1) and P(2) to Ni(1) of 2.1673(9) and 2.1590(7) Å, respectively. In contrast the distances for P(3) and P(4) ligated to Ni(2) are 2.2144(6) and 2.2011(6) Å, respectively. Further asymmetry is observed the PNiP angles within the solid-state structure of **8** with the larger as 122.69° and the smaller PNiP angles as 109.71 Å.

Additional views of the Ni_2Si_2 core of **8** in ellipsoid representation at 50 % probability can be seen in Figure 3.3-2. Highlighted is the asymmetry observed in the $P_4Ni_2Si_2$ core as revealed in the solid-state structure of **8**. The dinickel disilylene, **8**, features broad NMR spectroscopic data at room temperature. This broadness is attributed to an equilibrium process in the solution state in which an interconversion of the two nickel atoms is occurring within the Ni_2Si_2 core (Figure 3.3-2). The solid-state structure displays asymmetry for the PNiP angles as depicted in the diagram of Figure 3.3-2. Examination of the solid-state structure of **8** also reveals a C_2 axis of symmetry through the nickel centers (Figure 3.3-2). Given this, it was reasoned there must be an axis of symmetry perpendicular to the nickel centers through the silicon atoms. The variable temperature NMR studies of **8** confirm what is observed in the solid-state structure. At low temperature two resonances are revealed and indicative of two different phosphorous environments within **8**, while at low temperature the $^{29}Si\{^1H\}$ NMR displays one resonance at a δ 190 ppm. The resonance in the direct $^{29}Si\{^1H\}$ begins to exhibit splitting at low temperature likely due to coupling with the adjacent ^{31}P nuclei. A magnified view of the silicon resonance can be seen in Figure 3.3-1. The ^{31}P NMR confirms what is observed in the ^1H NMR variable temperature experiments. At –40 °C the ^1H NMR displays four sets of methylene proton resonances as diastereotopic while at high temperature they resolve into two sets of doublets at a δ = 3.83 (d, *J* = 11.2 Hz, 4H), and δ = 3.13 (d, *J* = 12.7 Hz, 4H, methine C-*H*), which is consistent with the observation for the two resonances observed in the ^{31}P NMR of **8** at the same low temperature.

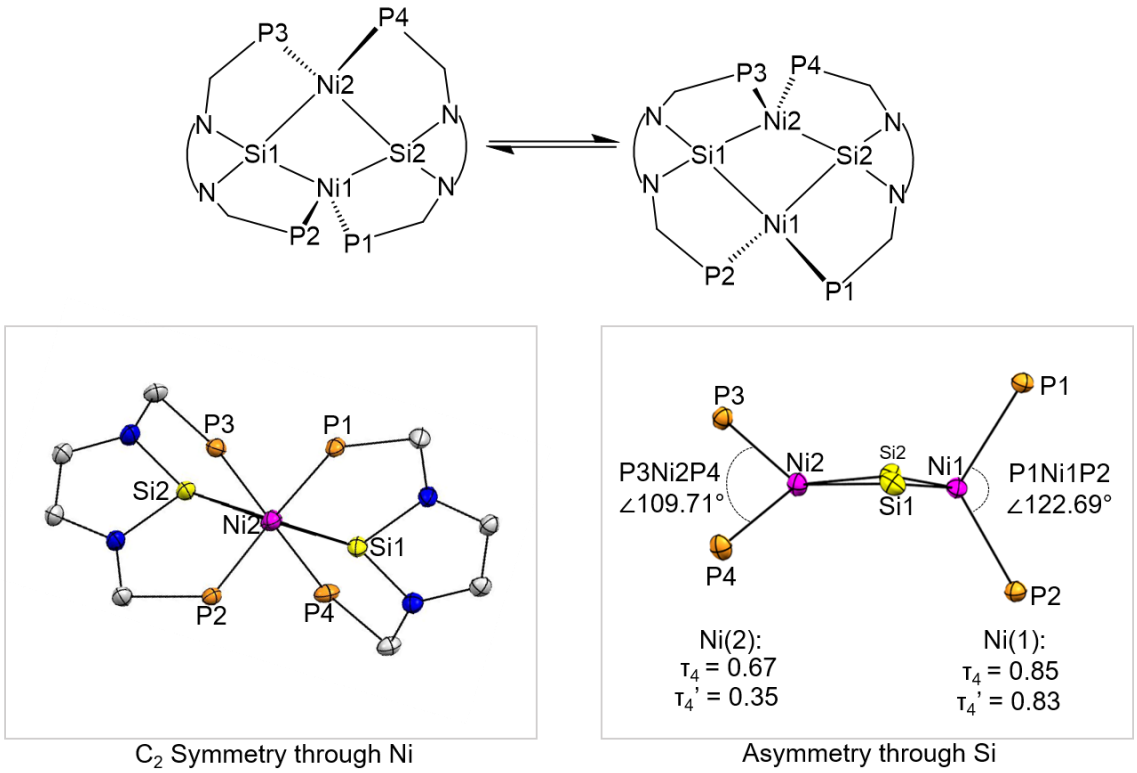

Figure 3.3-2. Representation of Ni_2Si_2 core demonstrating the equilibrium process of **8** in the solution state for interconversion of nickel centers (top). XRD data featuring core of **8** in thermal ellipsoid representation at 50% probability: view through the Ni2 atom reveals C_2 symmetry of the molecule (bottom left), and view through the Si2 atom demonstrating asymmetry in PNiP angles (°) in the solid-state structure (bottom right).

3.3.2 $(P^{Cy})_2SiNi(PPh_3)_2$ (**9**)

Given the dimerization of **8** in the absence of ancillary ligands or coordinating solvents the formation of a monometallic Ni^0–silylene complex was attempted in the presence of phosphine. When a solution of **4** is allowed to stir in the presence of excess triphenylphosphine (2.1 equivalents) followed treatment of two equivalents of potassium naphthalenide, the monometallic Ni^0-silylene, $(P^{Cy})_2SiNi(PPh_3)_2$, **9** is formed and isolated from concentrated toluene/hexane solution as a crystalline orange solid in 68% yield (Figure 3.3-3).

The additional 0.1 equivalents of triphenylphosphine was found to be necessary as two equivalents or less resulted in partial formation of **8** as evident by $^{31}P\{^{1}H\}$ NMR of the crude reaction mixture.

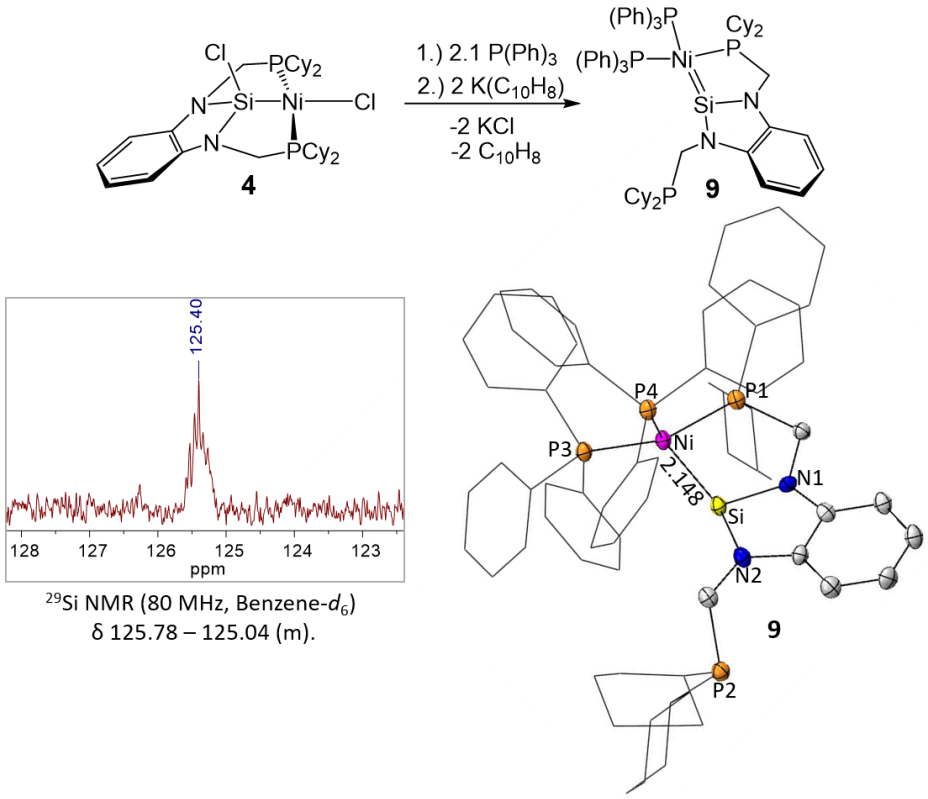

Figure 3.3-3 Synthesis of mono-metallic nickel–silylene **9** via reduction of **4** in the presence of triphenylphosphine (top). Magnified silicon resonance from direct $^{29}Si\{^{1}H\}$ NMR spectrum for **9** (bottom left). Ellipsoid representation of **9** at 50% probability (bottom right) with notable bond lengths (Å): Ni–Si = 2.148(1), Ni(1)–P(1) = 2.229(1), Ni(1)–P(3) = 2.206(1), Ni(1)–P(4) = 2.171(1), Si–N(1) = 1.753(3), Si–N(2) = 1.758(4). Selected angles (°): Si–Ni– P(1) = 86.02(4), Si–Ni– P(3) = 124.50(5), Si–Ni– P(4) = 97.97(5), P4–Ni– P1 = 113.53(4), P4–Ni– P3 = 110.14(4), P3–Ni– P1 = 121.17(4).

The ^{1}H NMR in C_6D_6 of **9** displays two resonances for the methylene protons at δ 3.81 (d, J = 4.5 Hz, 2H) and δ 2.92 (d, J = 4.6 Hz, 2H) with coupling due nearby ^{31}P nuclei. The $^{29}Si\{^{1}H\}$ NMR displays a resonance at δ 125.71 – 125.10 ppm in C_6D_6 as a multiplet with complex coupling to the nearby phosphorous atoms through the nickel center. A single

resonance in the direct $^{29}Si\{^{1}H\}$ NMR in C_6D_6 for **9** is shifted upfield indicating a more shielded silicon center when compared to that of **8** (+70 °C, δ 190.67 ppm, tol-d_8), but is at a similar resonance to nickel–silylene complexes reported independently in the laboratories of West and Driess.[30,31] The $^{31}P\{^{1}H\}$ NMR of **9** displays three resonances in C_6D_6 at δ 41.92 ppm (t, $J_{P–P}$ = 26.8 Hz), corresponding to one of the two dicyclohexylphosphine donors as still ligated to the nickel center, while the resonance at a δ 37.35 (d, $J_{P–P}$ = 26.5 Hz) is assigned to the two triphenylphosphine ancillary ligands, and a δ - 4.39 ppm, consistent with dissociation of one of the two dicyclohexylphosphine pincer arms, as this is displayed upfield as a single resonance with no coupling. In addition to NMR spectroscopic studies **9** was also examined by single crystal X-ray diffraction studies and an ellipsoid representation at 50% probability can be seen in Figure 3.3-3. The solid-state structure of **9** features a distorted tetrahedral, formally nickel (0) center, bonded to a distorted trigonal planar silicon. Additionally, the solid-state structure of **9** features Ni–Si bond length of 2.148(1) Å. This length is consistent with previously reported monometallic Ni–silylene complexes which have a significantly shorter bond length when viewed as a dative bond to a nickel center. For example, the nickel carbonyl silylene complex reported by West features a range of bond lengths between 2.207(2) and 2.216(2) Å.[2] Additionally, the monometallic nickel mixed chelated NHSi and NHC complex reported by Driess and co-workers in 2015 features a similar Ni–Si length (2.1740(18) Å)[32], of which is slightly longer than the Ni–Si length observed in **9** (2.148(1) Å). Though this short distance is typically associated with a dative bond between nickel and silicon, interestingly, the length

observed for **9** is similar to the Ni–Si distance observed in the covalent single bond revealed in the solid-state structure of **4**, which features a Ni–Si distance of 2.1468(5) Å.

Preliminary studies were done to investigate the reactivity of **9** with H_2, CO_2 and carbon monoxide. The reactivity of these small molecules with **9** afforded starting material, a mixture of various products, in addition to the presence of free triphenylphosphine by ^{31}P NMR. These results suggest the dissociation of the triphenylphosphine ancillary ligands as a slow process that could potentially be changed to increase reactivity by swapping to an appropriate ancillary ligand. With the intent of generating a more reactive mono-metallic nickel–silylene for the activation of small molecules the reduction of **4** was attempted in the presence of tricyclohexylphosphine. Initial attempts appeared promising by ^{31}P NMR of the crude reaction mixture; however, recrystallization attempts to isolate a monometallic metal–silylene complex with tricyclohexylphosphine as an ancillary ligand resulted in the dissociation of the tricyclohexylphosphine and the formation of **8** by $^{31}P\{^{1}H\}$ NMR post work-up. The reduction of **4** was also done in the presence tritertbutylphosphine and 1, 2-bis(diphosphino)ethane (DPPE). The reduction in the presence of tritertbutylphosphine was inconclusive. However, the reduction of **4** in the presence of DPPE followed by addition of potassium naphthalenide revealed three resonances in the ^{31}P NMR. Multiple attempts to isolate the compound proved difficult and the ^{31}P NMR was not consistent. The inconsistency in the formation of a single trapped product is likely due to the coordination geometry around nickel with DPPE converting from four coordinate tetrahedral Ni to square planar Ni given the coordinating and free motion of the DPPE ligand. This is in contrast to the geometry of **9** which displays a nickel center that is four-coordinate distorted

tetrahedral with stabilization provided by increased steric restraints of the triphenylphosphine ancillary ligands. The metal complex with DPPE was not fully characterized as a result, however, ^{1}H NMR and ^{31}P NMR spectroscopic data clearly indicate the DPPE is bound at the nickel center. This is suggested by the coupling evident in the ^{31}P NMR spectrum which displays four resonances as predicted: a triplet at a δ 78.03 ppm, two resonances at a δ 38.18 ppm and 38.09 ppm with slight coupling exhibited, assigned the DPPE ancillary ligands, and suggestive of the phosphorus atom within the DPPE ligand, in addition to a single upfield resonance at δ –13.28 ppm assigned to of one of the free and hemilabile dicyclohexylphosphine chelating arms. (Figure 3.3-4).

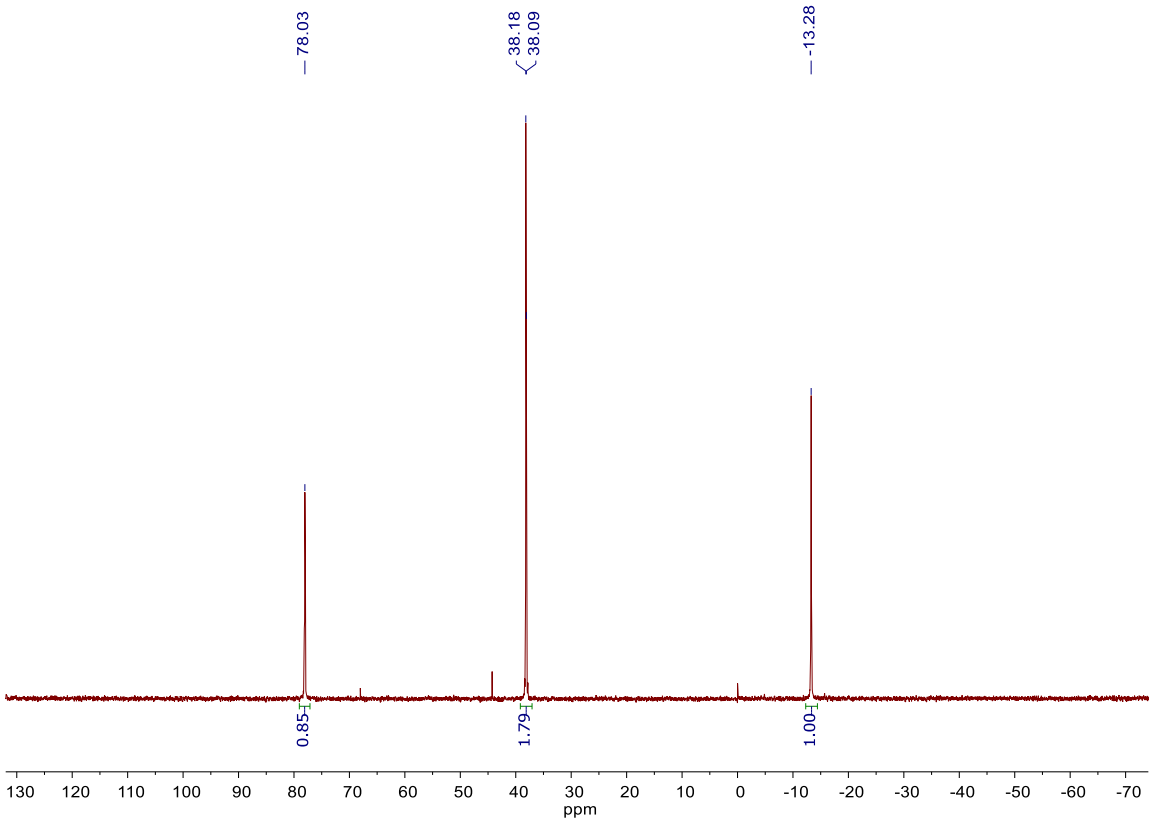

Figure 3.3-4. $^{31}P\{^{1}H\}$ NMR of DPPE trapped monometallic Ni–silylene.

Despite multiple attempts to unsuccessfully isolate the DPPE metal complex for full characterization, isolation of the triphenylphosphine mono-metallic nickel silylene , **9**, proved successful. Continued efforts could focus in finding appropriate ancillary donors to trap a monometallic nickel complex which would potentially be more reactive towards small molecules such as dihydrogen, carbon monoxide and carbon dioxide.

3.3.3 $(P^{Cy})_4Pd_2Si_2$ (**10**)

Given the ability of **4** to generate **8** as a dimer the reduction of **5** was pursued. Upon addition of two equivalents of potassium naphthalenide in either THF or benzene a new broad resonance is evident in the ^{31}P NMR, closely overlapping with the sharp resonance of **5** ($^{31}P\{^1H\}$ NMR = δ 74.30 ppm). A reaction time o two hours by $^{31}P\{^1H\}$ NMR revealed **5** had been consumed. This new broad resonance was suggestive of the formation of bimetallic pallidum analogue, **10**, to that of **8**. The $^{31}P\{^1H\}$ NMR and ^1H NMR spectroscopic data at room temperature for **10** featured broad spectroscopic resonances, similar to room temperature spectroscopic data for **8**. This suggested **10** had dynamic behavior in the solution state similar to that of **8**. To investigate this further variable temperature $^{31}P\{^1H\}$ NMR experiments were carried out and revealed a coalescence point as single resonance for **10** at δ 72.42 at + 30 °C in d_8-toluene. Additionally, at a low temperature of –20 °C the peak resolves and sharpens to reveal two resonances at δ 77.95 and 67.15 ppm, confirming the presence of two different phosphorous environments (Figure 3.3-5). This data is consistent to what is observed for **8** in the solution state, suggesting evidence for the successful synthesis of the dimeric dipalladium disilylene, **10**.

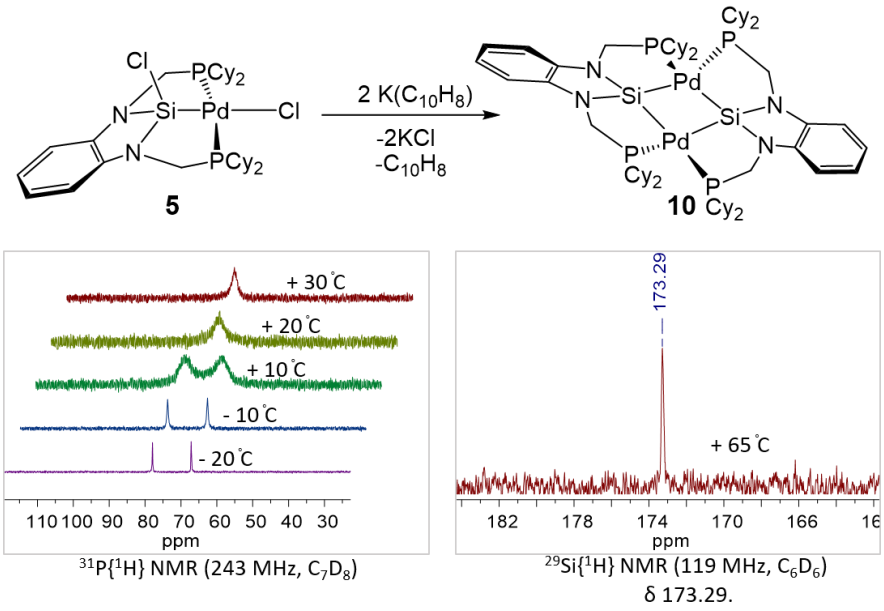

Figure 3.3-5. Synthesis of $(P^{Cy})_4Pd_2Si_2$, **10**, the result of addition of two equivalents of potassium naphthalenide to **5** (top scheme). VT $^{31}P\{^1H\}$ NMR at selected temperatures (bottom left). Magnified $^{29}Si\{^1H\}$ NMR of silicon resonance for **10** at +65 °C in C_6D_6 (bottom right).

The ^1H NMR spectroscopic data corroborates what is revealed in the variable temperature $^{31}P\{^1H\}$ NMR experiments, which displays two resonances at a δ 3.87 and 3.17 ppm for two sets of methylene protons at a temperature of +30 C in d_8-toluene in the ^1H NMR. These resonances split to display four resonances at a low temperature of –20 °C. The $^{29}Si\{^1H\}$ NMR for **10** reveals a resonance at a δ +173.29 ppm at a temperature of +65 °C which is significantly downfield shifted from the precursor **5** (δ +63.73 in C_6D_6). Preliminary reactivity carried with **10** in the presence of excess carbon dioxide revealed promising results but with dihydrogen fewer promising results, both of which are briefly described in Chapter 4 of this work. It is worth noting attempts to characterize **10** by single crystal XRD analysis proved difficult and instead resulted in the isolation of the water addition product for **10** (Figure 3.3-6)

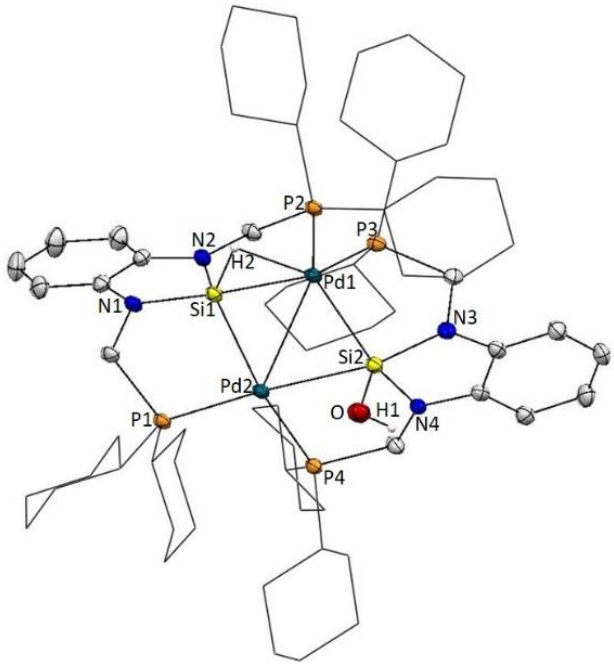

Figure 3.3-6. XRD data in ellipsoid representation for the water addition product, **10-H_2O**, at 50% probability. Notable distances (Å): Si(1)–Pd(1) = 2.317(1), Si(1)–Pd(2) = 2.3524(9), Si(2)–Pd(1) = 2.3657(9), Si(2)–Pd(2) = 2.640(1), Pd(1)---Pd(2) = 2.8347(5), Si(1)–H(2) = 1.54(4), Pd(1)–H(2) = 1.86(3), Si(2)–O = 1.688(2), O–H(1) = 1.688(2), Pd(1)–P(3) = 2.3157(9), Pd(1)–P(2) = 2.4033(7), Pd(2)–P(1) = 2.3227(9), Pd(2)–P(4) = 2.377(1), Si(1)–N(1) = 1.776(3), Si(1)–N(2) = 1.762(2), Si(2)–N(4) = 1.797(3), Si(2)–N(3) = 1.810(3). Selected angles (°): Pd(2)–Si(1)– Pd(1) = 74.75(3), Pd(1)–Si(2)– Pd(2) = 68.74(2), Si(1)–Pd(1)– Si(2) = 113.35(3), Si(1)–Pd(2)– Si(2) = 103.07(3), P(2)–Pd(1)– P(3) = 113.82(3), P(1)–Pd(2)– P(4) = 112.67(3), Si(1)–H(2)– Pd(1) = 85(1), H(2)–Pd(1)– Si(1) = 42(1), H(2)–Si(1)– Pd(1) = 53(1).

It is also noted a more careful and detailed report of **10** and its reactivity may be found in the dissertation of my fellow lab co-worker, Marissa Barrientos.

3.4 Concluding Remarks

We have successfully demonstrated the access to novel TM–silylene complexes, **8**, **9** and **10**, via the reduction of M(II)–silyl complexes **4** and **5**. The asymmetry observed in the solid-state structure of **8** suggests interesting bonding between the molecular orbitals of Ni and Si atoms within the core of the complex. A Natural Bond Order (NBO) analysis may provide insight into the type of bonding that occurs within the core and offer insight for the unusual asymmetric bond lengths observed in the solid-state single molecule

structure of **8**. Furthermore, we have demonstrated it is possible to trap a single nickel fragment, prior to its dimerization to form **8**, in the presence of ancillary phosphine ligands which results in the formation of the monometallic complex **9**. This monomer represents a trapped nickel fragment, prior to dimerization, which reacts with itself to form the bridging dinickel disilylene complex **8**. Each TM–silylene complex **8**, **9** and **10** have interesting spectroscopic features, most notably the downfield shift observed in the direct $^{29}Si\{^{1}H\}$ of **8** (δ 190.67) versus **9** (δ 125.71 – 125.10 (m)). The downfield shift observed for **8** is presumably attributed to the presence of a second nickel center resulting in a more deshielded silicon nucleus in contrast to **9** which only has one nickel center. Additionally, and expectedly, the Pd–silylene features a resonance similar to that of **8** within the $^{29}Si\{1H\}$ NMR.

3.5 Syntheses of Transition Metal–Silylene Complexes **8**, **9** and **10**

3.5.1 Standard Synthetic Methods and Materials

Standard synthetic methods and materials are the same as reported for Chapter 1 and 2.

3.5.2 $(P^{Cy})_4Ni_2Si_2$ (**8**)

A 200 mL round bottom flask was charged with 0.999 g of **4** (1.46 mmol) and dissolved in 100 mL benzene. Potassium naphthalenide, 0.673 g (2.92 mmol) was added slowly added in 3 portions. After one hour and thirty minutes the reaction was complete by ^{31}P NMR. The reaction mixture was filtered through a pad of Celite and the filtrate concentrated down to 20 mL. To the saturated solution of benzene, 100 mL hexane was added, the filtrate concentrated down to 30 mL and the solution was allowed to stand at –35 °C for 12 hours. The bronze microcrystalline solid was collected using a fine frit and washed with 2×5 mL

of cold hexane. After second crop collection 0.4531 g (51% yield) was obtained. Crystals suitable for X-ray were grown from concentrated benzene with hexane layering. ^{1}H NMR (600 MHz, Toluene-d_8) δ 6.84 (dt, *J* = 6.8, 3.4 Hz, 4H, Aryl-*H*), 6.75 (dt, *J* = 6.7, 3.4 Hz, 4H, Aryl-*H*), 3.83 (d, *J* = 11.2 Hz, 4H, methine C-*H*), 3.13 (d, *J* = 12.7 Hz, 4H, methine C-*H*), 2.02 (d, *J* = 13.4 Hz, 5H, cyclohexyl C-*H*), 1.90 – 1.78 (m, 8H, cyclohexyl C-*H*), 1.74 (d, *J* = 11.6 Hz, 9H, cyclohexyl C-*H*), 1.71 – 1.61 (m, 10H, cyclohexyl C-*H*), 1.61 – 1.51 (m, 6H, cyclohexyl C-*H*), 1.50 – 1.41 (m, 3H, cyclohexyl C-*H*), 1.35 – 1.20 (m, 15H, cyclohexyl C-*H*), 1.15 (ddt, *J* = 25.1, 12.4, 3.4 Hz, 8H, cyclohexyl C-*H*), 1.10 – 1.01 (m, 4H, cyclohexyl C-*H*), 0.95 (q, *J* = 13.1 Hz, 5H, cyclohexyl C-*H*). ^{31}P{^{1}H} NMR (202 MHz, Toluene-d_8) +70 °C, δ 84.73. ^{29}Si{^{1}H} NMR (119 MHz, Toluene-$d_{8,}$) +70 °C, δ 190.67. ^{13}C NMR (151 MHz, Toluene-d_8) +70 °C, δ 143.24 (Aryl-C), 117.77 (Aryl-C), 108.24 (Aryl-C), 39.82 (methine C), 39.50 (methine C), 37.55 (cyclohexyl C), 30.59 (cyclohexyl C), 30.48(cyclohexyl C), 29.94 (cyclohexyl C), 28.38 (cyclohexyl C), 28.08 (cyclohexyl C), 27.89 (cyclohexyl C), 27.18 (cyclohexyl C). Accurate Mass Predicted for $C_{64}H_{104}N_4Ni_2P_4Si_2$: 1224.5457. Mass found for $C_{64}H_{104}N_4Ni_2P_4Si_2$ by LIFDI: [M^+]: 1226.5. An accurate mass was not obtained given the high molecular weight, however, the predicated isotopic pattern matched well with the observed. Elemental Analysis predicted for $C_{64}H_{104}N_4Ni_2P_4Si_2$: C, 62.65; H, 8.54; N, 4.57. Elemental Analysis found for $C_{64}H_{104}N_4Ni_2P_4Si_2$: C, 62.80; H, 8.34; N, 4.42.

3.5.3 $(P^{Cy})_2SiNi(PPh_3)_2$ (**9**)

In a 20 mL scintillation vial, with stir bar, 0.100 g (0.146 mmol) of **4** was added. Triphenylphosphine, 0.085 g (0.307 mmol) dissolved in minimum benzene was added to a

solution of **4** and allowed to stir for several minutes. To this homogenous mixture 0.067 g (0.292 mmol) of potassium naphthalenide was added in three small portions. The vial containing potassium naphthalenide was rinsed with 0.5 mL of benzene to ensure all was transferred. After 3 hours the reaction was complete by ^{31}P NMR. The mixture was filtered through Celite and solvent removed in *vacuo*. Minimum toluene was added (1 mL), followed by 6 mL hexane. After sitting at room temperature overnight, orange crystalline solid was collected on paper tipped pipet and washed with 3 x 1mL hexane followed by 3 x 1 mL of ether to give 0.113 g of **9** as an orange solid in 68 % yield after first crop collection. ^{1}H NMR (600 MHz, Benzene-d_6) δ 7.57 (td, *J* = 8.6, 7.9, 3.1 Hz, 12H), 7.32 – 7.27 (m, 1H), 7.12 – 7.07 (m, 2H), 7.06 – 6.96 (m, 19H), 6.84 – 6.80 (m, 1H), 3.81 (d, *J* = 4.5 Hz, 2H), 2.92 (d, *J* = 4.6 Hz, 2H), 2.07 – 1.94 (m, 4H), 1.93 – 1.83 (m, 5H), 1.83 – 1.77 (m, 2H), 1.74 (td, *J* = 11.3, 10.6, 2.2 Hz, 2H), 1.70 – 1.55 (m, 5H), 1.54 – 1.32 (m, 13H), 1.30 – 1.13 (m, 6H), 1.06 (ddt, *J* = 16.2, 12.8, 3.5 Hz, 3H), 0.75 (qt, *J* = 12.9, 3.7 Hz, 2H). ^{31}P{^{1}H} NMR (243 MHz, Benzene-d_6) δ 41.92 (t, *J* = 26.8 Hz), 37.35 (d, *J* = 26.5 Hz), -4.39 (s). ^{29}Si{^{1}H} NMR (80 MHz, Benzene-d_6) δ 125.71 – 125.10 (m). ^{13}C NMR (151 MHz, C_6D_6) δ 143.55, 141.71, 141.34, 134.89, 134.68, 129.40, 129.13, 119.10, 118.34, 110.85, 109.19, 43.03, 40.67, 39.55, 34.45, 31.32, 30.77, 30.48, 28.39, 27.59, 26.93. Elemental Analysis predicted for $C_{68}H_{82}N_2NiP_4Si$: 71.76, 7.26, 2.46, Elemental Analysis found for $C_{68}H_{82}N_2NiP_4Si$: 71.90, 7.38, 2.21.

3.5.4 $(P^{Cy})_4Pd_2Si_2$ (**10**)

A 20 mL scintillation vial was charged with 0.050 g of **5** (0.068 mmol) and dissolved in 10 mL benzene. Potassium naphthalenide, 0.031 g (0.136 mmol), was added slowly in three

portions. After two hours the reaction was complete by $^{31}P\{^{1}H\}$ NMR. The reaction mixture was filtered through a pad of Celite and solvent removed in *vacuo*. The residue was extracted with ether, filtered through Celite a second time and allowed to stand for 12 hours at –35 C. The yellow/green microcrystalline solid was collected on a paper tipped pipet and washed with 4×2 mL of cold ether. After second crop collection, 0.0331 g (74 % yield) of **10** was obtained as a light green/yellow (dichromic) crystalline solid. ^{1}H NMR (600 MHz, d_8-Tol, +30 °C) δ 3.87 (br s), 3.17 (br, s). Note that methylene resonances are reported only and due to poor resolution coupling was not observed. ^{31}P NMR (243 MHz, d_8-Tol, +30° C) δ 72.42. ^{13}C NMR (151 MHz, Benzene-d_6, +65 °C) δ 142.87, 117.72, 108.11, 39.24 (t, J = 12.1 Hz), 38.30, 35.90, 30.02, 29.55, 28.12 (d, J = 18.8 Hz), 27.89 – 27.41 (m), 26.98 (d, J = 17.3 Hz). $^{29}Si\{^{1}H\}$ NMR (119 MHz, C_6D_6, 65 °C) δ 173.29.

3.6 References

(1) Gehrhus, B.; Hitchcock, P. B.; Lappert, M. F.; Maciejewski, H. *Organometallics* **2002**, *17* (26), 5599–5601.

(2) Denk, M.; Hayashi, R. K.; West, R. *J. Chem. Soc., Chem. Commun.* **1994**, 33–34.

(3) So, C. W.; Roesky, H. W.; Magull, J.; Oswald, R. B. *Angewandte Chemie - International Edition* **2006**, *45* (24), 3948–3950.

(4) Wang, W.; Inoue, S.; Yao, S.; Driess, M. *Journal of the American Chemical Society* **2010**, *132* (45), 15890–15892.

(5) Raoufmoghaddam, S.; Zhou, Y.-P.; Wang, Y.; Driess, M. *Journal of Organometallic Chemistry* **2017**, *829*, 2–10.

(6) Mitchell, G. P.; Tilley, T. D. *Journal of the American Chemical Society* **1997**, *119* (46), 11236–11243.

(7) Blom, B.; Stoelzel, M.; Driess, M. *Chemistry - A European Journal* **2013**, *19* (1), 40–62.

(8) Corey, J. Y. *Chemical Reviews* **2016**, *116* (19), 11291–11435.

(9) Blom, B.; Gallego, D.; Driess, M. *Inorganic Chemistry Frontiers* **2014**, *1* (2), 134.

(10) Zybill, C.; Müller, G. *Angewandte Chemie International Edition in English* **1987**, *26* (7), 669–670.

(11) Grumbine, S. K.; Tilley, T. D.; Arnold, F. P.; Rheingold, A. L. *J. Am. Chem. Soc* **1994**, *116*, 5495–5496.

(12) Grumbine, Steven D., Tilley, D. T. *J. Am. Chem. Soc* **1993**, *115*, 360–361.

(13) Grumbine, S. D.; Tilley, T. D.; Arnold, F. P.; Rheingold, A. L. *J. Am. Chem. Soc.* **1993**, *115* (17), 7884–7885.

(14) Handwerker, Hermann; Paul, Martin; Blumel, Janet; Zybill, C. *Angew. Chem., Int. Ed. Engl* **1993**, *32* (9), 1313–1315.

(15) Protchenko, A. V.; Bates, J. I.; Saleh, L. M. A.; Blake, M. P.; Schwarz, A. D.; Kolychev, E. L.; Thompson, A. L.; Jones, C.; Mountford, P.; Aldridge, S. *Journal of the American Chemical Society* **2016**, *138* (13), 4555–4564.

(16) Protchenko, A. V; Birjkumar, K. H.; Dange, D.; Schwarz, A. D.; Vidovic, D.; Jones, C.; Kaltsoyannis, N.; Mountford, P.; Aldridge, S. *J. Am. Chem. Soc* **2012**, *134*, 6503.

(17) Klei, S. R.; Don Tilley, T.; Bergman, R. G. *Organometallics* **2002**, *21* (16), 3376–3387.

(18) Azhakar, R.; Sarish, S. P.; Roesky, H. W.; Hey, J.; Stalke, D. *Inorg. Chem* **2011**, *50*, 5039–5043.

(19) Waterman, R.; Hayes, P. G.; Tilley, T. D. *Accounts of Chemical Research* **2007**, *40* (8), 712–719.

(20) Asay, M.; Jones, C.; Driess, M. *Chemical Reviews* **2011**, *111* (2), 354–396.

(21) Inoue, S.; Eisenhut, C. *Journal of the American Chemical Society* **2013**, *135* (49), 18315–18318.

(22) Gau, D.; Rodriguez, R.; Kato, T.; Saffon-Merceron, N.; De Cózar, A.; Cossío, F. P.; Baceiredo, A. *Angewandte Chemie - International Edition* **2011**, *50* (5), 1092–1096.

(23) Fürstner, A.; Krause, H.; Lehmann, C. W. *Chemical Communications* **2001**, *1* (22), 2372–2373.

(24) Enthaler, S.; Haberberger, M.; Wang, W.; Someya, C. I.; Inoue, S. *Chemistry Letters* **2013**, *42* (3), 286–288.

(25) Wang, Y.; Kostenko, A.; Yao, S.; Driess, M. *Journal of the American Chemical Society* **2017**, *139* (38), 13499–13506.

(26) Okuniewski, A.; Rosiak, D.; Chojnacki, J.; Becker, B. *Polyhedron* **2015**, *90*, 47–57.

(27) Yang, L.; Powell, D. R.; Houser, R. P. *Dalton Transactions* **2007**, No. 9, 955–964.

(28) Stoelzel, M.; Präsang, C.; Inoue, S.; Enthaler, S.; Driess, M. *Angewandte Chemie International Edition* **2012**, *51* (2), 399–403.

(29) Tavčar, G.; Sen, S. S.; Azhakar, R.; Thorn, A.; Roesky, H. W. *Inorganic Chemistry* **2010**, *49* (21), 10199–10202.

(30) Hadlington, T. J.; Szilvási, T.; Driess, M. *Angewandte Chemie - International Edition* **2017**, *56* (45), 14282–14286.

(31) Schmedake, T. A.; Haaf, M.; Paradise, B. J.; Powell, D.; West, R. *Organometallics* **2000**, *19* (17), 3263–3265.

(32) Tan, G.; Driess, M.; Enthaler, S.; Inoue, S.; Blom, B. *Angewandte Chemie International Edition* **2015**, *54* (7), 2214–2218.

3.7 Spectroscopic Data, Figures and Tables

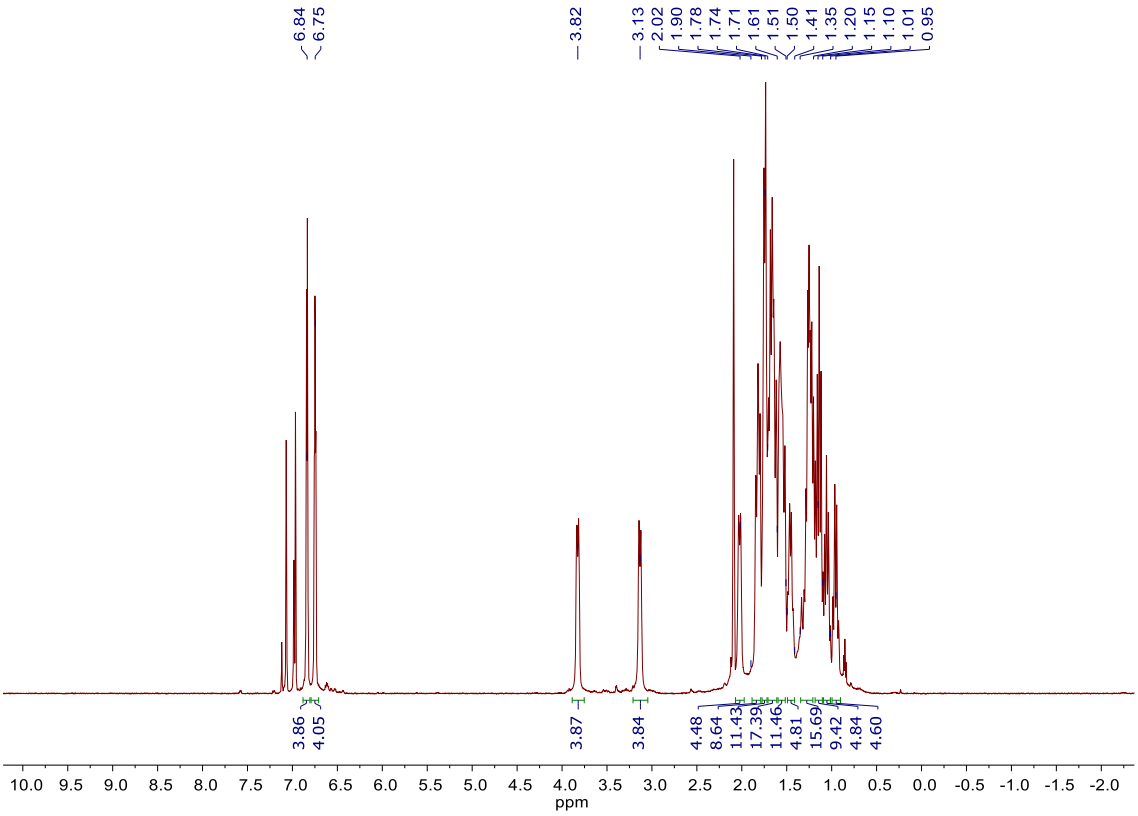

Figure 3.7-1. ^{1}H NMR of $(P^{Cy})_4Ni_2Si_2$, **8**, at +70 °C in d_8-toluene at 600 MHz.

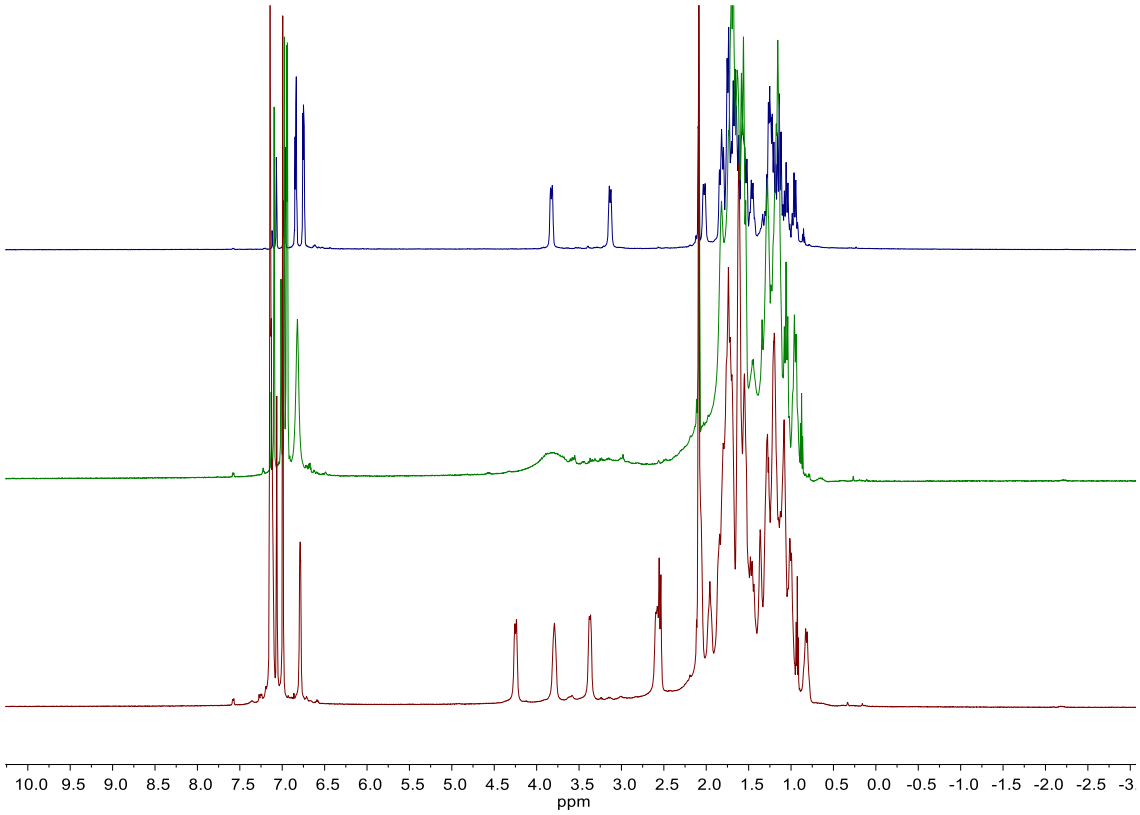

Figure 3.7-2 VT ^{1}H NMR of $(P^{Cy})_4Ni_2Si_2$, **8**, at selected temperatures; top, +70 °C, middle, +20 °C and bottom spectrum, –40 °C in d_8-toluene at 500 MHz.

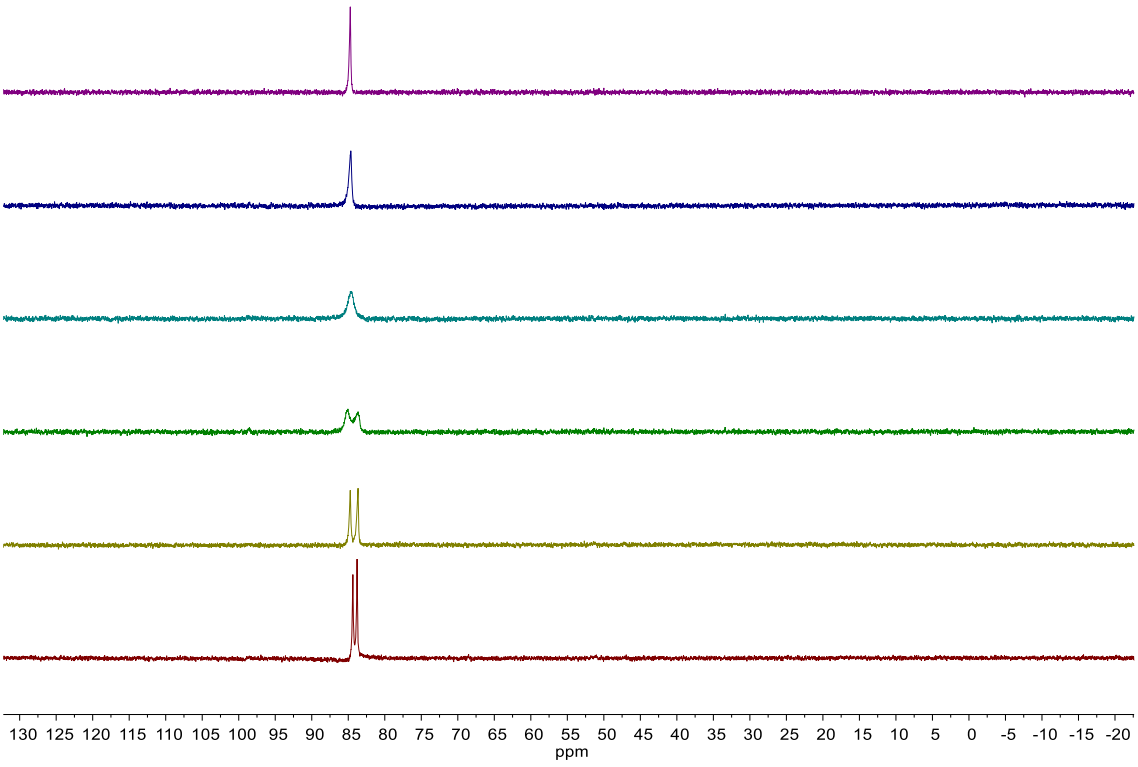

Figure 3.7-3 VT $^{31}P\{^{1}H\}$ NMR for $(P^{Cy})_4Ni_2Si_2$, **8**, at 202 MHz with selected temperatures in d^8-toluene at +70 °C (top spectrum), +40 °C, +18 °C, –15 °C, –21 °C and –40 °C (bottom spectrum), respectively.

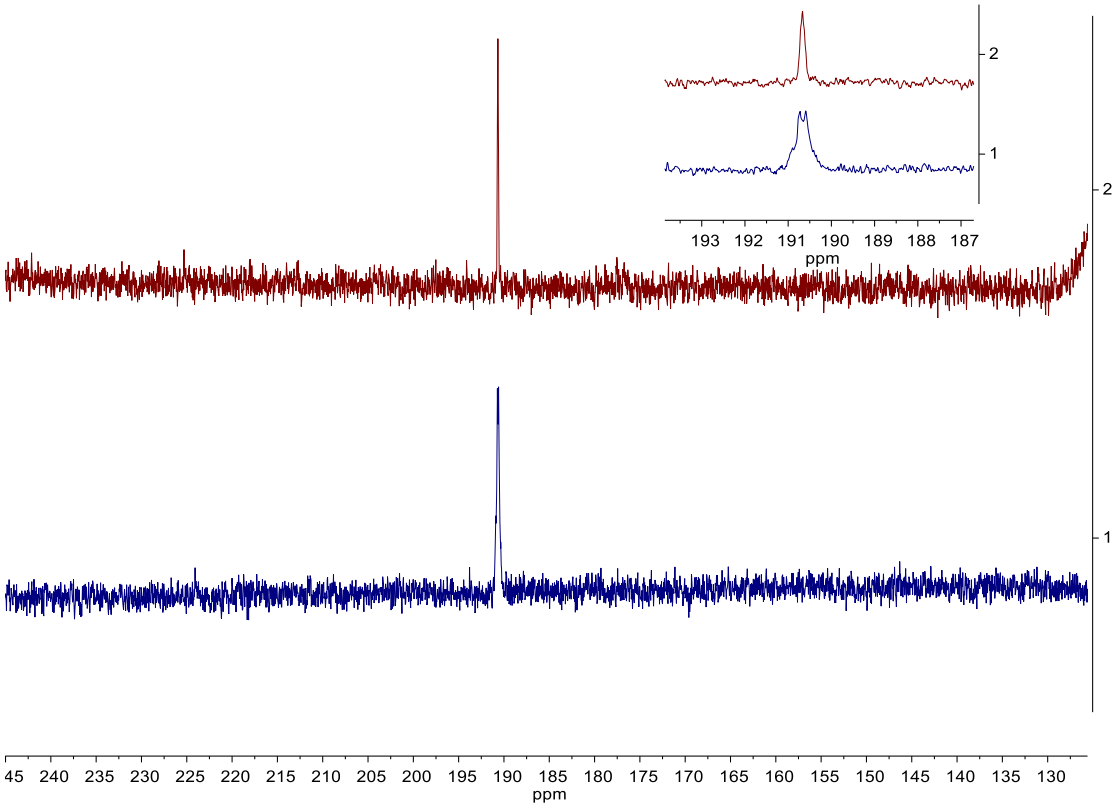

Figure 3.7-4 $^{29}Si\{^{1}H\}$ NMR of $(P^{Cy})_4Ni_2Si_2$, **8**, at +70 °C (top spectrum) and –40°C (bottom spectrum) in toluene-d^8 at 119 MHz. A single resonance is revealed at a δ 190.66 ppm with splitting evident and due to ^{29}Si coupling to the ^{31}P nearby nuclei.

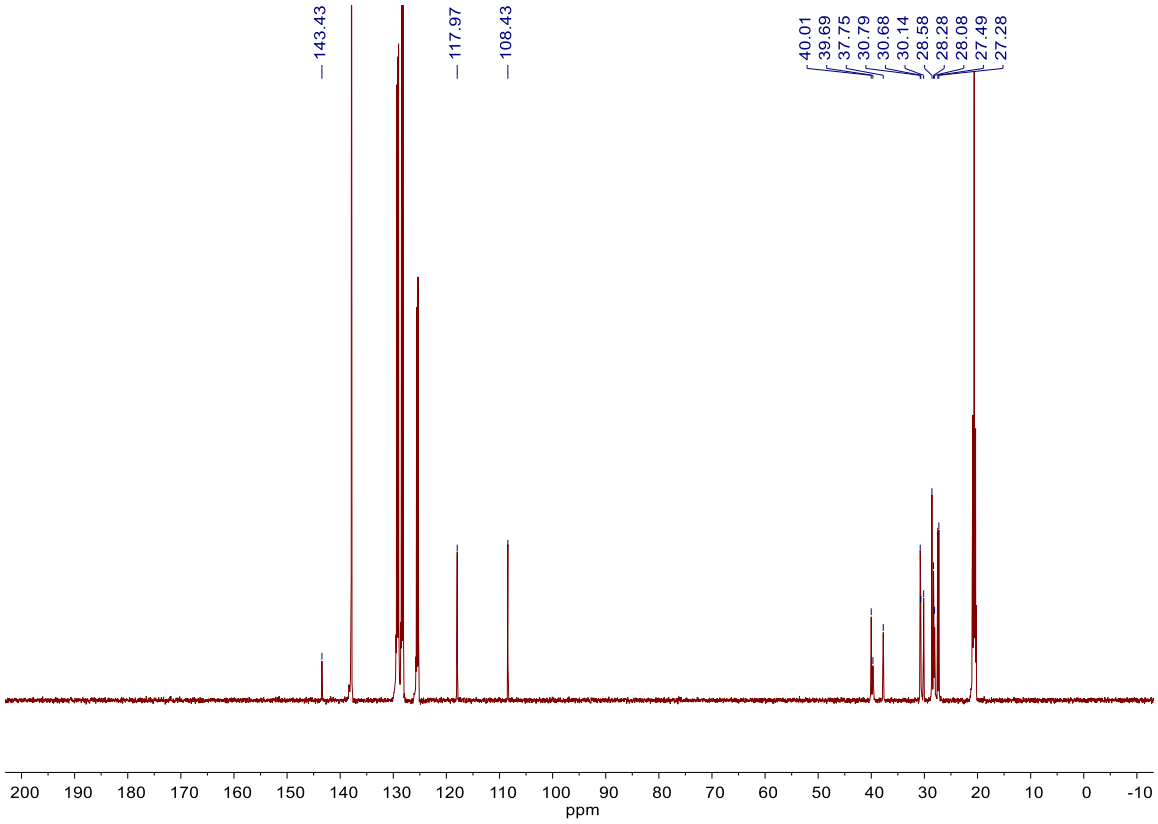

Figure 3.7-5 ^{13}C NMR of $(P^{Cy})_4Ni_2Si_2$, **8**, at +70 °C in toluene-d_8 at 151 MHz.

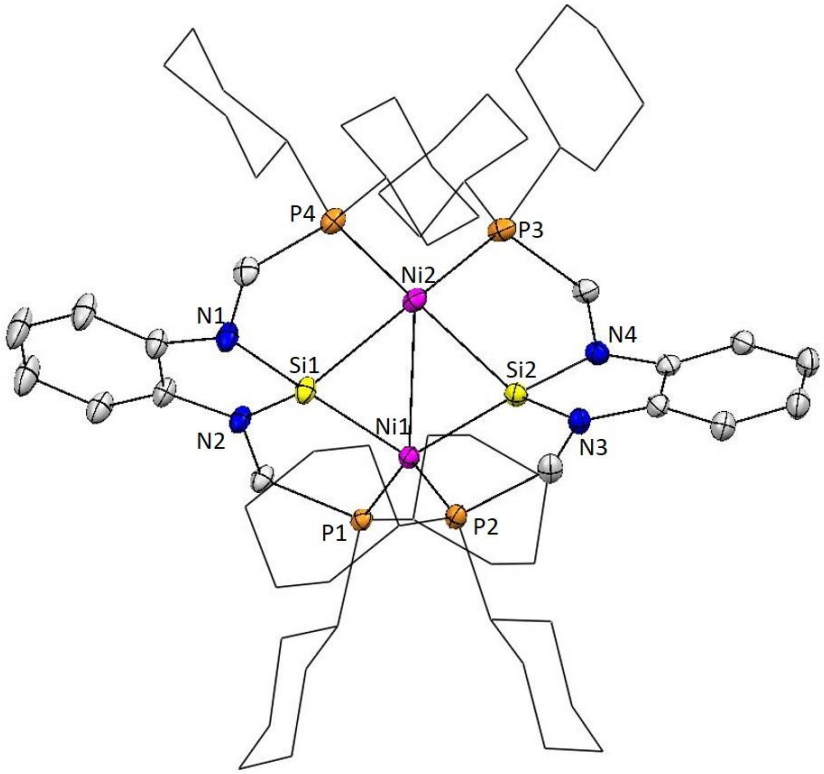

Figure 3.7-6 Thermal ellipsoid plot at 50% probability of $(P^{Cy})_4Ni_2Si_2$, **8**, Magenta, yellow, blue, orange, and gray ellipsoids represent nickel, silicon, nitrogen, phosphorus, and carbon respectively. Hydrogen atoms are omitted for clarity. Two diastereomer molecules of $C_{64}H_{104}N_4Ni_2P_4Si_2$ were present in the asymmetric unit of the unit cell.

Table 3.7-1 Crystallographic data for $(P^{Cy})_4Ni_2Si_2$, **8**.

Identification code	hh156AB15_0m	
Empirical formula	$C_{64}H_{104}N_4Ni_2P_4Si_2$	
Formula weight	1226.99	
Temperature	100(2) K	
Wavelength	0.71073 Å	
Crystal system	Monoclinic	
Space group	P 21/n	
Unit cell dimensions	a = 24.9907(11) Å	α = 90º.
	b = 20.4925(9) Å	β = 112.9237(6)º.
	c = 27.0162(12) Å	γ = 90º.
Volume	12742.9 (10) Å^3	
Z	8	
Density (calculated)	1.279 mg/m^3	
Absorption coefficient	0.771 mm^{-1}	
F(000)	5280	
Crystal size	0.500 x 0.352 x 0.215 mm^3	
θ range for data collection	1.637 to 30.507°.	
Index ranges	$-35 \le h \le 35, -29 \le k \le 29, -38 \le l \le 38$	
Reflections collected	305834	
Independent reflections	38894 [R_{int} = 0.0361]	
Completeness to θ = 25.242°	100.00%	
Absorption correction	Semi-empirical from equivalents	
Refinement method	Full-matrix least-squares procedure on F^2	
Data / restraints / parameters	38894 / 0 / 1369	
Goodness-of-fit on F^2	1.018	
Final R indices [$I > 2\sigma_1$]	R_1 = 0.0403, wR_2 = 0.1023	
R indices (all data)	R_1 = 0.0503, wR_2 = 0.1089	
Largest diff. peak and hole	1.785 and -1.256 e/Å^3	

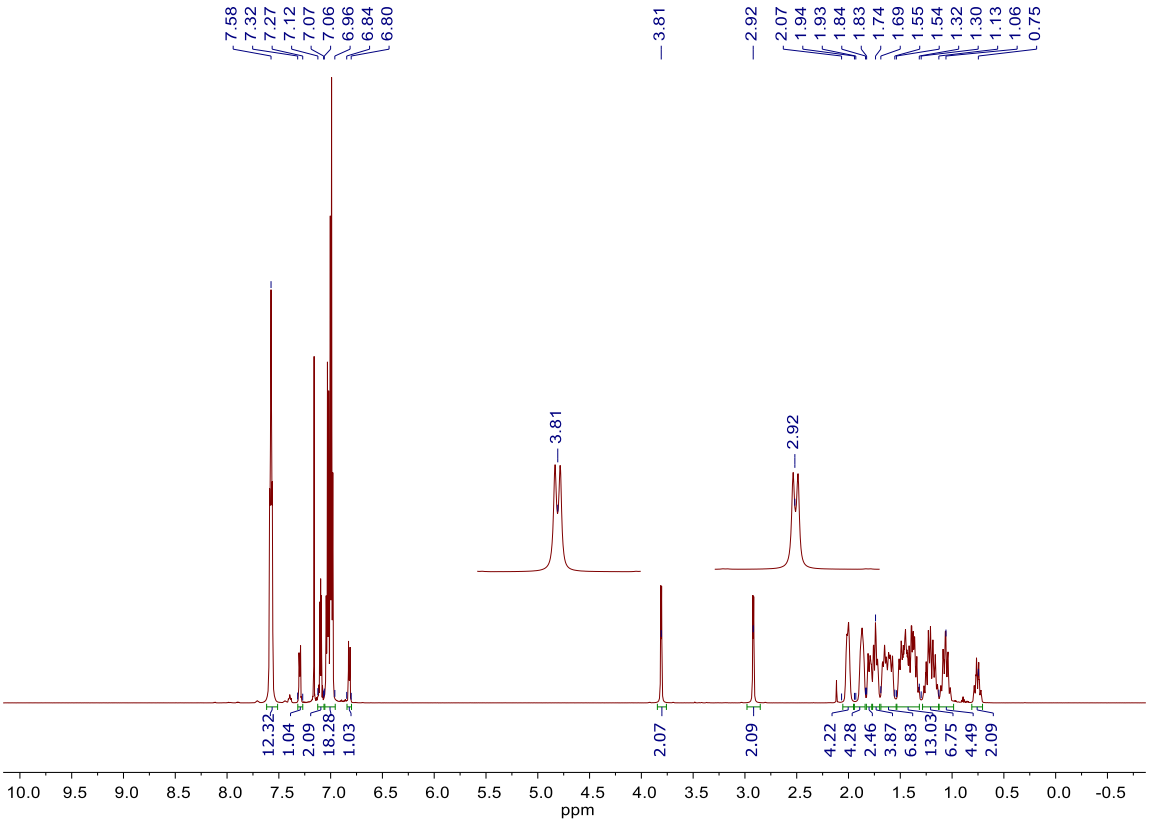

Figure 3.7-7 ^{1}H NMR of $(P^{Cy})_2SiNi(PPh_3)_2$, **9**, in C_6D_6 at 600 MHz.

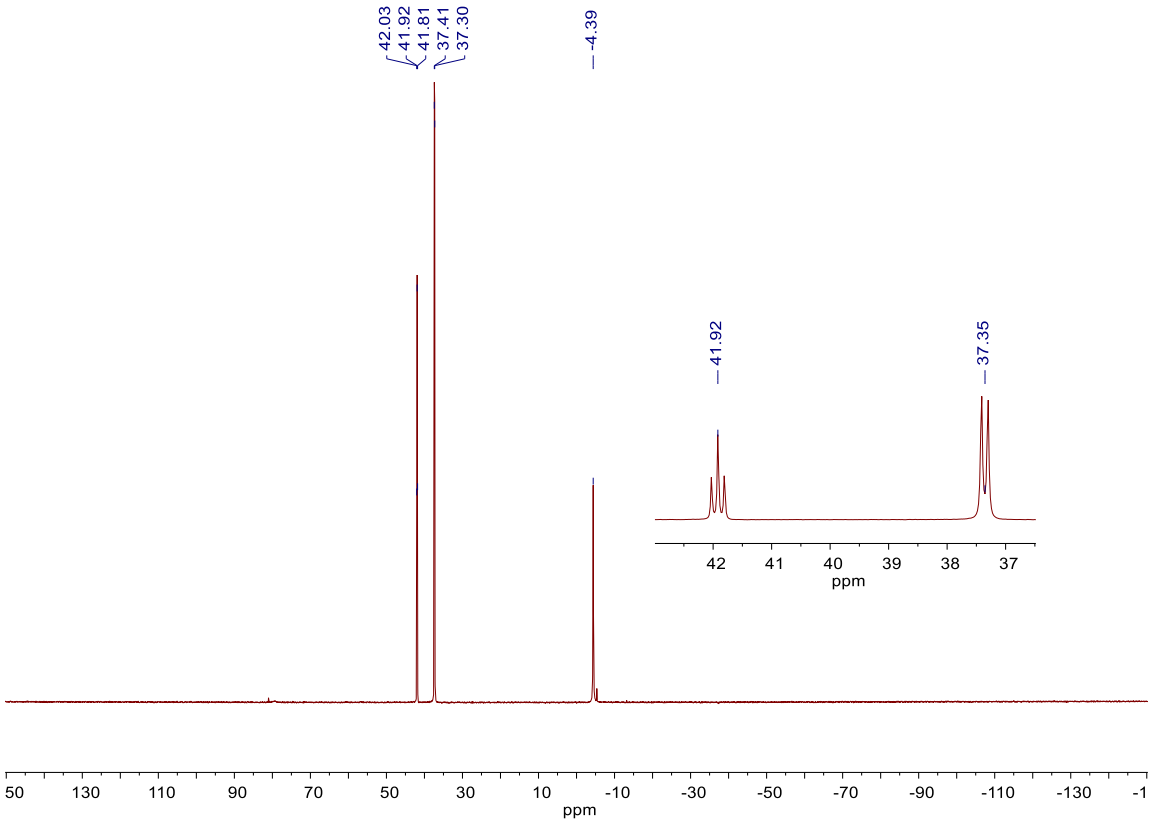

Figure 3.7-8 $^{31}P\{^{1}H\}$ NMR of $(P^{Cy})_2SiNi(PPh_3)_2$, **9**, in C_6D_6 at 243 MHz.

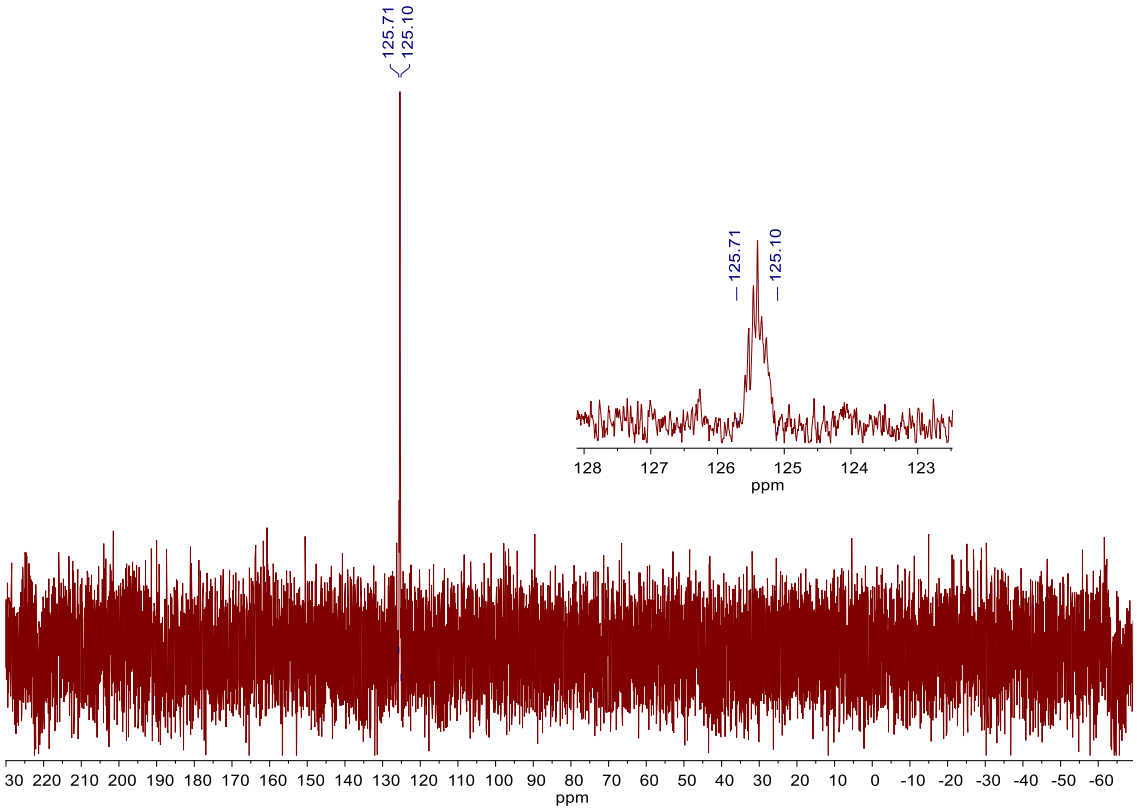

Figure 3.7-9 $^{29}Si\{^{1}H\}$ NMR of $(P^{Cy})_2SiNi(PPh_3)_2$, **9**, at 80 MHz in C_6D_6.

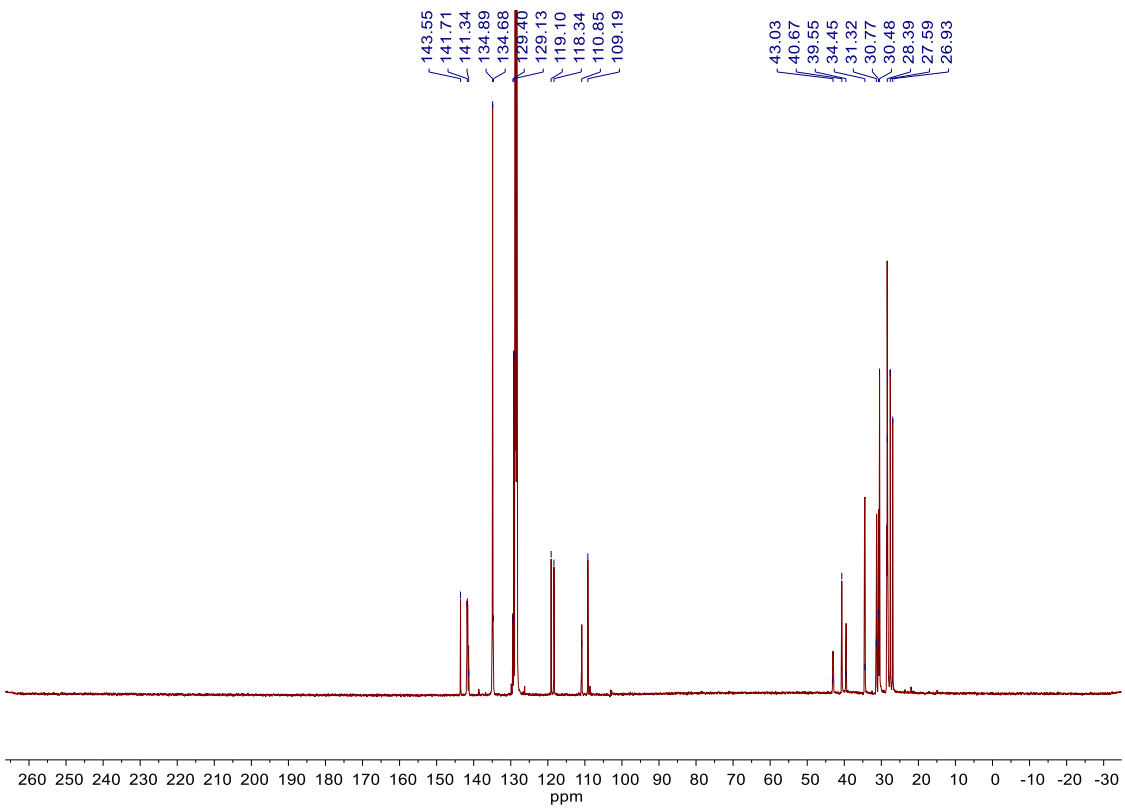

Figure 3.7-10 ^{13}C NMR of $(P^{Cy})_2SiNi(PPh_3)_2$, **9**, in C_6D_6 at 151 MHz.

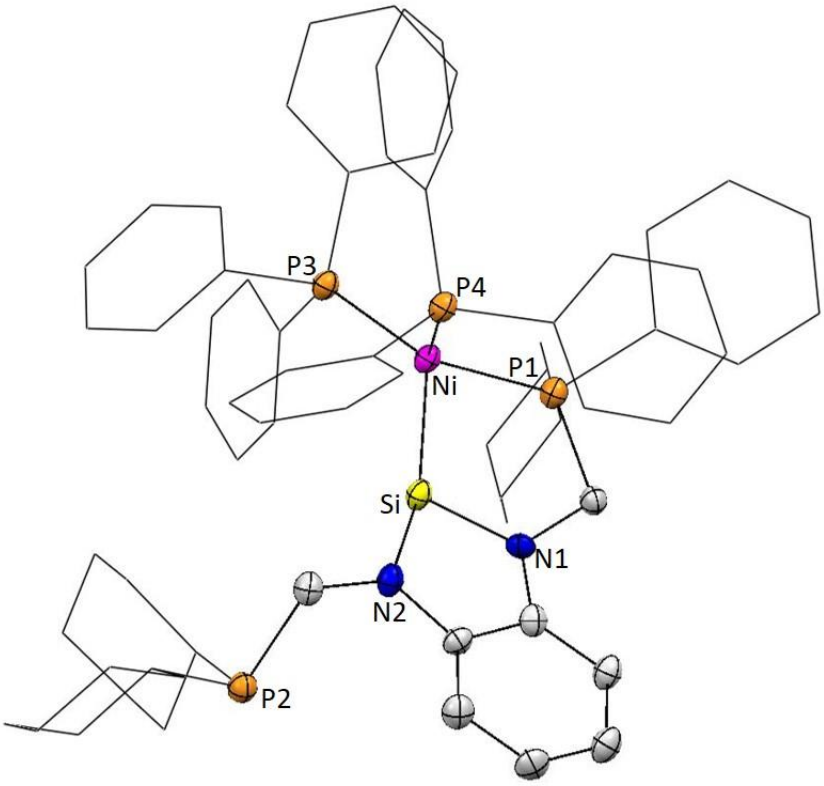

Figure 3.7-11 Thermal ellipsoid plot at 50% probability $(P^{Cy})_2SiNi(PPh_3)_2$, **9**. Magenta, yellow, blue, orange, and gray ellipsoids represent nickel, silicon, nitrogen, phosphorus, and carbon respectively. Hydrogen atoms and solvent molecules are omitted for clarity. Additionally, cyclohexyl and phenyl rings are displayed in wireframe for clarity. Direct methods of phase determination followed by two Fourier cycles of refinement led to an electron density map from which most of the non-hydrogen atoms were identified in the asymmetric unit of the unit cell. With subsequent isotropic refinement, all of the non-hydrogen atoms were identified. There was one molecule of $C_{68}H_{82}N_2NiP_4Si$ and one solvent molecule of toluene present in the asymmetric unit of the unit cell.

Table 3.7-2 Crystallographic data for $(P^{Cy})_2SiNi(PPh_3)_2$, **9**.

Identification code	hh285AB28r_0m	
Empirical formula	$C_{75}H_{90}N_2NiP_4Si$	
Formula weight	1230.16	
Temperature	100(2) K	
Wavelength	0.71073 Å	
Crystal system	Monoclinic	
Space group	P 21/c	
Unit cell dimensions	a = 12.847(2) Å	α = 90°.
	b = 41.635(7) Å	β = 106.707(2)°.
	c = 12.845(2) Å	γ = 90°.
Volume	6580.3(18) $Å^3$	
Z	4	
Density (calculated)	1.242 mg/m^3	
Absorption coefficient	0.455 mm^{-1}	
F(000)	2624	
Crystal size	0.396 x 0.304 x 0.078 mm^3	
θ range for data collection	2.212 to 27.482°.	
Index ranges	$-16 \le h \le 16$, $-54 \le k \le 54$, $-16 \le l \le 16$	
Reflections collected	98211	
Independent reflections	15051 [R_{int} = 0.0546]	
Completeness to θ = 25.242°	99.60%	
Absorption correction	Semi-empirical from equivalents	
Refinement method	Full-matrix least-squares on F^2	
Data / restraints / parameters	15051 / 0 / 749	
Goodness-of-fit on F^2	1.262	
Final R indices [$I > 2\sigma_1$]	R_1 = 0.0784, wR_2 = 0.1535	
R indices (all data)	R_1 = 0.0936, wR_2 = 0.1580	
Extinction coefficient	n/a	
Largest diff. peak and hole	0.972 and -0.591 $e/Å^{-3}$	

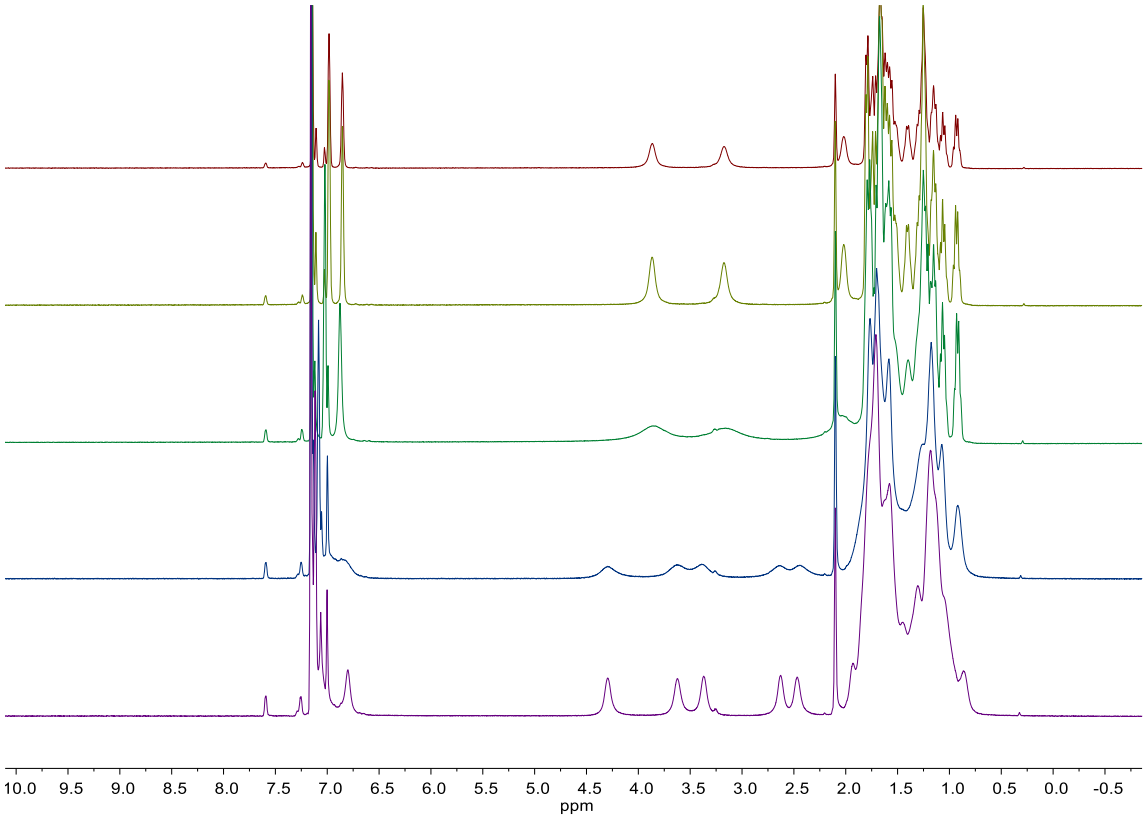

Figure 3.7-12 VT ^{1}H NMR of $(P^{Cy})_4Pd_2Si_2$, **10**, in d_8-Tol at 600 MHz at selected temperatures. From top, +30, +20, –10 and –20 °C, respectively.

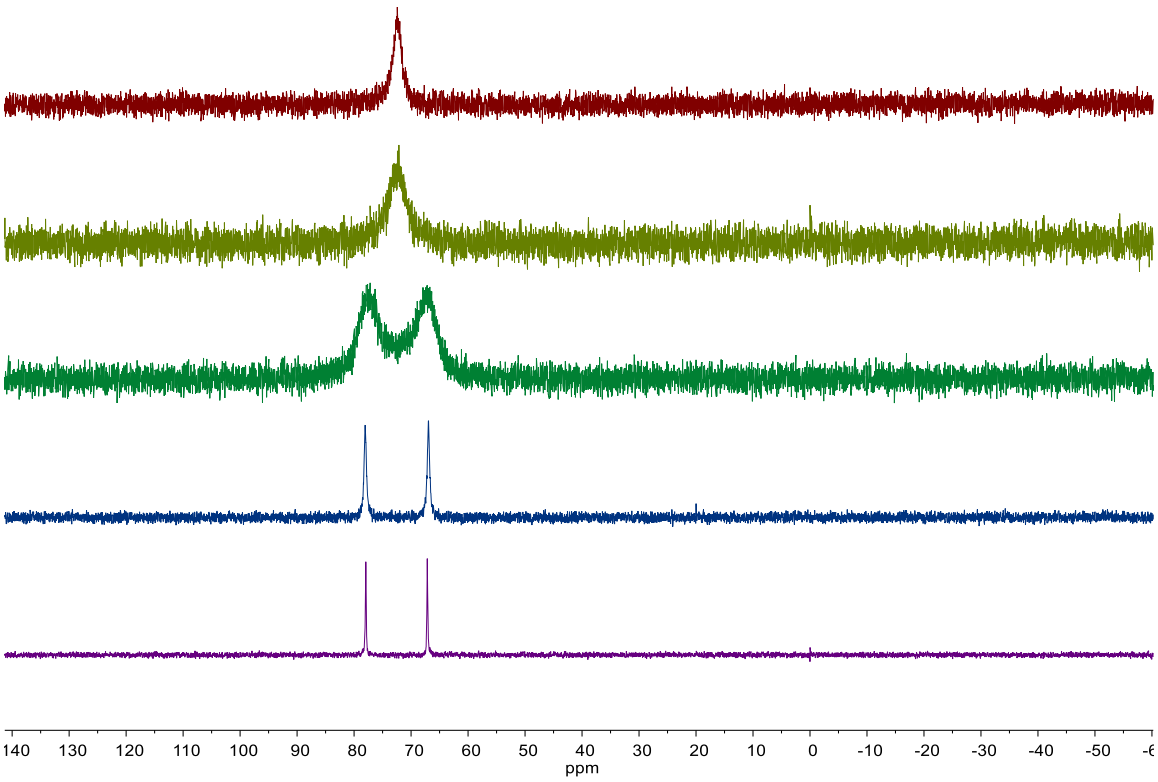

Figure 3.7-13 VT $^{31}P\{^{1}H\}$ NMR of $(P^{Cy})_4Pd_2Si_2$, **10**, at 243 MHz in d_8-toluene at selected temperatures. From top spectrum, +30, +20, +10, –10 and –20 °C, respectively.

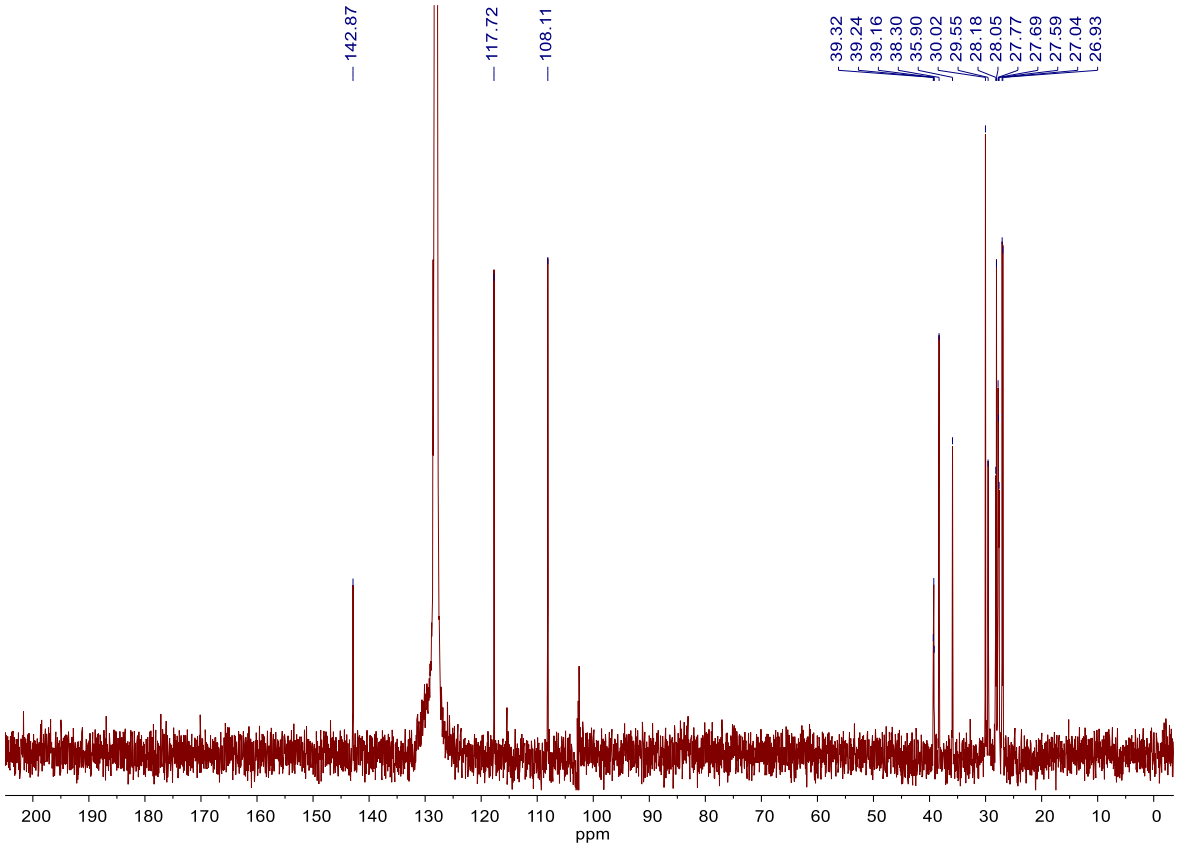

Figure 3.7-14 ^{13}C NMR at 151 MHz in C_6D_6 of $(P^{Cy})_4Pd_2Si_2$, **10**, at +60 °C.

Table 3.7-3 Crystallographic data for $(P^{Cy})_4Pd_2Si_2$-H_2O, **10-H_2O**.

Identification code	hh276AB26_0m	
Empirical formula	$C_{64}H_{106}N_4OP_4Pd_2Si_2$	
Formula weight	1340.38	
Temperature	100(2) K	
Wavelength	0.71073 Å	
Crystal system	Triclinic	
Space group	P -1	
Unit cell dimensions	a = 11.5465(10) Å	α = 100.7186(13)°.
	b = 15.2265(13) Å	β = 98.5413(14)°.
	c = 20.5181(18) Å	γ = 109.4368(13)°.
Volume	3255.1(5) Å^3	
Z	2	
Density (calculated)	1.368 mg/m^3	
Absorption coefficient	0.731 mm^{-1}	
F(000)	1412	
Crystal size	0.346 x 0.318 x 0.014 mm^3	
θ range for data collection	1.466 to 28.282°.	
Index ranges	,-15 ≤ h ≤ 15, -20 ≤ k ≤ 20, -27 ≤ l ≤ 27	
Reflections collected	66806	
Independent reflections	16115 [R_{int} = 0.0445]	
Completeness to θ = 25.242°	99.90%	
Absorption correction	Semi-empirical from equivalents	
Refinement method	Full-matrix least-squares on F^2	
Data / restraints / parameters	16115 / 0 / 698	
Goodness-of-fit on F_2	1.042	
Final R indices [$I > 2\sigma_1$]	R_1 = 0.0384, wR_2 = 0.0851	
R indices (all data)	R_1 = 0.0544, wR_2 = 0.0911	
Extinction coefficient	n/a	
Largest diff. peak and hole	1.792 and -1.234 e/Å^{-3}	

CHAPTER 4 E–H and E–E Activation with Dinickel Disilylene

4.1 Abstract

Small molecule activation across the Ni–Si interaction of dinickel disilylene, **8**, with small molecule substrates including dihydrogen, phenol, thiophenol and diphenyl disulfide were investigated and the resulting products are reported here. Using Covalent Bond Theory (CBC)[1] Ni(II) is assigned to each nickel center with an X-type ligand from the silyl moiety and an X-type ligand from the second nickel center to create a family of diamagnetic, formally 18e$^-$, dinickel Ni(II)–disilyl complexes. Small molecule substrate addition to **8** allows access to several Ni(II)–disilyl complexes that feature interesting bonding motifs within the Ni_2Si_2 core of **8**.

4.2 Introduction

TM–silyl syntheses interest stems from ease of access for oxidative addition products resulting from Si–H bond activation with transition metal fragments versus the more difficult activation of C–H bonds.[2] The access to TM–silylene complexes using a Si(IV) precursor, such as a hydrosilane derivative, and its addition to transition metal fragments is a route that involves substituent migration, largely demonstrated in reports by Tilley as well as Tobita and co-workers.[3] For example, several reports of tungsten and ruthenium silylenes were prepared using the latter route by Tobita and coworkers.[4–6] The laboratory of Tilley has also reported the use of a ruthenium methoxide reagent with CyMeSiH(OMe) followed by H_2 evolution which affords a Ru–silylene after an alkoxy transfer reaction.[7,8] Traditionally the prior route to form TM–silylenes is more difficult versus initial generation

of a silylene followed by treatment with a transition metal fragment, protocol of which was largely established by Lappert and co-workers. Transition metal fragments and their reactivity with various hydrosilanes has provided access to various TM–complexes that represent reaction intermediates. These isolated reaction intermediates are important in transformations for hydrosilyaltion, silane dehydrocoupling or similar metal mediated reactions, in addition to revealing complexes that feature interesting binding modes at the metal center with small molecules.[3,9] The multitude of TM–silylene complexes and their resulting silyl complexes are in part due to the various binding modes capable for the TM–H–Si moiety. In recent years (2011-2017) with the growing number of complexes featuring varying degrees of interaction between the three atoms within the TM–H–Si moiety a number of reviews have been written with the goal of classifying the interactions.[3,9,10] Regardless of each classification it is emphasized that the reactivity between the three atoms (TM–H–Si) in each bonding classification can be viewed as a continuum, with various examples of TM-silyl and silylene complexes falling into one or more classification. Three centered two electron bonds (3c–2e) are an important feature in many TM–Si complexes and a variety of examples are reported in the literature.[3] The most common way to generate TM–silyl complex is through treatment of a TM fragment, possessing open coordination, with a hydrosilane derivative. A relatively recent route to TM–Silicon containing compounds involves stabilization of tricoordinate Si(II) systems with NHSis and NHC.[3] Noted in the literature are several examples which feature a TM–H–Si moiety, a few of which are highlighted in Figure 4.2-1 which feature a dinickel disilyl dihydrido core. These include complexes featuring a Ni_2Si_2 made through the activation of

an aryl silane with a metal fragment in the groups of Osakada and Johnson in 2012.[11–13] In contrast, Tilley and coworkers reported a similar system featuring a Ni_2Si_2 core via activation of molecular hydrogen with a Ni-silylene complex.[14]

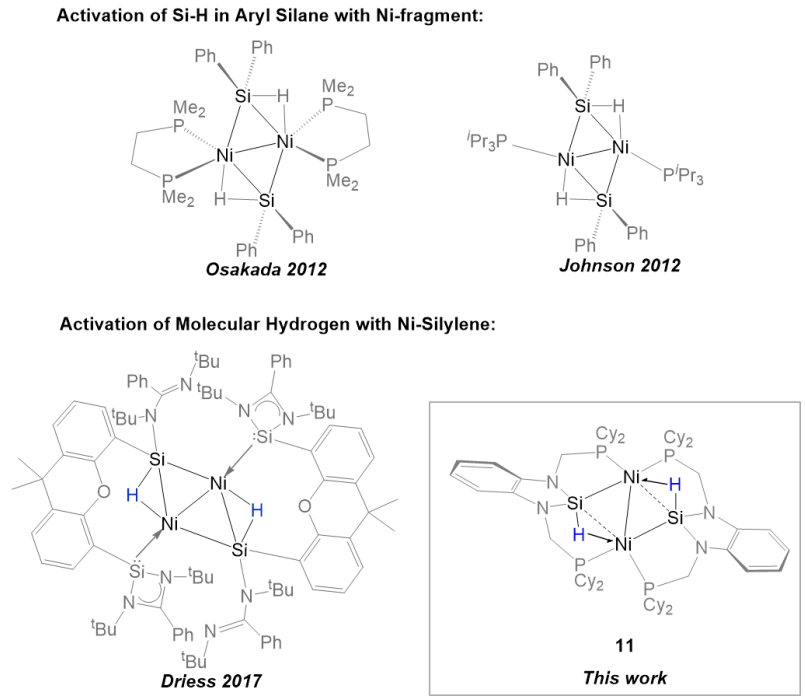

Figure 4.2-1. Previously reported complexes featuring $Ni_2Si_2H_2$ core. Those made via Si–H activation of an aryl silane with a nickel transition metal fragment (top). Those made through activation of molecular H_2 with Ni-silylene complex.

Transition metal complexes featuring a TM–H–Si moiety with nickel have been demonstrated in a variety of geometries and oxidation states. The geometry at nickel may not be explicitly stated by investigators and at times can be unclear or described as tetrahedral or pseudo tetrahedral in part to its' "anomalous behavior" which is attributed to the "energy difference between tetrahedral and planar nickel (II) species [which] can be small."[15] With respect to Ni(I) complexes a recent review on spectroscopically and crystallographically characterized complexes was done by Power and Lin.[16] Complexes

which contain true Ni(I) are paramagnetic in nature given the unpaired electron, however, within this class of compounds are those which are diamagnetic due to the dimerization of Ni(I) fragments which feature a formal Ni–Ni bond to create Ni(II). The early work of Jones and Atwood have reported a diamagnetic $(CO)_2Ni(\mu\text{-}^tBu_2P)_2Ni(PR_3)$ (R = Me_3 and Et_3), in addition to a $[Ni(p\text{-}(^tBu)(H)P)\text{-}(PMe_3)_2]_2$ by Jones, with the latter report stating the bridging phosphide groups act as "three electron donors" (L to one nickel center and X to another when CBC classification is applied) which satisfies the 18-elecron rule at each nickel center.[17,18] Gade and coworkers in 2012 reported the synthesis of an unexpected $[PNP]_2(Ni_2)$ dimer upon the reaction of 2,5-bis((diphenyl-phosphino)methyl)-1H-pyrrole with $Ni(COD)_2$ featuring a Ni–Ni distance of 2.3259(2) Å.[19] Peters and Lin in 2014 reported the synthesis of a $[(^{Ph}PBP)Ni]_2$ which revealed a Ni–Ni distance of 2.2421(9) Å with unsymmetrical μ^2-boryl ligands to each Ni^INi^I dimer center.[20] Key examples toward small molecule activation in an effort to mimic the reaction site of NiFe hydrogenase with bimetallic Ni(I) dimers have also been reported.[16] These reports demonstrate interest in accessing multimetallic metal complexes for small molecule activation given the potential for additional binding modes, in contrast to those featuring a single metal center.[21]

The work reported here describes access to Ni(II)–disilyl complexes from the reaction of dinickel disilylene, **8**, with a variety of small substrates including molecular hydrogen, phenol, thiophenol, and diphenyl disulfide though activation of various E–H bonds and E–E bonds (E = H, O, S). We also report various binding modes of small molecule substrates can be accessed and are demonstrated within the Ni_2Si_2 core of **8**.

4.3 Results and Discussion

4.3.1 $P_4Ni_2Si_2(\mu\text{-}H)_2$ (**11**)

Addition of excess H_2 at atmospheric pressure to **8** in benzene after a three freeze, pump, thaw cycles results in a color change from red to orange indicating in the formation of the diamagnetic dinuclear $P_4Ni_2Si_2(\mu\text{-}H)_2$–silyl complex, **11**, isolated in 51 % yield after first crop collection as a bright orange crystalline solid from THF/hexane. The $Ni_2Si_2H_2$ core of **11** reveals molecular hydrogen bond is cleaved resulting in a bridging hydrido ligand between two Ni–Si interactions to reveal a 3c–2e bond interaction evident by ^{1}H NMR. Also worth noting is the synthesis of **11** when **8** is treated with excess potassium metal in benzene or sodium amalgam in THF. In this alternative synthetic route, the dinuclear $P_4Ni_2Si_2(\mu\text{-}H)_2$–silyl complex, **11**, can be isolated as a bright red/orange crystalline material in 50% and 40% yield, respectively. In this latter route **11** is thought to form through a proton abstraction pathway with the solvent. Each of these synthetic routes are depicted in Figure 4.3-1.

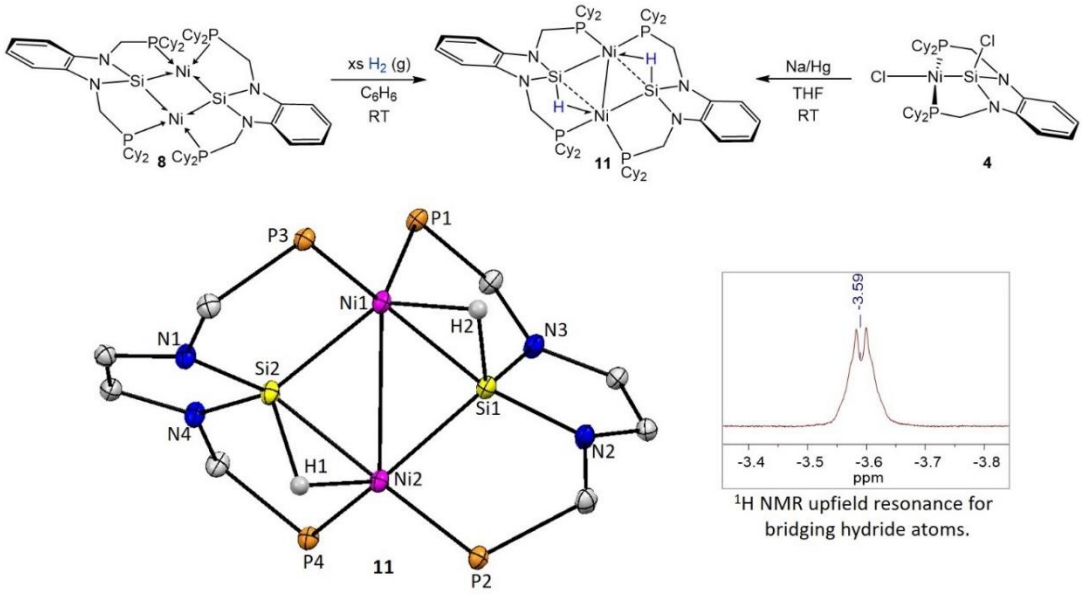

Figure 4.3-1. Synthesis of **11** upon addition of H_2 (g) to **8** (top). Core fragment of the molecular structure for **11** in an ellipsoid representation at 50% probability (bottom left). Hydrogen atoms with exception of the two bridging the Ni and Si atoms (H1and H2) have been omitted for clarity (bottom left). Notable distances (Å): Ni1–Ni2 = 2.7735(5), Si1–Ni1 = 2.181(1), Si1–Ni2 = 2.2228(7), Ni1–H2 = 1.58(2), Si1–H2 = 1.68(1), Si2–Ni1 = 2.2209(8), Si2–Ni2 = 2.176(1), Ni2–H1 = 1.54(1), Si2–H1 = 1.68(2). Selected angles (°): Ni1–Si2–Ni2 = 78.20(3), Ni1–Si1–Ni2 = 78.06(3), Si2–Ni1–Si1 = 100.44(3), Si1–Ni2–Si2 = 100.53(3), H1–Ni2–Si2 = 50.2(6), H1–Si2–Ni2 = 45.0(5), H2–Si1–Ni1 =.46.0(6), H2–Ni1–Si1 = 49.8(6). Resonance in ^{1}H NMR of **11** for the bridging hydride atoms at a shift of –3.59 ppm in C_6D_6 at 500 MHz (bottom right).

The ^{1}H NMR of **11** features a broad resonance as a complex doublet as not well resolved and significantly upfield shifted assigned to the bridging hydrido within the Ni–H–Si moiety at a δ –3.59 ppm (2H, J = 9.0 Hz). The observation of characteristic silicon satellites was unable to be resolved in the ^{1}H NMR but despite this the IR spectrum of **11** exhibits strong absorption around 1500 cm^{-1} observed in previously reported dinuclear Ni complexes featuring a Ni–H–Si fragment.[14,22,23] Additionally, the four sets of methylene protons are displayed at δ 3.75 ppm (dd, J = 12.9, 7.8 Hz, 2H), δ 3.48 – 3.34 ppm (m, 4H), and δ 2.96 ppm (dd, J = 12.8, 7.6 Hz, 2H). Each resonance at δ 3.75 ppm and δ 2.96 ppm feature a doublet of doublets coupling pattern with geminal ^{1}H–^{1}H coupling of 8 Hz and, a

coupling constant of 13 Hz for $^{1}H–^{31}P$ nuclei coupling. The $^{31}P\{^{1}H\}$ NMR displays two sets of triplets at a δ 94.47 and 46.65 ppm for the two sets of inequivalent phosphorous environments displaying $^{31}P–^{31}P$ coupling constants of J = 27.2 Hz. Similar splitting pattern and coupling is consistent with previously reported binuclear nickel–phosphine complexes featuring two sets of inequivalent phosphorous atoms.[24] The $^{29}Si\{^{1}H\}$ NMR of **11** displays a single resonance at δ 124.0 ppm for the two equivalent silicon atoms for the μ-(Si–H) bridging silyl groups within the Ni–H–Si fragment and features complicated $^{29}Si–^{31}P$ heteronuclei coupling that was unable to be resolved. This shift (δ 124.0 ppm) is similarly downfield and comparable to previously reported μ-(Si–H)Ni complexes which typically range from δ 114.0 to 123.7ppm.[14,22,23,25] The single resonance for the silicon atoms in **11** is upfield from that of **8** (δ 190 ppm). There are few crystallographically characterized complexes with a $Ni_2Si_2(\mu\text{-}H)_2$ motif featuring a bridging hydride across the Ni–Si interaction. The work of Osakada in 2012 reported a similar bonding motif featuring dinuclear Ni–silyl compounds with a $Ni_2Si_2H_2$ core as the result of $Ni(COD)_2$, DMPE or PMe_3 and H_2SiPh_2 .[12,25] The work reported in 2012 by Beck and Johnson featured a range of interesting mononuclear, dinuclear, trinuclear and tertranuclear nickel complexes with silyl and silylene ligands.[11] These complexes were the result of $(^{i}Pr_3P)_2Ni^0$ precursors with Ph_2SiHCl, Ph_2SiH_2, $PhSiH_3$, and Ph_3SiH featuring bridging hydridic character within the Ni–H–Si interaction. Additionally, in 2014 a report from the Radius lab reported a complex featuring a similar $Ni_2Si_2H_2$ core within $[\{(iPr_2Im)Ni\text{-}\mu_2\text{-}(HSiPh_2)\}_2]$.[22] The latter a result of $[Ni_2(iPr_2Im)_4(COD)]$ with two equivalents diphenylsilane at 110 °C. Each of these examples facilitate the formation of Ni–H–Si fragments via S–H bond activation by nickel

with some form of silane derivative. Recently Driess and co-workers in 2017 reported the synthesis of η^2-(Si−H)→Ni complex as the result of H_2 addition to [Si^{II}(Xant)Si^{II}]- Ni(η^2-1,3-cod)$_2$.[14] This example was the first report of a dinuclear Ni complex featuring a Ni_2Si_2 core obtained from the activation of H_2, in contrast to previously generated η^2-(Si−H)→Ni complexes via Si–H activation with derivatives of phenylsilane by nickel fragments.

Single crystal X-ray diffraction analysis confirmed the structure of **11** and is consistent with the spectroscopic data. The molecular structure of complex **11** features a Ni–Ni distance of 2.773 Å which is longer than previously reported Ni–Ni bond lengths (2.2393(7)–2.693(2).[16] While the Ni–Ni bond in **11** is longer than most reported, similar lengths are been observed in nickel dimers within the work of Jones which contain formal Ni(I) metal centers.[17,26] The two bridging hydrido ligands, μ-H, located between Ni and Si atoms in **11** have varying distances with a longer Si–H (1.68(1) and 1.68(2) Å) when compared to that in the Ni–H interaction (1.58(2) and 1.54(1) Å). These lengths in **11** for Si–H are similar to the Si–H distance reported in Driess silicon assisted H_2 activation product, which was also stated to match well with the computationally optimized structure in their report suggesting an η^2-(Si–H) σ–complex.[14] These results are also consistent with for a Ni_2Si_2 complex as reported by Beck and Johnsons which also featured bridging hydrido ligands. The Ni–Si distances with μ-H is 2.181(1) and 2.176(1) Å with each silicon center adopting a pseudo tetrahedral arrangement (discounting the Ni–Si interaction within the Ni–H–Si moiety), when viewing the hydrido from the apical position with distorted geometry attributed to the 3c–2e interaction. The distance for each Ni–Si bond lacking the μ–H is 2.2209(8) and 2.2228(7) Å) consistent with other σ-bound Ni–Si distances.[23] All

Ni–Si distances observed in the solid state of **11** are within the range of previously reported Ni–Si bonds (2.21 – 2.30 Å), with Ni–Si distances within the Ni–H–Si fragment as slightly shorter and consistent with 3c–2e bonds.[27] From inspection of the crystal structure the two Ni centers are equivalent and the two phosphine donors are inequivalent. Consistent with this observation the ^{31}P NMR spectrum of **11** exhibits two sets of triplets at δ 94.47 and δ 47.74 both exhibiting ^{31}P coupling ($J_{P–P}$ = 27.93 Hz) for the two sets of chemically inequivalent phosphorous atoms coupling to one another through the Ni atoms.

4.3.2 $P_4Ni_2Si_2(\mu$-H)(OPh) (**12**)

The addition of one equivalent of phenol to **8** in a solution of benzene results in the $Ni_2Si_2(\mu$-H)(OPh), **12**, featuring a μ–H hydrido ligand between the Ni and Si atoms and phenoxide on the second Si center (Figure 4.3-2). The ^{1}H NMR of **12** features an upfield resonance with a doublet of triplets coupling pattern for the μ–H at δ -1.45 ppm with J = 19.3, 9.3 Hz. This resonance for the μ-H in **12** is a higher chemical shift than that observed for **11** (δ -3.59 ppm) and may suggest less hydridic character in **12**.[23] The ^{31}P{^{1}H} NMR of **12** features four distinctive shifts, δ 85.82 (ddd, J = 29.0, 20.1, 12.0 Hz), 78.96 – 78.54 (m), 32.93 (t, J = 10.6 Hz), 26.09 (d, J = 27.3 Hz), for each of the four inequivalent ligated phosphorous atoms, highlighting the asymmetry of the complex. Additionally, the ^{29}Si NMR for **12** displays two resonances at δ 118.14 – 116.15 (m) and 46.34 – 44.97 (m) with unresolved coupling to phosphorous.

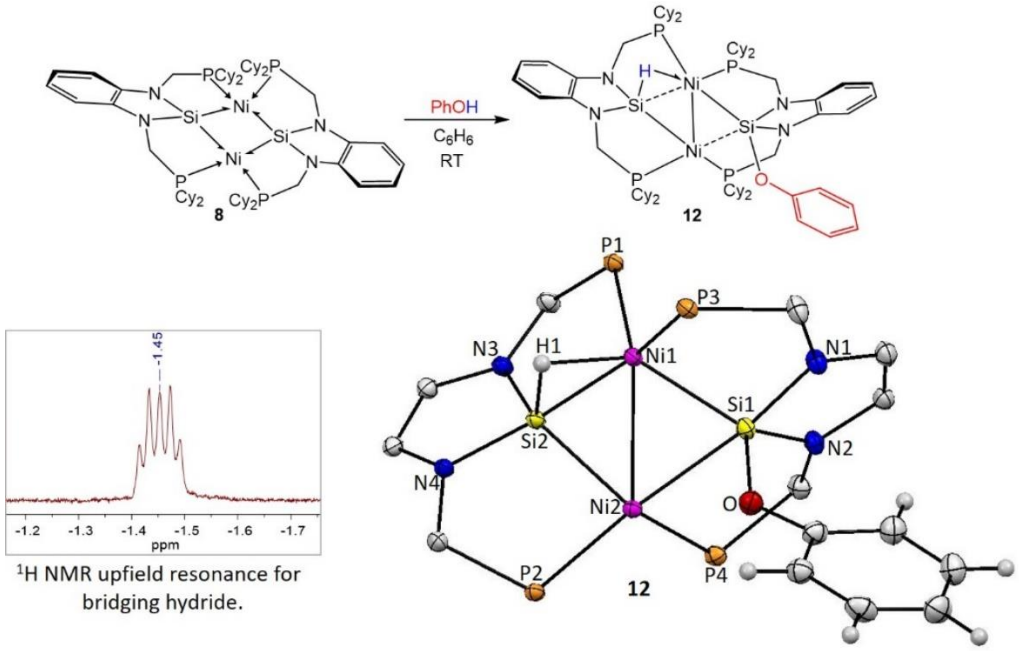

Figure 4.3-2. Synthesis of $P_4Ni_2Si_2(\mu\text{-H})(OPh)$, **12**, from addition of phenol with **8** (top). Resonance in the ^{1}H NMR for **12** revealing the bridging hydride atom at a shift of –1.45 ppm in C_6D_6 at 500 MHz (bottom left). Core fragment of XRD ellipsoid representation of **12** at 50% probability. Hydrogen atoms, but for the one bridging the Ni1–Si1 (H1) and those on phenoxide aryl ring have been omitted for clarity. Notable distances (Å): Ni1–Ni2 = 2.6989(4), Si1–Ni1 = 2.2536(6), Si1–Ni2 = 2.4418(4) Ni1–H1 = 1.60(2), Si2–H1 = 1.64(2), Si2–Ni1 = 2.1603(4), Si2–Ni2 = 2.2230(5), Si1–O = 1.731(1). Selected angles (°): Ni1–Si2–Ni2 = 75.99(2), Ni1–Si1–Ni2 = 70.04(2), Si2–Ni1–Si1 = 110.47(2), Si1–Ni2–Si2 = 101.94(2), H1–Ni1–Si2 = 49.1(6), H1–Si1–Ni1 = 47.3(6).

With reference provided by the ^{29}Si{^{1}H} resonance observed for **11** (δ 124.0 ppm) the resonance at δ 118.14 – 116.15 (m) for **12** is assigned to silicon within the Ni–H–Si fragment with the μ-H hydrido ligand and the lower chemical shift (46.34 – 44.97 (m) ppm) assigned to the bridging silyl bound to phenoxide [Si(OPh)]. A solid-state X-ray diffraction study confirmed the structure of **12** and the bridging hydrido was located in the electron density map. Upon inspection of the XRD data the Ni–Ni distance for **12** is 2.6989(4) Å. This Ni–Ni distance is similar to that revealed in the solid-state structure for **11** but significantly longer than most reported Ni–Ni bonds in dimeric systems, as previously

mentioned.[23] The diamagnetic nature of **11** and **12** supports these formally Ni(II)–disilyl complexes can be viewed as Ni(I) dimer fragments.[23]

4.3.3 $P_4Ni_2Si_2(\mu\text{-H})(\mu\text{-SPh})$ (**13**)

Addition of an equivalent of thiophenol in THF to **8** results in the formation of diamagnetic $Ni_2Si_2(\mu\text{-H})(\mu\text{-SPh})$, **13**. This product is the result of oxidative addition of thiophenol into a Ni–Si to afford a bridging thiolate group across one Ni–Si interaction and a bridging hydrido ligand across the second Ni–Si interaction. The ^{1}H NMR in C_6D_6 for **13** displays the methylene proton resonances at δ 3.83 (t, *J* = 10.8 Hz, 1H), 3.76 – 3.63 (m, 2H), 3.43 (t, *J* = 11.3 Hz, 1H), 3.23 (dd, *J* = 12.3, 4.4 Hz, 1H), 3.15 (t, *J* = 11.5 Hz, 1H), 3.04 (dd, *J* = 13.0, 5.2 Hz, 1H) and 2.47 (d, *J* = 12.4 Hz, 1H).

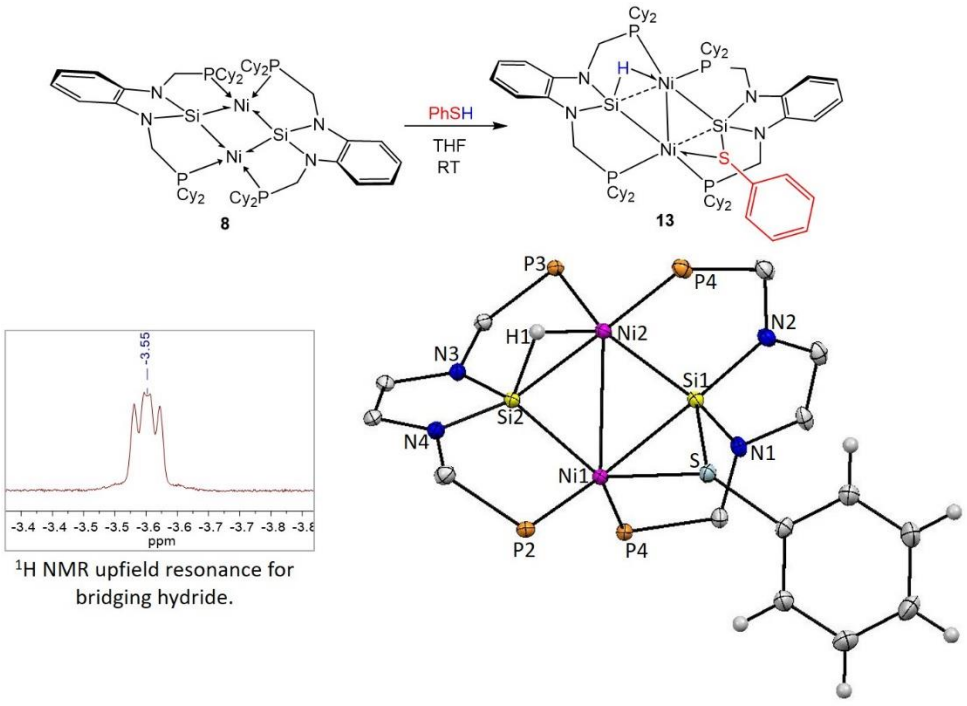

^{1}H NMR upfield resonance for bridging hydride.

Figure 4.3-3. Synthesis of $P_4Ni_2Si_2(\mu\text{-H})(\mu\text{-SPh})$, **13**, via addition of thiophenol to **8** (top). Resonance in the ^{1}H NMR for **13** revealing the bridging hydride atom at a shift of –3.55 ppm in C_6D_6 at 500 MHz (bottom left). Core fragment from XRD data in ellipsoid representation of **12** at 50% probability (bottom right). Hydrogen atoms but for the bridging hydrido across the Ni1–Si1 (H1) and those on phenoxide aryl ring have been omitted for clarity. Notable distances (Å): Ni1–Ni2 = 2.7510(5), Si1–Ni1 = 2.3867(6), Si1–Ni2 = 2.2321(6), Ni2–H1 = 1.52(2), Si2–H1 = 1.68(3), Si2–Ni1 = 2.2165(7), Ni1–S = 2.3657(5), Si1–S = 2.2992(7). Selected angles (°): Ni1–Si2–Ni2 = 75.99(2), Ni1–Si1–Ni2 = 77.90(2), Si2–Ni1–Si1 = 98.30(2), Si1–Ni2–Si2 = 105.00(2), H1–Ni1–Si2 = 73.03(2), H1–Si1–Ni2 = 44.5(7), H1–Si1–Ni2 = 50.9(8).

Each of the methylene protons located in the bridge of the phosphine arms are diastereotopic as expected and display coupling but for single resonance that displays as a multiplet, the result of two overlapping resonances. Additionally, the ^{1}H NMR of **13** features an upfield resonance with doublet of doublets coupling pattern for the μ-H at δ –3.54 (J = 15.7, 9.4 Hz, 1H). This shift is significantly more shielded in contrast to the μ-H resonance for **12**, but does display similar coupling (δ –1.45 ppm with J = 19.3, 9.3 Hz, 1H). The ^{31}P{^{1}H} NMR of **13** displays four distinctive resonances at δ 71.51 (dd, J = 32.2, 20.3 Hz), 70.78 (t, J = 33.3 Hz), 47.18 (t, J = 31.8 Hz), 26.04 (dd, J = 34.2, 20.1 Hz),

with ^{31}P–^{31}P two and three bond coupling evident.[17,23] The solid-state structure was confirmed by single crystal X-ray diffraction with the core fragment of the molecular structure of **13** represented in Figure 4.3-3. A noted difference in the structure of **12** when compared to that of **13** is the bridging thiolate group across the Ni–Si interaction, in contrast to **12** where phenoxide is only bound to silicon (see Figure 4.3-2). This difference in bonding may be attributed to the higher affinity of silicon for oxygen versus that of sulfur. This bonding motif [Ni–S–Si] is similar to previously reported Ni–Fe synthetic systems that feature (μ-S) ligands [Ni–S–Fe].[28] To the best of our knowledge, with respect to the [TM–S–Si] fragment featuring a μ-S the only reported is the 2002 Bergman and Tilley report of a Cp*–Ir complex featuring a similar bonding motif to that of **13**.[29] The Ni–Ni distance in **13** is 2.7510(5) is significantly longer than those typically reported Ni–Ni distances in representative similar dimeric nickel phosphine complexes, however similar two bond and three bond ^{31}P–^{31}P coupling evident in **13** have been reported.[17,23,30,31] The C–S bond length in **13** is 1.788(2) Å which is slightly longer than that of the C–S bond length found in free thiophenol (1.775 Å).[32] The Ni1–S distance of 2.3657(5) and Si1–S distance of 2.2992(7) are slightly longer than those reported in the work of Hammes-Schiffer, Rauchfuss and Lubitz who reported (μ^2-S)Ni–Fe complexes (Ni1−S_{avg}, 2.1645(7) and Fe1–S_{avg} = 2.2208(7).[16,28] This lengthening in the distance to the thiolate group within the [Si–S–Ni] moiety is presumably the result of σ–donation from the adjacent silicon and nickel atoms (Si1–Ni2, 2.2321(6) Å and Ni1–Si2, 2.2165(7) Å), which have Ni–Si distances similar to those previously reported for Ni–Si σ-bonds.[23,33] Distances for the μ-H to Ni and Si are 1.52(2) and 1.68(3), respectively. These distances are similar to those

observed in the solid-state structure for **11** and **12**, suggesting a similar 3c–2e bond interaction for the Si–H–Ni fragment.

4.3.4 $P_4Ni_2Si_2(\mu\text{-}(SPh))_2$ (**14**)

Addition of diphenyl disulfide to **8** results in the symmetric complex $Ni_2Si_2(\mu\text{-}(SPh))_2$, **14.** The ^{31}P NMR of **14** features a set of doublet of doublets at δ 41.13 (dd, J = 32.7, 23.4 Hz), 25.29 (dd, J = 32.6, 23.5 Hz). Characteristic of TM-silyl complexes a resonance is observed in the $^{29}Si\{1H\}$ in the range of 40 ppm as complex multiplets at δ 40.10 – 39.48 (m), 39.50 – 38.93 (m) due to ^{29}Si–^{31}P coupling. The solid-state structure of **14** features a long Ni1–Ni2 distance of 2.7376(5) Å that is slightly shorter than the Ni1–Ni2 distance observed in the solid-state structure of **13** (2.7510(5) Å). Asymmetry is observed in the Ni–Si distances within the Ni_2Si_2 core highlighting the bonding interactions. The solid-state structure for **13** reveals the distance between Ni1–Si1 is 2.2466(7) Å and Ni2–Si2 as 2.2540(7) Å with these lengths consistent with previously reported Ni–silyl ligand σ-bond distances.

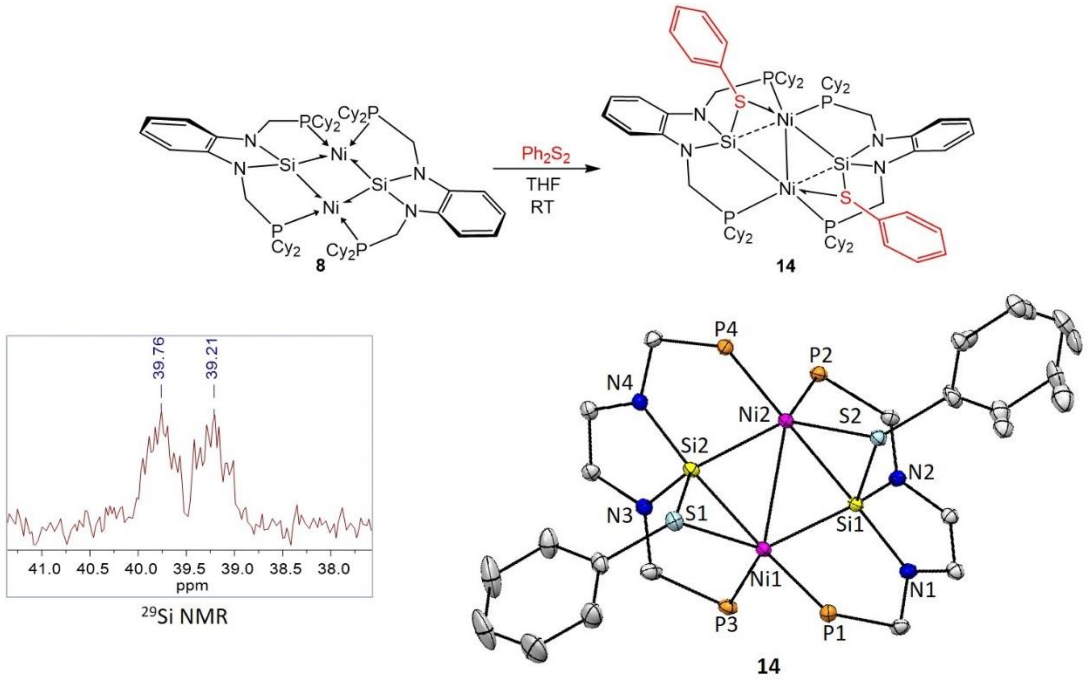

Figure 4.3-4. Synthesis of **14** via addition of diphenyl disulfide to **8** (top). Magnified resonance within $^{29}Si\{^{1}H\}$ NMR of **14** as a complex multiplet at a shift of 39.5 ppm in C_6D_6 at 600 MHz (bottom left). Core fragment of XRD ellipsoid representation of 14 at 50% probability. Hydrogen atoms have been omitted for clarity. Notable distances (Å): Ni1–Ni2 = 2.7376(5), Si1–Ni1 = 2.2466(7), Si1–Ni2 = 2.3106(6), Si1–S2 = 2.2904(7), Ni2–S1 = 2.3843(6), Ni2–Si2 = 2.2540(7), Ni2–S2 = 2.3843(6), Si2–Ni1 = 2.3228(6), Si2–S1 = 2.2858(5), Ni2–S1 = 2.3911(6). Selected angles (°): Ni1–Si2–Ni2 = 73.83(2), Ni1–Si1–Ni2 = 73.46(2), Si2–Ni1–Si1 = 100.51(2), Si1–Ni2–Si2 = 100.66(2), Si2–S1–Ni1 = 59.51(2), S1–Ni1–Si2 = 57.99(2), S1–Si1–Ni1 = 62.50(2).

The distance between the Ni and Si interactions with the bridging thiolate moiety for Ni2–Si1 and Ni1–Si2 is 2.3106(6) and 2.3228(6) Å, respectively. An interesting feature with respect to the bond angles is seen in the P4Ni2P2 angle which is 106.06° and P4Ni2S2 as 106.81° with the ligated phosphorous atom resulting in a distorted square pyramidal geometry surrounding the Ni2 center. Additionally, the sum of the angles surrounding Ni2 are 332.1°.

4.4 Concluding Remarks

We have demonstrated the reactivity of the dinickel disilylene complex **8** to activate small molecule substrates within the Ni_2Si_2 core. All products resulting in addition of H_2, phenol, thiophenol, diphenyl disulfide to **8** are diamagnetic $18e^-$ complexes. A comparative summary of the various bond lengths within the Ni_2Si_2 core for **11**, **12**, **13**, and **14** to that of the Ni_2Si_2 core of **8** can be seen in Figure 4.4-1.

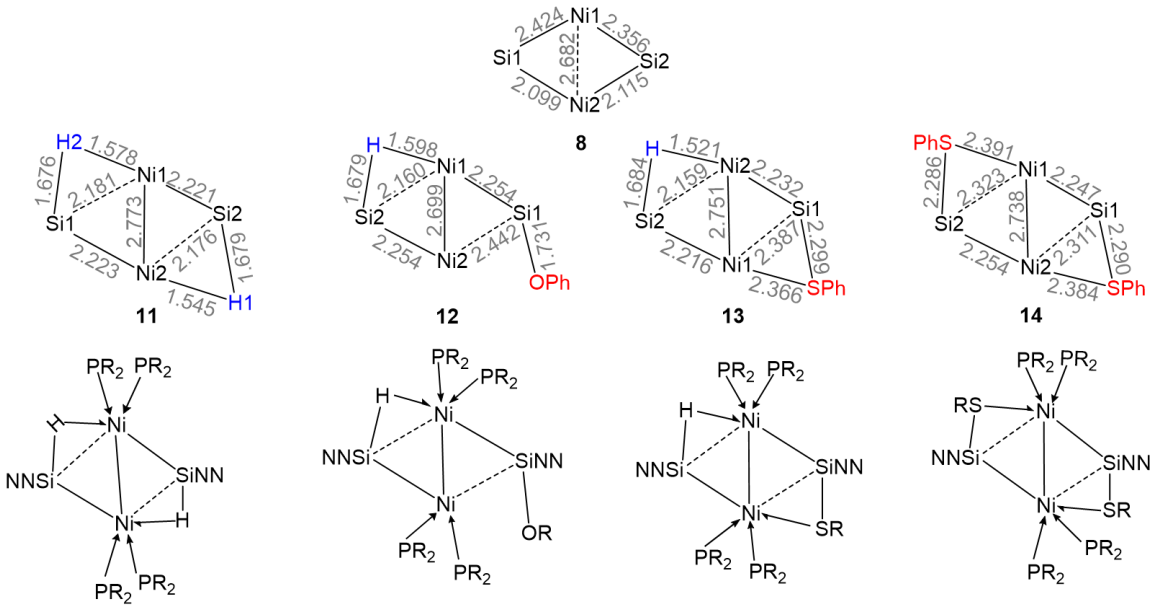

Figure 4.4-1. Representation of the core for complex **8** with that of complexes **11**, **12**, **13** and **14** with reported bond lengths from the XRD experimental data (top). Possible resonance structure using CBC representation of the bonding within the core of **11**, **12**, **13** and **14** (bottom).

As described in Chapter 3 the Ni_2Si_2 core features asymmetry. An interesting comparison can be made in the structures of **12** and **13** as the products of **8** with phenol and thiophenol, respectively. With addition of substrate, the Ni–Si interaction with the sulfur bridging substrate has the longer bond length. The products resulting from small molecule activation have Ni–Ni bond lengths ranging from about 2.7 to 2.9 Å, which is a longer distance compared to most Ni–Ni σ–bond distances. However, a Ni–Ni bond is

invoked as the complexes are diamagnetic. These long distances observed in the Ni–Ni bonds are typically seen in multi-metallic nickel complexes and rarely in dimeric systems, however, stabilization at Ni within each dinickel disilyl is presumably a result of the coordinated phosphine and silyl ligands. In each of the complexes, **11**, **12**, and **13** the ^{1}H NMR displays a characteristically upfield shift for the Ni–H–Si moiety treated as 3c–2e bond interaction. Furthermore, though the Ni–Ni distance is longer than those generally observed in similar Ni–silyl complexes the diamagnetic nature suggests Ni(I)–fragments which form a Ni–Ni bond to afford the diamagnetic formally 18e^{-} dication dinickel disilyl family of complexes reported in this work.

4.5 Syntheses of Ni(II)–Silyl Dimer Complexes **11**, **12**, **13** and **14**

4.5.1 Standard Synthetic Methods and Materials

Standard synthetic methods and materials are the same as reported in Chapter 1 but for the following additional details. Research grade hydrogen gas was purchased for Air Gas and used for the synthesis of **11**. Phenol, thiophenol and diphenyl disulfide were purified and dried according to literature procedures prior to use.

4.5.2 $P_4Ni_2Si_2(\mu\text{-}H)_2$ (**11**)

To a 100 mL Strauss flask with stir bar 70.0 mg of **8** (.057 mmol) in 10 mL of benzene was added. The solution was freeze pump thawed three times after which time H_2 was added. The reaction mixture was allowed to vigorously stir over an H_2 atmosphere for 20 mins. In the Glove Box the solution was concentrated down to 4 mL and 2 mL of hexane added. Sitting overnight afforded 42.2 mg (51% yield) of orange crystalline material after first crop collection. ^{1}H NMR (500 MHz, Benzene-d_6) δ 7.00 – 6.92 (m, 4H), 6.77 – 6.65 (m,

4H), 3.75 (dd, *J* = 12.9, 7.8 Hz, 2H), 3.48 – 3.34 (m, 4H), 2.96 (dd, *J* = 12.8, 7.6 Hz, 2H), 2.19 (d, *J* = 12.8 Hz, 2H), 2.06 (d, *J* = 11.0 Hz, 2H), 1.98 – 1.89 (m, 5H), 1.89 – 1.77 (m, 12H), 1.76 – 1.66 (m, 18H), 1.61 (t, *J* = 15.8 Hz, 8H), 1.56 – 1.46 (m, 10H), 1.39 (dd, *J* = 12.9, 9.8 Hz, 5H), 1.34 – 1.26 (m, 6H), 1.25 – 1.20 (m, 6H), 1.19 – 1.00 (m, 18H), -3.59 (d, *J* = 9.0 Hz, 2H). ^{31}P NMR (202 MHz, Benzene-d_6) δ 93.37 (t, *J* = 27.2 Hz), 46.65 (t, *J* = 27.2 Hz). ^{29}Si NMR (119 MHz, C_6D6) δ 124.40 (m). ^{13}C NMR (126 MHz, C_6D_6) δ 142.68, 141.68, 141.61, 117.36, 117.26, 106.95, 106.23, 40.14, 40.09, 39.21, 38.19, 37.99, 37.35, 37.30, 34.31, 34.20, 30.56, 30.33, 29.82, 29.70, 29.37, 28.68, 28.64, 28.57, 28.47, 28.18, 28.10, 27.94, 27.55, 27.36, 27.24, 26.90, 26.75. Anal. Calcd. for $C_{64}H_{106}N_4Ni_2P_4Si_2$: C, 62.55%; H, 8.69%; N, 4.56% Anal. Found for $C_{64}H_{106}N_4Ni_2P_4Si_2$: C, 52.42%; H, 8.60%; N, 3.53% Note: Due to the high molecular weight of the complexes, an exact mass was not obtained, however the LIFDI analysis did well match the theoretical isotope pattern.

Exact Mass Predicted for $C_{64}H_{106}N_4Ni_2P_4Si_2$: 1226.5613 Mass found by LIFDI for $C_{64}H_{106}N_4Ni_2P_4Si_2$: M, 1226.6

4.5.3 $P_4Ni_2Si_2(\mu$-H)(OPh) (**12**)

A 20 mL vial was charged with 39.5 mg (0.032 mmol), stir bar and 2 mL benzene. Phenol, 3 mg (0.032 mmol) in 0.5 mL benzene was added to **8**. Stirring overnight resulted in formation of a red precipitate, which was collected using a paper tipped pipette. The precipitate was rinsed with ether and collected with THF. The THF was concentrated down to about 1 mL and 2 mL hexane added. After sitting overnight at 35 °C, dark red crystals where isolated in 60% yield. ^{1}H NMR (500 MHz, Benzene-d_6) δ 7.14 (m, overlapping with C_6D_6, 1H), 7.11 (t, *J* = 7.4 Hz, 1H), 6.99 (t, *J* = 8.0 Hz, 4H), 6.87 (d, *J* = 7.3 Hz, 1H), 6.84

(t, *J* = 4.4 Hz, 1H), 6.76 (d, *J* = 7.3 Hz, 1H), 6.72 (d, *J* = 8.1 Hz, 2H), 6.61 (d, *J* = 6.9 Hz, 2H), 3.85 (t, *J* = 11.3 Hz, 1H), 3.42 (d, *J* = 10.8 Hz, 2H), 3.36 – 3.19 (m, 3H), 3.11 (dd, *J* = 12.4, 5.5 Hz, 1H), 2.53 (d, *J* = 13.8 Hz, 1H), 2.48 (d, *J* = 17.0 Hz, 1H), 2.33 (s, 1H), 2.23 (d, *J* = 12.0 Hz, 1H), 2.11 (s, 3H), 2.05 (s, 3H), 1.96 (d, *J* = 13.3 Hz, 2H), 1.94 – 1.82 (m, 10H), 1.81 – 1.73 (m, 8H), 1.71 – 1.56 (m, 19H), 1.55 – 1.36 (m, 15H), 1.35 – 1.28 (m, 6H), 1.27 – 1.16 (m, 7H), 1.15 – 1.03 (m, 14H), 0.97 (q, *J* = 11.5, 10.6 Hz, 10H), 0.72 (t, *J* = 12.0 Hz, 3H), 0.20 (q, *J* = 13.7, 13.3 Hz, 1H), -1.45 (dt, *J* = 19.4, 9.3 Hz, 1H). ^{31}P NMR (202 MHz, Benzene-d_6) δ 85.82 (ddd, *J* = 29.0, 20.1, 12.0 Hz), 78.96 – 78.54 (m), 32.93 (t, *J* = 10.6 Hz), 26.09 (d, *J* = 27.3 Hz). ^{29}Si NMR (119 MHz, Benzene-d_6) δ 118.14 – 116.15 (m), 46.34 – 44.97 (m). ^{13}C NMR (151 MHz, C_6D_6) δ 157.08, 144.19, 144.08, 142.91, 142.20, 142.10, 141.26, 141.19, 129.46, 121.30, 119.64, 118.71, 118.64, 117.71, 116.92, 109.23, 107.73, 107.32, 105.80, 45.37, 41.39, 41.33, 39.79, 39.71, 39.21, 38.95, 38.74, 37.27, 36.91, 36.85, 35.81, 35.70, 33.54, 33.46, 33.04, 31.88, 31.76, 31.51, 30.49, 30.40, 30.30, 30.04, 29.97, 29.72, 29.65, 29.50, 29.43, 29.25, 28.85, 28.79, 28.69, 28.45, 28.38, 28.31, 28.18, 28.09, 27.95, 27.85, 27.78, 27.63, 27.59, 27.52, 27.43, 27.00, 26.77, 25.24. Note: Due to the high molecular weight of the complexes, an exact mass was not obtained, however the LIFDI did well match the theoretical isotope pattern. Exact Mass Predicted $C_{70}H_{110}N_4Ni_2OP_4Si_2$: 1318.5876 Mass found by LIFDI for $C_{70}H_{110}N_4Ni_2OP_4Si_2$: M^+, 1318.6

4.5.4 $P_4Ni_2Si_2$(μ-H)(μ-SPh) (**13**)

To a 50 mL Strauss flask equipped with stir bar, 47.3 mg (0.0385 mmol) in 13 mL of benzene was added. While under an inert atmosphere of N_2, 3.9 μL (0.0385 mmol) of dried

thiophenol was added via an analytical syringe. After thirty minutes of stirring, the reaction mixture was pumped down and recrystallized from a THF/ether mixture at -35 °C in 35% yield. ^{1}H NMR (500 MHz, Benzene-d_6) δ 7.34 (d, J = 7.5 Hz, 2H), 7.10 (d, J = 7.3 Hz, 1H), 7.07 (d, J = 8.1 Hz, 1H), 6.95 (h, J = 7.1 Hz, 2H), 6.91 – 6.82 (m, 3H), 6.77 (q, J = 7.6, 5.8 Hz, 1H), 6.69 (q, J = 8.5 Hz, 3H), 3.82 (t, J = 11.1 Hz, 1H), 3.76 – 3.63 (m, 2H), 3.42 (t, J = 11.6 Hz, 1H), 3.23 (d, J = 11.9 Hz, 1H), 3.16 (t, J = 11.6 Hz, 1H), 3.08 – 2.97 (m, 2H), 2.55 – 2.42 (m, 2H), 2.39 – 2.24 (m, 6H), 2.24 – 2.12(m, 2H), 2.11 – 2.00 (m, 5H), 1.99 – 1.84 (m, 9H), 1.83 – 1.77 (m, 4H), 1.76 – 1.67 (m, 6H), 1.66 – 1.55 (m, 10H), 1.54 – 1.37 (m, 10H), 1.36 – 1.22 (m, 9H), 1.21 – 0.98 (m, 15H), 0.96 – 0.79 (m, 4H), 0.60 (q, J = 13.1 Hz, 2H), -3.55 (t, J = 12.3 Hz, 1H). ^{31}P NMR (202 MHz, Benzene-d_6) δ 71.51 (dd, J = 32.2, 20.3 Hz), 70.78 (t, J = 33.3 Hz), 47.18 (t, J = 31.8 Hz), 26.04 (dd, J = 34.2, 20.1 Hz). ^{13}C NMR (151 MHz, C_6D_6) δ 142.97, 142.60, 141.75, 141.30, 140.58, 134.24, 128.89, 125.71, 118.26, 118.22, 118.00, 117.66, 107.90, 107.77, 107.68, 106.79, 45.93, 39.24, 38.41, 37.56, 37.18, 37.12, 36.73, 36.50, 35.65, 33.96, 33.36, 32.96, 31.01, 30.21, 29.98, 29.73, 29.49, 29.38, 29.22, 29.00, 28.67, 28.59, 28.51, 28.44, 28.01, 27.54, 27.46, 27.29, 27.22, 27.00, 26.23. Note: Due to the high molecular weight of the complex, an exact mass was not obtained, however the LIFDI did well match the theoretical isotope pattern. Exact Mass Predicted: 1334.5647, Mass found by LIFDI: M^+, 1336.5.

4.5.5 $P_4Ni_2Si_2(\mu\text{-}(SPh))_2$ (**14**)

To a 20 mL vial **4**, 100 mg (0.146 mmol) was added and dissolved in toluene. With stirring, 67.3 mg (0.292 mmol) potassium naphthalenide was added in three portions. After 40 mins, the reaction was complete by ^{31}P NMR to generate **8** in situ. The reaction mixture was

filtered through a pipette Celite filter, to remove KCl, into a clean 20 mL vial. With stirring, 15.9 mg (0.0.73 mmol) of diphenyl disulfide in 0.5 mL of toluene was added. The reaction was found to be complete after 20 mins with stirring. The toluene solution was concentrated down to about 1-2 mL and ether added. Cooling at -30 C yielded 70 mg (69 % yield) of **14**, after first crop collection. ^{1}H NMR (600 MHz, Benzene-d_6) δ 7.20 – 7.16 (m, 3H, partially overlapping with benzene), 7.11 (td, *J* = 7.5, 1.3 Hz, 1H), 7.06 (td, *J* = 7.5, 1.3 Hz, 1H), 6.87 (dd, *J* = 7.5, 1.3 Hz, 1H), 6.81 (t, *J* = 7.6 Hz, 2H), 6.76 – 6.70 (m, 1H), 6.67 (dd, *J* = 7.4, 1.3 Hz, 1H), 3.75 (dd, *J* = 12.1, 6.5 Hz, 1H), 3.42 (dd, *J* = 13.0, 5.8 Hz, 1H), 3.36 – 3.23 (m, 1H), 3.15 (dd, *J* = 12.1, 3.7 Hz, 1H), 3.11–3.02 (m, 1H), 2.83 (dd, *J* = 13.0, 3.6 Hz, 1H), 2.65 (d, *J* = 12.8 Hz, 1H), 2.39 (d, *J* = 12.4 Hz, 1H), 2.25 (t, *J* = 12.8 Hz, 1H), 2.09 – 1.98 (m, 3H), 1.99 – 1.91 (m, 2H), 1.91 – 1.53 (m,13H), 1.52 – 1.41 (m, 2H), 1.41 – 1.29 (m, 4H), 1.28 – 1.08 (m, 7H), 1.06 – 0.92 (m, 2H), 0.78 – 0.66 (m, 1H), 0.63 – 0.53 (m, 1H), 0.52 – 0.43 (m, 1H). ^{31}P NMR (243 MHz, Benzene-d_6) δ 41.13 (dd, *J* = 32.7, 23.4 Hz), 25.29 (dd, *J* = 32.6, 23.5 Hz).^{29}Si NMR (119 MHz, Benzene-d_6) δ 40.10 – 39.48 (m), 39.50 – 38.93 (m). ^{13}C NMR (151 MHz, C_6D_6) δ 142.12, 141.66, 140.78, 133.57, 129.09, 125.38, 118.81, 118.09, 108.76, 107.81, 44.26, 42.83, 40.41, 38.96, 38.28, 35.96, 32.42, 31.47, 31.06, 30.68, 30.30, 30.22, 29.33, 29.26, 29.07, 29.00, 28.94, 28.71, 28.63, 28.51, 28.46, 27.79, 27.72, 27.61, 27.46, 27.18, 26.86. Note: Due to the high molecular weight of the complexes, an exact mass was not obtained, however the LIFDI did well match the theoretical isotope pattern. Exact Mass Predicted for $C_{76}H_{114}N_4Ni_2P_4S_2Si_2$: 1442.5681. Mass found by LIFDI for $C_{76}H_{114}N_4Ni_2P_4S_2Si_2$: M^+, 1444.6

4.6 References

(1) Green, M. L. H. *Journal of Organometallic Chemistry* **1995**, *500* (1–2), 127–148.

(2) Iluc, V. M.; Hillhouse, G. L. *Tetrahedron* **2006**, *62* (32), 7577–7582.

(3) Corey, J. Y. *Chemical Reviews* **2016**, *116* (19), 11291–11435.

(4) Watanabe, T.; Hashimoto, H.; Tobita, H. *Chemistry - An Asian Journal* **2012**, *7* (6), 1408–1416.

(5) Suzuki, E.; Okazaki, M.; Tobita, H. *Chemistry Letters* **2005**, *34* (7), 1026–1027.

(6) Sakaba, H.; Watanabe, S.; Kabuto, C.; Kabuto, K. *Journal of the American Chemical Society* **2003**, *125* (10), 2842–2843.

(7) Dysard, J. M.; Tilley, T. D. *Organometallics* **2002**, *19* (23), 4726–4732.

(8) Campion, B. K.; Heyn, R. H.; Tilley, T. D. *Organometallics* **1992**, *11*, 3918–3920.

(9) Scherer, W.; Meixner, P.; Barquera-Lozada, J. E.; Hauf, C.; Obenhuber, A.; Brück, A.; Wolstenholme, D. J.; Ruhland, K.; Leusser, D.; Stalke, D. *Angewandte Chemie - International Edition* **2013**, *52* (23), 6092–6096.

(10) Corey, J. Y. *Chemical Reviews* **2011**, *111* (2), 863–1071.

(11) Beck, R.; Johnson, S. A. *Organometallics* **2012**, *31*, 3599–3609.

(12) Tanabe, M.; Yumoto, R.; Osakada, K. *Chem. Commun. Chem. Commun* **2012**, *48* (48), 2125–2127.

(13) Tanabe, M.; Takahashi, A.; Yamada, T.; Osakada, K. *Organometallics* **2013**, *32*, 34.

(14) Wang, Y.; Kostenko, A.; Yao, S.; Driess, M. *Journal of the American Chemical Society* **2017**, *139* (38), 13499–13506.

(15) Gerloch, M. *Polyhedron* **2016**, *120*, 205–207.

(16) Lin, C.-Y.; Power, P. P. *Chem. Soc. Rev* **2017**, *46*, 5347.

(17) Jones, R. A.; Stuart, A. L.; Atwood, J. L.; Hunter, W. E. *Organometallics* **1983**, *2*, 874–878.

(18) Jones, Richard A. Norman, Nicholas C., and Seeberger, M. H. *Organometallics* **1983**, *2* (11), 1629–1634.

(19) Grüger, N.; Wadepohl, H.; Gade, L. H. *Dalton Transactions* **2012**, *41* (46), 14028.

(20) Lin, T.-P.; Peters, J. C. *J. Am. Chem. Soc* **2014**, *136*.

(21) Suzuki, H. *Eur. J. Inorg. Chem.* **2002**, 1009–1023.

(22) Schmidt, D.; Zell, T.; Schaub, T.; Radius, U. *Dalton Transactions* **2014**, *43* (28), 10816.

(23) Beck, R.; Johnson, S. A. *Organometallics* **2012**, *31* (9), 3599–3609.

(24) Vicic, D. A.; Jones, W. D. *Journal of the American Chemical Society* **1997**, *119* (44), 10855–10856.

(25) Tanabe, M.; Yumoto, R.; Osakada, K.; Sanji, T.; Tanaka, M. *Organometallics* **2012**, *31* (19), 6787–6795.

(26) Jones, R. A.; Whittlesey, B. R. *Inorganic Chemistry* **1986**, *25* (6), 852–856.

(27) Iluc, V. M.; Hillhouse, G. L. *Journal of the American Chemical Society* **2010**, *132* (34), 11890–11892.

(28) Chambers, G. M.; Huynh, M. T.; Li, Y.; Hammes-Schiffer, S.; Rauchfuss, T. B.; Reijerse, E.; Lubitz, W. *Inorganic Chemistry* **2016**, *55* (2), 419–431.

(29) Klei, S. R.; Don Tilley, T.; Bergman, R. G. *Organometallics* **2002**, *21* (16), 3376–3387.

(30) Sorensen, S.; Jakobsen, H. J. *Organic Magnetic Resonance* **1977**, *9* (2), 101–104.

(31) Beck, R.; Johnson, S. A. *Chem. Commun* **2011**, *47*, 9233–9235.

(32) Batiha, M.; Altarawneh, M.; Al-Harahsheh, M.; Altarawneh, I.; Rawadieh, S. *Computational and Theoretical Chemistry* **2011**, *970*, 1–5.

(33) Tan, G.; Driess, M.; Enthaler, S.; Inoue, S.; Blom, B. *Angewandte Chemie International Edition* **2015**, *54* (7), 2214–2218.

4.7 Spectroscopic Data, Figures and Tables

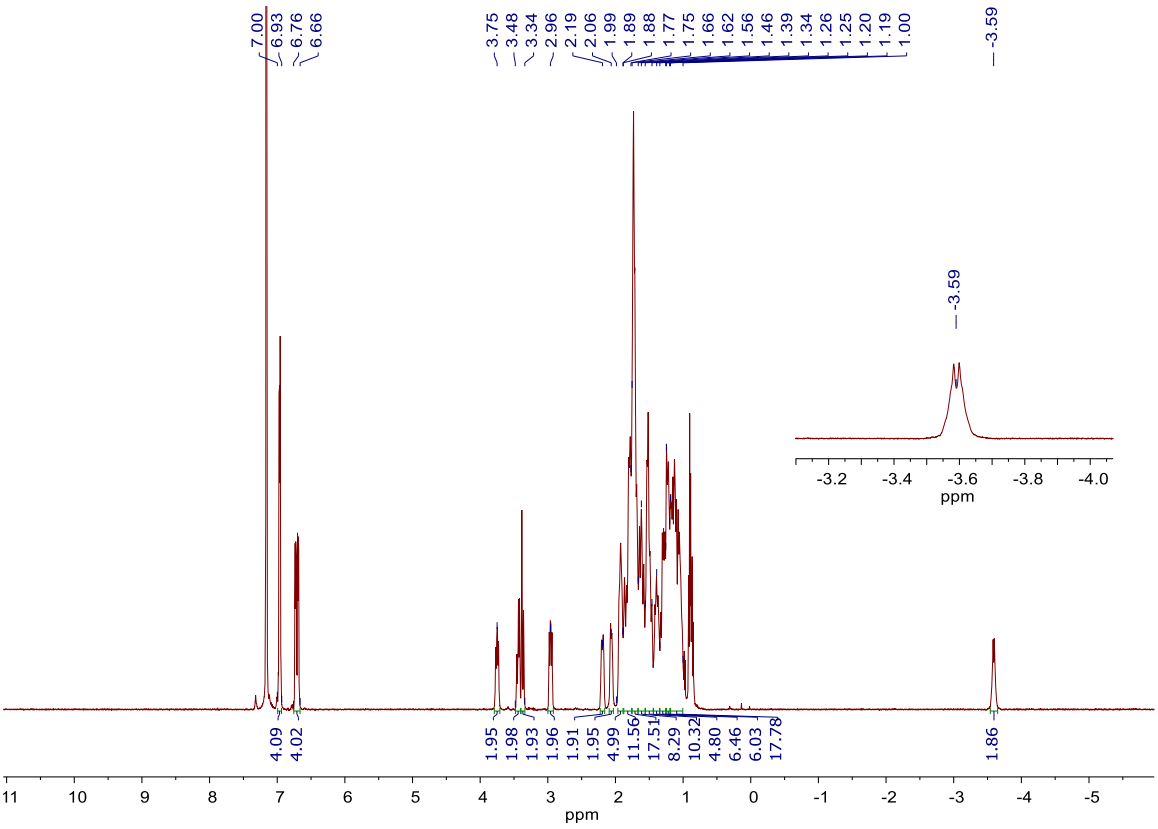

Figure 4.7-1. ^{1}H NMR of $P_4Ni_2Si_2(\mu\text{-H})_2$, **11**, in C_6D_6 at a frequency of 500 MHz.

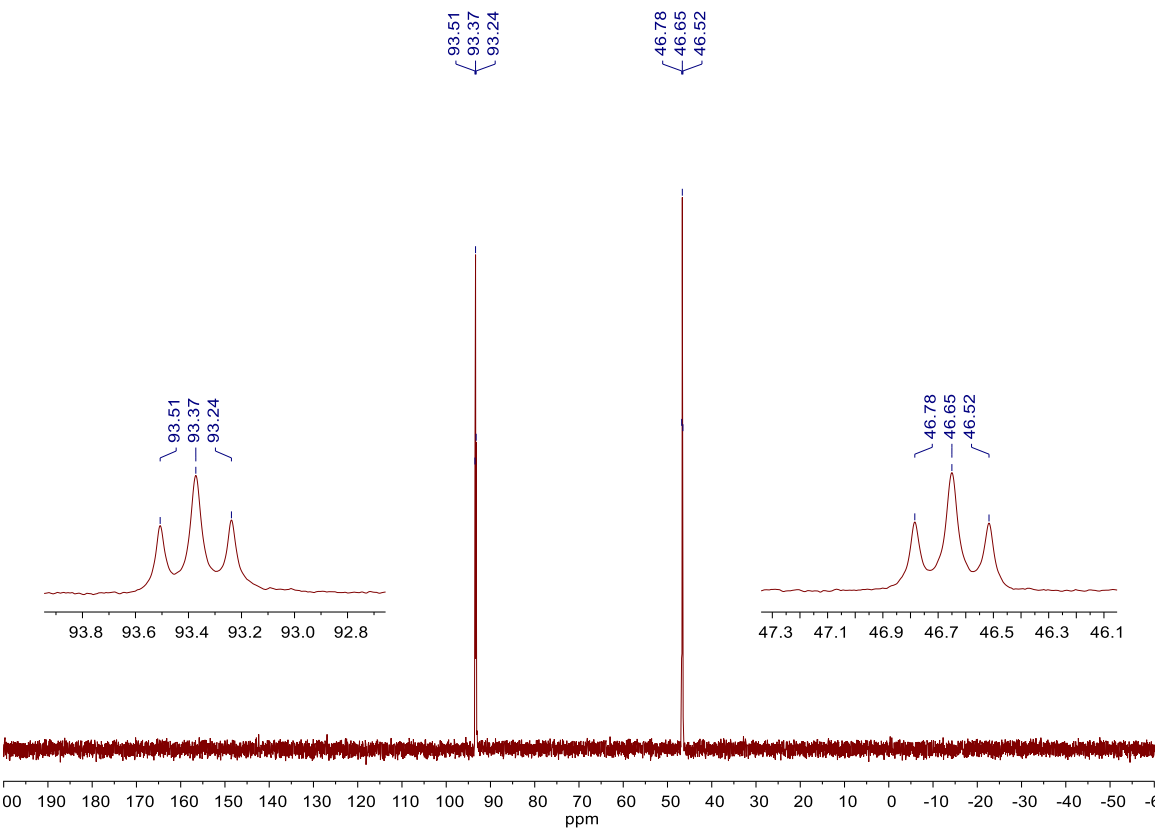

Figure 4.7-2 $^{31}P\{^{1}H\}$ NMR of $P_4Ni_2Si_2(\mu\text{-H})_2$, **11**, in C_6D_6 at a frequency of 202 Hz.

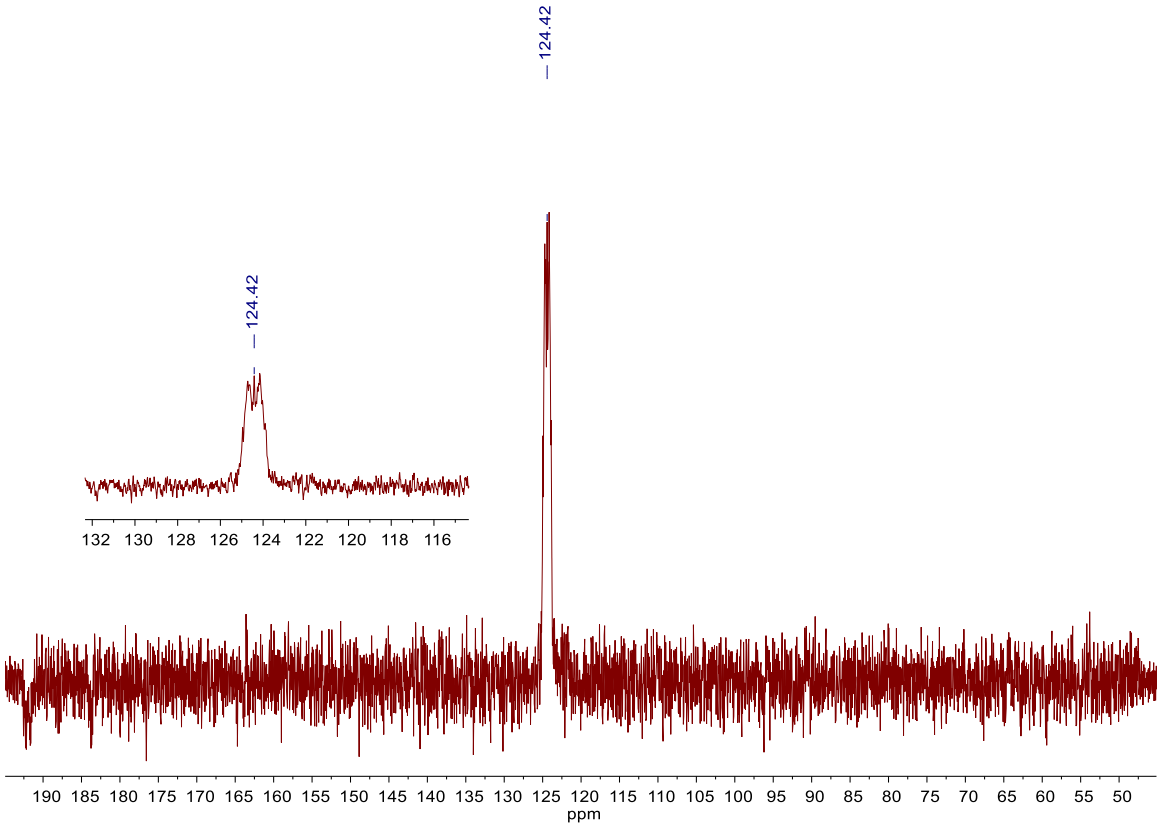

Figure 4.7-3 $^{29}Si\{^{1}H\}$ NMR of $P_4Ni_2Si_2(\mu\text{-}H)_2$, **11**, in C_6D_6 at 119 Hz.

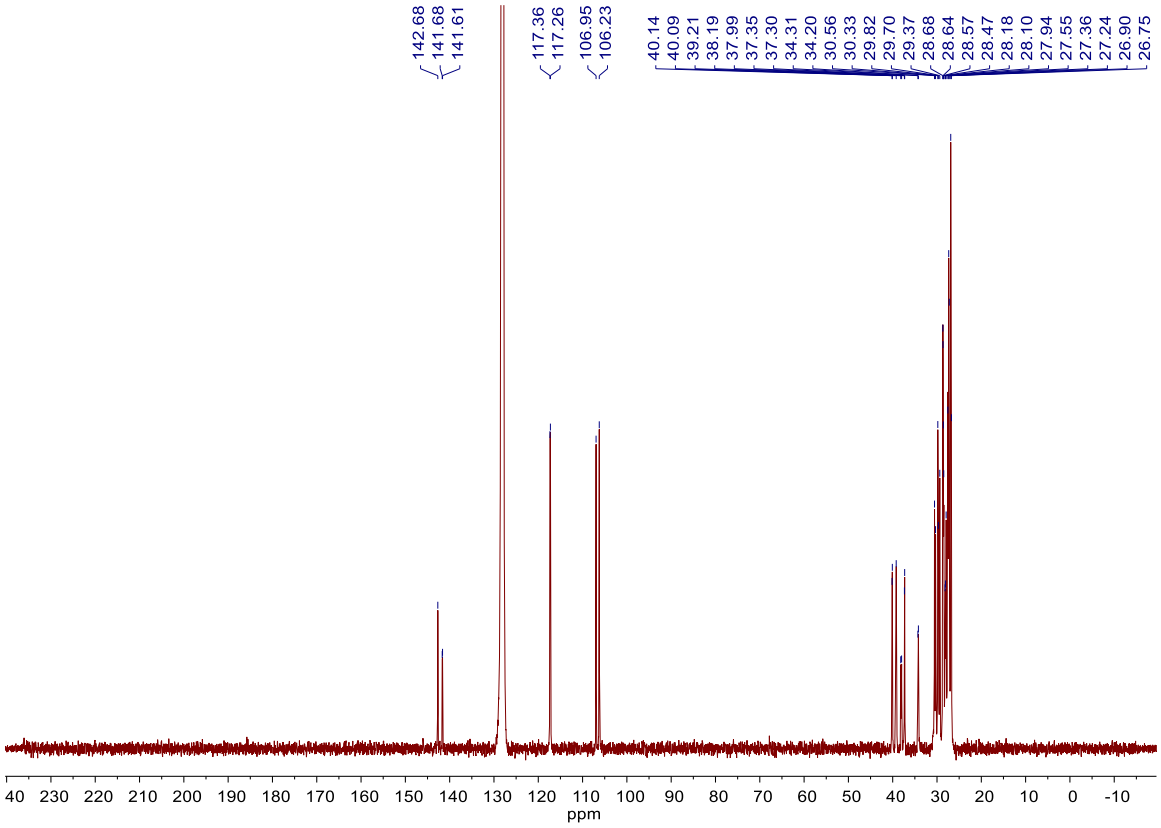

Figure 4.7-4 ^{13}C NMR of $P_4Ni_2Si_2(\mu\text{-H})_2$, **11**, in C_6D_6 at 126 MHz.

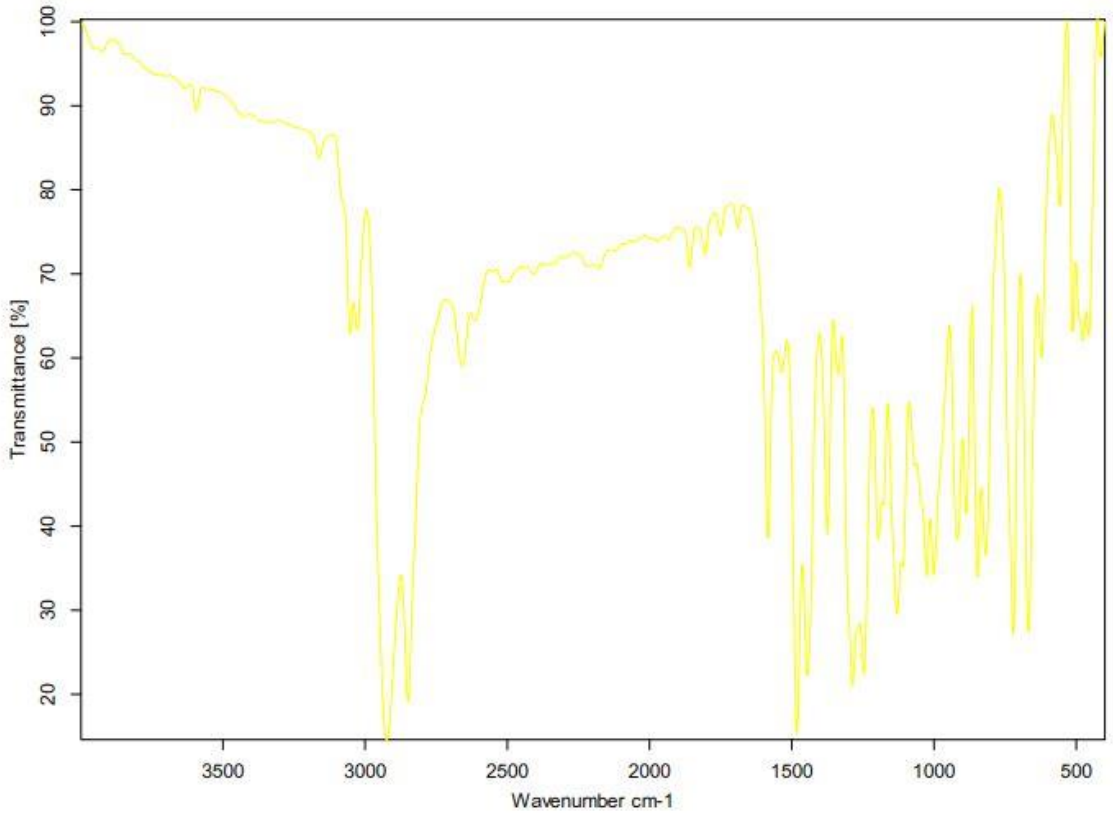

Figure 4.7-5 IR spectrum obtained using a KBR pellet of $P_4Ni_2Si_2(\mu\text{-H})_2$, **11**, featuring strong absorption around 1500 cm^{-1} indicative of Si–H fragment.

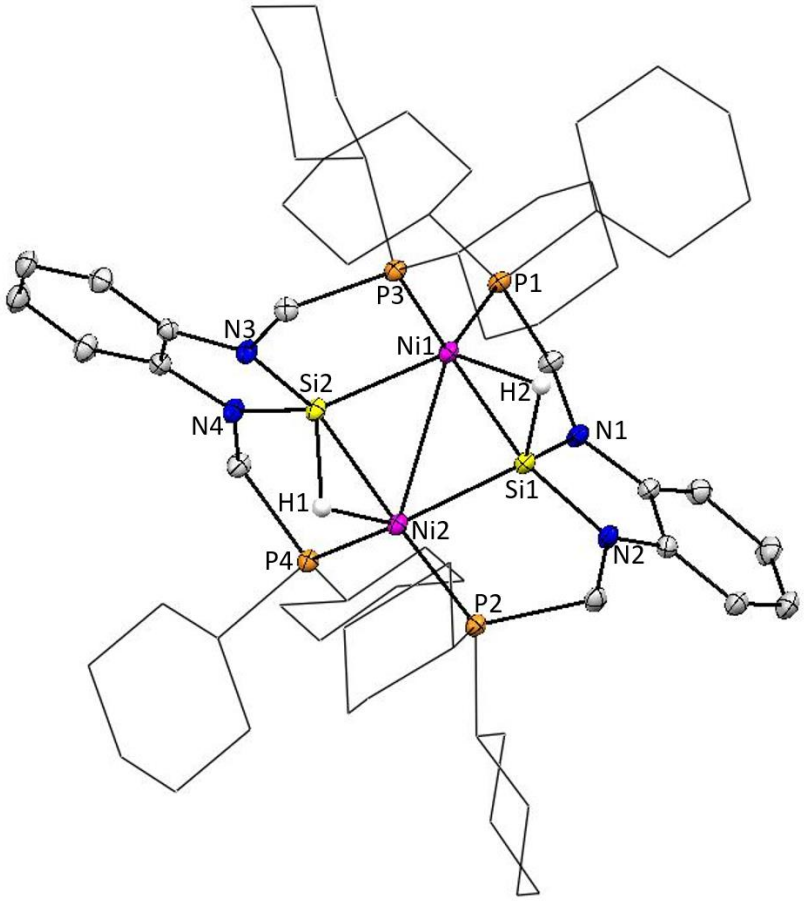

Figure 4.7-6 ORTEP representation of $P_4Ni_2Si_2(\mu\text{-H})_2$, **11**. Magenta, yellow, blue, orange, and gray ellipsoids represent nickel, silicon, nitrogen, phosphorus, and carbon respectively. For clarity, hydrogen atoms and solvent molecules are omitted and cyclohexyl rings on phosphorous are displayed as wireframe. There was one molecule of $C_{64}H_{106}N_4Ni_2P4_4Si_2$ and half a disordered molecule of C_7H_8 present in the asymmetric unit of the unit cell. The disordered C_7H_8 was located at the 1/4-diagonal glide plane parallel to the ab-plane and modeled as 50%/50% disordered site occupancy ratio.

Table 4.7-1 Crystallographic data for $P_4Ni_2Si_2(\mu\text{-H})_2$, **11**.

Identification code	hh99AB9_0m	
Empirical formula	$C_{67.50}H_{110}N_4Ni_2P_4Si_2$	
Formula weight	1275.07	
Temperature	100(2) K	
Wavelength	0.71073 Å	
Crystal system	Monoclinic	
Space group	C 2/c (#15)	
Unit cell dimensions	a = 39.9660(14) Å	α = 90°.
	b = 15.9105(6) Å	β = 113.8334(6)°.
	c = 22.9410(8) Å	γ = 90°.
Volume	13343.7(8) Å^3	
Z	8	
Density (calculated)	1.269 mg/m^3	
Absorption coefficient	0.739 mm^{-1}	
F(000)	5496	
Crystal size	0.328 x 0.158 x 0.110 mm^3	
θ range for data collection	1.396 to 30.508°.	
Index ranges	$-57 \le h\ 57, \le -22 \le k \le 22, -32 \le l \le 32$	
Reflections collected	193503	
Independent reflections	20365 [R_{int} = 0.0518]	
Completeness to θ = 25.242°	100.00%	
Absorption correction	Semi-empirical from equivalents	
Refinement method	Full-matrix least-squares on F^2	
Data / restraints / parameters	20365 / 16 / 743	
Goodness-of-fit on F^2	1.027	
Final R indices [$I > 2\sigma_1$]	R_1 = 0.0313, wR_2= 0.0728	
R indices (all data)	R_1 = 0.0450, wR_2 = 0.0789	
Largest diff. peak and hole	0.512 and -0.299 e/Å^3	

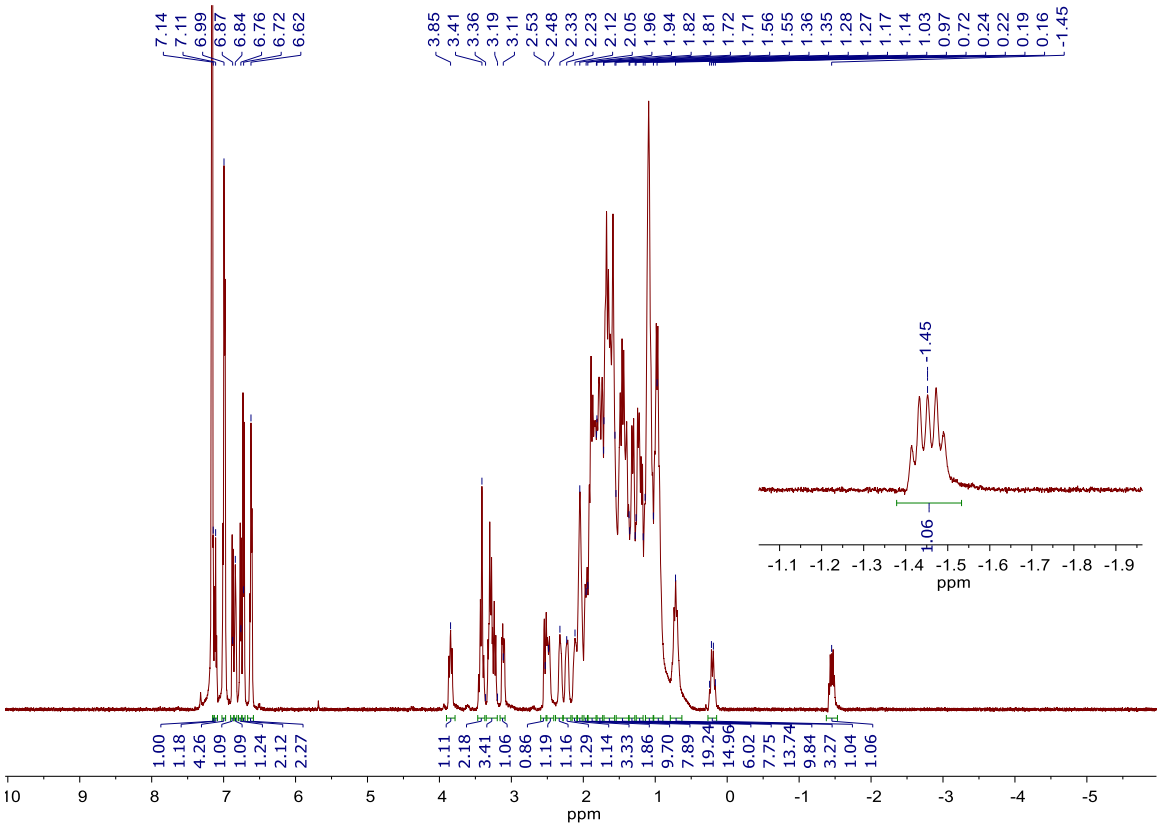

Figure 4.7-7 ^{1}H NMR of $P_4Ni_2Si_2(\mu\text{-H})(OPh)$, **12**, in C_6D_6 at 500 MHz.

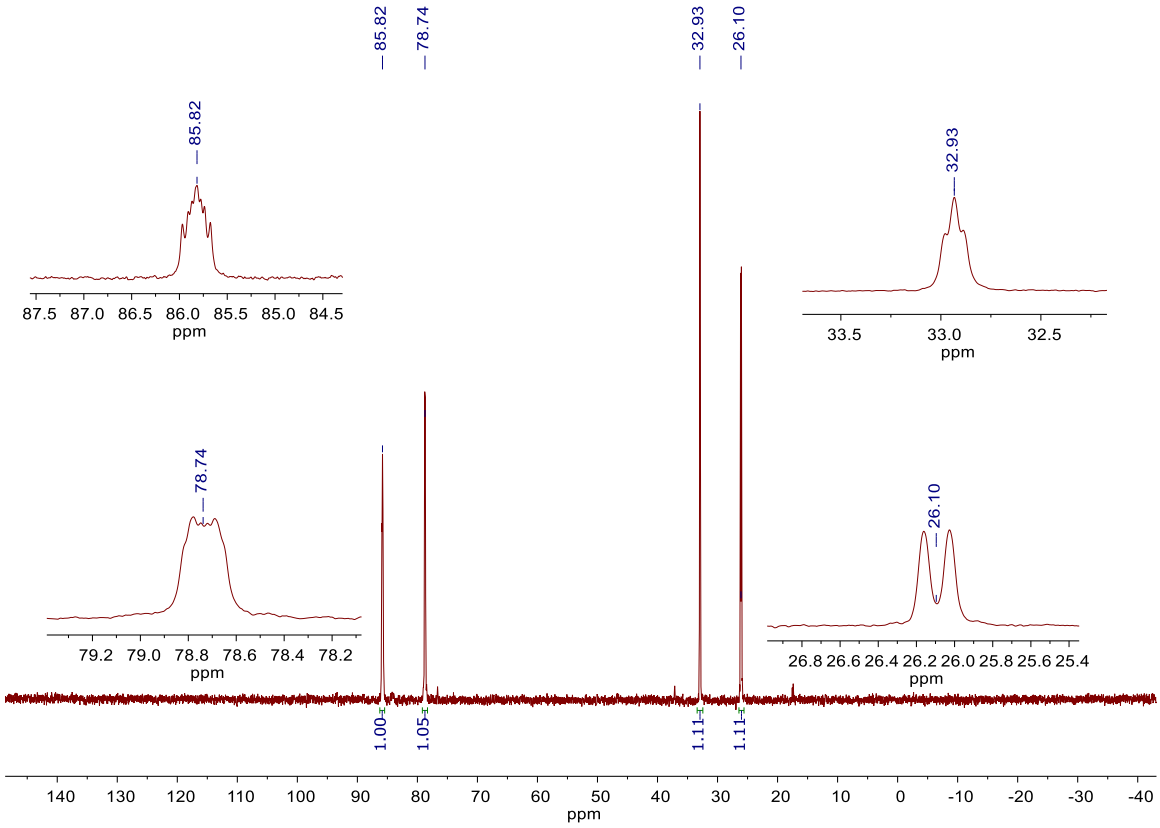

Figure 4.7-8 $^{31}P\{^{1}H\}$ NMR of $P_4Ni_2Si_2(\mu\text{-H})(OPh)$, **12**, in C_6D_6 at a frequency of 202 MHz.

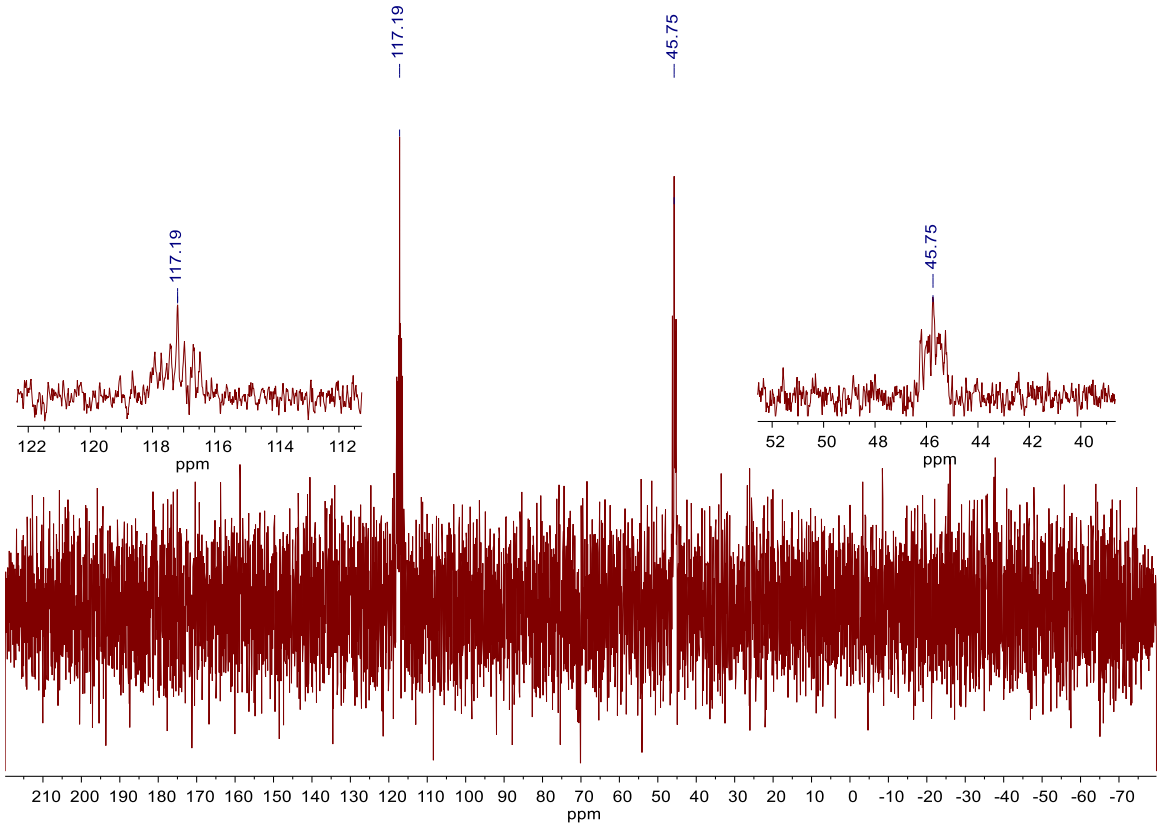

Figure 4.7-9 $^{29}Si\{^{1}H\}$ NMR of $P_4Ni_2Si_2(\mu\text{-}H)(OPh)$, **12**, in C_6D_6 at a frequency of 119 MHz.

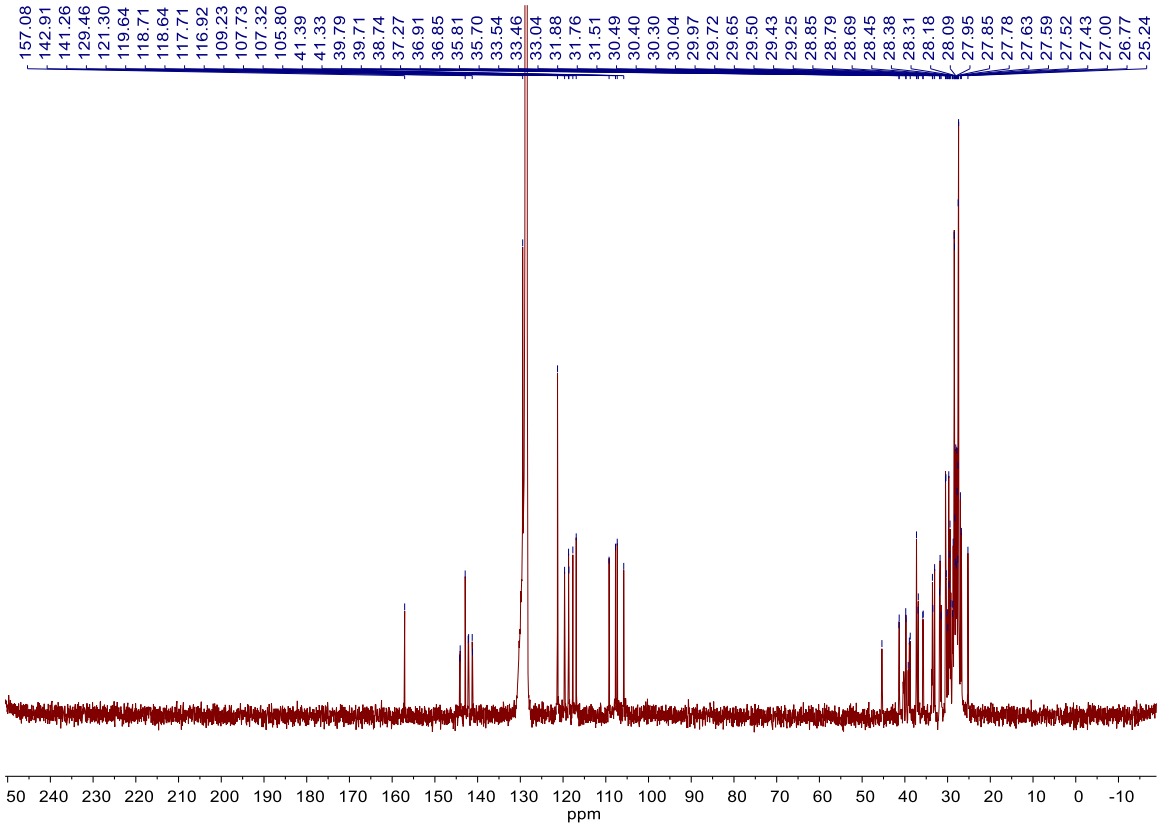

Figure 4.7-10 ^{13}C NMR of $P_4Ni_2Si_2(\mu\text{-}H)(OPh)$, **12**, in C_6D_6 at 151 MHz

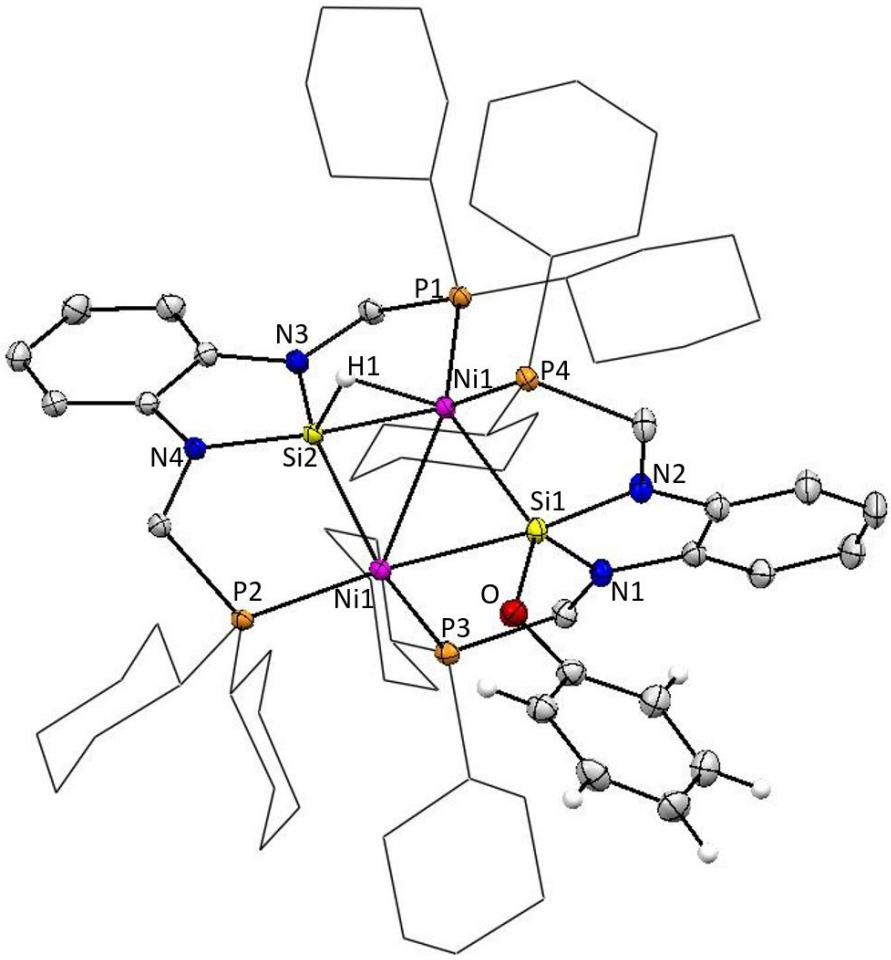

Figure 4.7-11 Thermal ellipsoid plot at 50% probability of $P_4Ni_2Si_2(\mu\text{-}H)(OPh)$, **12**, Magenta, yellow, blue, orange, red and gray ellipsoids represent nickel, silicon, nitrogen, phosphorus, oxygen and carbon respectively. For clarity, hydrogen atoms and solvent molecules are omitted and cyclohexyl rings on phosphorous are displayed as wireframe. There was one molecule of $C_{70}H_{110}N_4Ni_2OP_4Si_2$, and two half molecule of benzene present in the asymmetric unit of the unit cell. The two benzene molecules were located at the inversion symmetry.

Table 4.7-2 Crystallographic data for $P_4Ni_2Si_2(\mu\text{-H})(OPh)$, **12**.

Identification code	hh118AB12_0m	
Empirical formula	$C_{76}H_{116}N_4Ni_2OP_4Si_2$	
Formula weight	1399.2	
Temperature	100(2) K	
Wavelength	0.71073 Å	
Crystal system	Triclinic	
Space group	P -1	
Unit cell dimensions	a = 12.9855(4) Å	α = 75.6841(5)°.
	b = 15.4083(5) Å	β = 79.2287(5)°.
	c = 20.6575(6) Å	γ = 65.1543(5)°.
Volume	3617.99(19) $Å^3$	
Z	2	
Density (calculated)	1.284 mg/m^3	
Absorption coefficient	0.689 mm^{-1}	
F(000)	1504	
Crystal size	0.549 x 0.493 x 0.129 mm^3	
θ range for data collection	1.483 to 28.282°.	
Index ranges	$-17 \le h \le 17$, $-20 \le k \le 20$, $-27 \le l \le 27$	
Reflections collected	130499	
Independent reflections	17951 [R_{int} = 0.0270]	
Completeness to θ = 25.242°	100.00%	
Absorption correction	Semi-empirical from equivalents	
Refinement method	Full-matrix least-squares on F^2	
Data / restraints / parameters	17951 / 0 / 805	
Goodness-of-fit on F^2	1.029	
Final R indices [$I > 2\sigma_1$]	R_1 = 0.0277, wR_2 = 0.0706	
R indices (all data)	R_1 = 0.0320, wR_2 = 0.0734	
Largest diff. peak and hole	0.696 and -0.299 e/$Å^3$	

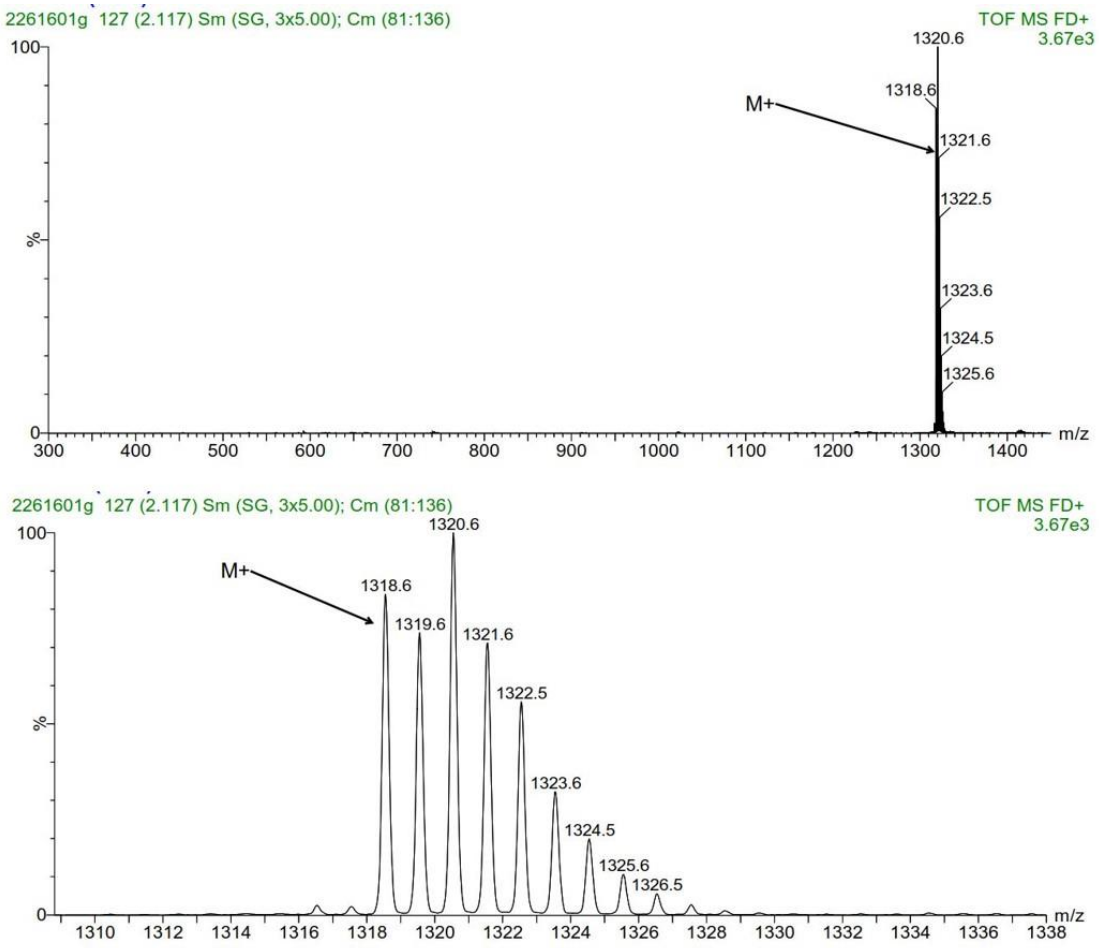

Figure 4.7-12. Mass Spectrometry operating in LIFDI mode for $P_4Ni_2Si_2(\mu\text{-}H)(OPh)$, **12**. Accurate mass calculated (1318.5876) was not obtained due to high molecular weight (1321.1288 g/mol) of **12**, however, the calculated isotopic pattern matched well with the observed.

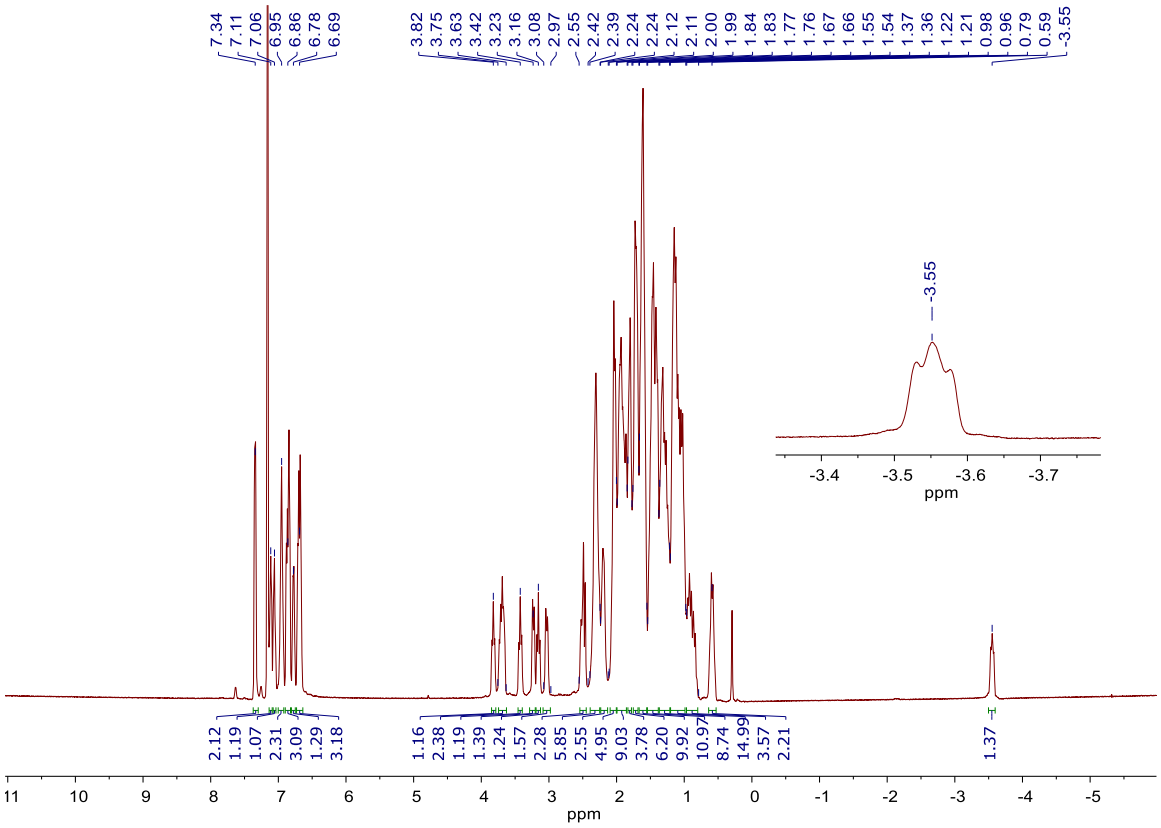

Figure 4.7-13 ^{1}H NMR of $P_4Ni_2Si_2(\mu\text{-H})(\mu\text{-SPh})$, **13**, in C_6D_6 at 500 MHz.

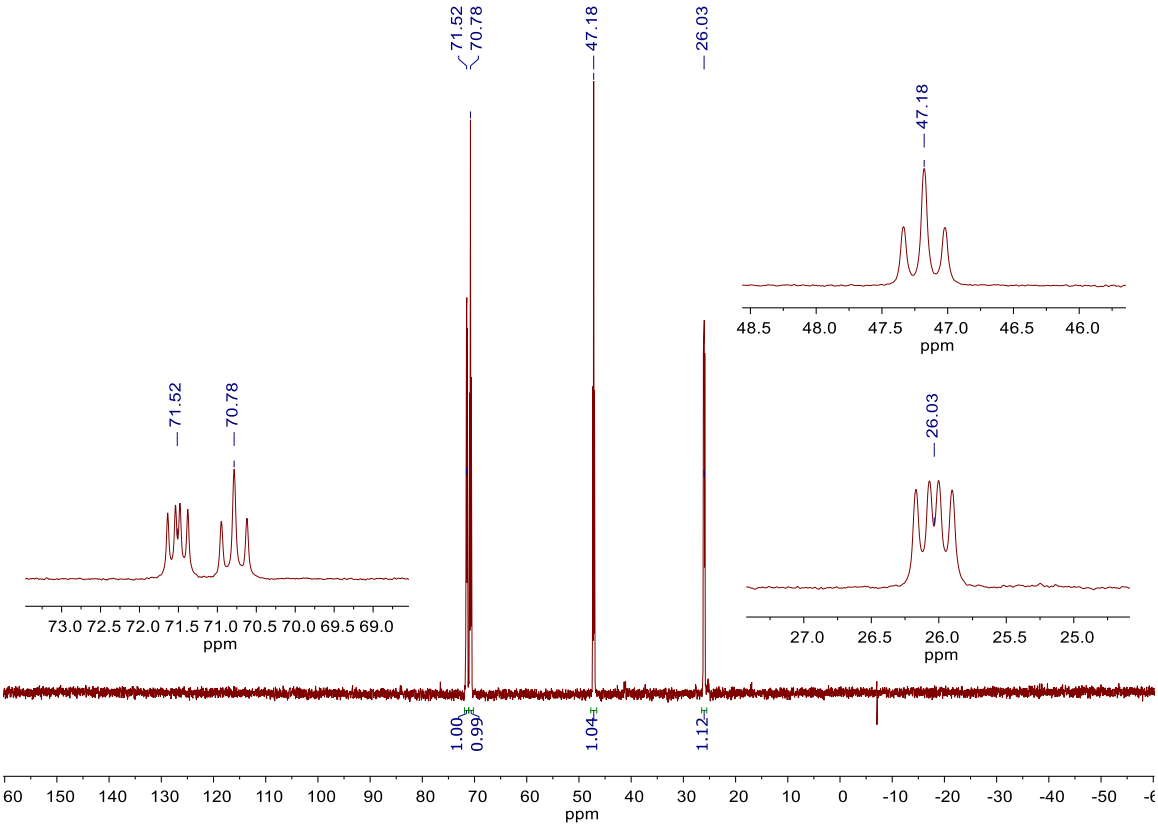

Figure 4.7-14 $^{31}P\{^{1}H\}$ NMR of $P_4Ni_2Si_2(\mu\text{-H})(\mu\text{-SPh})$, **13** in C_6D_6 at 202 MHz.

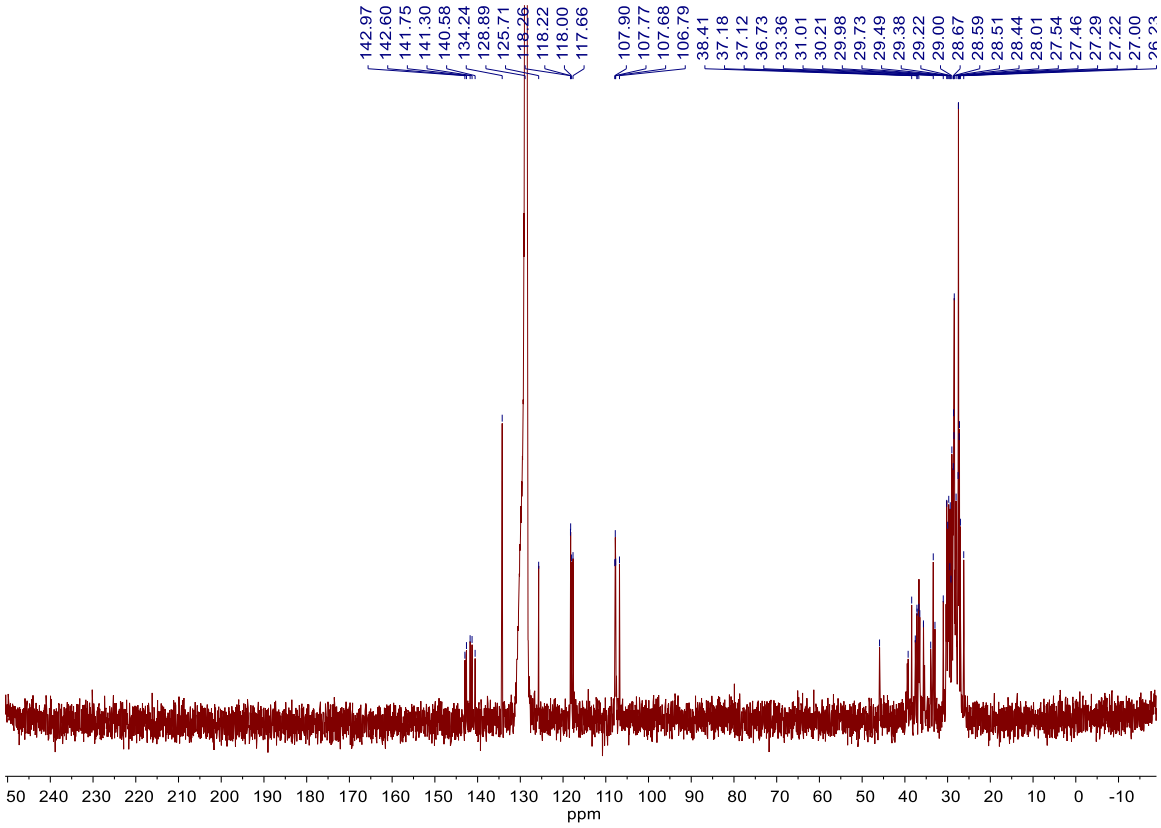

Figure 4.7-15 ^{13}C NMR of $P_4Ni_2Si_2(\mu\text{-H})(\mu\text{-SPh})$, **13**, in C_6D_6 at 151 MHz.

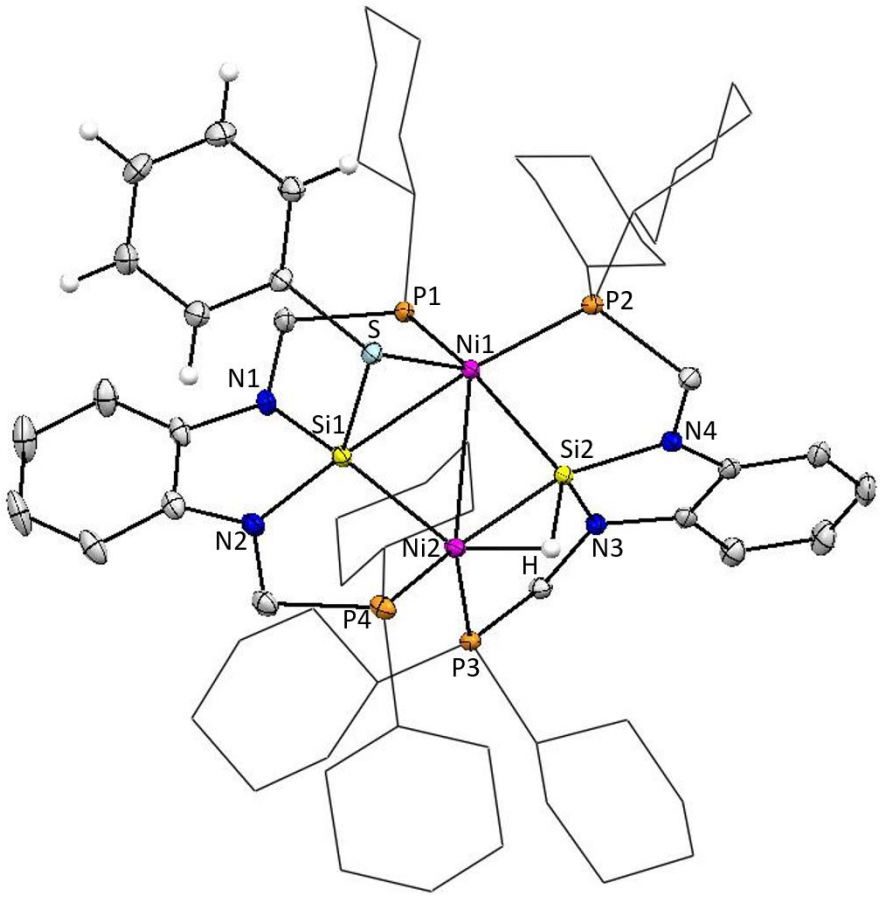

Figure 4.7-16 Thermal ellipsoid plot at 50% probability of $P_4Ni_2Si_2(\mu\text{-H})(\mu\text{-SPh})$, **13**. Magenta, yellow, blue, orange, light blue and gray ellipsoids represent nickel, silicon, nitrogen, phosphorus, sulfur and carbon respectively. For clarity, hydrogen atoms and solvent molecules are omitted and cyclohexyl rings on phosphorous are displayed as wireframe. There was one molecule of $C_{70}H_{110}N_4Ni_2P_4SSi_2$, where two of the cyclohexyl groups were modeled with disorder (disordered site occupancy ratios were 77%/23% and 83%/17%), and one solvent molecule of $C_4H_{10}O$ present in the asymmetric unit of the unit cell. The check cif alert level B and short H4A...H38C, H30B...H46B and O3S…C38D contacts were due to the two disordered cyclo-hexyl-groups.

Table 4.7-3 Crystallographic data for $P_4Ni_2Si_2(\mu\text{-H})(\mu\text{-SPh})$, **13**.

Identification code	hh184AB16_0m	
Empirical formula	$C_{74}H_{120}N_4Ni_2OP_4SSi_2$	
Formula weight	1411.27	
Temperature	100(2) K	
Wavelength	0.71073 Å	
Crystal system	Triclinic	
Space group	P -1	
Unit cell dimensions	a = 13.7797(5) Å	α = 81.8029(7)°.
	b = 14.8343(6) Å	β = 80.0920(7)°.
	c = 20.5432(8) Å	γ = 62.8856(6)°.
Volume	3672.2(2) Å^3	
Z	2	
Density (calculated)	1.276 mg/m^3	
Absorption coefficient	0.706 mm^{-1}	
F(000)	1520	
Crystal size	0.288 x 0.104 x 0.044 mm^3	
θ range for data collection	1.546 to 28.282°.	
Index ranges	-18≤ h ≤ 18, -19≤ k ≤19, -27≤ l ≤ 27	
Reflections collected	77200	
Independent reflections	18217 [R_{int} = 0.0466]	
Completeness to θ = 25.242°	100.00%	
Absorption correction	Semi-empirical from equivalents	
Refinement method	Full-matrix least-squares on F^2	
Data / restraints / parameters	18217 / 97 / 845	
Goodness-of-fit on F^2	1.019	
Final R indices [$I > 2\sigma_1$]	R_1 = 0.0363, wR_2 = 0.0778	
R indices (all data)	R_1 = 0.0537, wR_2 = 0.0847	
Largest diff. peak and hole	0.839 and -0.508 e/Å^3	

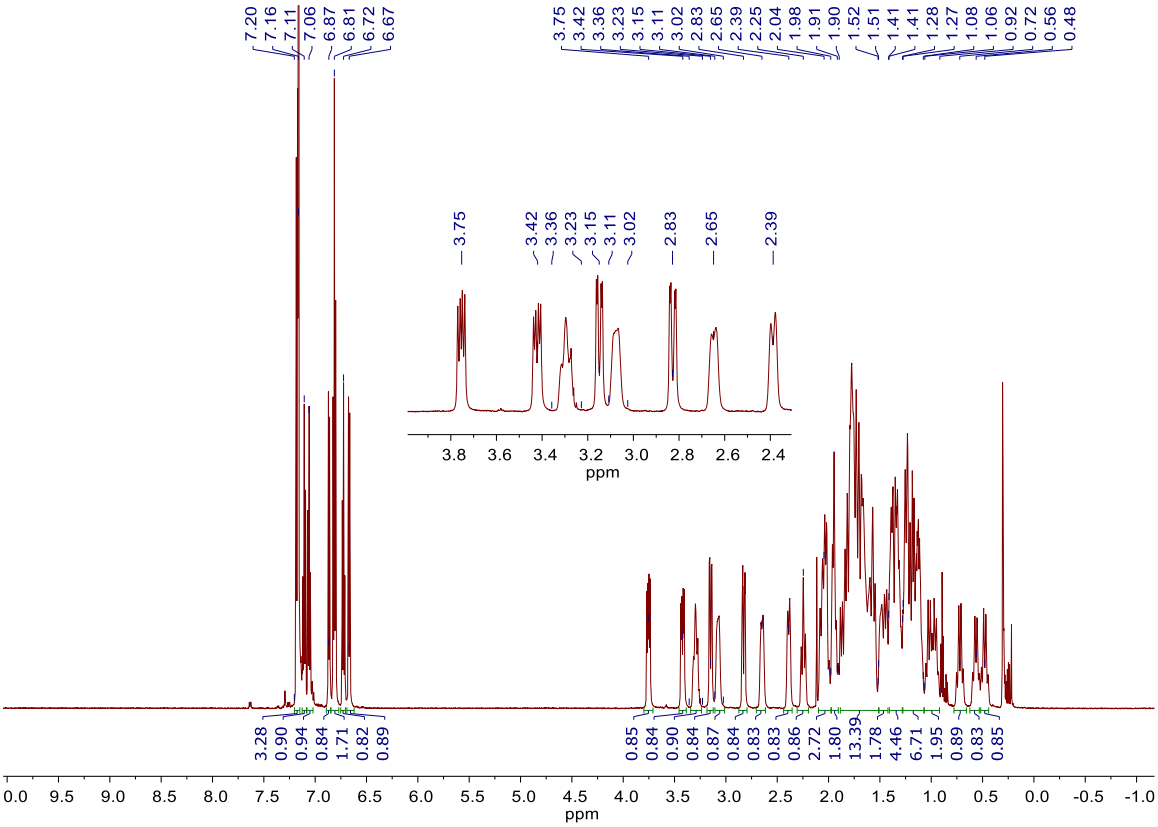

Figure 4.7-17 ^{1}H NMR of $P_4Ni_2Si_2(\mu\text{-}(SPh))_2$, **14**, in C_6D_6 at 600 MHz. Note H-grease at 0.30 ppm.

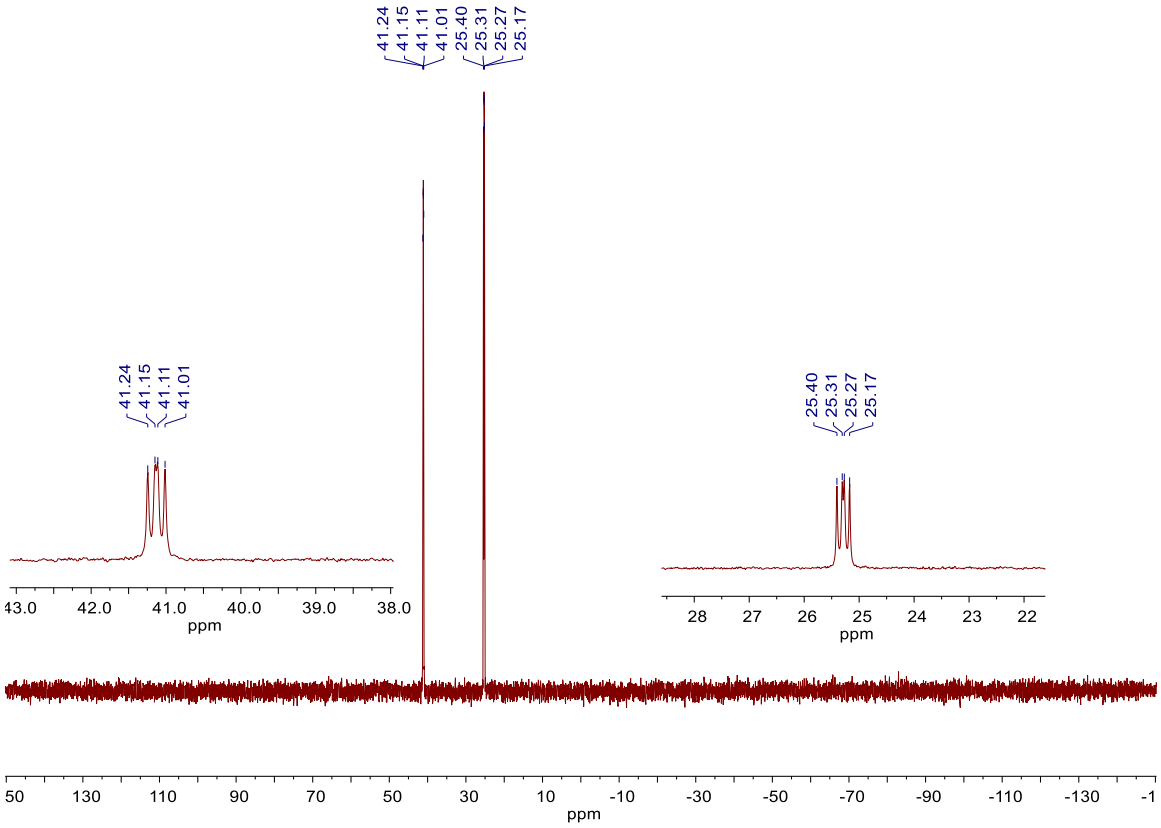

Figure 4.7-18 $^{31}P\{^{1}H\}$ NMR of $P_4Ni_2Si_2(\mu\text{-}(SPh))_2$, **14**, in C_6D_6 at 243 MHz.

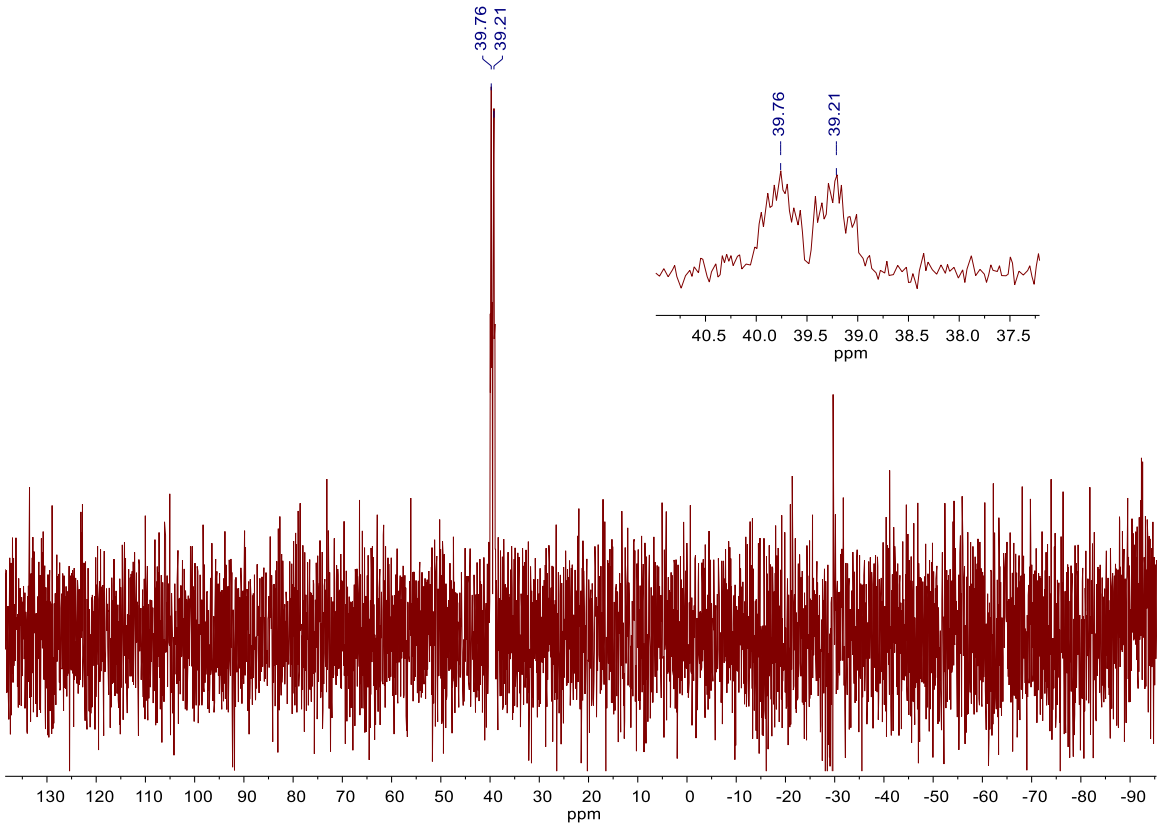

Figure 4.7-19 $^{29}Si\{^{1}H\}$ NMR of $P_4Ni_2Si_2(\mu\text{-}(SPh))_2$, **14**, in C_6D_6 at 119 MHz.

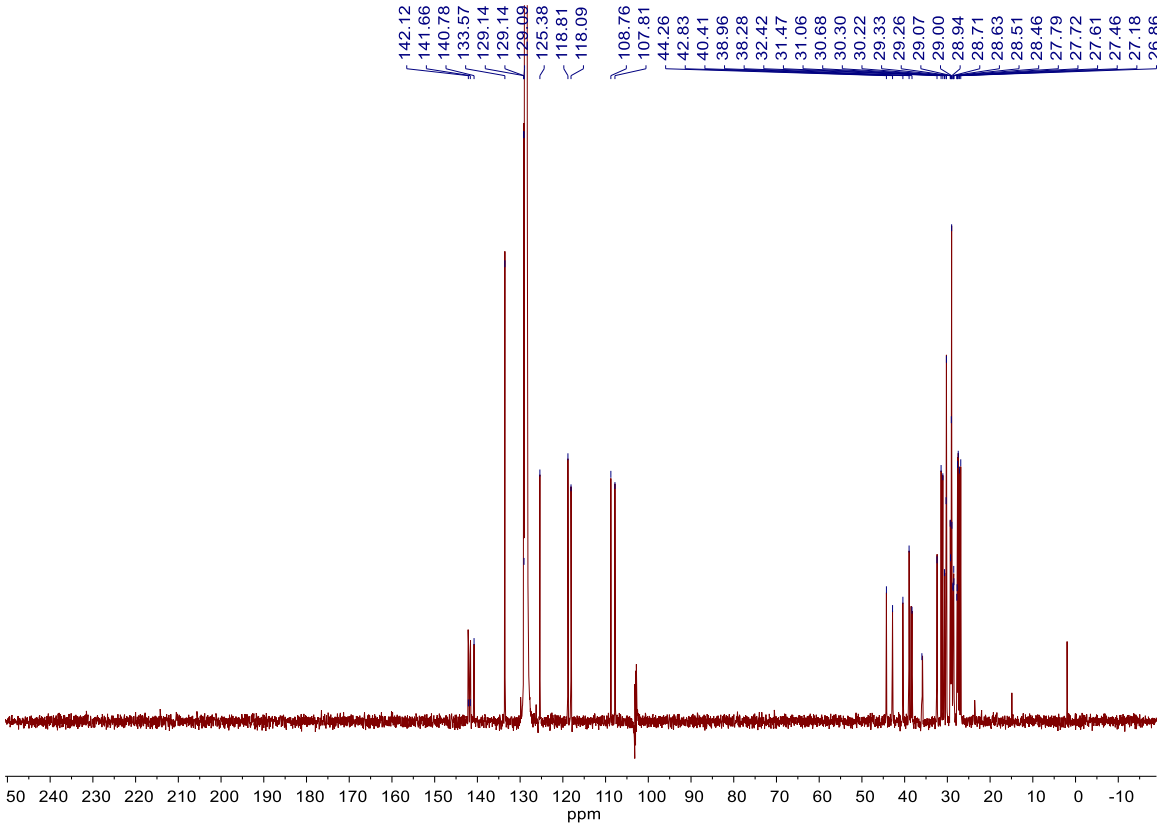

Figure 4.7-20 ^{13}C NMR of $P_4Ni_2Si_2(\mu\text{-}(SPh))_2$, **14**, in C_6D_6 at 151 MHz.

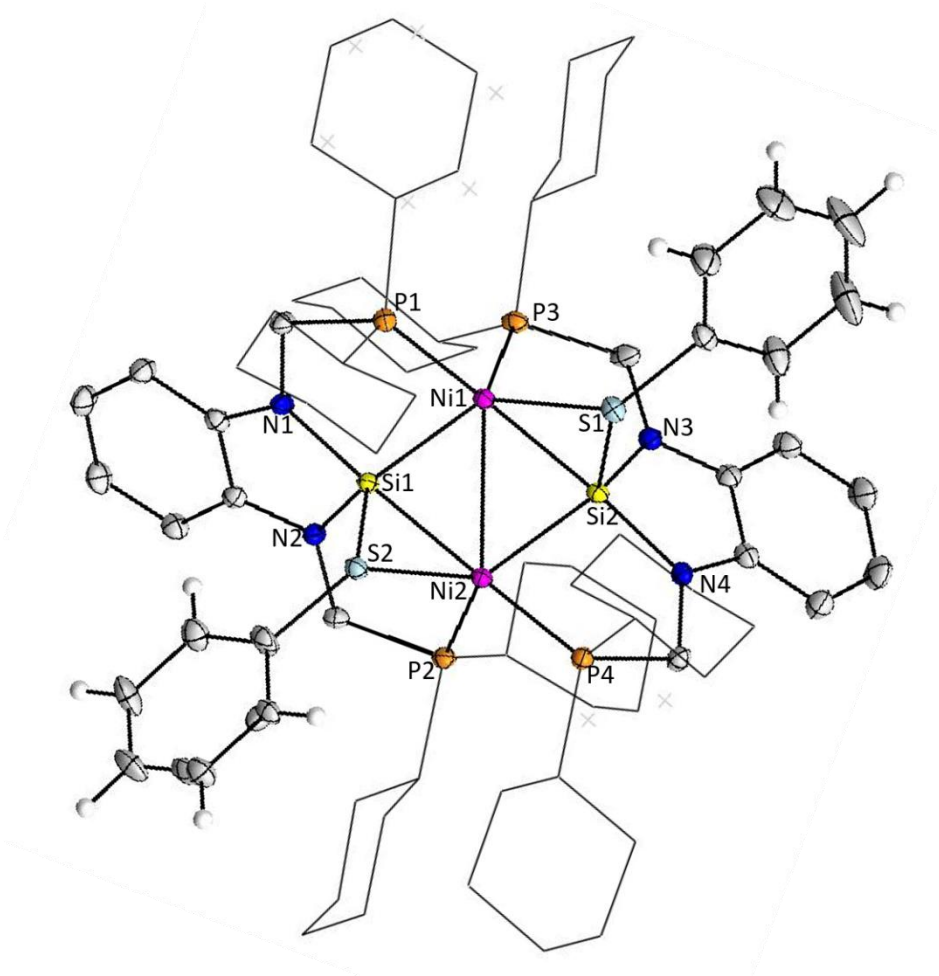

Figure 4.7-21 Thermal ellipsoid plot at 50% probability of $P_4Ni_2Si_2(\mu\text{-}(SPh))_2$, **14**. Magenta, yellow, blue, orange, light blue and gray ellipsoids represent nickel, silicon, nitrogen, phosphorus, sulfur and carbon respectively. For clarity, hydrogen atoms but for those on the thiophenoxide and solvent molecules are omitted and cyclohexyl rings on phosphorous are displayed as wireframe. The compound $C_{76}H_{114}N_4Ni_2P_4S_2Si_2$ crystallized with two half molecules of toluene. The phenyl ring on one thiophenoxide ligand and two separate cyclohexyl rings exhibited disorders that were each modeled over two positions. The disorder ratios were refined freely and converged at 70:30, 51:49, and 86:14, respectively.

Table 4.7-4 Crystallographic data for $P_4Ni_2Si_2(\mu\text{-}(SPh))_2$, **14**.

Identification code	hh296ab_sq	
Empirical formula	$C_{76}H_{114}N_4Ni_2P_4S_2Si_2$	
Formula weight	1445.31	
Temperature	100(2) K	
Wavelength	0.71073 Å	
Crystal system	Triclinic	
Space group	P-1	
Unit cell dimensions	a = 12.3716(6) Å	α = 91.662(2)°.
	b = 13.1476(6) Å	β = 94.987(2)°.
	c = 25.6907(12) Å	γ = 108.670(2)°.
Volume	3936.7(3) Å^3	
Z	2	
Density (calculated)	1.219 mg/m^3	
Absorption coefficient	0.685 mm^{-1}	
F(000)	1548	
Crystal color	red	
Crystal size	0.389 x 0.056 x 0.040 mm^3	
Theta range for data collection	1.594 to 29.130°	
Index ranges	$-16 \le h \le 16$, $-18 \le k \le 18$, $-35 \le l \le 35$	
Reflections collected	129042	
Independent reflections	21159 [R_{int} = 0.0587]	
Completeness to θ = 25.242°	100.00%	
Absorption correction	Semi-empirical from equivalents	
Refinement method	Full-matrix least-squares on F^2	
Data / restraints / parameters	21159 / 820 / 970	
Goodness-of-fit on F^2	1.011	
Final R indices [I>2σ$_1$ = 16332 data]	R_1 = 0.0344, wR_2 = 0.0734	
R indices (all data)	R_1 = 0.0540, wR_2 = 0.0802	
Largest diff. peak and hole	0.460 and -0.379 e/Å^{-3}	

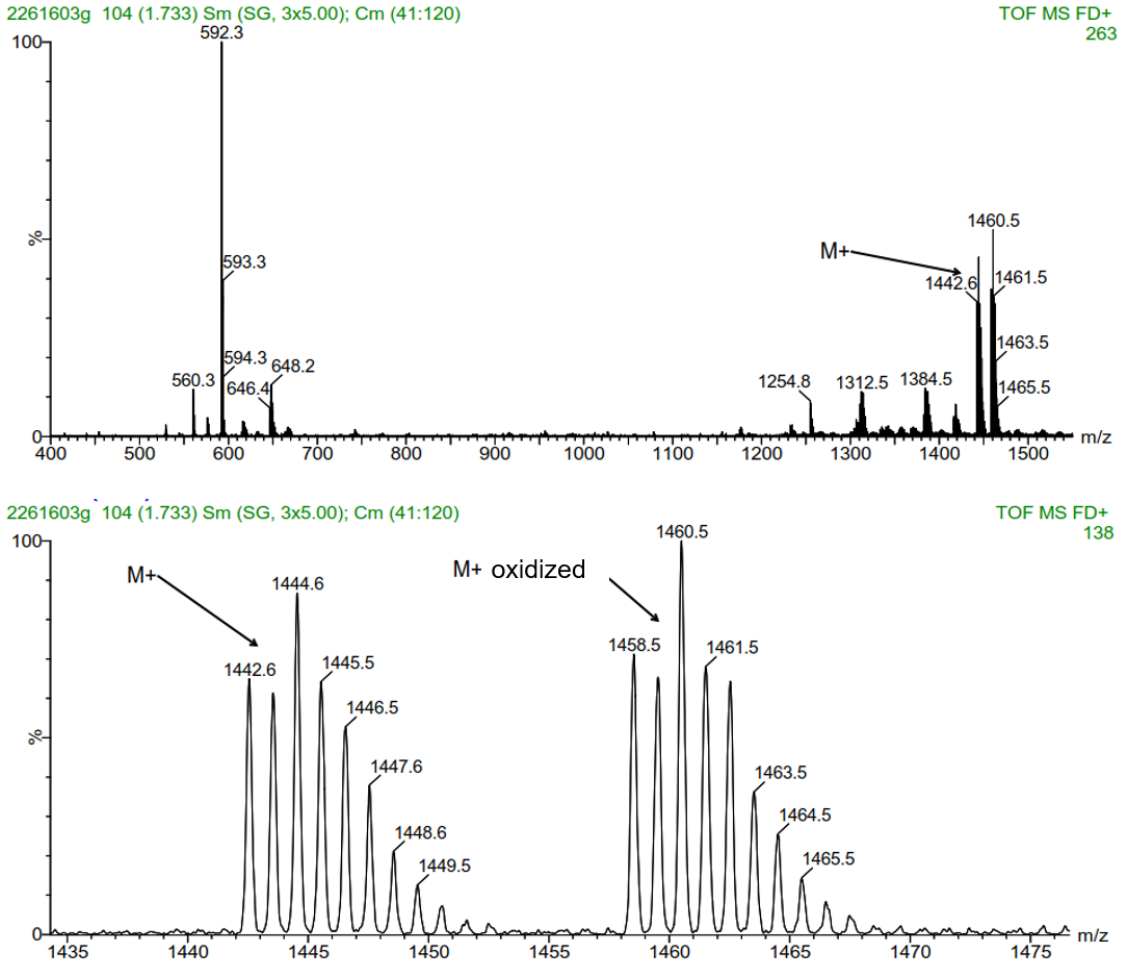

Figure 4.7-22 Mass Spectrometry operating in LIFDI mode for $P_4Ni_2Si_2(\mu\text{-}(SPh))_2$, **14**. Accurate mass calculated (1442.5681) was not obtained due to high molecular weight (1445.3478 g/mol) of **14**, however, the calculated isotopic pattern matched well with the observed.

CHAPTER 5 Reactivity of Dinickel Disilylene with Carbon Dioxide and Carbon Monoxide

5.1 Abstract

The demonstrated ability of $(P^{Cy})_4Ni_2Si_2$, **8**, to activate various E–H and E–E bonds (discussed in Chapter 4) led us to investigate its reactivity with CO_2 and the results are detailed here. Addition of excess CO_2 to $(P^{Cy})_4Ni_2Si_2$ revealed a new product, $(P^{Cy})_4Ni_2(\mu\text{–}CO)\ Si_2O$, featuring a bridging CO across the two Ni centers. The loss of CO is observed under certain conditions to reveal an oxo-bridged $16e^-$ $Ni_2(Si_2O)$ complex as the product of CO_2 deoxygenation. A transient side-bound CO_2 intermediate was hypothesized to initially form across one of the two Ni–silylene interactions prior to the formation of $(P^{Cy})_4Ni_2(\mu\text{–}CO)Si_2O$. Trapping experiments with TMSCl revealed an intermediate can be isolated, $(P^{Cy})_4NiClNi(CO)Si_2O$-TMS, featuring a terminal Ni–CO and a siloxyl moiety, $Si–O–Si(CH_3)_3$, on one of the two Si centers, suggesting the cooperativity of the Ni–Si bond in activating CO_2. The TM–silyl and silylene complexes as the result of CO_2 and CO addition are reported here and have been characterized by a range of spectroscopic techniques and confirmed by single crystal X-ray diffraction.

5.2 Introduction

Carbon dioxide is a stable and inert compound. Additionally, it is a greenhouse gas which makes the idea of CO_2 to fuels ideal as a carbon neutral process. The use of carbon dioxide as a feedstock in the formation of C–C bonds mediated by transition metal complexes has been a topic of research interest that dates to the early sixties.[1] The challenge

with carbon dioxide reduction to liquid fuels or fuel precursors, is that proton-coupled multi-electron steps are generally more favorable than single electron reductions, as thermodynamically more stable molecules are produced.[2,3] One way to utilize CO_2 as a feedstock for the generation of fuels involves non-catalyzed thermal reduction of CO_2 using concentrations of solar power. This method requires very high temperatures, up to 1500 K, and are limited by the day and night cycle minimizing the amount of solar energy accessible.[4]

In nature enzymes catalyze reduction-oxidation reactions with extreme efficiency. This leads researchers to seek out synthetic routes of generating transition-metal complexes capable of mimicking these active sites within enzymes. With respect to carbon dioxide reduction, a particular enzyme of importance which offers inspiration in this endeavor is Carbon Monoxide Dehydrogenase II (CODH II). It was the work of Dobbek and Jeoung which first reported the crystal structure of CODH II from the bacteria *Carboxydothermus hydrogenoformans* in 2001 in three different states.[5,6] Of great significance in the work of Dobbek and co-workers was the finding that carbon dioxide was found to bridge both a nickel and iron site within the enzyme, with each metal site cooperatively participating in a frustrated Lewis Pair (FLP) type interaction. [5,6] In this FLP-type interaction the nickel site can be thought of as acting as the Lewis base and the iron as the Lewis acid.

The propensity of nickel and palladium to react with carbon dioxide within in transition metal complexes has been well established and reported since the 1970s. [7] From a synthetic active site perspective the first reported transition metal–CO_2 complex was with nickel, $(PCy_3)_2Ni(\eta^2\text{-}CO_2)$, in 1975 by Aresta and co-workers, followed by Hillhouse who reported

isolated CO_2 and CS_2 single nickel site complexes.[8,9] In 1993 and the years following it was the work of Kubiak who established bi-and tri-nuclear nickel clusters to reduce both CO_2 and CS_2 [10,11] With respect to main group TM complexes, TM–silylene and carbene complexes have been reported in the literature which have shown to activate and reduce carbon dioxide.[12–15] In 1995 the work of Banaszak and co-workers demonstrated a Pt–germylene complex capable of binding carbon dioxide in a side-bound fashion across the Pt–Ge interaction.[16] In addition, the work of Sadighi in 2005 reported a binuclear Ni(0)–NHC complex capable of reducing carbon dioxide.[17,18] Recently, the work of Lee and co-workers demonstrated (PNP)Ni(0)–CO to afford a Ni(II)–carboxylate species followed by CO expulsion.[12,19] Work has continued in the endeavor for the synthesis of novel transition metal complexes to investigate the activation of carbon dioxide, in addition to uncovering new binding modes.[20]

The work here-in describes the reactivity of a dinickel disilylene, $(P^{Cy})_4Ni_2Si_2$, **8**, with CO_2 and CO. The resulting products have been characterized by a range of spectroscopic techniques. In addition, the reactivity of the reaction products of **8** with CO_2, were further explored by addition of CO with interesting results.

5.3 Results and Discussion

5.3.1 Reactivity of $(P^{Cy})_4Ni_2Si_2$, **8**, with CO_2 and CO

Upon exposure of excess carbon dioxide, after three freeze-pump-thaw cycles, to **8** in benzene at atmospheric pressure a color change from dark crimson red to a lighter red is observed. The ^1H NMR indicates a break in symmetry of **8** as the methylene linker protons are displayed as five resonances indicating diastereotopic protons in deuterated benzene at

δ 4.50 ppm (d, *J* = 8.5 Hz, 1H), δ 4.23–3.93 ppm (m, 4H), δ 3.42 ppm (t, *J* = 10.8 Hz, 1H), δ 3.24 ppm (d, *J* = 8.1 Hz, 1H) δ = 3.02 (t, *J* = 9.4, 8.1 Hz, 1H) (Figure 5.7-1). A ^{31}P NMR analysis reveals a resonance for each of the four phosphine arms of the ligand at δ 64.33 ppm (d, *J* = 16.1 Hz), δ 61.38 ppm (t, *J* = 41.2 Hz), δ 28.63 ppm (d, *J* = 25.1 Hz), and δ -18.53 ppm (s). Based on Banaszak and co-workers' prior observations with a Pt–germylene complex[16] we anticipated that the ensuing product may be some CO_2 side-bound adduct within the core of **8** with CO_2 envisioned as bridging one of the two Ni–Si interactions (Scheme 5.3-1).

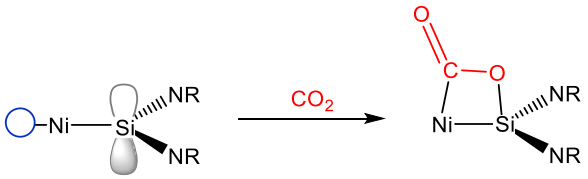

Scheme 5.3-1. Anticipated reactivity upon addition of excess CO_2 to $(P^{Cy})_4Ni_2Si_2$, **8**.

This type of reactivity would indeed give rise to four new resonances in the ^{31}P NMR, in addition to revealing diastereotopic methylene protons within the ^{1}H NMR. To our surprise excess carbon dioxide addition to **8** results not in the side bound adduct, as observed in in the Pt–Ge system[16], nor does it add in the same fashion as observed in the work of Aresta and Hillhouse at a single nickel site.[8,9] Rather a single crystal X-ray diffraction study revealed the formation of $(P^{Cy})_4Ni_2(\mu\text{-CO})Si_2O$, **15**, upon the addition of excess CO_2 to **8** (Figure 5.3-1), which is isolated as a brown crystalline solid from cold diethyl ether in 47% yield after first crop collection.

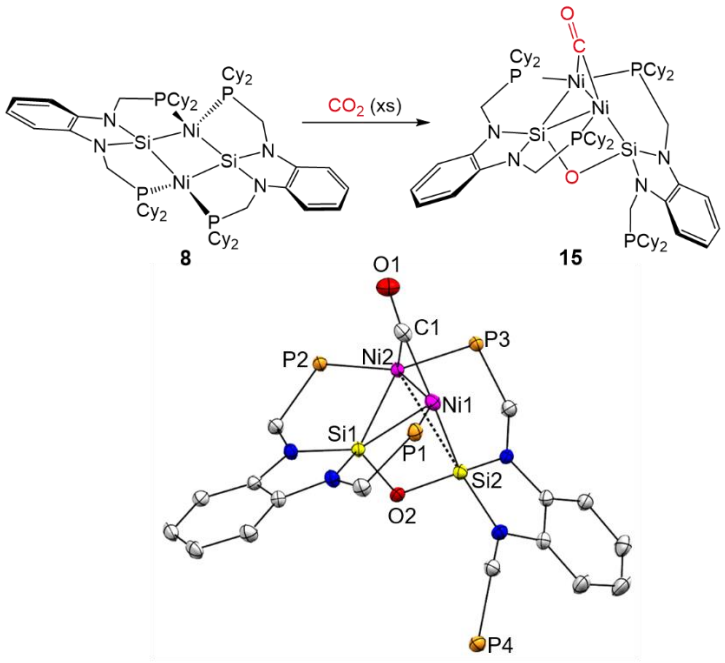

Figure 5.3-1. Formation of **15** via excess CO_2 addition to **8** (top). Core fragment of the solid-state structure for **15** in ellipsoid representation at 50 % probability (bottom). Notable bond lengths and distances (Å): Ni2–Ni1 = 2.3040(6), Si1–Ni2 = 2.348(1), Si1–Ni1 = 2.3489(9), Si2–Ni1 = 2.2885(8), Si2---Ni1 = 2.9485(9) , Si1–O2 = 1.680(2), Si2–O2 =1.674(2), Ni2–C1 = 1.998(3), Ni1–C1 =1.831(3), C1–O1 =1.169(3), P2–Ni2 = 2.1974(8) , P3–Ni2 = 2.2145(9) , P1–Ni1 = 2.1556(9).

The structure of **15** reveals a bridging carbonyl across two nickel centers with Ni(1) ligated to two silyl ligands: one terminal silyl, Si(2) , and one bridging silyl ligand, Si(1). Multiple resonance structures can be envisioned for **15**, such as invoking a formal Ni–Ni bond or not, and leads to various possible geometries surrounding each nickel site. However, the coordination geometry surrounding silicon supports the conclusion of assigning one silyl ligand as bridging, Si(1), and the other as terminal, Si(2). The geometry index, τ_5 value, for Si(1) in the bridging silyl is 0.13. This value is consistent with a distorted square pyramidal geometry as it is bonded to both the Ni(1) and Ni(2) sites, with bond lengths of 2.3489(9) and 2.348(1), respectively. The other silicon center, Si(2), within

the solid-state structure of **15** reveals it is no longer bonded to Ni(2) (Si2---Ni1 = 2.9485(9)) and so adopts a distorted tetrahedral geometry with $\tau_4 = 0.79$ and $\tau_4' = 0.76$. The Si(2)–Ni(1) bond length observed in the solid-state structure is observed to be 2.2885(8). The distance between Si(2) and Ni(2) is 2.9485(9) which is significantly longer than the average Ni–Si bond length and as such suggests no interaction. Noteworthy is the asymmetry observed in the Ni(2)–C(1) and Ni(1)–C(1) distances which has also been observed in similar methylcyclopentadienyl (Cp*) dinuclear nickel complexes as reported by Byers and Dahl.[21] The Ni(1) and Ni(2) bond length of 2.3040(6) Å is significantly shorter than the distance between the two nickel centers revealed in the solid-state structure of **8** ($d_{Ni–Ni}$ = 2.6823(6) Å). A bond length of 2.3040(6) Å is consistent with the median (2.576 Å) and average (2.619 Å) Ni–Ni distance as determined using a Crystal Structure Database (CSD) analysis. The solid-state structure of **15** also reveals a bridging siloxyl group as present, the result of oxygen atom cleavage within carbon dioxide. The Si(1)–O(2) and Si(2)–O(2) bonds are relatively equal with lengths of 1.680(2) and 1.674(2). This small difference in Si–O bond length ($\Delta = 0.006$ Å) is reasoned by steric factors given the shorter of the two Si–O bond lengths is observed in the silicon center bonded to only one nickel site. Additional heteronuclear NMR experiments carried out on **15** reveal interesting spectroscopic features consistent with the solid-state-structure provided by XRD results. The ^{29}Si NMR of **15** displays a resonance at δ 1.66 ppm (s), in addition to a resonance with a doublet of doublet of doublet coupling pattern at δ -3.94 ppm ($J_{Si\text{-}P}$ = 98.2, 26.4, 13.7 Hz), indicative of two bond coupling through nickel to three of the four total phosphine arms ligated to the nickel sites. This spectroscopic data is in good agreement with XRD results

based on the two silicon environments. The ^{13}C NMR of **15** displays a resonance downfield at a δ = 234.36 ppm consistent a bridging carbonyl. The bridging carbonyl is also revealed in the IR spectrum of **15** which features a peak at 1850.46 cm^{-1}.

Overtime at room temperature a set of new resonances appear in the $^{31}P\{^{1}H\}$ NMR for a solution of **15**. Believing this new species must be the result of gradual CO loss, curiosity led us to investigate if CO loss with **15** could be facilitated in a controlled fashion. Gentle heating at +40 °C for over the course of a week in deuterated benzene results in a color change from red to orange. The ^{1}H NMR revealed methylene proton resonances with δ 4.01 ppm (t, J = 11.8 Hz, 2H), δ 3.69 – 3.57 ppm (m, 4H), and δ 3.39 ppm (td, J = 8.7, 4.3 Hz, 2H). By $^{31}P\{^{1}H\}$ NMR symmetry was regained as two new resonances appear, while the four other resonances indicative of **15** disappear, each with a doublet coupling pattern within the $^{31}P\{^{1}H\}$ NMR at δ 46.18 ppm (d, $J_{P\text{-}P}$ = 18.6 Hz) and δ 44.56 (d, $J_{P\text{-}P}$ = 18.2 Hz) consistent with ^{31}P–^{31}P two bond coupling through Ni. ^{1}H NMR and $^{31}P\{^{1}H\}$ NMR experiments suggested this was the oxo-bridged silyl complex and single crystal X-ray diffraction studies confirmed the formation of **16** as product of CO loss from **15** (Figure 5.3-2). The solid-state structure of **16** reveals C_2 symmetry through both nickel and silicon sites as all four phosphine substituents are once more ligated to each nickel site. The solid-state structure for **16** also shows each nickel site adopts a distorted square planar geometry accompanied by a formal Ni–Ni bond with a length of 2.4833(6) Å. As expected with the loss of the bridging carbonyl ligand, this Ni–Ni distance in **16** is slightly elongated in length when compared to the length observed for **15** (Ni(1) –Ni(2) = 2.3040(6) Å).

Alternatively, it was demonstrated addition of pyridine N-oxide to a solution of **8** can independently yield **16** in 31 % yield after first crop collection as a bright orange crystalline solid from diethyl ether. This route to generate **16**, including the first discussed, is summarized in Figure 5.3-2.

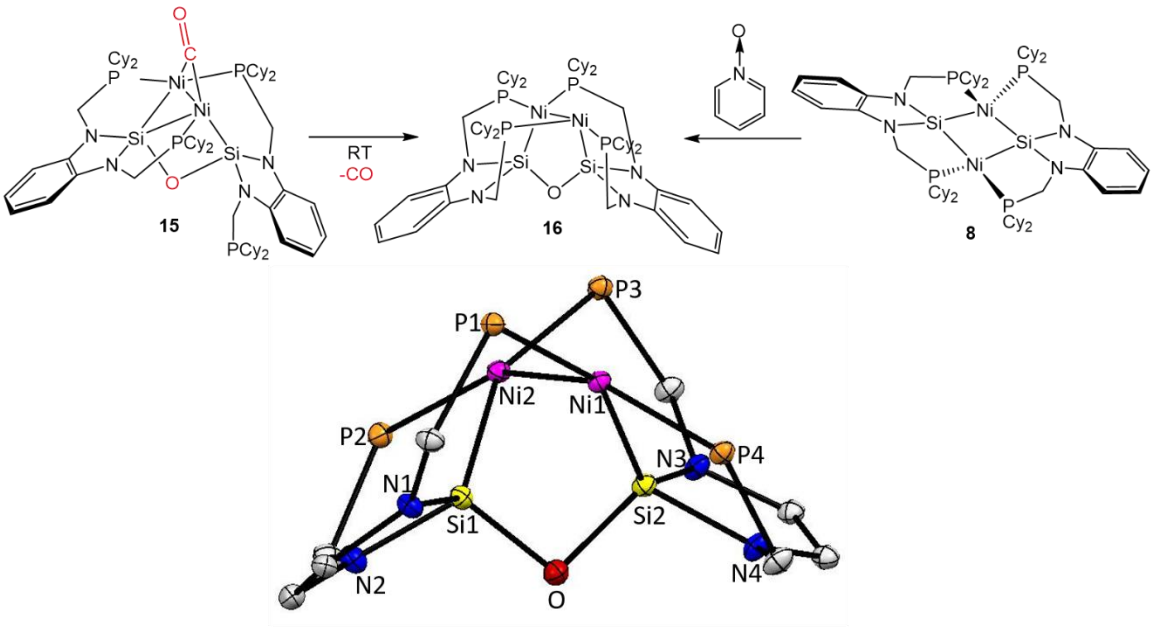

Figure 5.3-2. Synthetic route to generate **16** via CO dissociation from **15** (top, left to right) and addition of one equivalent of pyridine N-oxide to **8** (top, right to left). Core fragment of the solid-state structure of **16** in an ellipsoid representation at 50 % probability (bottom). Notable bond lengths (Å): Ni2–Ni1 = 2.4883 (6), Si1–Ni2 =2.2026(6), Si2–Ni1 = 2.2178(5), Si1–O = 1.700(1), Si2–O =1.696(1).

Given the reactivity and reported isolation of a side-bound CO_2 Pt–germylene complex by Banaszak, a transient side-bound CO_2 intermediate was hypothesized to initially form across one of the two Ni–silylene interactions of **8** prior to the formation of $(P^{Cy})_4Ni_2(\mu\text{–}CO)Si_2O$, **15**. It was then reasoned we may be able to intercept a possible intermediate by adding an exogenous electrophile (Figure 5.3-3).

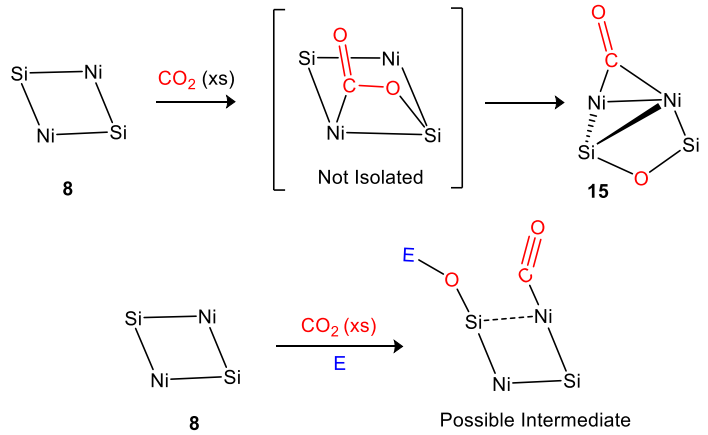

Figure 5.3-3. Schematic representation for the expected reactivity of **8** with CO_2 versus observed. Synthesis of **15** from **8** after excess CO_2 addition with hypothesized intermediate (top). Schematic representation outlining approach for generation of a possible intermediate via trapping experiments with a general electrophile (E).

This approach proved successful and with the addition of CO_2 in the presence of excess trimethylsilylchloride we can isolate the TMSCl trapped product, $(P^{Cy})_4NiClNi(CO)Si_2O$-TMS, **17**, as a bright yellow precipitate in 44% yield after first crop collection (Scheme 5.3-2). The addition of TMSCl traps the oxygen from CO_2 onto one of the silicon centers, resulting in a terminal carbonyl on one nickel center, while the chloride goes on to add into the coordination sphere of the remaining nickel site.

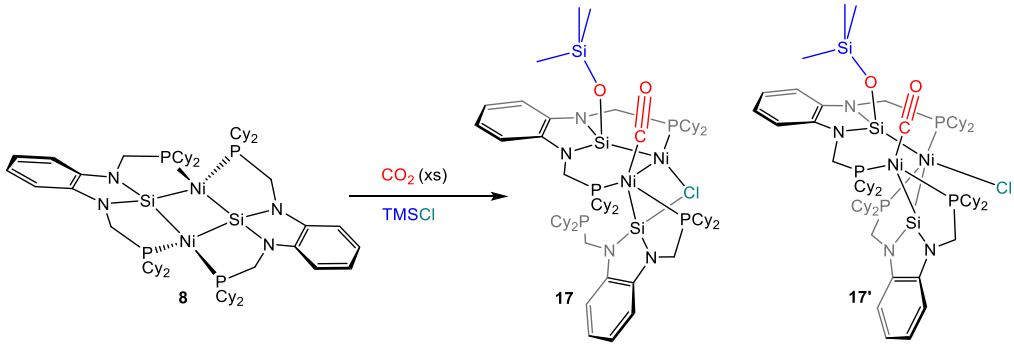

Scheme 5.3-2 Synthesis of trapped intermediate, **17**, upon the addition of excess CO_2 to **8** in the presence of trimethylsilylchloride.

The ^{1}H NMR of **17** features a resonance for each of the eight total diastereotopic methylene protons, as expected. Additionally, in deuterated benzene **17** shows four ^{31}P NMR resonances for each phosphine substituent at δ 63.97 ppm (d, $J_{P\text{-}P}$ = 35.1 Hz), δ 50.14 ppm (ddd, $J_{P\text{-}P}$ = 34.8, 15.3, 3.4 Hz), δ 35.02 ppm (dd, $J_{P\text{-}P}$ = 14.8, 4.2 Hz), and δ 5.46 ppm (s). The spectroscopic data suggests initial isolation of the trapped intermediate in solution exists as **17**. In the solution state, the ^{31}P{^{1}H} NMR reveals one of the four phosphorous resonances upfield as a single peak at δ 5.46 ppm and this suggests **17** as the isomer that dominates in the solution state. A single crystal X-ray diffraction study revealed two different molecules of **17** with molecular formula $C_{68}H_{113}ClN_4Ni_2O_2P_4Si_3$ and four solvent molecules of pentane present in the asymmetric unit of the unit cell which are omitted for clarity (Figure 5.3-4).

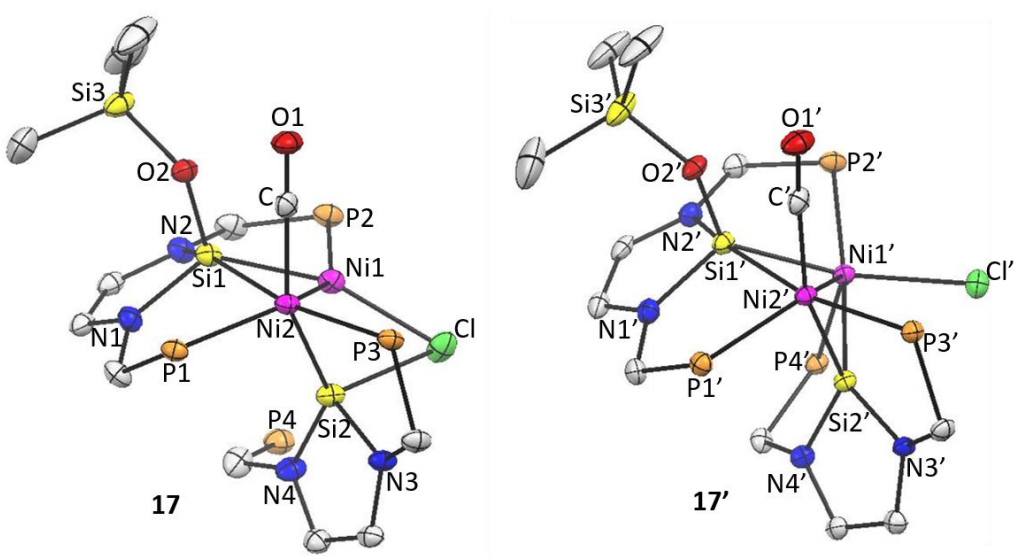

Figure 5.3-4. Core fragment of the solid-state structure of **17** and **17'** at 50 % probability. Notable distances and bond lengths (Å); 17: Ni2–Ni1 = 2.5415(6), Si1–Ni1 = 2.2151(9), Si1–Ni2 = 2.7247(9), Si1–O2 = 1.652(2), O2–Si3 =1.642(2), Ni2–C = 1.789(3), C–O1 = 1.148(4), Si2–Ni2 = 2.2338(9), Si2–Ni1 = 2.242(1), Si2–Cl = 2.503(1), Ni1–Cl = 2.2663(8), 17': Ni2'---Ni1' = 2.7541(6), Si1'–Ni1' = 2.2744(9), Si1'–Ni2' = 2.6195(9), Si1'–O2' = 1.668(2), O2'–Si3' =1.642(2), Ni2'–C' = 1.792(3), C'–O1' = 1.143(4), Si2'–Ni2' = 2.1805(9), Si2'–Ni1' = 2.2210(8), Ni1'–Cl' = 2.3312(8), Si2'---Cl' = 3.072(1).

The solid-state structure featuring the core of **17** can be seen in Figure 5.3-4. The Cl atom is bridging the Ni(1)–Si(2) atoms in **17** and the Cl' is terminally bonded to Ni(1') in **17'** for the two different $C_{68}H_{113}ClN_4Ni_2O_2P_4Si_3$ molecules. The distance between Si(2') and Cl' in **17'** is 3.072(1) Å, which suggests no bridging character exists, as evident in structure of **17**. The distance between Si(2) and Ni(2) in **17** of 2.242(1) Å is suggestive of some interaction between the two atoms, and a computational Natural Bond Order analysis is warranted for further investigation. Overtime, within days, a resonance in the ^{31}P NMR appears at a δ 68 ppm which may suggest **17'** in the solution state has all four phosphine atoms bound to the two nickel sites, with further confirmation needed. To investigate this VT NMR studies were carried out to probe the possibility of converting **17** to **17'**. Observed was simply the disappearance of the upfield shift around 5 ppm but no evidence of a resonance growing in at a downfield position that would suggest all four phosphine substituents are once more ligated to each nickel center. This suggests a lower temperature (below –40 °C) may be needed to further probe the possibility of one isomer **17** to convert to the other, **17'**. Overall, the results of **8** with CO_2 in the presence of TMSCl proved successful as one of the two silylene ligands are still intact while the other has participated in activating CO_2 independently. In each isomer this would correspond to Si(1) and Ni(2) in **17** and Si(1') and Ni(2') in **17'**. Heteronuclear experiments, specifically $^{29}Si\{^1H\}$ NMR, prove valuable in providing evidence of a bridging silylene versus that of a silyl moiety within these systems. The $^{29}Si\{^1H\}$ NMR, consistent with XRD results, exhibits three silicon resonances at δ 102.26 ppm (dd, $J_{Si\text{-}P}$ = 94.7, 34.6 Hz, Ni–*Si*–Ni), assigned to the bridging silylene ligand, δ 3.26 ppm (s, –O–*Si*$(CH_3)_3$), assigned to the TMS moiety and

δ – 10.29 ppm (m, Ni–*Si*–O–Si(CH_3)) assigned to silicon site which has deoxygenated CO_2. The presence of a terminal carbonyl in the structure of **17** is further confirmed in the ^{13}C NMR and IR spectrum. The ^{13}C NMR of **17** exhibits a downfield resonance at δ 200.85 ppm indicative of the terminal carbonyl ligand, as expected, in contrast to the bridging carbonyl resonance for **15** (δ = 234.36 ppm). Additionally, the IR spectrum displays a peak at 1988.27 cm^{-1} consistent with a terminal carbonyl. The spectroscopic data and XRD results are highly suggestive that the activation of CO_2 within this system is largely driven by the cooperativity of one of the four Ni–Si interactions present within the core of **8**.

With the success of isolating the trapped CO_2 intermediate **17**, we next turned our attention to the possibility of generating the cationic species of **17** via chloride abstraction which presumably leads to the isolation of **18** (Scheme 5.3-3).

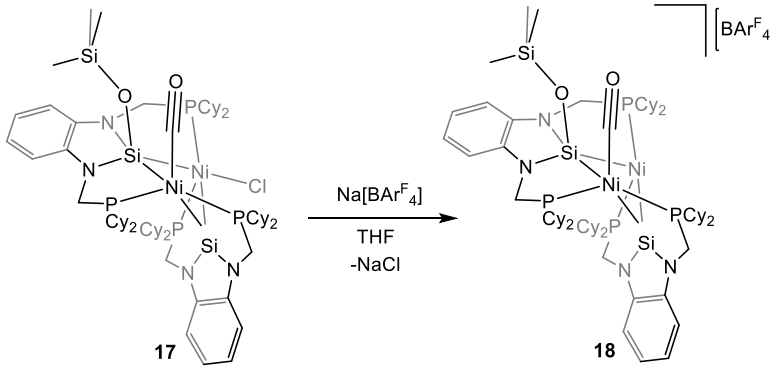

Scheme 5.3-3. Synthesis of **18** from the addition of $NaBAr^F_4$ to **17**.

When sodium tetrakis[3,5-bis(trifluoromethyl)phenyl]borate is added to a slurry of **17** in ether, an immediate color change from orange to deep purple is observed. The $^{31}P\{^1H\}$ NMR and ^1H NMR are suggestive of successful halide abstraction and generation of the cationic species. After filtration of the reaction mixture through Celite, an analysis

of the $^{31}P\{^{1}H\}$ NMR in deuterated acetonitrile exhibits four new resonances at δ 78.29 (d, *J* = 13.6 Hz), 74.59 (d, *J* = 19.6 Hz), 53.85 (dd, *J* = 20.2, 7.8 Hz), 37.24 (t, *J* = 10.9 Hz) downfield from the starting material. Furthermore, each phosphorous shift exhibits ^{31}P–^{31}P coupling in the $^{31}P\{^{1}H\}$ NMR spectrum, evidence the ligation of all four phosphine donors to each Ni is possible once more given the removal of chloride from the inner sphere of nickel. As expected, the ^{1}H NMR in deuterated acetonitrile for **18** exhibits seven distinctive resonances, one resonance as a multiplet with integration of two protons for each of the eight chemically inequivalent methylene protons. Due to the sensitive nature of the cationic species in solution, repeated attempts to obtain a single crystal for X-ray diffraction studies have been unsuccessful thus far. Overtime in solution while set-up to recrystallize the dissociation of the anion gave way to various decomposition products.

To gain further insight into the reactivity of **8**, with knowledge that **8** can form metal complexes featuring both terminal and bridging carbonyl ligands under certain conditions, the addition of carbon monoxide was also investigated. Upon addition of excess CO to a solution of **8** in deuterated benzene, after three free pump thaw cycles, an immediate color change is observed from deep crimson red to a light red/orange which generates **19** as a yellow precipitate in 77 % yield after first crop collection (Figure 5.3-5).

A $^{31}P\{^{1}H\}$ NMR analysis of **19** indicates four resonances at a δ 97.20 ppm (s), δ 59.86 ppm (d, J_{P-P} = 31.2 Hz, δ 55.48 ppm (d, J_{P-P} = 31.1 Hz), and a δ -11.39 ppm upfield as a singlet.

The IR spectrum using a KBr pellet of **19** confirms the presence of two terminal carbonyl ligands present on each nickel atom at 1958.22 cm^{-1} and 1939.86 cm^{-1}. Additionally, the ^{13}C NMR indicates two distinctive resonances for each terminal carbonyl ligand at a δ 200.17 ppm and δ 198.66 ppm.

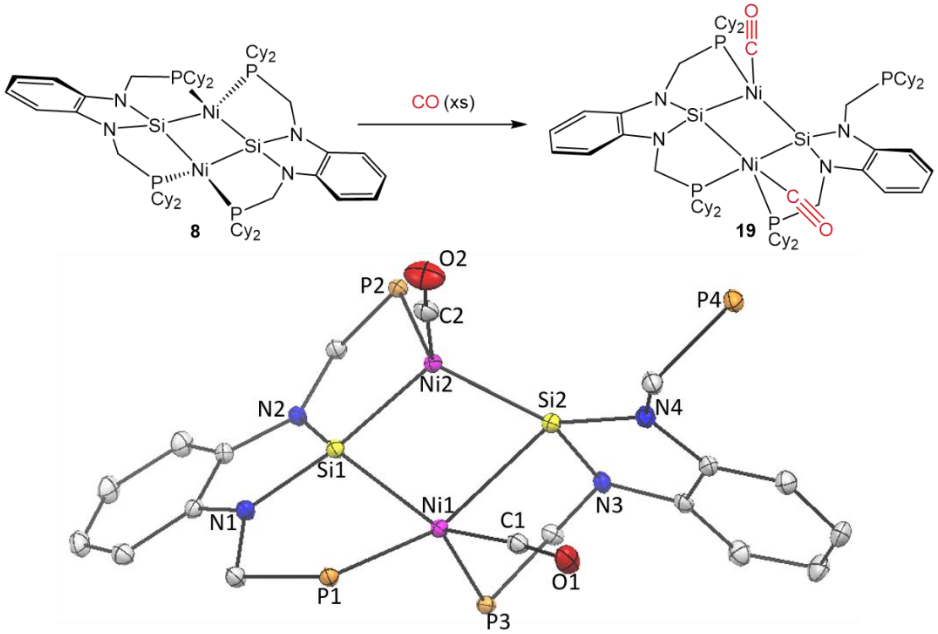

Figure 5.3-5. Formation of **19** via CO (xs) addition to **8** (top). Ellipsoid representation at 50% probability of **19** (bottom). Cyclohexyl and hydrogen have been omitted for clarity. Notable distances (Å): dNi2---Ni1 = 2.6947(5), Si1–Ni1 = 2.3691(7), Si1–Ni2 = 2.1847(7), Ni2–C2 = 1.767(2), C2–O2 = 1.153(3), Si2–Ni2 = 2.01451(8), Si2–Ni1 = 2.5528(7), Ni1–C1 = 1.775(2), C1–O1 = 1.154(3), P1–Ni1 = 2.2439(6), P3–Ni1 = 2.2471(8), P2–Ni2 = 2.1670(6).

A single crystal X-ray diffraction study confirms the formation of the asymmetric nickel carbonyl complex, **19**, in which one of the four phosphine atoms is no longer ligated to a nickel center. Each nickel site has taken on a terminal carbonyl ligand and reveals Ni(1) to adopt a distorted square pyramidal geometry, while Ni(2) adopts a distorted tetrahedral geometry where one of the two phosphine donors is no longer ligated.

The solid-state structure of **19** shows each silicon center adopts a tetrahedral geometry, with Si(1)–Ni(1) distance of 2.3691(7) Å and Si(1)–Ni(2) distance of 2.1847(7) Å. The distances for Si(2)-Ni(1) and Si(2)-Ni(2) are 2.5528(7) and 2.01451(8) Å. These Si–Ni distances are in range of reported Si–Ni bonds in silyl and silylene complexes.[22–32] The Si(1)-Ni(2) length, 2.01451(8) Å, is the shortest of the Si–Ni distances featured within the core of **19**. This Si(1)-Ni(2) length is slightly shorter than the silylene Ni(0)(η^6–Arene) complexes (2.0369(6) Å), and the silylene–$Ni(CO)_3$ (2.1663(12)–2.2403(12) Å) reported by Driess.[33,34] Additionally, a comparison of shortest Ni–Si length in **19** reveals this distance as shorter than the Ni–Si bond length reported in the base stabilized silylene nickel carbonyl complexes reported by Roesky, ranging from 2.1854(7) –2.2111(8).[35] As observed with previously reported silylene nickel carbonyl complexes, the decreased distance of Si(1)-Ni(2) within the solid-state structure of **19** may suggest possible π-back-bonding within the Si–Ni interation.[26,35] The distance between Si(2)–Ni(1) of 2.5528(7) is longer than the typical Si–Ni interaction and has been reported in only a few complexes. Notably, silicon and germanium heterocyclotriyne Ni(0) complexes, in addition to nickel metallosilatranes, the latter with DFT calculations suggesting M→Si dative bond interaction.[36,37] The $^{29}Si\{^1H\}$ NMR for **19** displays two resonances; δ 171.90 ppm with a triplet of triplets coupling pattern that displays ^{29}Si–^{31}P coupling of 16.7, 6.9 Hz and a resonance at δ 148.72 ppm as a triplet with ^{29}Si–^{31}P coupling of 14.8 Hz. Analysis of the solid-state structure of **19** provides insight to shift assignment within the $^{29}Si\{^1H\}$ NMR. The more downfield resonance at δ 171.90 ppm is assigned to the Si(1) center with one bond coupling to three phosphine arms through Ni(1) and Ni(2).

The upfield resonance in the $^{29}Si\{^{1}H\}$ NMR at δ 148.72 ppm can be assigned to the Si(2) site bonded to the Ni(2) center with this upfield shift suggestive of Ni–Si π-back-donation, as evidenced with other silylene nickel complexes.[34] The bond length of 2.01451(8) is significantly shorter than the Si–Ni distance for the trapped monometallic complex **9** which has a Ni–Si distance of 2.148(1) Å (discussed in Chapter 3). This difference may be attributed to the fact that **9** features all phosphorous atom donors to nickel, while **19** features a P atom donor in addition to an electron withdrawing CO ligand with more π-back-donation. Furthermore, **9** displays a more shielded resonance in the $^{29}Si\{^{1}H\}$ NMR at δ 125.71 – 125.10, as a multiplet due to complex $^{29}Si–^{31}P$ coupling, when compared to **19** (δ 171.90 ppm and 148.72 ppm). When a comparison of the ^{29}Si shifts of **19** ($^{29}Si\{^{1}H\}$ NMR: C_6D_6, δ 171.90 (tt, J = 16.7, 6.9 Hz), 148.72 (t, J = 14.8 Hz) are made to that of **8** ($^{29}Si\{^{1}H\}$ NMR, Tol-d_8, +70 ºC, δ = 190.67 ppm) both resonances for **19** are slightly more upfield but still significantly more downfield than the silyl complexes reported within the collection of this work. By referring to the library of ^{29}Si chemical shifts with this ligand framework and their transition metal complexes, we can suppose silylene character is retained in **19** based on the downfield shifted resonance. While at this time XRD results and direct $^{29}Si\{^{1}H\}$ NMR are the only insight on silylene character, a computational analysis would provide further insight into the orbitals accessed within the Ni–Si interactions and provide further clarification into bonding scenarios.

Given the labile nature of the phosphine substituents within this ligand platform, additional reactivity with **15**, **16** and **17** were explored. Upon addition of CO to **15** in

deuterated benzene a color change from red to yellow occurs. The $^{31}P\{^{1}H\}$ NMR displays four new resonances at δ 87.12 (d, J = 14.7 Hz), 49.87 (t, J = 14.9 Hz), 42.77 (s), –11.83 (d, J = 15.4 Hz) and the disappearance of the $^{31}P\{^{1}H\}$ NMR shifts indicating **15**. Additionally, the reaction between excess CO and **16** results in a color change from orange to yellow with a $^{31}P\{^{1}H\}$ NMR analysis revealing the same four resonances as seen upon addition of excess CO to **15** to form the tentatively assigned new product **20** (Scheme 5.3-4). The resulting $^{31}P\{^{1}H\}$ and ^{1}H NMR of **15** and **16** after addition of excess CO reveal the same product is formed (Refer to Section 5.7). Solid state IR using a KBr pellet reveals two peaks at 2066.29 cm^{-1} and 1981.04 cm^{-1}, confirming the presence of two terminal carbonyl ligands. Multiple attempts to isolate the proposed bimetallic Ni-dicarbonyl bridging oxo-silyl complex, **20**, for XRD analysis were unsuccessful given its transient nature. Repeated crystallization attempts instead resulted in the isolation of the diamagnetic complex **21**, which displays one resonance by $^{31}P\{^{1}H\}$ NMR. A reactivity summary of **15** and **16** with excess CO, and the subsequent isolation of **21**, is outlined in Scheme 5.3-4.

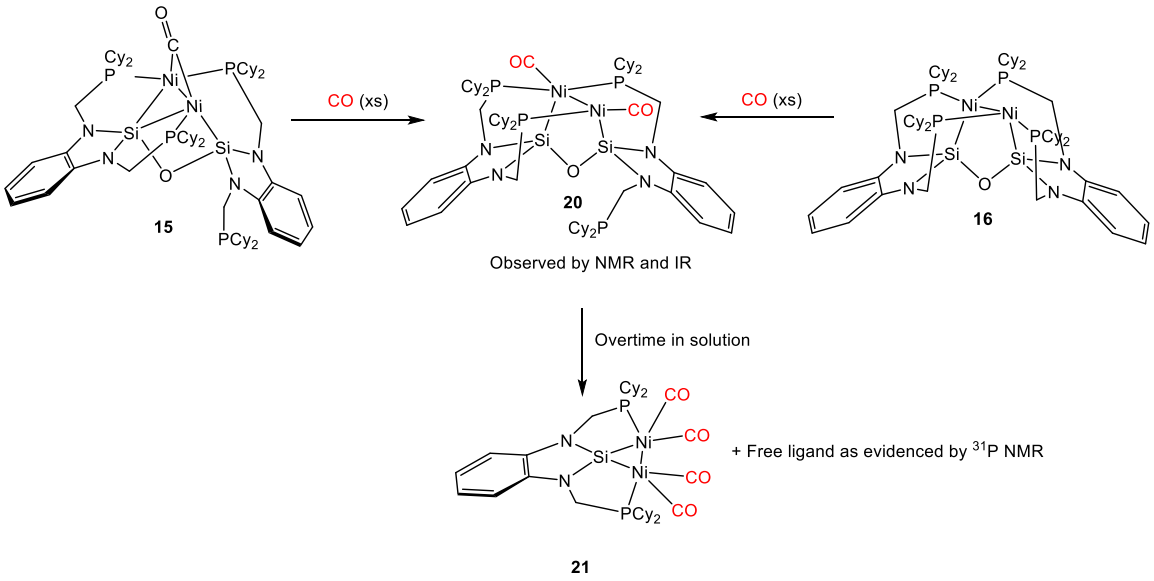

Scheme 5.3-4. Addition of excess CO to both **15** and **16** resulted in observation of the new product, **20**, tentatively assigned as a dicarbonyl bridging oxo-silyl complex based on IR spectroscopic data and also ^{1}H and ^{31}P{^{1}H} NMR spectroscopic data. Isolation of **21** by NMR and XRD was the result of repeated attempts to isolate intermediate **20** from solutions of ether.

The ^{1}H NMR of **21** displays a resonance as a doublet at δ 3.22 ppm with ^{1}H–^{31}P two bond coupling of 3.6 Hz for the methylene protons. The ^{31}P{^{1}H} NMR for **21** shows a single resonance at δ 77.81 ppm which gives rise to the expected triplet observed in the ^{29}Si{^{1}H} NMR at δ 169.74 ppm with ^{29}Si nuclei coupling to the two identical ^{31}P atoms in **21** with J = 20.1 Hz. The ^{13}C NMR of **21** shows a resonance at δ 201.83 ppm which is consistent with previously reported Ni–carbonyl complexes featuring terminal carbonyl ligands.[33,38] The IR spectroscopic data also confirms the terminal carbonyl ligands on each Ni site with peaks present at 2029.29, 1983.82, 1956.23 cm^{-1}. The solid-state structure of **21** reveals the distance between each of the Ni sites is 2.7126(4) Å and is unusually long to invoke a formal Ni–Ni bond and relatively rare. However, similar Ni---Ni distances have been previously reported. Distances of about 2.7 Å between nickel atoms are common in

cluster chemistry as reported in the work of Johnson on di, tetra and pentanuclear nickel silyl and silylene complexes in 2012.[39] Similar distances have been observed in bismuth nickel carbonyl clusters by Sevov and co-workers and more recently within molecular nickel phosphide carbonyl nanoclusters by Femoni, Zacchini and Zanotti.[40,41] The mechanism of formation for **21** from the intermediate complex, **20**, is unknown at this time. However, both $^{31}P\{^{1}H\}$ and ^{1}H NMR show evidence of some form of free ligand within the filtrate and mother liquor from crystallizations set-up in an attempt to isolate the transient intermediate **20**. For the transformation of **20** to **21** silicon–oxygen bond cleavage must be promoted. Traditionally this is not a facile transformation given the Si–O bond strength, however there is precedent for selective Si–O bond cleavage with allylic and vinylic trimethylsilyl ethers with $RuH_2(PPh_3)_4$ complexes which result in evolution of propylene and propane to afford carbonyl complexes $RuH_2(CO)(PPh_3)_3$ and $Ru(CO)_3(PPh_3)_2$.[42] However, the role of a metal hydride for nucleophilic attack on the silyl ether moiety within **20** is not likely but it is interesting to note the TM–carbonyl formation following Si–O bond cleavage in such systems. Another possibility for the repeated formation of **21** from **20** may involve an acid catalyzed route promoted by trace amounts of water within the highly coordinating diethyl ether solvent used for recrystallization. Coordinating solvents have been suggested to help facilitate such transformations in some studies regarding Si–O bond cleavage.[43] In addition, solvation can stabilize any potentially formed charged intermediates.[44] With the mechanism still unknown, and the possibility of complex mechanistic route, a more rigorous study is warranted for the formation of **21** from **20**. Given the reaction of $Co_2(CO)_4$ with **1** to generate **7** (Chapter 2), the potential of

generating **21** independently through a more concise synthetic route would involve treatment of two equivalents of $Ni(CO)_4$ to a solution of the **1** by means of Si–Cl oxidative addition. However, this synthetic route was not pursued given the toxicity of $Ni(CO)_4$.

5.3.2 Preliminary Reactivity of $(P^{Cy})_4Pd_2Si_2$, **10**

Preliminary results with $(P^{Cy})_4Pd_2Si_2$, **9**, with excess CO_2 spectroscopically appeared promising. Addition of excess CO_2 to **9** resulted in a color change from light green to yellow with $^{31}P\{^1H\}$ NMR analysis indicating the presence of two new species. One species confirmed by XRD as a bridging carbonate complex in which the two oxygen atoms are bound to each of the silicon atoms within the Pd_2Si_2 core. The other species present by $^{31}P\{^1H\}$ NMR is hypothesized to be a bridging oxo-silyl complex analogous to complex **16**. A more in-depth discussion on the investigation of $(P^{Cy})_4Pd_2Si_2$, **9**, with small molecules can be found in the work of my lab co-worker Marissa Barrientos.

5.4 Concluding Remarks

This study has demonstrated the reactivity of the dinickel disilyene complex **8** and its activation of CO_2 within the asymmetric Ni_2Si_2 core, in addition to investigating **8** with CO. Addition of excess CO_2 to **8** reveals the formation of $(P^{Cy})_4Ni_2(\mu\text{-CO})\ Si_2O$, **15**, featuring a bridging carbonyl across the two nickel centers and siloxyl moiety as the result of deoxygenating CO_2. The loss of the bridging carbonyl ligand leads to the formation of **16**, which can be independently synthesized by addition of pyridine N-oxide to **8**. In the presence of trimethylsilylchloride we have shown a trapped intermediate, $Ni_2Si_2(CO)(O\text{-TMS})Cl$, **17**, can be successfully isolated, supporting our hypothesis that CO_2 is initially activated across the Ni–Si interaction prior to the formation of **15**. The solid-state structure

of **15** confirms a terminal CO ligand on one of the two nickel centers, with an oxygen from CO_2 trapped on silicon with the TMS unit and chloride bound to the second nickel site which completes its coordination sphere. We have also demonstrated an interesting result with the reaction of excess CO to **8** which features a Ni–Si bond length (Si2–Ni2 = 2.01451(8)) that is shorter than Ni–Si bond lengths reported in both Ni(silylene) arene and carbonyl complexes which may suggest the possibility of strong Ni–Si π-back-donation.[26,34] Each of the complexes synthesized and discussed within this chapter exhibit interesting spectroscopic and solid-state features that provide a fundamental understanding of the reactivity of the Ni_2Si_2 core of **8** towards CO_2 activation and CO addition.

Assignment of oxidation states is complex and is dependent on the assignment of ligands as bridging X or L donors.[45] There is precedent in the literature for mixed valent nickel clusters as reported by Henkel and coworkers for mixed nickel sulfide thiolate complexes.[46] It is highlighted that sterically demanding ligands are capable of stabilizing unusual oxidation states of nickel, specifically with sulfur coordination in the prior report. Presumably a similar stabilization occurs with **15** and **17** and **17'** in which stabilization of unusual oxidation states can be provided by labile bis(phosphino) ligation and the N-heterocyclic silyl and silylene ligands.

5.5 Syntheses of Carbon Dioxide and Carbon Monoxide Reaction Products

5.5.1 Standard Synthetic Methods and Materials

All manipulations were carried out under an atmosphere of N_2 using a GloveBox or standard Schlenk techniques. All dry solvents were passed through a purification solvent system from JC Meyer Solvent Systems followed by storage over 4 Å molecular sieves.

dicylcohexylphoshine and $Ni(COD)_2$ were made according to literature procedures or purchased from Strem Chemicals, Inc. Tetrachlorosilane and triethylamine were distilled under nitrogen prior to use. All gases used were research grade and purchased form Aig Gas. Spectroscopic data was collected using a Varian 400, 500 or Bruker 400 and 600 MHz instruments. Chemical shifts in ^{1}H NMR are referenced to deuterated solvents. Chemical shifts in ^{31}P NMR are referenced to phosphoric acid and ^{29}Si NMR are referenced to a trimethylvinylsilane standard (TMS). Original ^{29}Si NMR spectra were processed using MestReNova 11.0.4 to eliminate background signal from the borosilicate NMR tube. All spectroscopic data was taken at room temperature unless otherwise noted. X-ray diffraction was performed on a Bruker-AXS diffractometer. Mass spectra were recorded using either an Agilent LCTOF mass spectrometer or a Waters GCT high-resolution mass spectrometer operating in LIFDI mode. Elemental analyses were performed by Midwest Microlab, LLC, Indianapolis, IN.

5.5.2 $(P^{Cy})_4Ni_2(\mu\text{-}CO)Si_2O$ (**15**)

To a 20 mL vial, 0.100 g (0.146 mmol) of **4** was dissolved in 15 mL of benzene. A suspension of potassium naphthalenide, 0.0673 g (0.292 mmol), in one to two mL of benzene was added to **4** with stirring. After one hour, by ^{31}P NMR, the reaction was complete in the formation of **8**. The reaction mixture was filtered through a pad of Celite to remove KCl, and the filtrate used immediately for the addition of CO_2. Filtrate was transferred to a 50 mL Strauss flask and three freeze/pump/thaw cycles were performed. When the solution reached room temperature, CO_2 was added. The solution was stirred over an atmosphere of CO_2 for 30 mins at which time a color change from dark red/brown

to a lighter red was observed. The reaction was checked for by ^{31}P NMR for completion. Benzene was removed in vacuo and 3 mL diethyl ether was added and vial placed in freezer at –35 ℃ for 12 hours. The precipitate was collected on a filter-tipped pipet to give 44 mg (47% yield) of **15** as a brown crystalline solid. Crystals suitable for X-ray analysis were grown from a concentrated solution of toluene with diethyl ether layering. ^{1}H NMR (600 MHz, Benzene-d_6) δ 7.61 (d, *J* = 6.8 Hz, 1H, Aryl-C*H*), 7.05 – 7.00 (m, 1H, Aryl-C*H*), 6.99 – 6.93 (m, 2H, Aryl-C*H*), 6.80 (t, *J* = 8.0 Hz, 4H, Aryl-C*H*), 4.50 (d, *J* = 8.5 Hz, 1H, methine C-*H*), 4.23–3.93 (m, 4H, methine C-*H*), 3.42 (t, *J* = 10.8 Hz, 1H, methine C-*H*), 3.24 (d, *J* = 8.1 Hz, 1H, methine C-*H*), 3.02 (t, *J* = 9.4, 8.1 Hz, 1H, methine C-*H*), 2.52 (s, 2H, cyclohexyl C-*H*), 2.24 (d, *J* = 9.8 Hz, 2H, cyclohexyl C-*H*), 2.18 – 2.05 (m, 4H, cyclohexyl C-*H*), 2.05 – 1.93 (m, 6H, cyclohexyl C-*H*), 1.92 – 1.78 (m, 14H, cyclohexyl C-*H*), 1.76 – 1.61 (m, 16H, cyclohexyl C-*H*), 1.61 – 1.53 (m, 8H, cyclohexyl C-*H*), 1.51 – 1.36 (m, 19H, cyclohexyl C-*H*), 1.34 – 1.21 (m, 11H, cyclohexyl C-*H*), 1.18 – 1.06 (m, 11H, cyclohexyl C-*H*), 1.05 – 1.00 (m, 3H, cyclohexyl C-*H*), 1.00 – 0.85 (m, 3H, cyclohexyl C-*H*), 0.44 (s, 1H, cyclohexyl C-*H*). ^{31}P{^{1}H} NMR (202 MHz, Benzene-d_6) δ 64.33 (d, *J* = 16.1 Hz), 61.38 (t, *J* = 41.2 Hz), 28.63 (d, *J* = 25.1 Hz), -18.53. ^{29}Si{^{1}H} NMR (119 MHz, C_6D_6) δ 1.66, -3.94 (ddd, $J_{Si\text{-}P}$ = 98.2, 26.4, 13.7 Hz).^{13}C NMR (151 MHz, C_6D_6) δ 234.36 (carbonyl *C*O), 140.73, 140.49, 139.54, 128.59, 128.35, 118.31, 117.29, 117.21, 116.49, 110.47, 107.81, 106.65, 45.29, 45.07, 41.63, 41.48, 41.05, 40.88, 40.34, 40.22, 37.72, 37.62, 36.68, 36.47, 35.58, 35.49, 35.19, 35.09, 33.81, 33.60, 33.49, 33.36, 33.28, 32.24, 32.10, 31.94, 31.84, 31.69, 31.56, 31.27, 31.19, 30.73, 30.25, 29.63, 29.54, 29.19, 29.10, 28.89, 28.83, 28.37, 28.21, 28.08, 27.92, 27.62, 27.53, 27.43, 27.23,

27.06, 26.87, 26.69, 26.38, 26.23, 26.16, 25.87. Repeated attempts to obtain elemental analysis were unsuccessful due to the hydroscopic and oxygen sensitive nature of **15**.

IR: $\nu_{(C\text{-}O)\ bridging} = 1850.46\ cm^{-1}$

5.5.3 $(P^{Cy})_4Ni_2(Si_2O)$ (**16**)

In a 20 mL vial, **4**, 0.1064 g (0.155 mmol), was dissolved in 15 mL of benzene. A suspension of potassium naphthalenide, 0.0752 g (0.326 mmol), in one to two mL of benzene was added to the $NiSiCl_2$ with stirring. After one hour, by ^{31}P NMR, the reaction was complete. The reaction mixture was filtered through a pad of Celite to remove KCl. To the filtrate, pyridine n-oxide, 0.0074g (0.0774 mmol), in a minimum slurry of benzene, was added, with the assumption the reduction would be stoichiometric. The reaction was allowed to stir at room temperature for one hour and by ^{31}P NMR was complete. Benzene was removed in *vacuo*, minimum ether added and vial was placed in fridge at -30° C. Using a paper tipped pipet, **16**, (30.0 mg) was collected as an orange solid and washed with cold ether to yield the oxo-bridged complex in 31% yield after first crop collection. Crystals suitable for X-ray analysis were grown from minimum benzene. ^1H NMR (600 MHz, C_6D_6) δ 7.14 (td, *J* = 7.7, 1.3 Hz, 2H, Aryl-H), 7.03 (td, *J* = 7.6, 1.1 Hz, 2H, Aryl-H), 6.92 (dd, *J* = 7.5, 1.0 Hz, 2H, Aryl-H), 6.83 (dd, *J* = 7.4, 1.0 Hz, 2H, Aryl-H), 4.01 (t, *J* = 11.8 Hz, 2H, methine C-H), 3.69 – 3.57 (m, 4H, methine C-H), 3.39 (td, *J* = 8.7, 4.3 Hz, 2H, methine C-H), 2.53 (d, *J* = 12.5 Hz, 2H, cyclohexyl C-H), 2.35 (m, 2H, cyclohexyl C-H), 2.30 (t, *J* = 12.1 Hz, 2H, cyclohexyl C-H), 2.21 – 2.08 (m, 6H, cyclohexyl C-H), 2.03(m, 4H, cyclohexyl C-H), 1.99 – 1.91 (m, 3H, cyclohexyl C-H), 1.77 (m, 8H, cyclohexyl C-H), 1.72 – 1.47 (m, 30H, cyclohexyl C-H), 1.46 – 1.35 (m, 6H, cyclohexyl C-H), 1.34 – 1.14

(m, 20H, cyclohexyl C-H), 1.04 (dt, J = 12.7, 3.7 Hz, 2H, cyclohexyl C-H), 1.00 – 0.95 (m, 2H, cyclohexyl C-H). $^{31}P\{^{1}H\}$ NMR (243 MHz, C_6D_6) δ 46.18 (d, $J_{P\text{-}P}$ = 18.6 Hz), 44.56 (d, $J_{P\text{-}P}$ = 18.2 Hz). $^{29}Si\{^{1}H\}$ NMR (119 MHz, C_6D_6) δ 9.14 (d, $J_{Si\text{-}P}$ = 112.4 Hz). ^{13}C NMR (151 MHz, C_6D_6) δ 143.12 (Aryl C), 140.65 (Aryl C), 118.92 (Aryl C), 115.85 (Aryl C), 109.33 (Aryl C), 106.04 (methine C), 65.94, 44.99, 44.92, 43.10, 42.92, 39.24, 38.31, 33.28, 33.23, 32.61, 31.25, 30.75, 29.81, 29.31, 29.12, 28.99, 28.58, 28.05, 27.97, 27.73, 27.67, 27.06, 27.00, 26.30, 26.17, 15.62.

Anal. Calcd. for $C_{64}H_{104}N_4Ni_2OP_4Si_2$: C, 61.84 H, 8.43 N, 4.51. Anal. Found for $C_{64}H_{104}N_4Ni_2OP_4Si_2$: C, 61.33 H, 8.40 N, 3.77. IR: $\nu_{Si\text{-}O\text{-}Si}$= 1251.69 cm^{-1}.

5.5.4 $(P^{Cy})_4NiClNi(CO)Si_2O$-TMS, (**17**)

To a 20 mL vial, 0.2000 g (0.163 mmol) of Ni_2Si_2 was dissolved in 15 mL of benzene and transferred to a 50 mL Strauss flask equipped with stir bar. Excess TMSCl, 2 drops via pipet, was added prior to CO_2 addition. After three freeze pump thaw cycles, CO_2 was added at room temperature, after which time a color change is observed from red to orange. The mixture was allowed to stir for 60 mins. The reaction was checked by ^{31}P NMR after one hour and found to be complete. The solvent was removed in vacuo and hexane added. The product was collected as a bright yellow precipitate on a paper tipped pipette, 98.9 mg, 44 % yield, after first crop collection. Bright orange crystals suitable for X-ray analysis were grown from a concentrated solution of minimum benzene with hexane layering. ^{1}H NMR (600 MHz, C_6D_6) δ 6.99 (td, J = 7.5, 1.2 Hz, 1H, Aryl C*H*), 6.95 – 6.89 (m, 3H, Aryl C*H*), 6.89 – 6.84 (m, 1H, Aryl C*H*), 6.68 – 6.65 (m, 1H, Aryl C*H*), 6.63 (dd, J = 7.4, 1.3 Hz, 1H, Aryl C*H*), 6.60 (dd, J = 7.6, 1.2 Hz, 1H, Aryl C*H*) 3.74 (dd, J = 13.5, 4.2 Hz, 1H,

methine C*H*), 3.67 – 3.55 (m, 2H, methine C*H*), 3.47 (dd, *J* = 12.2, 5.2 Hz, 1H, methine C*H*), 3.39 (dd, *J* = 12.0, 6.0 Hz, 1H, methine C*H*), 3.25 – 3.18 (m, 1H, methine C*H*), 3.08 (dd, *J* = 12.2, 5.6 Hz, 1H, methine C*H*), 3.05 – 2.98 (m, 2H, cyclohexyl C-*H*), 2.97 (d, *J* = 3.5 Hz, 1H, methine C*H*), 2.96 – 2.91 (m, 1H, cyclohexyl C-*H*), 2.88 – 2.82 (m, 2H, cyclohexyl C-H), 2.79 (dd, *J* = 13.1, 1.9 Hz, 1H, methine C-*H*), 2.53 (t, *J* = 7.3 Hz, 2H, cyclohexyl C-*H*), 2.25 (d, *J* = 12.0 Hz, 2H, cyclohexyl C-*H*), 2.21 – 2.14 (m, 3H, cyclohexyl C-*H*), 2.11 – 2.00 (m, 2H, cyclohexyl C-*H*), 1.94 (d, *J* = 10.8 Hz, 2H, cyclohexyl C-*H*), 1.88 (dd, *J* = 13.1, 3.5 Hz, 2H, cyclohexyl C-*H*), 1.84 – 1.72 (m, 9H, cyclohexyl C-*H*), 1.72 – 1.59 (m, 7H, cyclohexyl C-*H*), 1.57 – 1.45 (m, 2H, cyclohexyl C-*H*), 1.42 (dt, *J* = 12.2, 3.1 Hz, 2H, cyclohexyl C-*H*), 1.39 – 1.33 (m, 2H, cyclohexyl C-*H*), 1.32 – 1.13 (m, 8H, cyclohexyl C-*H*), 1.10 – 1.02 (m, 1H, cyclohexyl C-*H*), 0.94 (tdd, *J* = 12.5, 9.1, 3.4 Hz, 1H, cyclohexyl C-*H*), 0.88 – 0.64 (m, 4H), 0.15 0.15 (s, 9H, –Si(CH_3)$_3$).^{31}P{^{1}H} NMR (162 MHz, C_6D_6) δ 63.97 (d, $J_{P\text{-}P}$ = 35.1 Hz), 50.14 (ddd, $J_{P\text{-}P}$ = 34.8, 15.3, 3.4 Hz), 35.02 (dd, $J_{P\text{-}P}$ = 14.8, 4.2 Hz), 5.46 (s). ^{29}Si{^{1}H} NMR (119 MHz, C_6D_6) δ 102.26 (dd, $J_{Si\text{-}P}$ = 94.7, 34.6 Hz, Ni_2-*Si*), 3.26 (s, -O-*Si*$(CH_3)_3$), -10.29 (m, Ni-*Si*-O-Si(CH_3)).^{13}C NMR (151 MHz, Benzene-d_6) δ 200.85 (Carbonyl *C*O), 141.44, 141.29 (d, *J* = 12.8 Hz), 140.73 (t, *J* = 16.7 Hz), 128.36, 126.08, 118.23, 117.86, 116.04, 108.85, 108.74, 107.11, 106.43, 42.48 (d, *J* = 7.5 Hz), 41.19 – 40.84 (m), 40.30 (d, *J* = 12.5 Hz), 39.46 (d, *J* = 12.6 Hz), 39.30 – 39.01 (m), 38.40 (d, *J* = 11.6 Hz), 38.13 (d, *J* = 5.8 Hz), 37.98, 37.82, 37.37 (d, *J* = 15.7 Hz), 36.63 (d, *J* = 34.3 Hz), 34.64 (d, *J* = 16.3 Hz), 33.34 (d, *J* = 17.8 Hz), 33.00 (d, *J* = 17.9 Hz), 32.57, 32.09 (d, *J* = 8.9 Hz), 31.55 (d, *J* = 6.2 Hz), 31.31 (d, *J* = 6.1 Hz), 31.04 (d, *J* = 12.2 Hz), 30.86, 30.66, 30.49 (d, *J* = 6.6 Hz), 30.31,

30.11, 29.92, 29.77, 29.51, 28.95 (d, *J* = 13.0 Hz), 28.63, 28.53, 28.40 (t, *J* = 7.0 Hz), 28.05, 27.96, 27.80, 27.60, 27.55, 27.16, 26.99, 26.85, 26.58 (d, *J* = 6.2 Hz), 2.13. Exact Mass Calcd. for $C_{68}H_{113}ClN_4Ni_2O_2P_4Si_3$: 1376.5517 Exact Mass Found by ESI for $C_{68}H_{113}ClN_4Ni_2O_2P_4Si_3$ [MH^+]: 1379.5246, Mass found matched well with the theoretical isotopic pattern. IR: $\nu_{(C\text{-}O)\ terminal}$ = 1988.27 cm^{-1}

5.5.5 $[Ni_2Si_2(CO)(O\text{-}TMS)]BAr^F{}_4$ (**18**)

To a 20 mL vial, **17**, 0.120 mg (0.087 mmol) in minimum ether. NaBarF, 0.077 mg (0.087 mmol) also in minimum ether, was added to slurry of **17**, after which time an immediate color change was observed from orange to a deep purple. The material was filtered through a paper tipped pipet with a pad of Celite and solvent removed in *vaccuo* to obtain **18** as a purple glaze. ^{1}H NMR (600 MHz, Acetonitrile-d_3) δ 7.69 (dt, *J* = 5.2, 2.1 Hz, 8H, BAr^F), 7.67 (s, 2H, BAr^F), 6.92 – 6.80 (m, 4H, Ar–*H*), 6.72 (dtd, *J* = 14.4, 7.5, 1.4 Hz, 2H, Ar–*H*), 6.64 (td, *J* = 7.4, 1.6 Hz, 1H, Ar–*H*), 6.57 (dd, *J* = 7.6, 1.3 Hz, 1H, Ar–*H*), 3.93 – 3.82 (m, 2H, methine C–*H*), 3.65 (dd, *J* = 13.2, 4.8 Hz, 1H, methine C–*H*), 3.60 (dd, *J* = 13.2, 10.4 Hz, 1H, methine C–*H*), 3.48 (dd, *J* = 13.7, 6.7 Hz, 1H, methine C–*H*), 3.24 (dd, *J* = 13.3, 6.4 Hz, 1H, methine C–*H*), 2.86 (t, *J* = 14.5 Hz, 1H, methine C–*H*), 2.68 (dd, *J* = 13.2, 2.2 Hz, 1H,methine C–*H*), -0.10 (s, 8H, Si–C*H*$_3$). ^{31}P NMR (243 MHz, Acetonitrile-d_3) δ 78.29 (d, *J* = 13.6 Hz), 74.59 (d, *J* = 19.6 Hz), 53.85 (dd, *J* = 20.2, 7.8 Hz), 37.24 (t, *J* = 10.9 Hz).

5.5.6 $Ni_2Si_2(CO)_2$ [Reaction of excess CO with $(P^{Cy})_4Ni_2Si_2$] (**19**)

In a 20 mL vial, 0.100 g (0.146 mmol) of **4** was dissolved in 15 mL of benzene. A suspension of potassium naphthalenide, 0.0673 g (0.292 mmol), in one to two mL of

benzene was added to (1,2-C_6H_4)($NCH_2P(Cy)_2)_2SiNiCl_2$, **4**, with stirring. After one hour, by ^{31}P NMR, the reaction was complete. The reaction mixture was filtered through a pad of Celite to remove KCl, and transferred to a Straus flask. After three freeze pump thaw cycles, excess CO was added at room temperature and the mixture allowed to stir for 30 minutes after which time a color change was observed form deep red to yellow. The reaction was checked by ^{31}P NMR and found to be complete. The solvent was removed in *vaccuo* and ether added. The product was collected as a yellow solid on a paper tipped pipet in .072 g, 77 % yield. Crystals for X-ray analysis were grown from benzene/ether layering. ^1H NMR (400 MHz, Benzene-d_6) δ 7.66 (dd, *J* = 7.9, 1.3 Hz, 1H), 7.07 (dtd, *J* = 7.6, 4.5, 2.3 Hz, 2H), 7.02 (td, *J* = 7.5, 1.3 Hz, 1H), 6.94 (td, *J* = 7.6, 1.2 Hz, 1H), 6.86 (dd, *J* = 7.5, 1.4 Hz, 1H), 6.80 (d, *J* = 7.7 Hz, 1H), 6.76 (dd, *J* = 7.5, 1.4 Hz, 1H), 4.91 (dd, *J* = 14.4, 3.8 Hz, 1H), 4.20 (dd, *J* = 14.3, 7.7 Hz, 1H), 4.12 (dd, *J* = 13.7, 8.3 Hz, 1H), 3.62 (dd, *J* = 12.6, 6.5 Hz, 1H), 3.56 (dd, *J* = 12.2, 9.7 Hz, 1H), 3.12 (dd, *J* = 12.6, 5.4 Hz, 1H), 2.77 (dd, *J* = 12.2, 4.8 Hz, 1H), 2.67 (dd, *J* = 13.7, 10.1 Hz, 1H), 2.40 (t, *J* = 17.1 Hz, 1H), 2.20 (q, *J* = 11.1, 10.1 Hz, 4H), 2.14 – 1.87 (m, 13H), 1.87 – 1.74 (m, 7H), 1.73 – 1.55 (m, 15H), 1.52 – 1.43 (m, 7H), 1.42 – 1.30 (m, 7H), 1.21 (dt, *J* = 22.8, 11.2 Hz, 5H), 1.13 – 0.96 (m, 10H), 0.86 – 0.68 (m, 2H), 0.68 – 0.60 (m, 1H), 0.59 – 0.47 (m, 1H). ^{31}P NMR (243 MHz, Benzene-d_6) δ 97.20, 59.86 (d, *J* = 31.2 Hz), 55.48 (d, *J* = 31.1 Hz), -11.39. $^{29}Si\{^1H\}$ NMR (119 MHz, Benzene-d_6) δ 171.90 (tt, *J* = 16.7, 6.9 Hz), 148.72 (t, *J* = 14.8 Hz). IR: $\nu_{CO(terminal)}$ = 1958.22 cm^{-1}, 1939.86 cm^{-1} ^{13}C NMR (151 MHz, C_6D_6) δ 200.17 (carbonyl *C*O), 198.66 (carbonyl *C*O), 143.58, 143.50, 142.73, 141.52, 140.64, 140.57, 126.08, 119.56, 118.20, 118.01, 117.35, 112.02, 111.94, 108.97, 108.62, 106.82, 43.87,

43.79, 41.64, 41.49, 40.68, 40.49, 40.36, 40.17, 40.05, 39.11, 38.99, 38.66, 38.57, 37.64, 36.95, 36.91, 34.74, 34.62, 33.40, 33.30, 31.98, 31.87, 31.57, 31.51, 31.14, 31.05, 30.85, 30.52, 30.39, 30.32, 30.07, 29.44, 29.30, 29.21, 29.18, 29.02, 28.69, 28.65, 28.58, 28.53, 28.46, 28.42, 28.34, 28.29, 28.24, 28.13, 28.08, 27.99, 27.90, 27.74, 27.69, 27.64, 27.60, 27.55, 27.51, 27.26, 27.20, 27.14, 27.07, 26.99, 26.92, 26.86, 26.67, 26.61, 26.57, 26.25, 26.04.

5.5.7 $Ni_2Si_2O(CO)_2$ [**15** or **16** + CO] (kinetic product) (**20**)

In a J-young tube with 0.020 mg of either **15** or **16** in C_6D_6, three freeze pump thaw cycles are carried out prior to excess CO(g) addition at atmospheric pressure, followed by manipulated agitation (shake the tube). With **15** an immediate color change from red to yellow is observed. With **16**, an immediate color change from orange to yellow is observed. Spectroscopically by ^1H and ^{31}P NMR full consumption of starting material is successful to yield **20** in solution. Note that multiple attempts to isolate **20** as a solid for single crystal X-ray analysis were unsuccessful due to decomposition but solution state spectroscopic data was acquired. ^1H NMR (600 MHz, Benzene-d_6) δ 7.10 (d, J = 7.6 Hz, 1H), 7.03 – 6.95 (m, 2H), 6.94 – 6.84 (m, 2H), 6.75 (d, J = 6.3 Hz, 2H), 4.34 – 4.24 (m, 2H), 4.12 (ddd, J = 13.2, 8.4, 4.5 Hz, 1H), 3.90 – 3.80 (m, 2H), 3.69 (dd, J = 13.3, 10.2 Hz, 1H), 3.63 (d, J = 13.0 Hz, 1H), 3.52 (dd, J = 13.6, 6.7 Hz, 1H), 2.73 (tdd, J = 15.4, 10.7, 3.1 Hz, 1H), 2.37 (tdd, J = 13.0, 6.8, 2.7 Hz, 1H), 2.17 (ddq, J = 12.6, 8.8, 4.3 Hz, 2H), 2.12 – 2.02 (m, 2H), 1.99 (d, J = 12.9 Hz, 1H), 1.94 – 1.88 (m, 3H), 1.88 – 1.78 (m, 10H), 1.77 – 1.71 (m, 5H), 1.70 – 1.63 (m, 8H), 1.62 – 1.58 (m, 4H), 1.58 – 1.56 (m, 2H), 1.55 – 1.41 (m, 15H), 1.41 – 1.35 (m, 4H), 1.35 – 1.25 (m, 13H), 1.23 – 1.15 (m, 6H), 1.14 – 1.11 (m, 1H), 1.11 – 1.01

(m, 5H), 1.10 – 0.87 (m, 5H), 0.73 (ddt, *J* = 16.3, 12.8, 6.4 Hz, 1H), 0.65 (dddd, *J* = 16.6, 13.0, 8.2, 3.5 Hz, 1H), 0.54 (tdd, *J* = 16.8, 7.3, 4.5 Hz, 2H). ^{31}P NMR (243 MHz, C_6D_6) δ 87.12 (d, *J* = 14.7 Hz), 49.87 (t, *J* = 14.9 Hz), 42.77, -11.83 (d, *J* = 15.4 Hz). ^{29}Si NMR (119 MHz, C_6D_6) δ 21.85 (d, J = 33.8 Hz), 7.75 (dd, J = 79.6, 19.8 Hz). ^{13}C NMR (151 MHz, C_6D_6) δ 204.32 (carbonyl *C*O), 198.51 (carbonyl *C*O), 184.47 (free *C*O), 141.78, 141.68, 140.10, 139.96, 128.59, 118.11, 110.56, 109.85, 108.36, 107.81, 65.94, 43.17, 41.53, 39.64, 38.41, 36.97, 36.44, 36.14, 35.99, 34.66, 34.05, 32.55, 31.68, 31.40, 31.15, 30.84, 30.55, 30.33, 30.12, 29.84, 29.80, 29.51, 29.18, 29.00, 28.86, 28.67, 28.58, 28.21, 27.91, 27.85, 27.64, 27.40, 27.21, 27.02, 26.93, 26.71, 26.57, 26.44, 26.34. IR: $\nu_{(C\text{-}O)\ terminal}$ = 2066.29 cm^{-1}, 1981.04 cm^{-1}.

5.5.8 $Ni_2Si(CO)_4$ [**15** or **16** + CO] (thermodynamic product) (**21**)

After a freeze pump thaw cycle with 0.050 g of either **15** or **16** in C_6D_6, CO gas is added at high pressure. An immediate color change from red (**15**) to yellow is observed. With **16**, an immediate color change from orange to yellow is observed. Spectroscopically by ^{1}H and ^{31}P NMR full consumption of starting material is successful to yield **20** in solution. Multiple attempts to isolate **20** as a solid for single crystal X-ray analysis were unsuccessful due to decomposition, but rather consistently resulted in the formation of **21** when set up to recrystallize in concentrated ether and isolated as a bright yellow crystalline solid. (6.0 mg, 20 % yield from **15**). ^{1}H NMR (600 MHz, Benzene-d_6) δ 7.11 (dd, *J* = 5.7, 3.2 Hz, 2H), 6.85 (dd, *J* = 5.6, 3.3 Hz, 2H), 3.22 (d, *J* = 3.6 Hz, 4H), 1.92 – 1.82 (m, 5H), 1.75 (tdt, *J* = 12.5, 6.6, 3.0 Hz, 4H), 1.71 – 1.61 (m, 4H), 1.53 (dd, *J* = 21.3, 8.5 Hz, 11H), 1.29 (qdd, *J* = 12.6, 5.7, 3.5 Hz, 4H), 1.18 (ddd, *J* = 12.6, 5.2, 3.3 Hz, 2H), 1.10 (tt, *J* = 12.3, 3.0 Hz,

3H), 1.07 – 0.99 (m, 7H). ^{31}P NMR (243 MHz, C_6D_6) δ 77.81. ^{29}Si{^{1}H} NMR (119 MHz, Benzene-d_6) δ 169.74 (t, J = 20.1 Hz). ^{13}C NMR (151 MHz, C_6D_6) δ 201.83, 141.28, 119.19, 109.23, 36.18, 36.00, 35.86, 35.75, 28.22, 27.84, 27.06, 26.99, 26.93, 26.42. IR: $\nu_{(C\text{-}O)\ terminal}$ = 2029.29, 1983.82, 1956.23 cm^{-1}

5.6 References

(1) Hopff, H.; Zimmermann, T. *Helvetica Chimica Acta* **1964**, *47* (5), 1293–1294.

(2) Benson, E. E.; Kubiak, C. P.; Sathrum, A. J.; Smieja, J. M. *Chemical Society reviews* **2009**, *38* (1), 89–99.

(3) Appel, A. M.; Bercaw, J. E.; Bocarsly, A. B.; Dobbek, H.; Dubois, D. L.; Dupuis, M.; Ferry, J. G.; Fujita, E.; Hille, R.; Kenis, P. J. A.; et al. *Chemical Reviews* **2013**, *113* (8), 6621–6658.

(4) Aresta, M.; Dibenedetto, A.; Angelini, A. *Chemical Reviews* **2014**, *114* (3), 1709–1742.

(5) Dobbek, H. *Science* **2001**, *293* (5533), 1281–1285.

(6) Jeoung, J.-H.; Dobbek, H. *8. P. Fekkes, A. J. M. Driessen, Microbiol. Mol. Biol. Rev* **2002**, *295* (11), 3.

(7) Braunstein, P.; Matt, D.; Nobel, D. *Chemical Reviews* **1988**, *88* (5), 747–764.

(8) Aresta, M.; Nobile, C. F.; Albano, V. G.; Forni, E.; Manassero, M. *Journal of the Chemical Society, Chemical Communications* **1975**, No. 15, 636–637.

(9) Anderson, J. S.; Iluc, V. M.; Hillhouse, G. L. *Inorganic Chemistry* **2010**, *49* (21), 10203–10207.

(10) Morgenstern, D. A.; Wittrig, R. E.; Fanwick, P. E.; Kubiak, C. P. *Energy Resources Through Photochemistry and Catalysis*; UTC, **1993**; Vol. 115.

(11) Simón-Manso, E.; Kubiak, C. P. *Organometallics* **2005**, *24* (1), 96–102.

(12) Kim, Y. E.; Kim, J.; Lee, Y. *Chemical Communications* **2014**, *50* (78), 11458–11461.

(13) Suh, H. W.; Guard, L. M.; Hazari, N. *Chemical Science* **2014**, *5* (10), 3859–3872.

(14) Murphy, L. J.; Hollenhorst, H.; McDonald, R.; Ferguson, M.; Lumsden, M. D.; Turculet, L. *Organometallics* **2017**, *36* (19), 3709–3720.

(15) Louie, J.; Gibby, J. E.; Farnworth, M. V; Tekavec, T. N. *J. Am. Chem. Soc.* **2002**, *124*, 0.

(16) Litz, K. E.; Henderson, K.; Gourley, R. W.; Banaszak Holl, M. M. *Organometallics* **1995**, *14* (11), 5008–5010.

(17) Laitar, D. S.; Mü, P.; Sadighi, J. P. *J. Am. Chem. Soc.* **2005**, *1* (1), 17196–17197.

(18) Chang, H. L.; Laitar, D. S.; Mueller, P.; Sadighi, J. P. *J. Am. Chem. Soc* **2007**, *129* (45), 13802–13803.

(19) Yoo, C.; Kim, Y.; Lee, Y. *Accounts of Chemical Research* **2018**, *51*, 1144–1152.

(20) Paparo, A.; Okuda, J. *Coordination Chemistry Reviews* **2017**, *334*, 136–149.

(21) Byers, L. R.; Dahl, L. F. *Inorg. Chem* **1980**, *19*, 680–692.

(22) Mitton, S. J.; McDonald, R.; Turculet, L. *Angewandte Chemie - International Edition* **2009**, *48* (45), 8568–8571.

(23) Nova, A.; Suh, H. W.; Schmeier, T. J.; Guard, L. M.; Eisenstein, O.; Hazari, N.; Maseras, F. *Angewandte Chemie - International Edition* **2014**, *53* (4), 1103–1108.

(24) Blom, B.; Stoelzel, M.; Driess, M. *Chemistry - A European Journal* **2013**, *19* (1), 40–62.

(25) Demott, J. C.; Gu, W.; Mcculloch, B. J.; Herbert, D. E.; Goshert, M. D.; Walensky, J. R.; Zhou, J.; Ozerov, O. V. *Organometallics* **2015**, *34*, 35.

(26) Stoelzel, M.; Präsang, C.; Inoue, S.; Enthaler, S.; Driess, M. *Angewandte Chemie International Edition* **2012**, *51* (2), 399–403.

(27) Hadlington, T. J.; Szilvási, T.; Driess, M. *Angewandte Chemie - International Edition* **2017**, *56* (26), 7470–7474.

(28) Schmidt, D.; Zell, T.; Schaub, T.; Radius, U. *Dalton Transactions* **2014**, *43* (28), 10816.

(29) Hadlington, T. J.; Szilvási, T.; Driess, M. *Angewandte Chemie - International Edition* **2017**, *56* (45), 14282–14286.

(30) Schmedake, T. A.; Haaf, M.; Paradise, B. J.; Powell, D.; West, R. *Organometallics* **2000**, *19* (17), 3263–3265.

(31) Gehrhus, B.; Hitchcock, P. B.; Lappert, M. F.; Maciejewski, H. *Organometallics* **2002**, *17* (26), 5599–5601.

(32) Baus, J. A.; Mück, F. M.; Schneider, H.; Tacke, R. *Chemistry - A European Journal* **2017**, *23* (2), 296–303.

(33) Meltzer, A.; Präsang, C.; Driess, M. *Journal of the American Chemical Society* **2009**, *131* (21), 7232–7233.

(34) Meltzer, A.; Präsang, C.; Milsmann, C.; Driess, M. *Angewandte Chemie - International Edition* **2009**, *48* (17), 3170–3173.

(35) Tavčar, G.; Sen, S. S.; Azhakar, R.; Thorn, A.; Roesky, H. W. *Inorganic Chemistry* **2010**, *49* (21), 10199–10202.

(36) Guo, L.; Bradshaw, J. D.; McConville, D. B.; Tessier, C. A.; Youngs, W. J. *Organometallics* **1997**, *16* (8), 1685–1692.

(37) Truflandier, L. A.; Brendler, E.; Wagler, J.; Autschbach, J. *Angewandte Chemie - International Edition* **2011**, *50* (1), 255–259.

(38) Wang, Y.; Kostenko, A.; Yao, S.; Driess, M. *Journal of the American Chemical Society* **2017**, *139* (38), 13499–13506.

(39) Beck, R.; Johnson, S. A. *Organometallics* **2012**, *31* (9), 3599–3609.

(40) Capacci, C.; Ciabatti, I.; Femoni, C.; Iapalucci, M. C.; Funaioli, T.; Zacchini, S.; Zanotti, V. *Inorganic Chemistry* **2018**, *57* (3), 1136–1147.

(41) Goicoechea, J. M.; Hull, M. W.; Sevov, S. C. *Journal of the American Chemical Society* **2007**, *129* (25), 7885–7893.

(42) Komiya, S.; Yamamoto, A. J.; Yamamoto, T.; Ishizu, J.; Kohara, T.; Yamamoto, A.; Ibid ; Vizi-Orosz, A.; Marko, L. *Angew. Chem., Int. Ed. Engl* **1985**, *4* (9), 1505.

(43) Lee, C. H.; Park, J. W. *Organometallics* **1999**, *18* (26), 5713–5716.

(44) Cypryk, M.; Apeloig, Y. *Organometallics* **2002**, *21* (11), 2165–2175.

(45) Green, J. C.; Green, M. L. H.; Parkin, G. *Chem. Commun* **2012**, *48*, 11481–11503.

(46) Kruger, T.; Krebs, B.; Henkel, G. **1989**, *28*, 61–62.

5.7 Spectroscopic Data, Figures and Tables

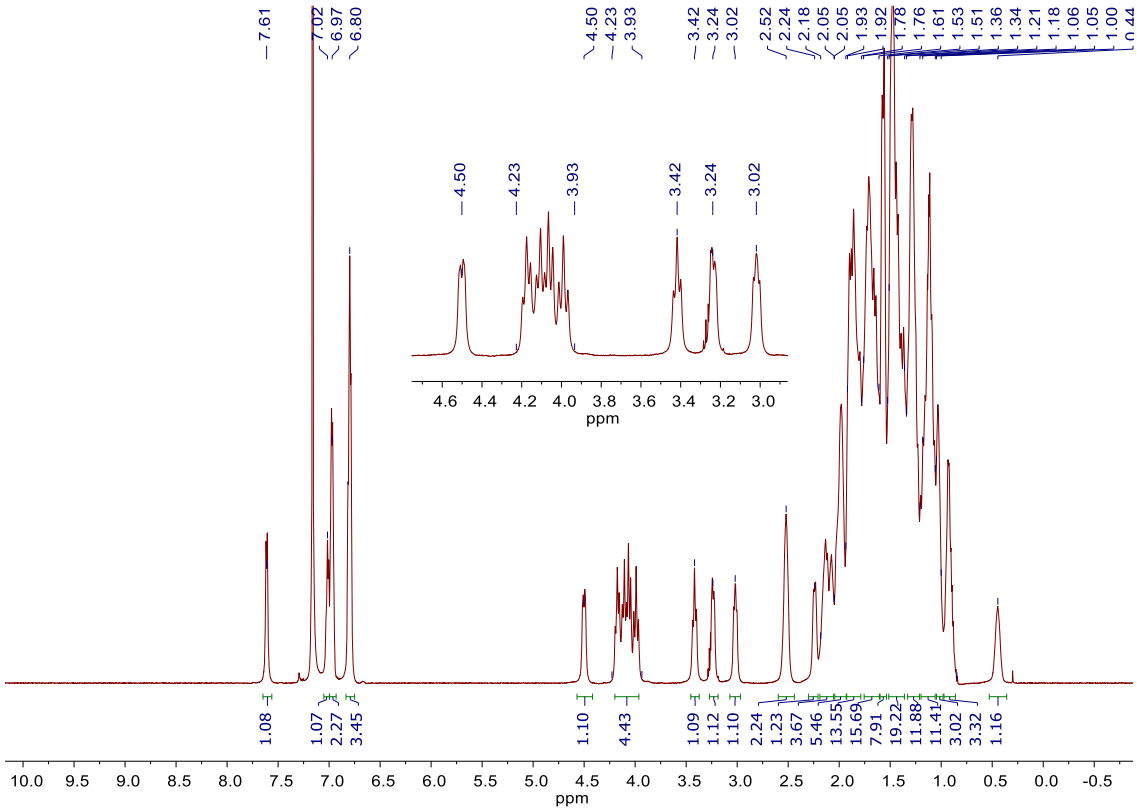

Figure 5.7-1 ^{1}H NMR of $(P^{Cy})_4Ni_2(\mu\text{-}CO)Si_2O$, **15**, in C_6D_6 on a 400 MHz instrument.

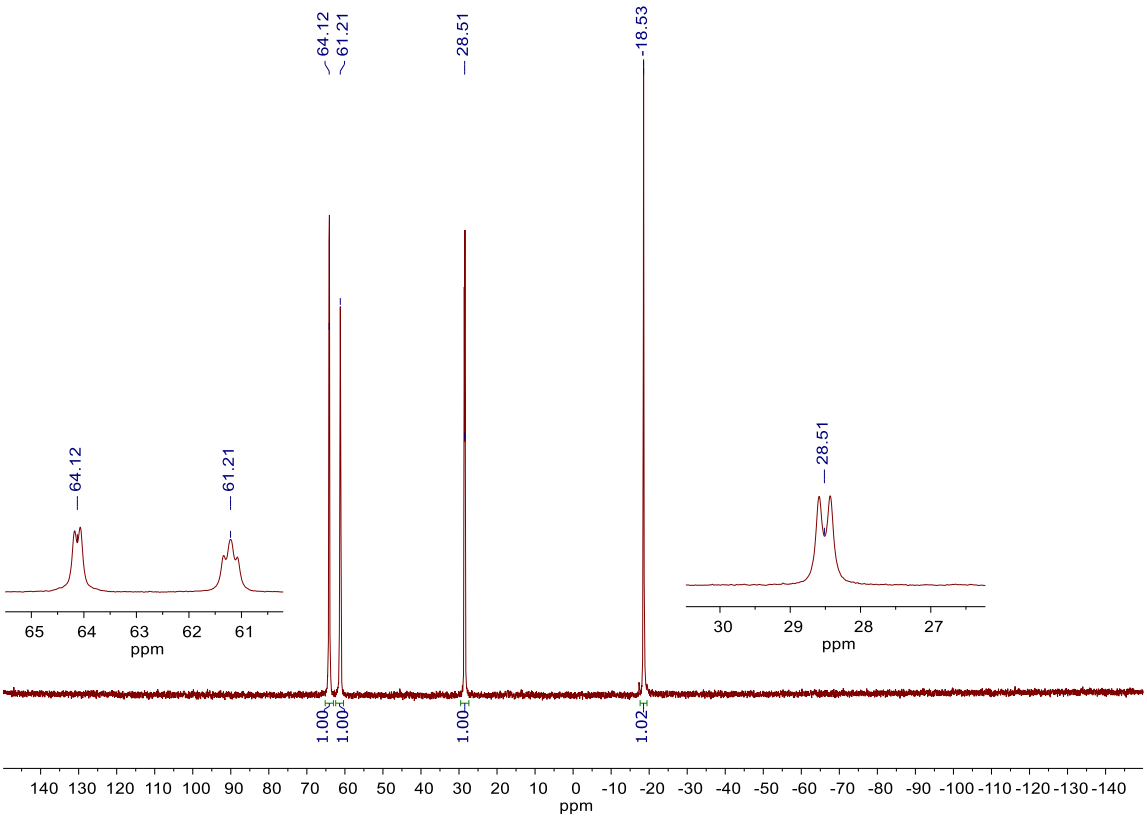

Figure 5.7-2 $^{31}P\{^{1}H\}$ NMR of $(P^{Cy})_4Ni_2(\mu\text{-}CO)Si_2O$, **15**, in C_6D_6 at 202 MHz.

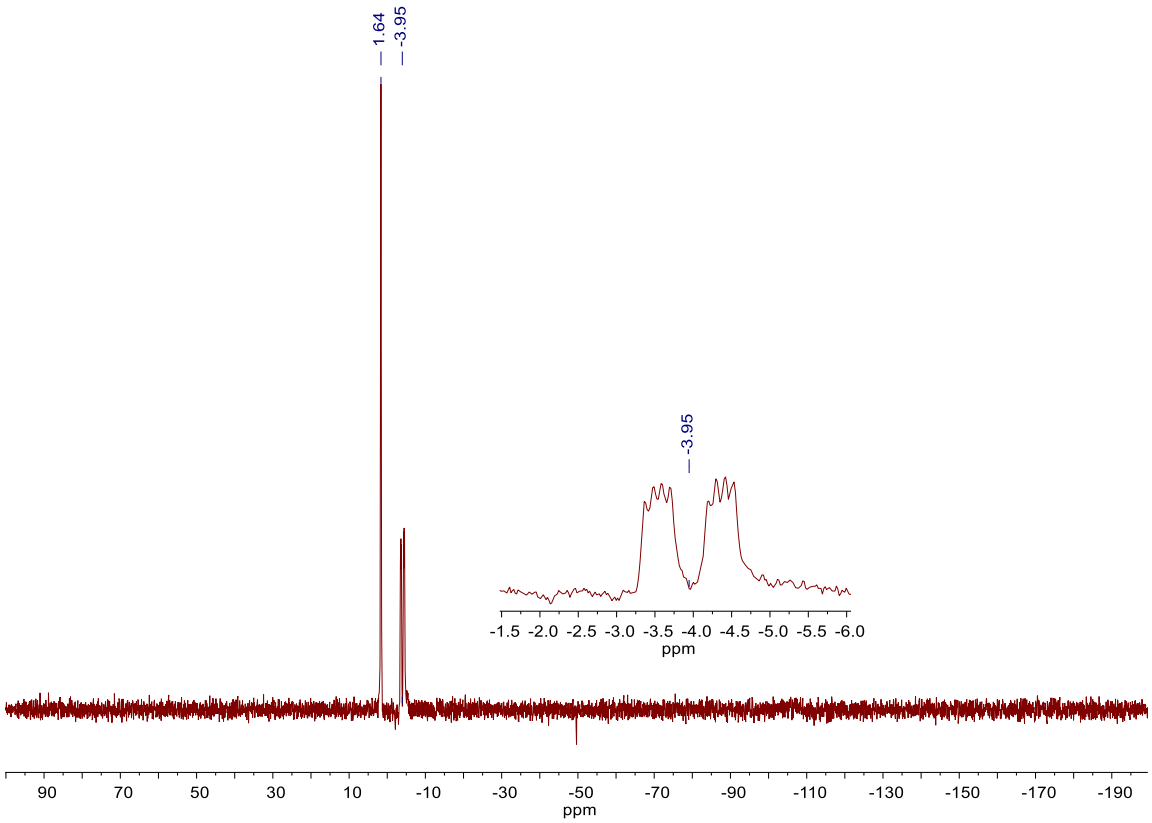

Figure 5.7-3 $^{29}Si\{^{1}H\}$ NMR of $(P^{Cy})_4Ni_2(\mu\text{-}CO)Si_2O$, **15**, in C_6D_6 at 119 MHz.

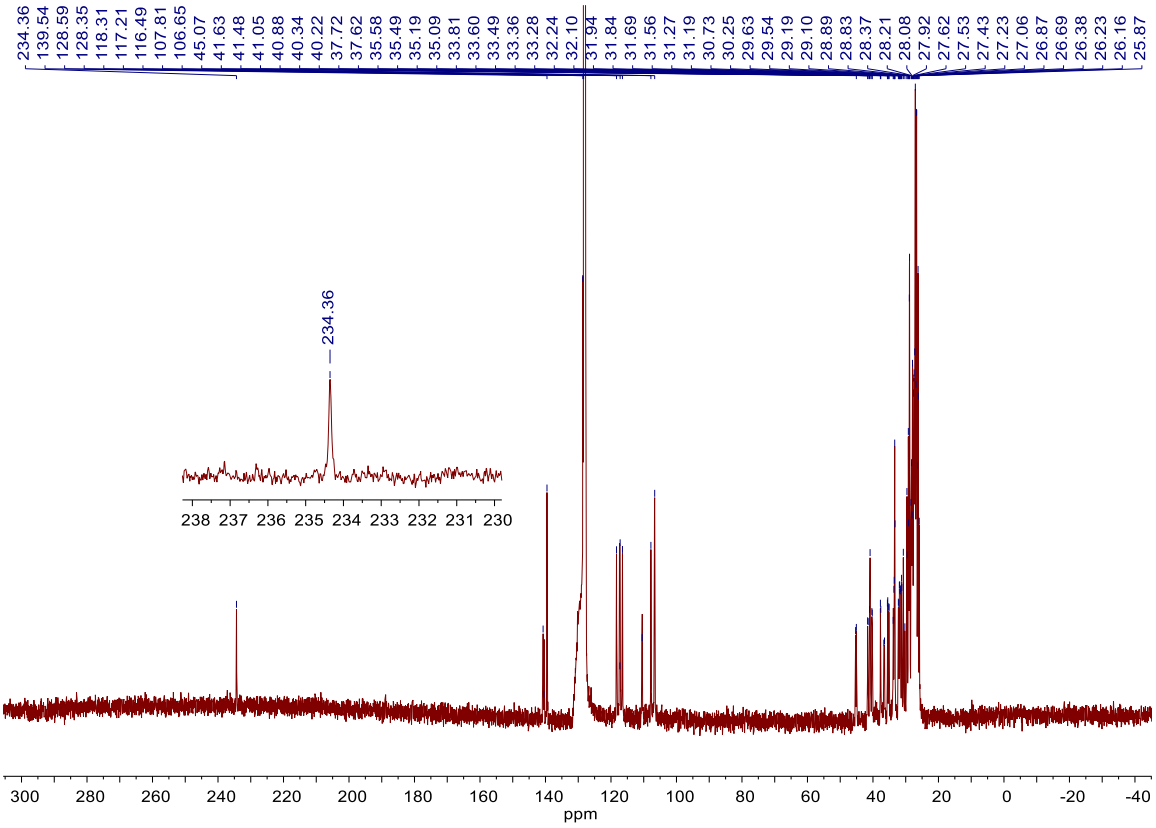

Figure 5.7-4 ^{13}C NMR of $(P^{Cy})_4Ni_2(\mu\text{-}CO)Si_2O$, **15**, in C_6D_6 at 151 MHz.

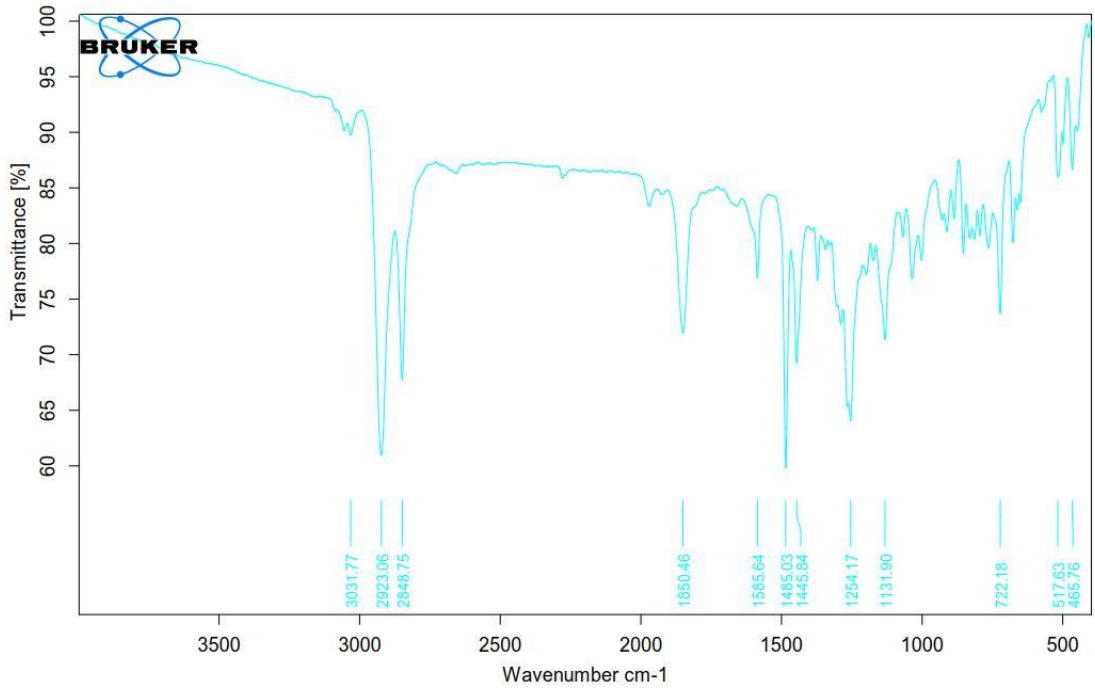

Figure 5.7-5. IR using KBR pellet of $(P^{Cy})_4Ni_2(\mu\text{-}CO)Si_2O$, **15**, featuring shift for bridging carbonyl at 1850.46 cm^{-1}.

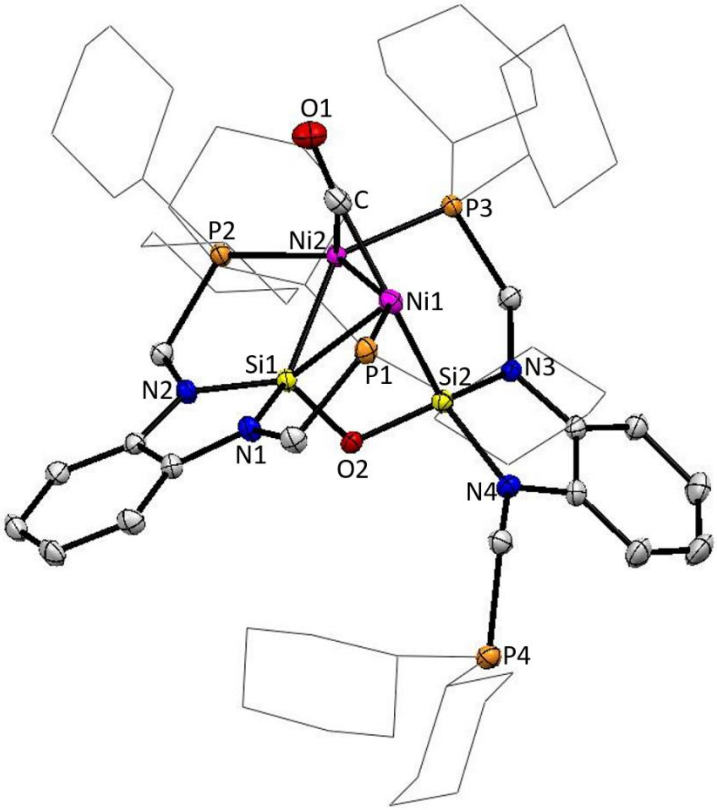

Figure 5.7-6 Thermal ellipsoid plot at 50% probability of $(P^{Cy})_4Ni_2(\mu\text{-}CO)Si_2O$, **15**. Magenta, yellow, blue, orange, red and gray ellipsoids represent nickel, silicon, nitrogen, phosphorus, oxygen and carbon atoms, respectively. For clarity, hydrogen atoms are omitted and cyclohexyl rings on phosphorous are displayed as wireframe. There was one molecule of $C_{65}H_{104}N_4Ni_2O2P_4Si_2$, and disordered molecules of THF and ether present in the asymmetric unit of the unit cell. Half of the disordered THF (disordered site occupancy ratio was 29%/21%) was located at the inversion center. The other ether/THF disorders were in general positions (ether/ether/THF/THF disordered site occupancy ratios were 42%/18%/17%/23%).

Table 5.7-1 Crystallographic data for $(P^{Cy})_4Ni_2(\mu\text{-}CO)Si_2O$, **15**.

Identification code	hh272AB25_0m	
Empirical formula	$C_{71}H_{117.20}N_4Ni_2O_{3.50}P_4Si_2$	
Formula weight	1380.37	
Temperature	100(2) K	
Wavelength	0.71073 Å	
Crystal system	Triclinic	
Space group	P -1	
Unit cell dimensions	a = 12.3779(8) Å	α = 94.4230(12)°.
	b = 14.1408(9) Å	β = 90.5941(12)°.
	c = 22.3753(14) Å	γ = 109.3863(12)°.
Volume	3680.7(4) Å^3	
Z	2	
Density (calculated)	1.246 mg/m^3	
Absorption coefficient	0.678 mm^{-1}	
F(000)	1486	
Crystal size	0.418 x 0.048 x 0.020 mm^3	
θ range for data collection	1.532 to 26.372°.	
Index ranges	$-15 \le h \le 15$, $-17 \le k \le 17$, $-27 \le l \le 27$	
Reflections collected	67077	
Independent reflections	15036 [R_{int} = 0.0703]	
Completeness to θ = 25.242°	100.00%	
Absorption correction	Semi-empirical from equivalents	
Refinement method	Full-matrix least-squares on F^2	
Data / restraints / parameters	15036 / 770 / 962	
Goodness-of-fit on F^2	1.030	
Final R indices [$I > 2\sigma_1$]	R_1 = 0.0443, wR_2 = 0.0989	
R indices (all data)	R_1 = 0.0737, wR_2 = 0.1096	
Largest diff. peak and hole	0.621 and -0.568 e/Å^3	

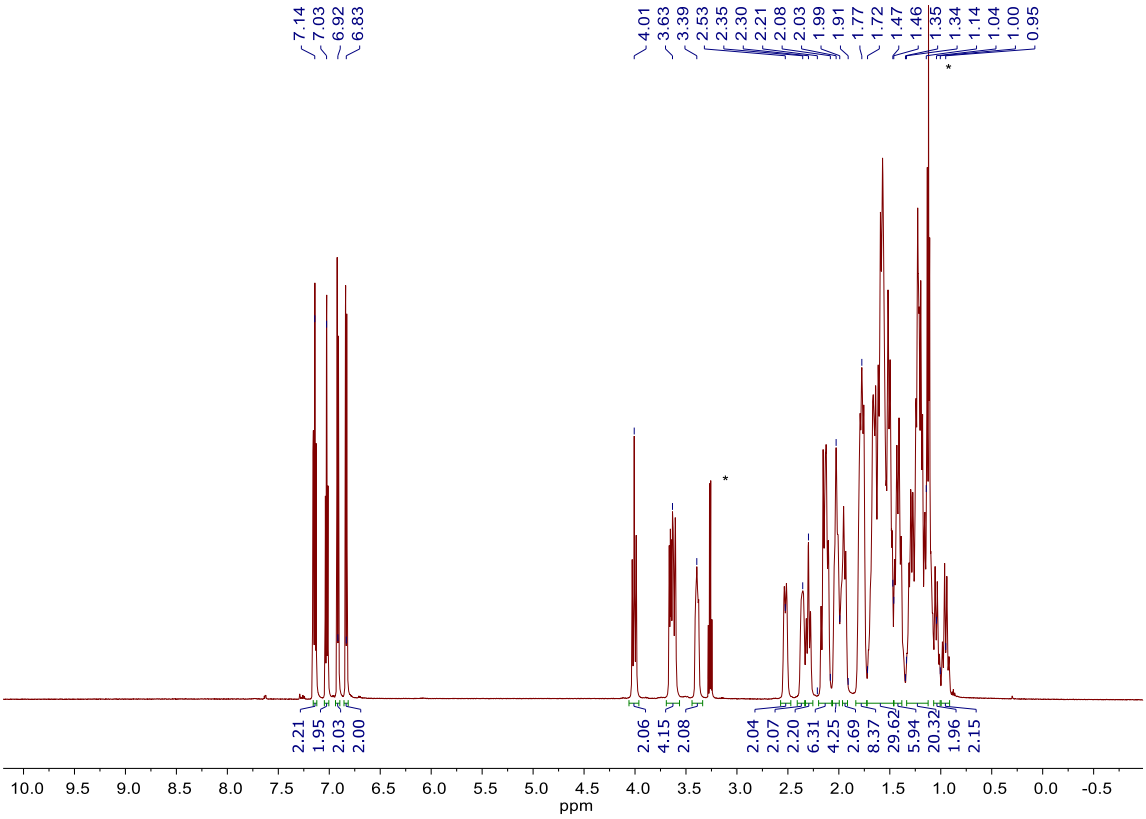

Figure 5.7-7 ^{1}H NMR of Ni_2Si_2O, **16**, in C_6D_6 on a 600 MHz instrument. *indicates ether.

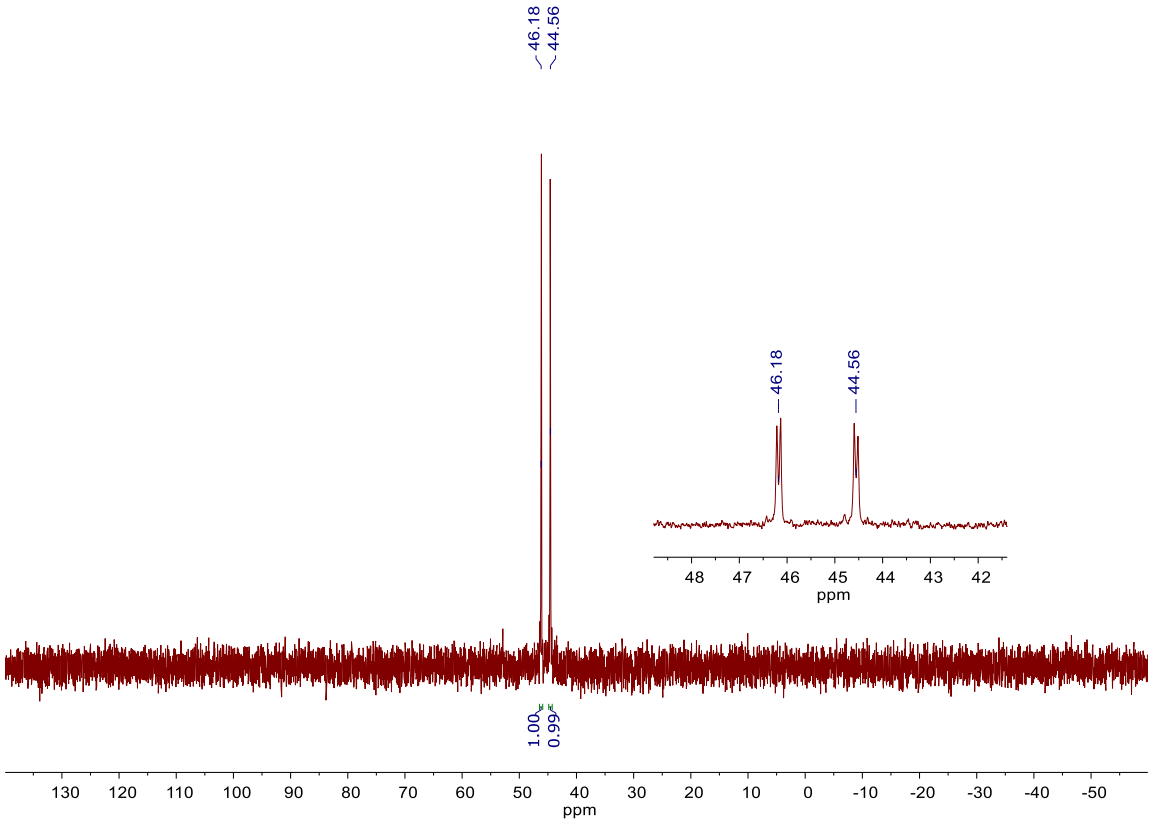

Figure 5.7-8 $^{31}P\{^{1}H\}$ NMR of Ni_2Si_2O, **16**, in C_6D_6 at 243 MHz.

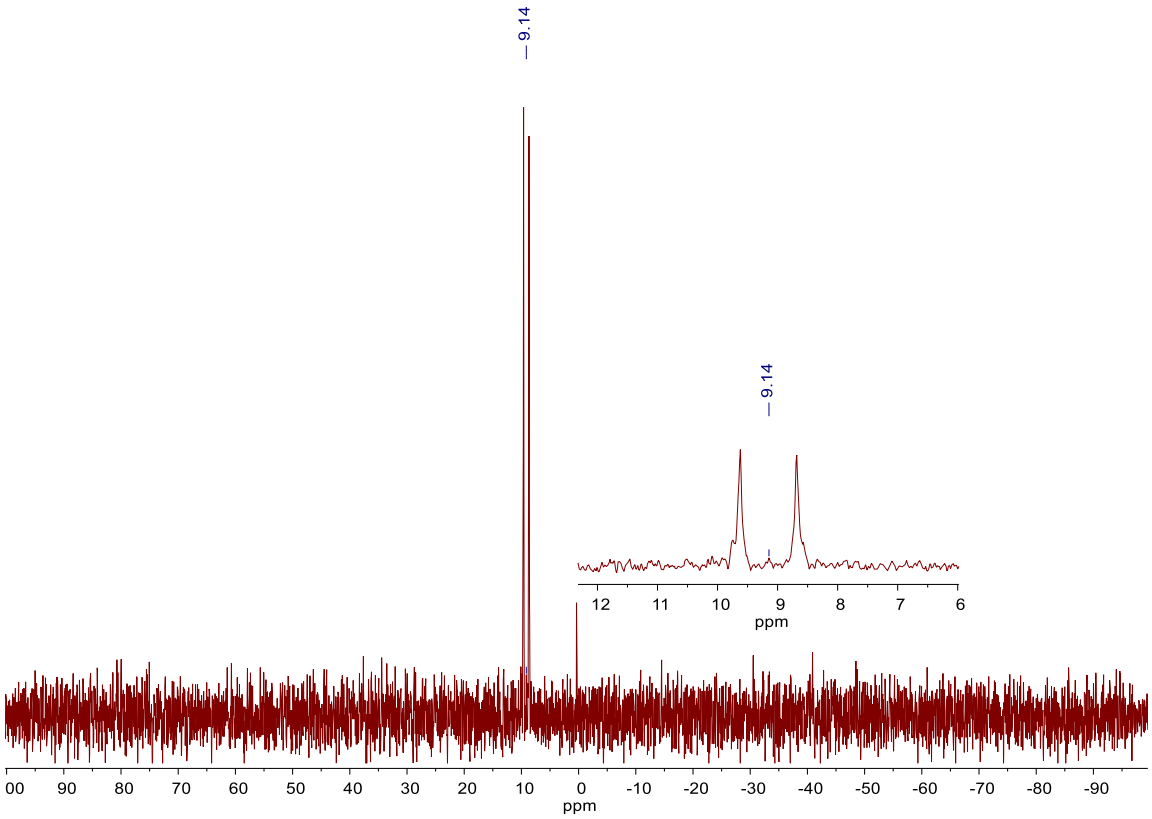

Figure 5.7-9 $^{29}Si\{^{1}H\}$ NMR of $(P^{Cy})_4Ni_2(Si_2O)$, **16**, in C_6D_6 at 119 MHz. Note artifact in spectrum at 0 ppm which is a glitch that occurred where the spectrum was centered.

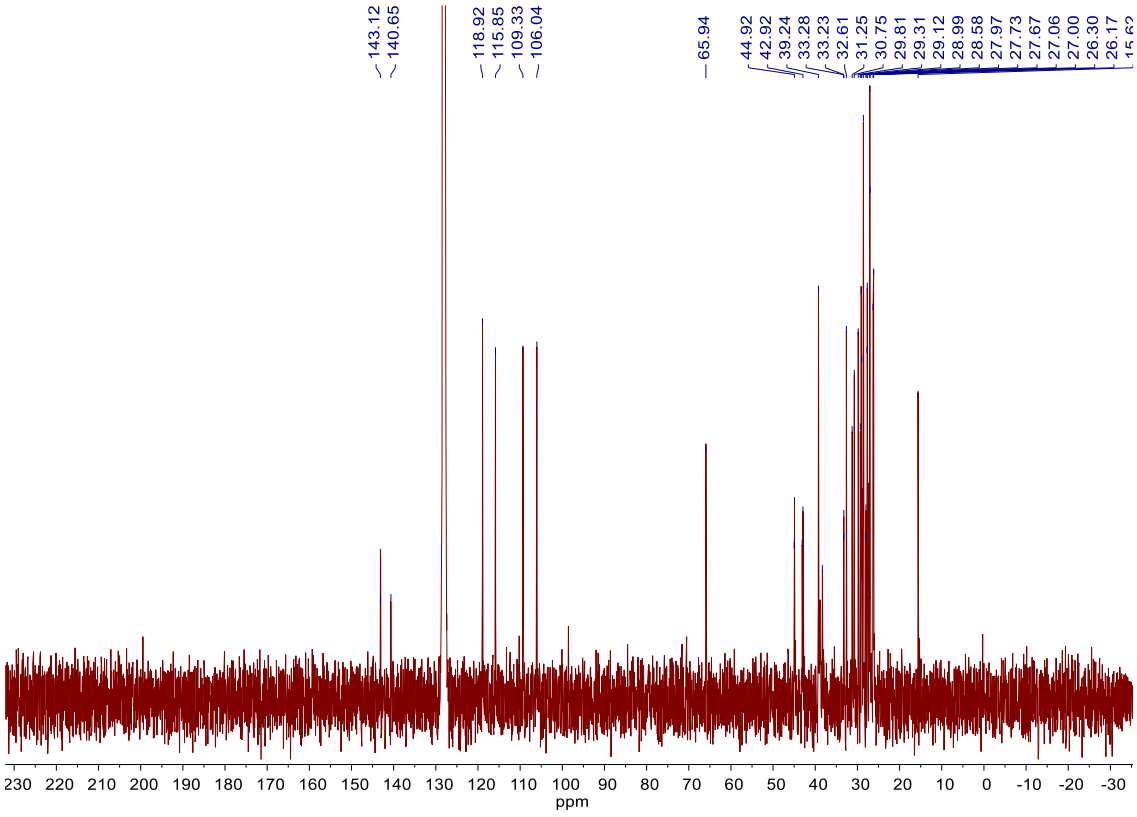

Figure 5.7-10 ^{13}C NMR of $(P^{Cy})_4Ni_2(Si_2O)$, **16**, in C_6D_6 at 151 MHz.

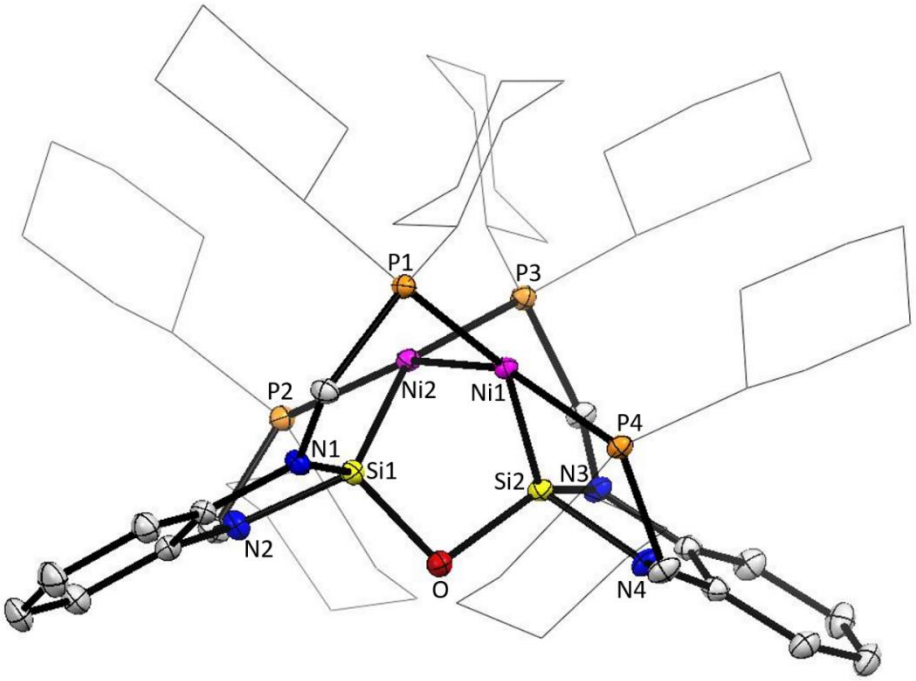

Figure 5.7-11 Thermal ellipsoid plot at 50% probability of $(P^{Cy})_4Ni_2(Si_2O)$, **16**. Magenta, yellow, blue, orange, red and gray ellipsoids represent nickel, silicon, nitrogen, phosphorus, oxygen and carbon respectively. For clarity, hydrogen atoms and solvent molecules are omitted and cyclohexyl rings on phosphorous are displayed as wireframe. There was one molecule of $C_{64}H_{104}N_4Ni_2OP_4Si_2$ and three solvent molecules of benzene present in the asymmetric unit of the unit cell. One of the three benzene molecules were modeled with disorder (disordered site occupancy ratio was 64%/36%).

Table 5.7-2 Crystallographic data for $(P^{Cy})_4Ni_2(Si_2O)$, **16**.

Identification code	hh270AB24_0m	
Empirical formula	$C_{82}H_{122}N_4Ni_2OP_4Si_2$	
Formula weight	1477.31	
Temperature	100(2) K	
Wavelength	0.71073 Å	
Crystal system	Monoclinic	
Space group	P 21/c	
Unit cell dimensions	a = 18.7564(11) Å	α = 90°.
	b = 21.4094(12) Å	β = 103.8439(10)°.
	c = 19.8830(12) Å	γ = 90°.
Volume	7752.3(8) Å^3	
Z	4	
Density (calculated)	1.266 mg/m^3	
Absorption coefficient	0.647 mm^{-1}	
F(000)	3176	
Crystal size	0.239 x 0.228 x 0.073 mm^3	
θ range for data collection	1.420 to 29.129°.	
Index ranges	$-25 \le h \le 25$, $-29 \le k \le 29$, $-27 \le l \le 27$	
Reflections collected	169964	
Independent reflections	20847 [R_{int} = 0.0475]	
Completeness to θ = 25.242°	100.00%	
Absorption correction	Semi-empirical from equivalents	
Refinement method	Full-matrix least-squares on F^2	
Data / restraints / parameters	20847 / 24 / 899	
Goodness-of-fit on F^2	1.017	
Final R indices [$I > 2\sigma_1$]	R_1 = 0.0296, wR_2 = 0.0669	
R indices (all data)	R_1 = 0.0420, wR_2 = 0.0722	
Largest diff. peak and hole	0.436 and -0.289 e/Å^3	

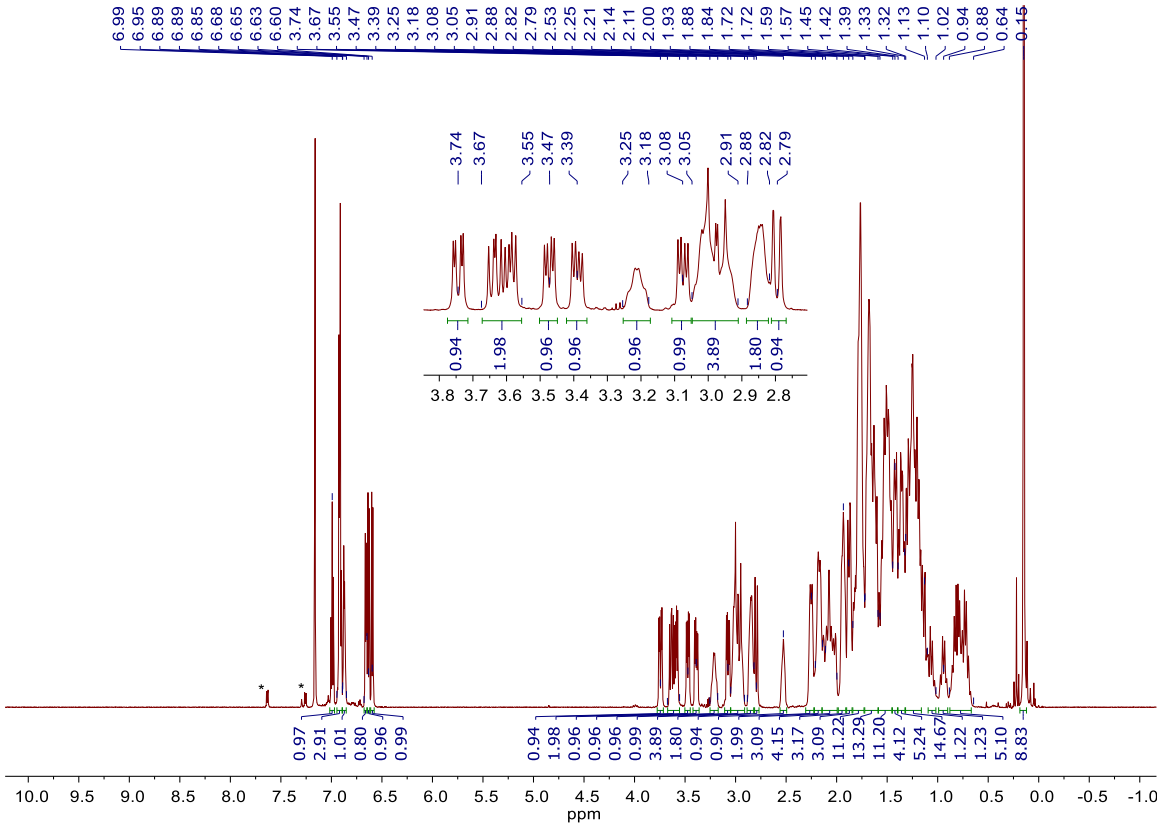

Figure 5.7-12 ^{1}H NMR of $(P^{Cy})_4NiClNi(CO)Si_2O$-TMS, **17**, in C_6D_6 on a 600 MHz instrument.*indicates naphthalene.

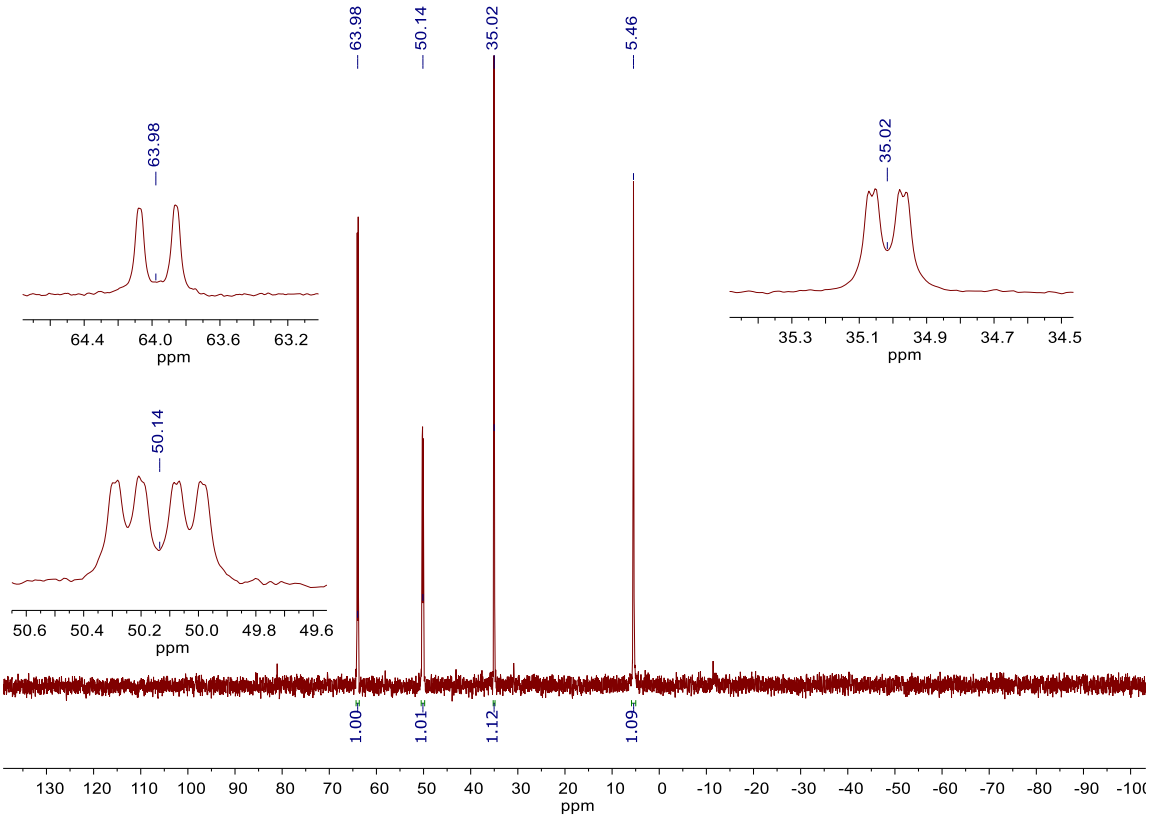

Figure 5.7-13 $^{31}P\{^{1}H\}$ NMR of $(P^{Cy})_4NiClNi(CO)Si_2O$-TMS, **17**, in C_6D_6 at 162 MHz.

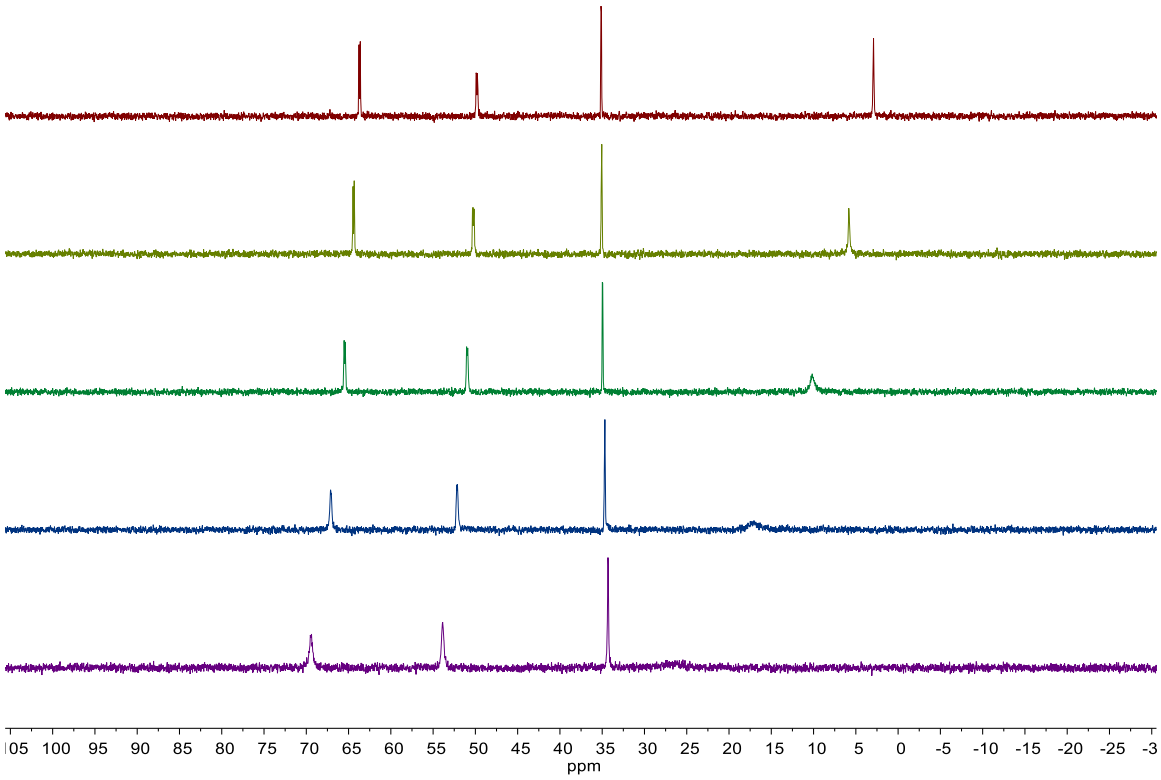

Figure 5.7-14. ^{31}P VT NMR of $(P^{Cy})_4NiClNi(CO)Si_2O$-TMS, **17**, at selected temperatures in d_8-toluene at 243 MHz. Temperatures starting with top spectrum; + 40,+ 20, 0, –20 and –40 °C.

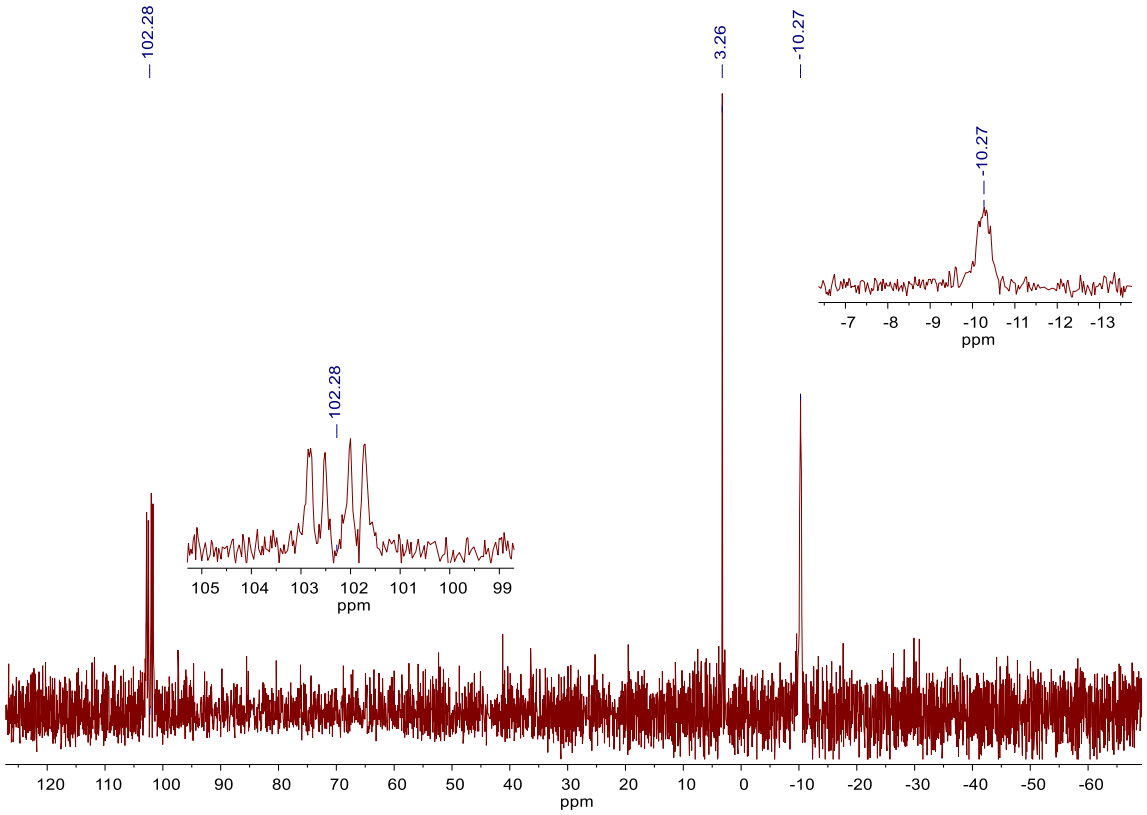

Figure 5.7-15 $^{29}Si\{^{1}H\}$ NMR of $(P^{Cy})_4NiClNi(CO)Si_2O$-TMS, **17**, in C_6D_6 at 119 MHz.

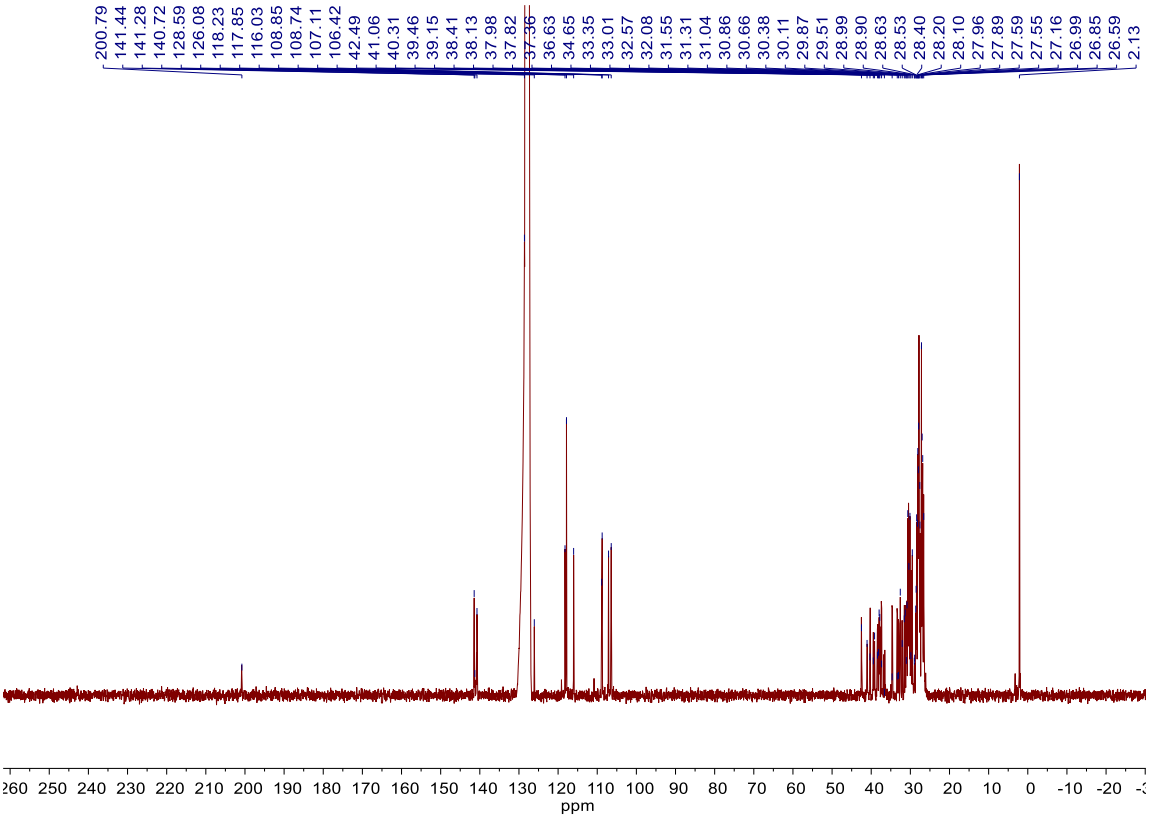

Figure 5.7-16 ^{13}C NMR of $(P^{Cy})_4NiClNi(CO)Si_2O$-TMS, **17**, in C_6D_6 at 151 MHz.

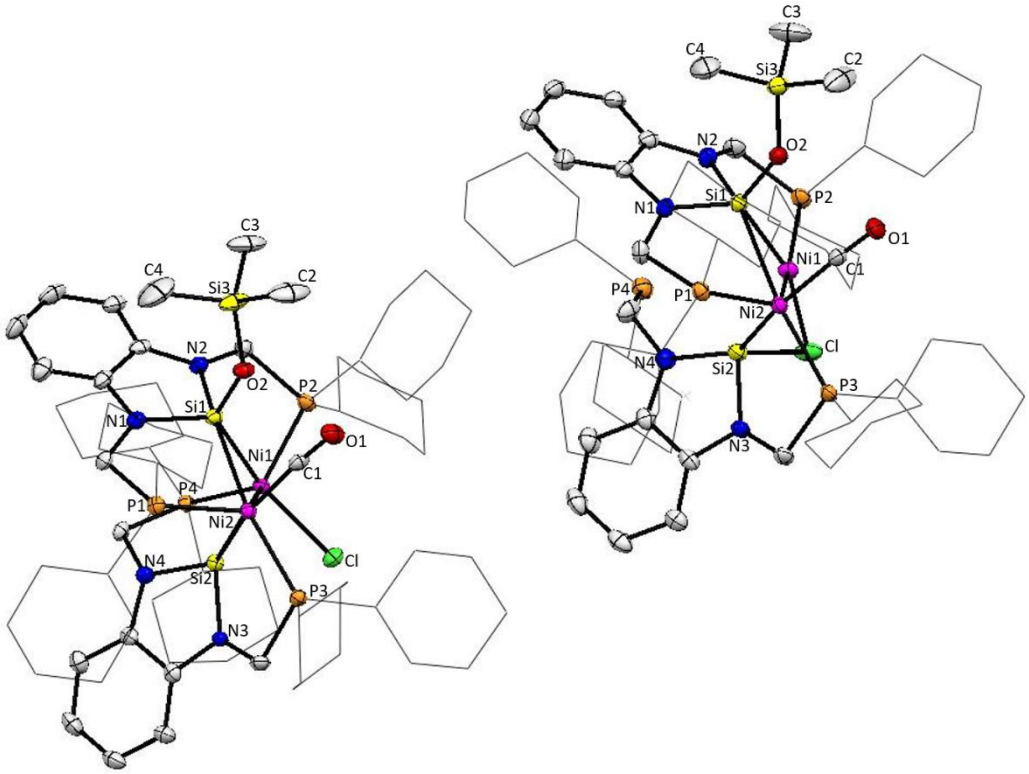

Figure 5.7-17 Thermal ellipsoid plot at 50% probability of $(P^{Cy})_4NiClNi(CO)Si_2O$-TMS, **17**, Magenta, yellow, blue, orange, red, green and gray ellipsoids represent nickel, silicon, nitrogen, phosphorus, oxygen, chlorine and carbon atoms, respectively. For clarity, hydrogen atoms and solvent molecules are omitted and cyclohexyl rings on phosphorous are displayed as wireframe. There were two different molecules of $C_{68}H_{113}ClN_4Ni_2O_2P_4Si_3$ and four solvent molecules of pentane present in the asymmetric unit of the unit cell. The Cl1A-atom is bridging the Ni1A-Si2A- atoms (right isomer) and the Cl1 is bonded to Ni1 for the two different $C_{68}H_{113}ClN_4Ni_2O_2P_4Si_3$ molecules (left isomer), respectively. Three of the eight cyclohexyl-groups where the $C_{68}H_{113}ClN_4Ni_2O_2P_4Si_3$ molecule has the Cl1A bridging effect were modeled with disordered (cyclohexyl disordered site occupancy ratios were 74%/26%, 59%/26%/15%, and 58%/42%). Three of the four pentane molecules were modeled with disorder, where one of the three pentane disorder is at the inversion symmetry (pentane disordered site occupancy ratios were 65%/35%, 59%/41%, and 50%/50%).

Table 5.7-3 Crystallographic data for $(P^{Cy})_4NiClNi(CO)Si_2O$-TMS, **17**.

Identification code	hh219AB18_0m	
Empirical formula	$C_{153.50}H_{268}Cl_2N_8Ni_4O_4P_8Si_6$	
Formula weight	3011.78	
Temperature	100(2) K	
Wavelength	0.71073 Å	
Crystal system	Triclinic	
Space group	P -1	
Unit cell dimensions	a = 16.9923(4) Å	α = 99.9169(5)°.
	b = 19.7638(4) Å	β = 98.4462(5)°.
	c = 24.8033(5) Å	γ = 97.0148(5)°.
Volume	8022.9(3) Å^3	
Z	2	
Density (calculated)	1.247 mg/m^3	
Absorption coefficient	0.673 mm^{-1}	
F(000)	3254	
Crystal size	0.122 x 0.103 x 0.060 mm^3	
θ range for data collection	1.364 to 26.373°.	
Index ranges	$-21 \le h \le 21$, $-24 \le k \le 24$, $-31 \le l \le 31$	
Reflections collected	122424	
Independent reflections	32815 [R_{int} = 0.0716]	
Completeness to θ = 25.242°	100.00%	
Absorption correction	Semi-empirical from equivalents	
Refinement method	Full-matrix least-squares on F^2	
Data / restraints / parameters	32815 / 979 / 1895	
Goodness-of-fit on F^2	1.01	
Final R indices [$I > 2\sigma_1$]	R_1 = 0.0485, wR_2 = 0.1061	
R indices (all data)	R_1 = 0.0871, wR_2 = 0.1203	
Largest diff. peak and hole	1.180 and -0.530 e/Å^3	

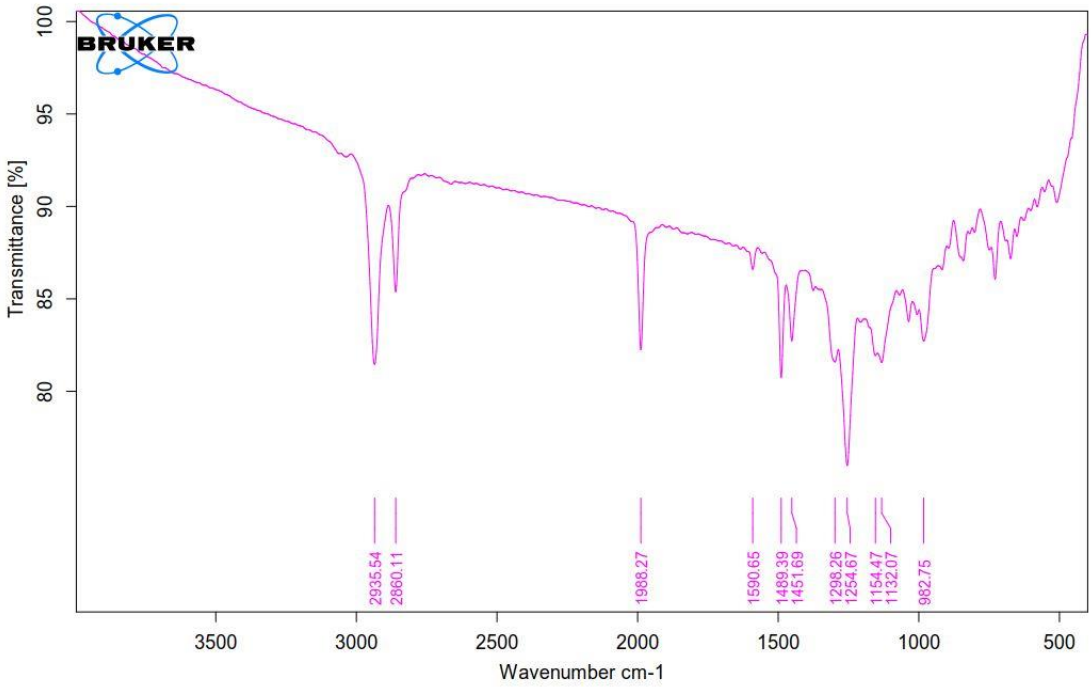

Figure 5.7-18. IR spectrum using a KBR pellet of $(P^{Cy})_4NiClNi(CO)Si_2O$-TMS, **17**, featuring shift for terminal carbonyl at 1988.65 cm^{-1}.

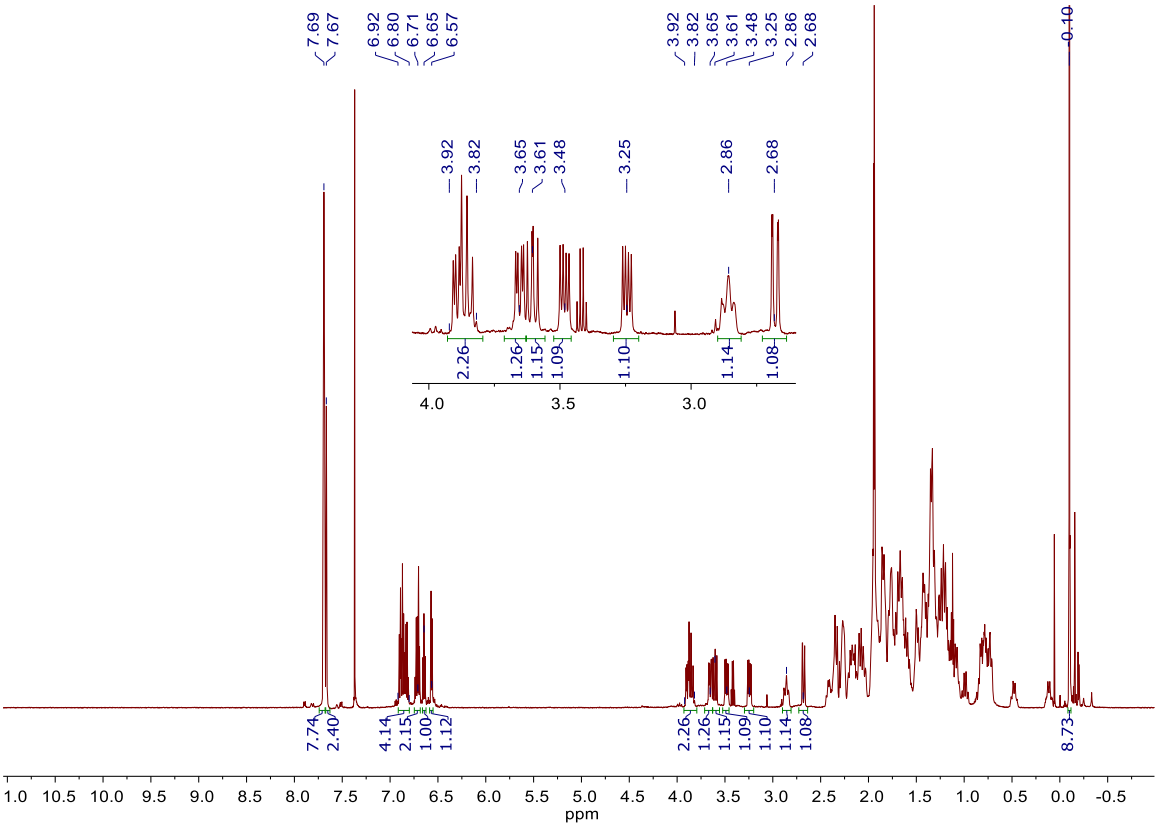

Figure 5.7-19. ^{1}H NMR of $[Ni_2Si_2(CO)(O\text{-}TMS)]BAr^F{}_4$, **18**, in CD_3CN at 600 MHz. Note ether at 3.42 ppm.

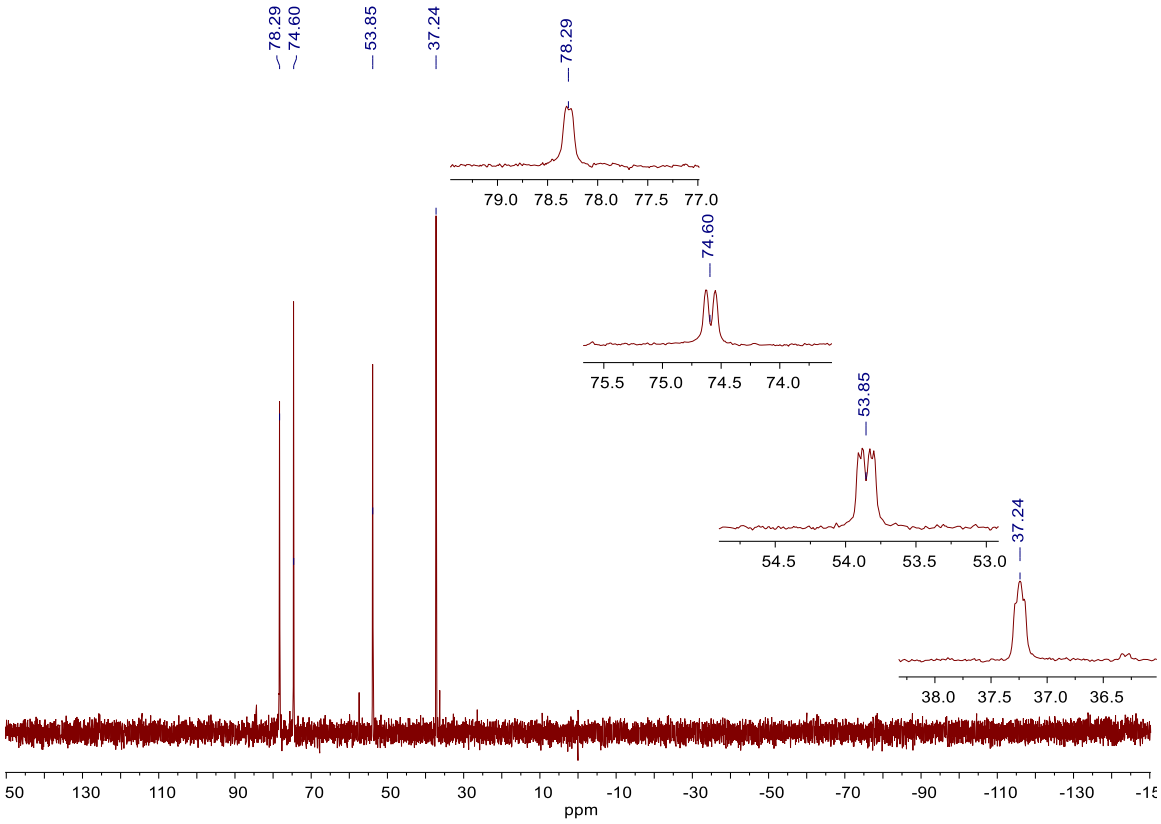

Figure 5.7-20. $^{31}P\{^{1}H\}$ NMR of $[Ni_2Si_2(CO)(O\text{-}TMS)]BAr^F{}_4$, **18**, in CD_3CN at 243 MHz.

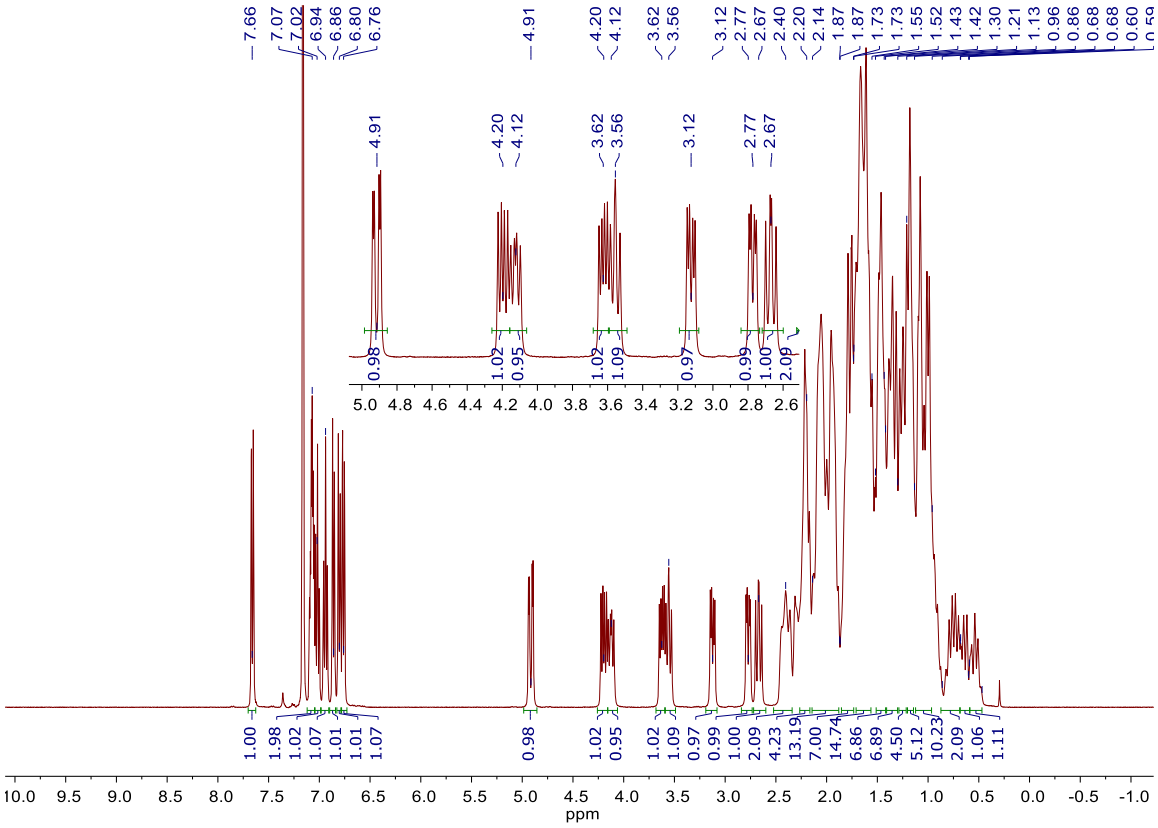

Figure 5.7-21 ^{1}H NMR of $P_4Ni_2Si_2(CO)_2$, **19**, in C_6D_6 at 400 MHz.

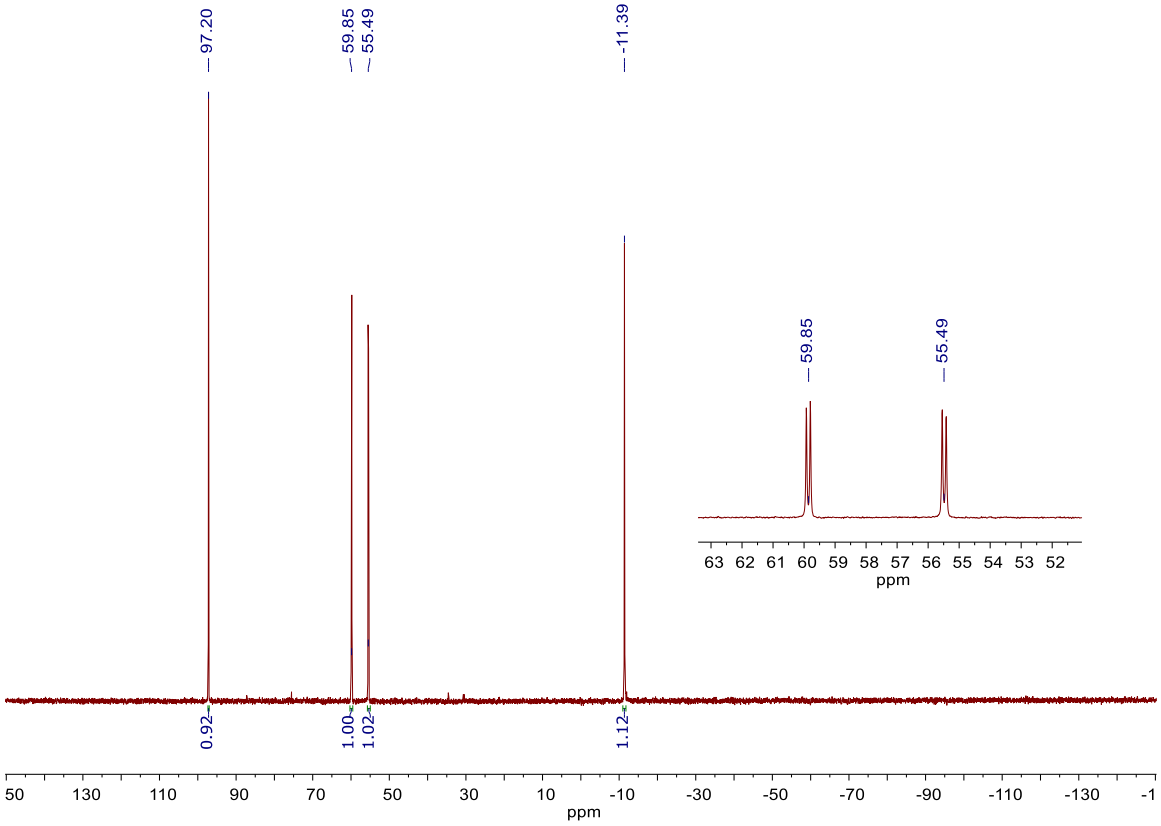

Figure 5.7-22 $^{31}P\{^{1}H\}$ $P_4Ni_2Si_2(CO)_2$, **19**, in C_6D_6 at 243 MHz.

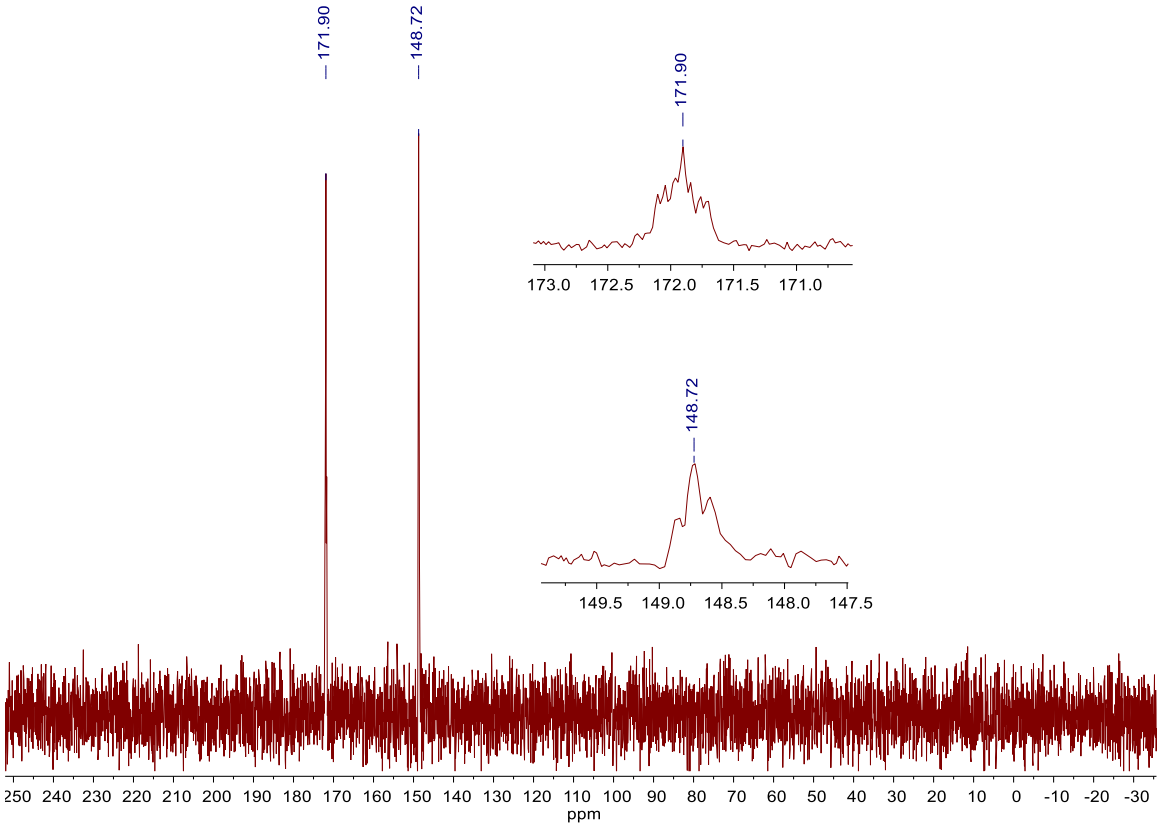

Figure 5.7-23. $^{29}Si\{^{1}H\}$ NMR of $P_4Ni_2Si_2(CO)_2$, **19**, in C_6D_6 in C_6D_6 at 119 MHz.

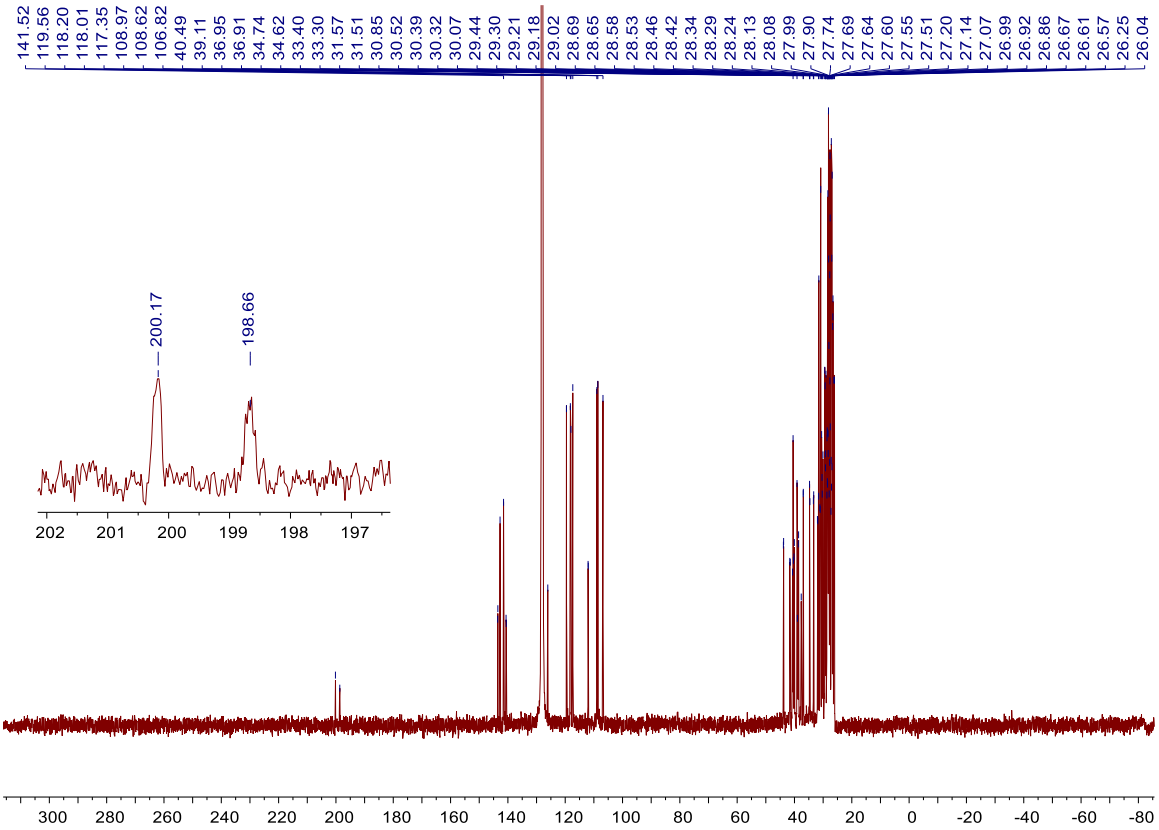

Figure 5.7-24. ^{13}C NMR of $P_4Ni_2Si_2(CO)_2$, **19**, in C_6D_6 at 151 MHz.

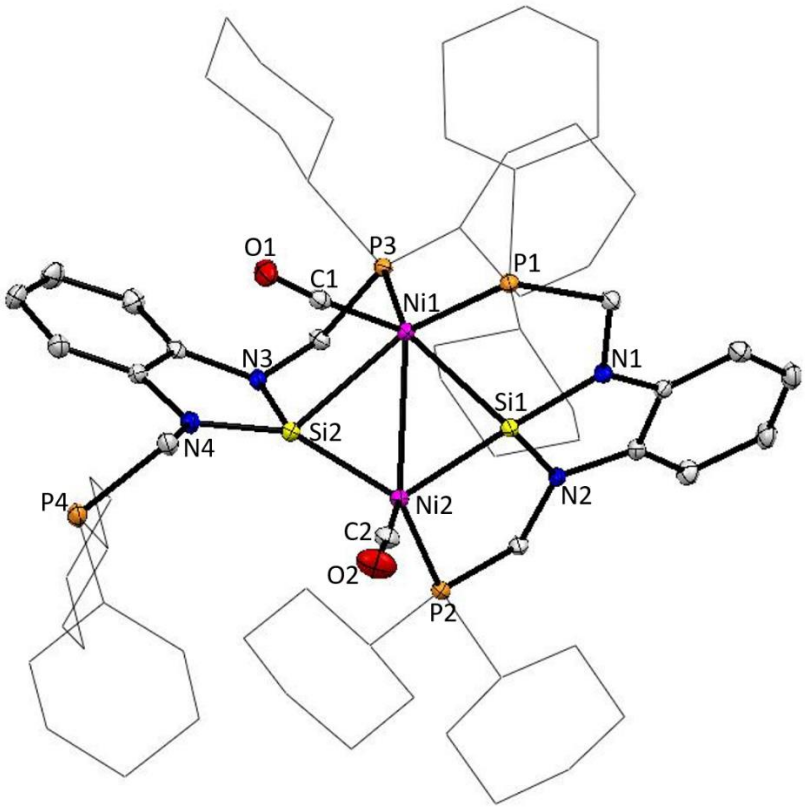

Figure 5.7-25. Thermal ellipsoid plot at 50% probability of $P_4Ni_2Si_2(CO)_2$, **19**. Magenta, yellow, blue, orange, red and gray ellipsoids represent nickel, silicon, nitrogen, phosphorus, oxygen and carbon atoms, respectively. For clarity, hydrogen atoms and solvent molecules are omitted and cyclohexyl rings on phosphorous are displayed as wireframe. Compound **19** crystallizes in the triclinic centrosymmetric space group P-1 with one molecule of **19** and three total molecules of benzene per asymmetric unit. One benzene molecule exhibits disorder that was modeled over two positions; the disorder ratio was refined freely and converged at 73:27. Two half-molecules of benzene are located on inversion centers. All benzene molecules were refined with the help of similarity restraints on 1,2- and 1,3- distances, as well as similarity and rigid-bond restraints on anisotropic displacement parameters. A planarity restraint was used on the minor portion of the disordered benzene.

Table 5.7-4 Crystallographic data for $P_4Ni_2Si_2(CO)_2$, **19**.

Identification code	hh294ab	
Empirical formula	$C_{84}H_{122}N_4Ni_2O_2P_4Si_2$	
Formula weight	1517.33	
Temperature	100(2) K	
Wavelength	0.71073 Å	
Crystal system	Triclinic	
Space group	P-1	
Unit cell dimensions	a = 12.5523(4) Å	α = 73.8627(16)°.
	b = 15.3540(5) Å	β = 84.8573(14)°.
	c = 21.6611(7) Å	γ = 85.1742(15)°.
Volume	3986.4(2) Å^3	
Z	2	
Density (calculated)	1.264 mg/m^3	
Absorption coefficient	0.631 mm^{-1}	
F(000)	1628	
Crystal color	orange	
Crystal size	0.195 x 0.083 x 0.037 mm^3	
θ range for data collection	1.383 to 30.508°	
Index ranges	$-17 \le h \le 17$, $-21 \le k \le 21$, $-30 \le l \le 30$	
Reflections collected	132804	
Independent reflections	24291 [R_{int} = 0.0915]	
Completeness to θ = 25.242°	100.00%	
Absorption correction	Semi-empirical from equivalents	
Refinement method	Full-matrix least-squares on F^2	
Data / restraints / parameters	24291 / 926 / 938	
Goodness-of-fit on F^2	1.009	
Final R indices [$I>2\sigma_1$ = 16485 data]	R_1 = 0.0469, *w* R_2 = 0.0965	
R indices (all data, ? Å)	R_1 = 0.0870, *w* R_2 = 0.1129	
Largest diff. peak and hole	1.770 and -0.462 e/Å^{-3}	

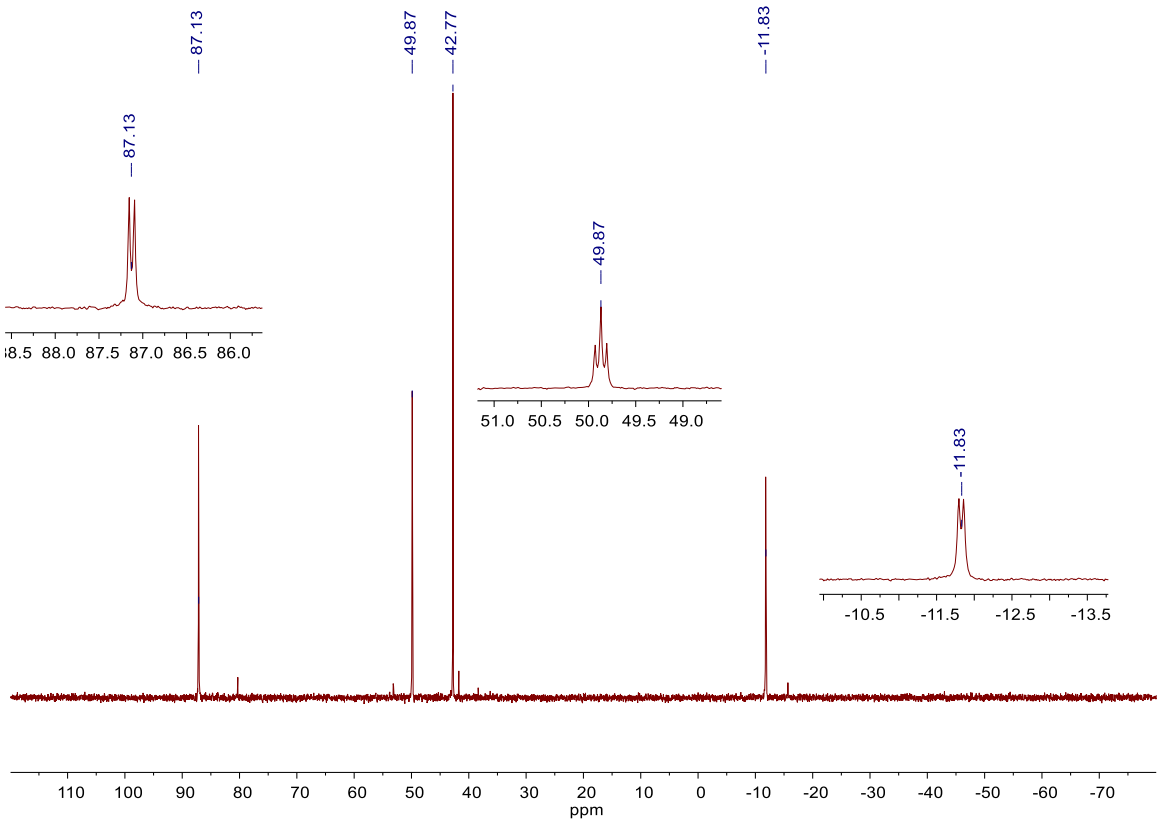

Figure 5.7-26. $^{31}P\{^{1}H\}$ NMR of product from reaction of excess CO with both **15** and **16** at 243 MHz in C_6D_6.

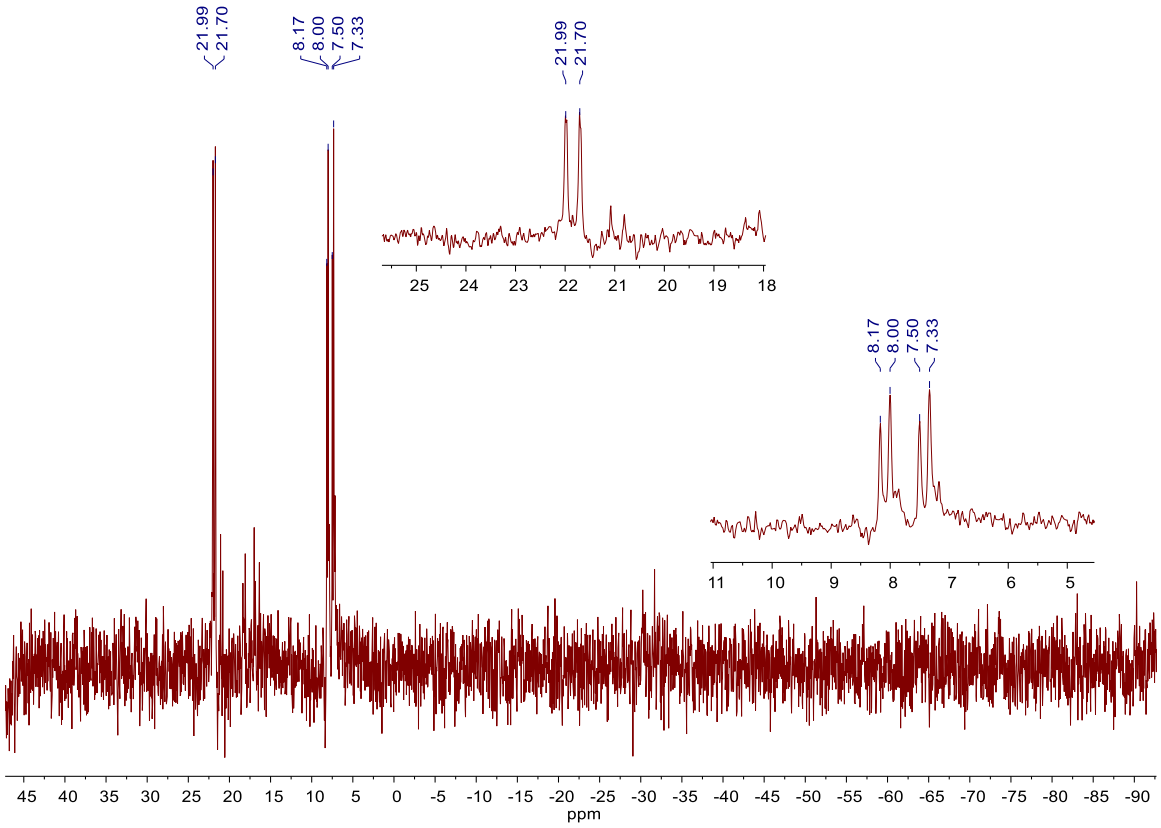

Figure 5.7-27. $^{29}Si\{^{1}H\}$ NMR of product from reaction of excess CO with both **15** and **16** at 119 MHz in C_6D_6.

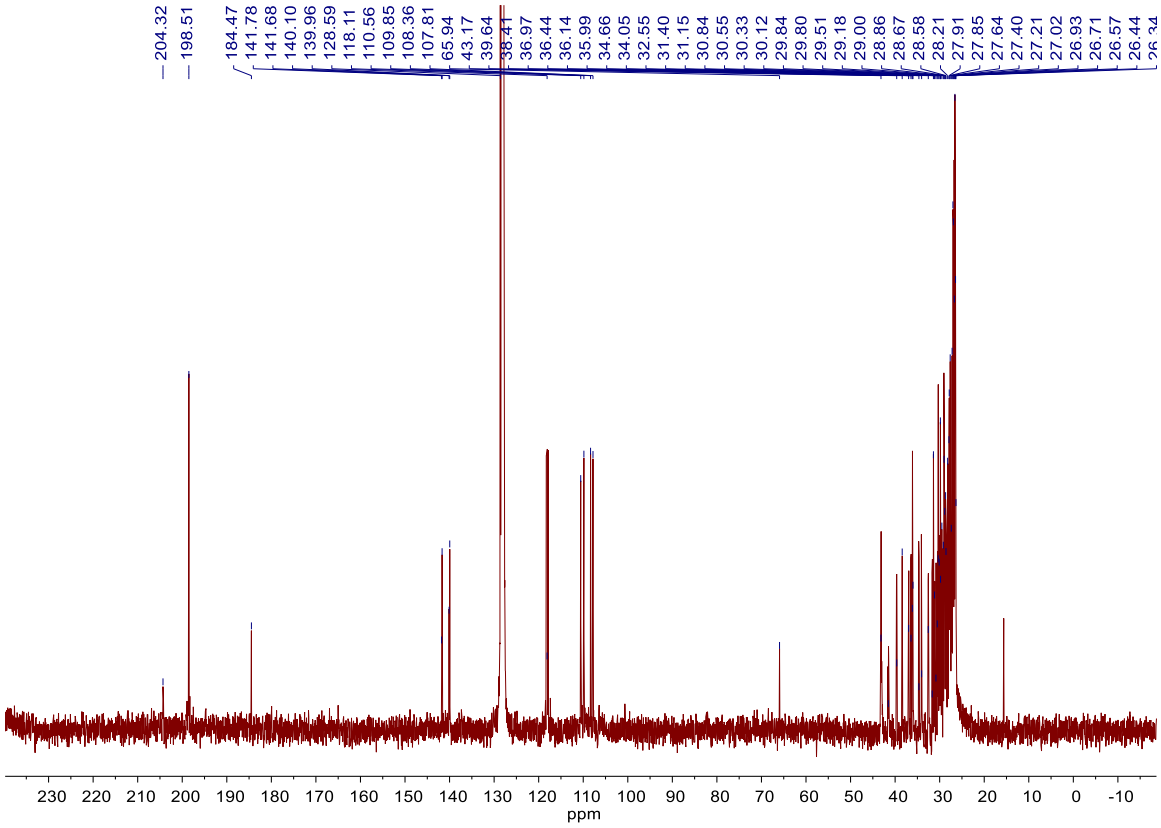

Figure 5.7-28. ^{13}C NMR of single product resulting from the exposure of excess CO to either **15** and **16** at 151 MHz in C_6D_6. Note free CO at 184.47 ppm.

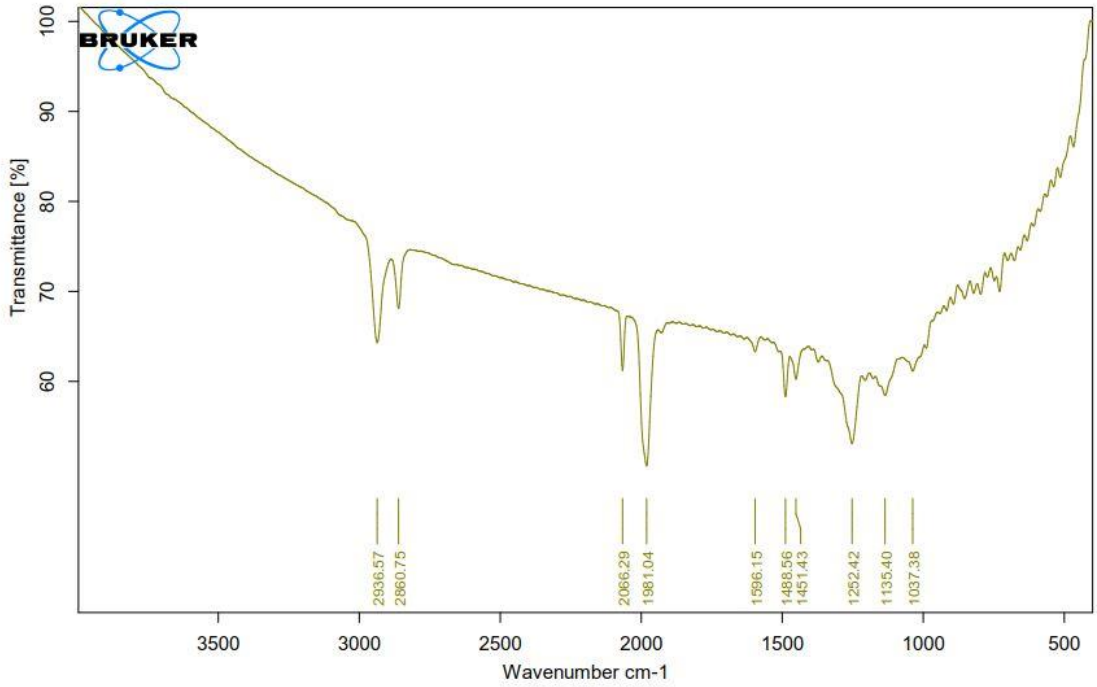

Figure 5.7-29 IR spectrum using KBr pellet for the single product resulting from exposure of excess CO to either **15** and **16.** Noted is the terminal carbonyl peak at 2066.29 cm^{-1} and another broad carbonyl peak at 1981.04 cm^{-1}.

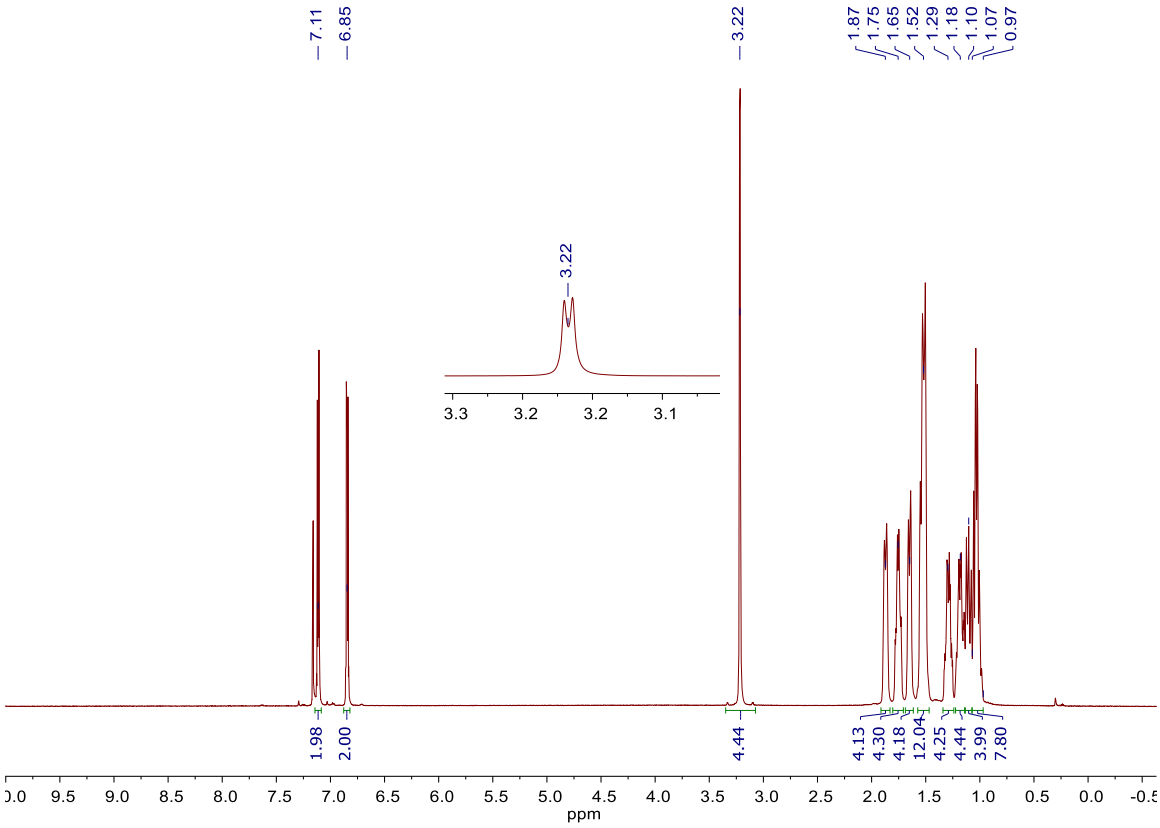

Figure 5.7-30. ^{1}H NMR of $P_2Ni_2Si(CO)_4$, **21**.in C_6D_6 at 600 MHz.

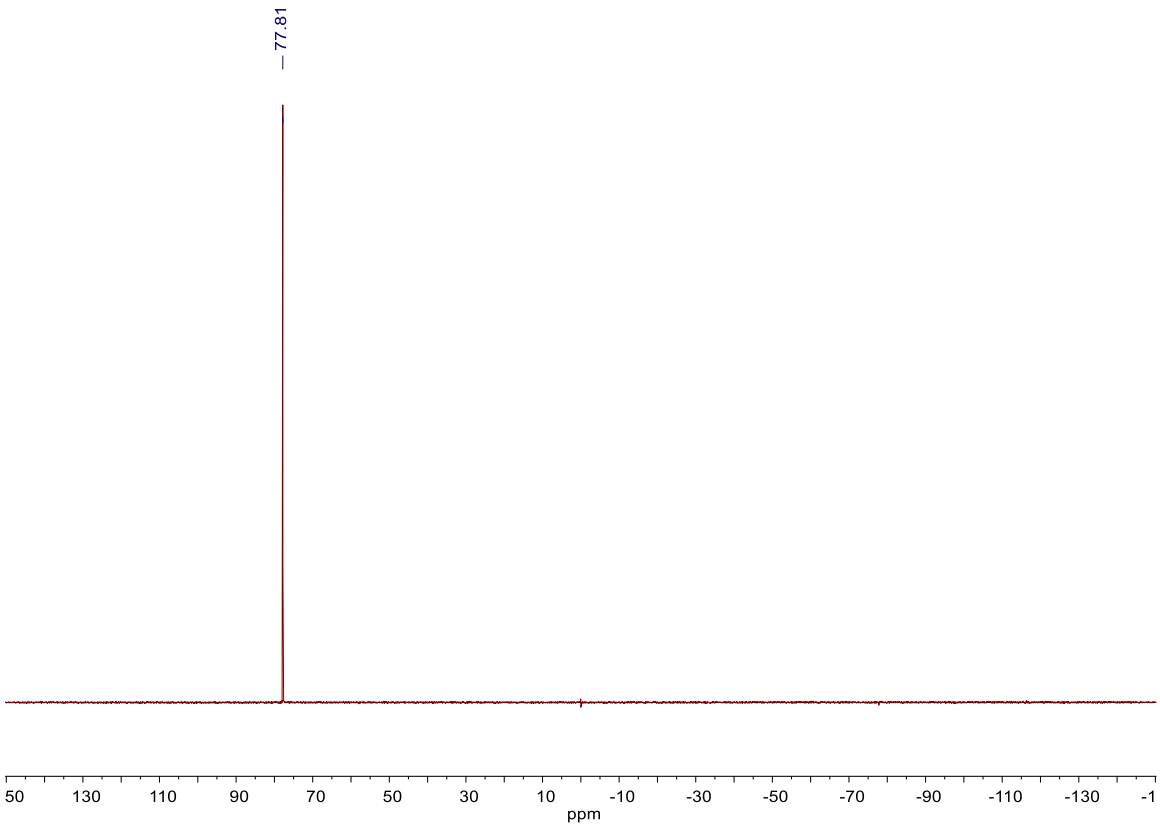

Figure 5.7-31 $^{31}P\{^{1}H\}$ NMR of $P_2Ni_2Si(CO)_4$, **21**.in C_6D_6 at 243 MHz.

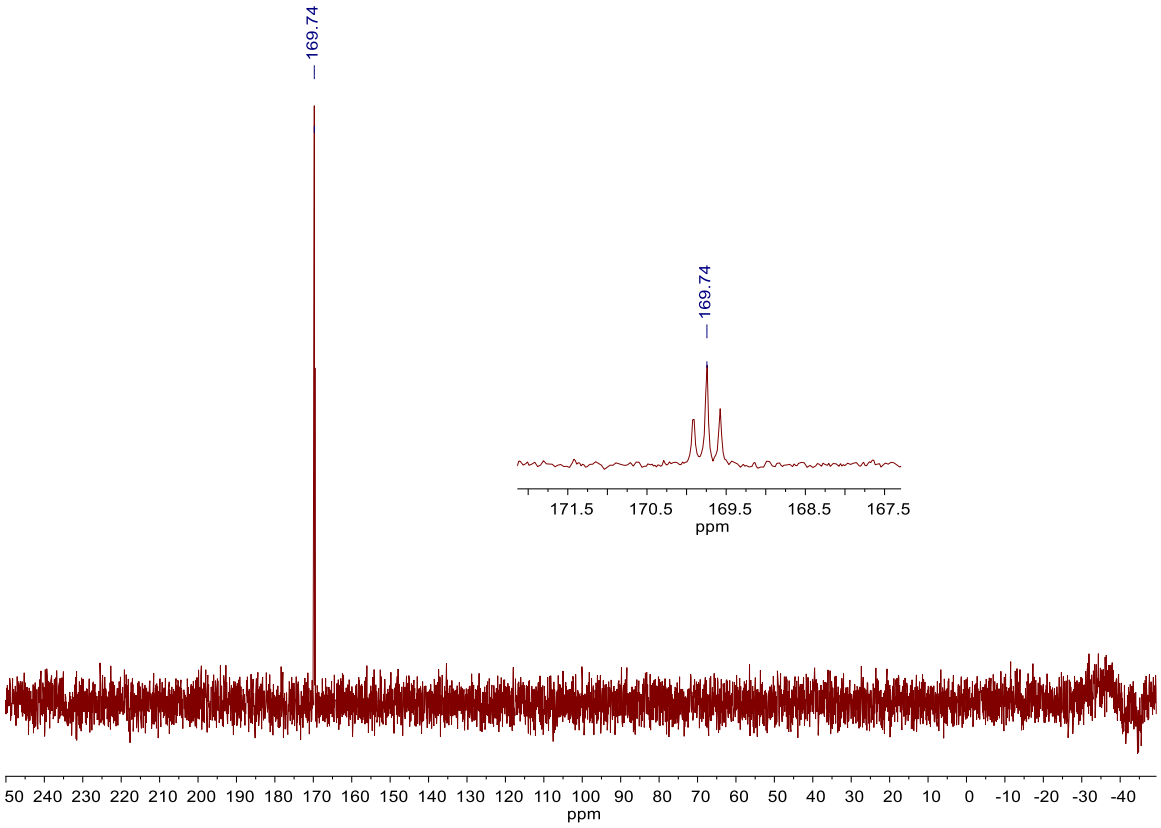

Figure 5.7-32 $^{29}Si\{^{1}H\}$ NMR of $P_2Ni_2Si(CO)_4$, **21**.in C_6D_6 at 119 MHz.

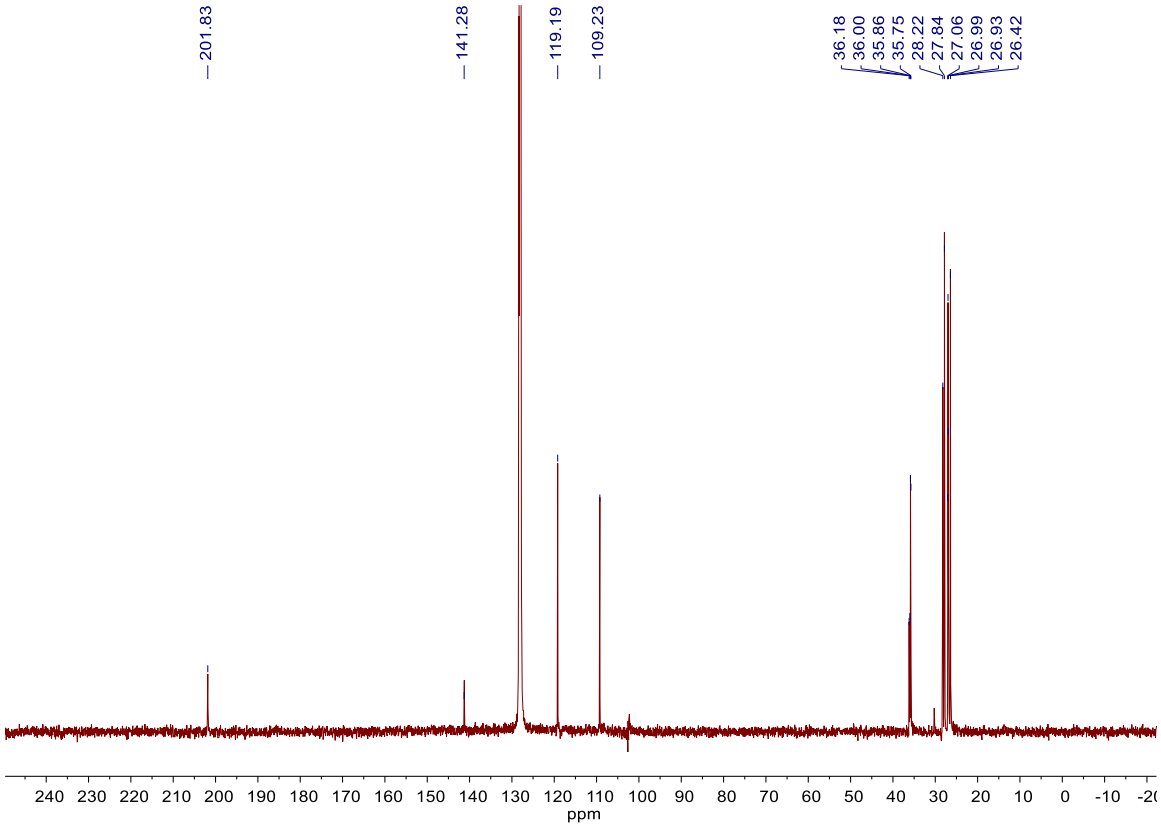

Figure 5.7-33 ^{13}C NMR of $P_2Ni_2Si(CO)_4$, **21**.in C_6D_6 at 151 MHz.

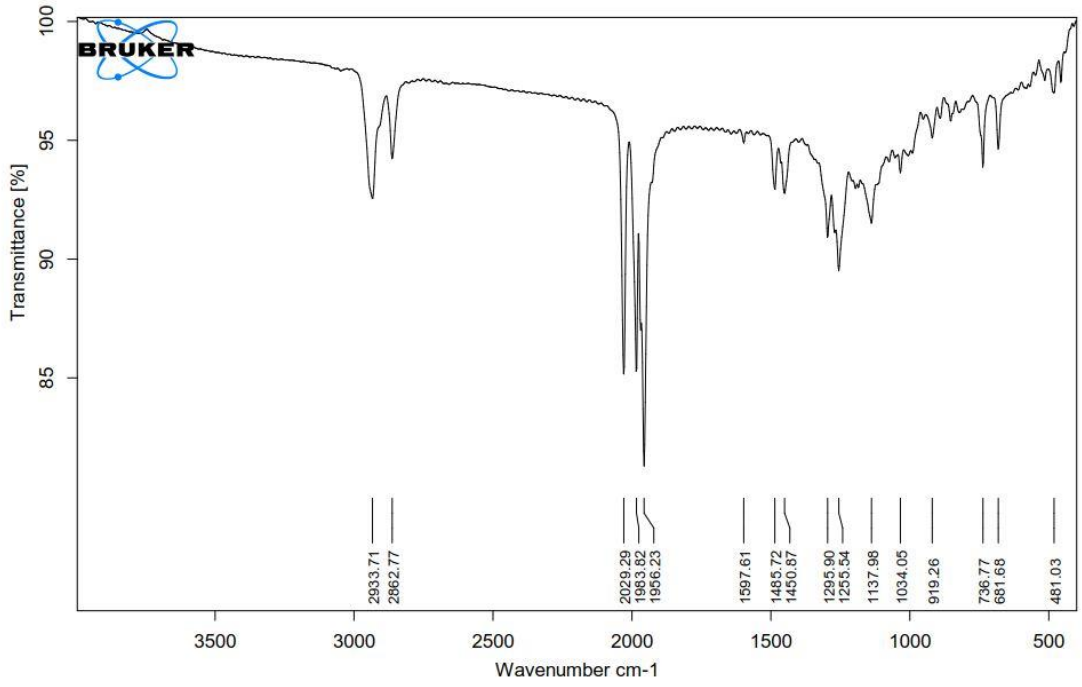

Figure 5.7-34 IR spectrum using KBr pellet of $P_2Ni_2Si(CO)_4$, **21**, featuring terminal carbonyl peaks at 2029.29, 1983.82, 1956.23 cm^{-1}. Note minor peak to the left of 1956.23 cm^{-1} that was not peak picked due to similarity in wavenumber

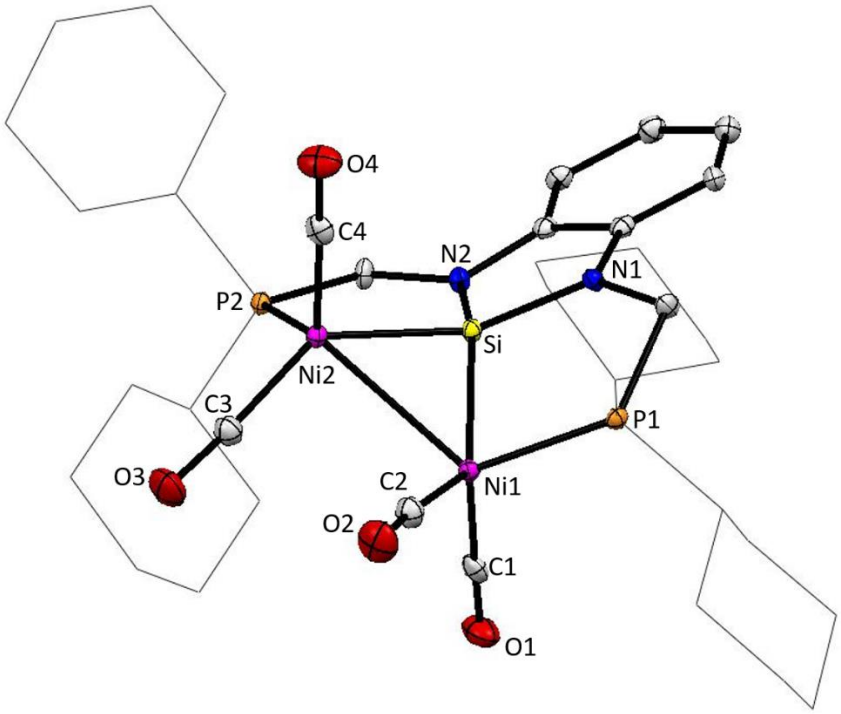

Figure 5.7-35 Thermal ellipsoid plot at 50% probability of $P_2Ni_2Si(CO)_4$, **21**. Magenta, yellow, blue, orange, red and gray ellipsoids represent nickel, silicon, nitrogen, phosphorus, oxygen and carbon atoms, respectively. For clarity, hydrogen atoms and solvent molecules are omitted and cyclohexyl rings are presented in wireframe for clarity.

Table 5.7-5 Crystallographic data for $P_2Ni_2Si(CO)_4$, **21**.

Identification code	hh297ab	
Empirical formula	$C_{36}H_{52}N_2Ni_2O_4P_2Si$	
Formula weight	784.24	
Temperature	100(2) K	
Wavelength	0.71073 Å	
Crystal system	Monoclinic	
Space group	C2/c	
Unit cell dimensions	a = 18.9321(6) Å	α = 90°.
	b = 13.2209(4) Å	β = 121.9505(11)°.
	c = 17.3880(9) Å	γ = 90°.
Volume	3692.9(2) Å^3	
Z	4	
Density (calculated)	1.411 Mg/m^3	
Absorption coefficient	1.179 mm^{-1}	
F(000)	1656	
Crystal color	yellow	
Crystal size	0.311 x 0.178 x 0.090 mm^3	
θ range for data collection	1.995 to 30.997°	
Index ranges	$-27 \leq h \leq 27$, $-19 \leq k \leq 19$, $-25 \leq l \leq 25$	
Reflections collected	42191	
Independent reflections	5891 [R_{int} = 0.0299]	
Completeness to θ = 25.242°	100.00%	
Absorption correction	Semi-empirical from equivalents	
Refinement method	Full-matrix least-squares on F2	
Data / restraints / parameters	5891 / 0 / 213	
Goodness-of-fit on F^2	1.039	
Final R indices [I>2σ$_1$ = 5244 data]	R_1 = 0.0223, w R_2 = 0.0572	
R indices (all data, 0.69 Å)	R_1 = 0.0270, w R_2 = 0.0597	
Largest diff. peak and hole	0.511 and -0.210 e/Å^{-3}	